International Conference
Materials Science and Nanotechnologies

Ekaterinburg, Russia
27—30 August 2023

ABSTRACT BOOK

Ural Federal University

urfu.ru

УДК **538.9**
ББК 22.37
С-423

Materials Science and Nanotechnology (MSN-2023). Abstract Book of International Conference (Ekaterinburg, August 27-30, 2023) Ekaterinburg, Ural Federal University, 2023- 179 с.
ISBN 978-5-9500624-6-9

Organizers

School of Natural Sciences and Mathematics, Ural Federal University named after the first President of Russia B.N. Yeltsin (UrFU)
http://www.urfu.ru

Ural Center for Shared Use “Modern Nanotechnology” UrFU
http://nanocenter.urfu.ru

Labfer Ltd.
http://www.labfer.com

Ferroelectric Laboratory, INSM UrFU
http://labfer.ins.urfu.ru

General chair

Prof. Vladimir Shur

Organizing committee

Vladimir Kruzhaev, Ural Federal University, Ekaterinburg, Russia
Alexander Sigov, MIREA - Russian Technological University, Moscow, Russia
Nikolai Mushnikov, M. N. Mikheev Institute of Metal Physics, Ekaterinburg, Russia
Leonid Korotkov, Voronezh State Technical University, Voronezh, Russia
Sergey Vakhrushev, Ioffe Institute, Saint-Petersburg, Russia
Alexander Vtyurin, Kirensky Institute of Physics, Krasnoyarsk, Russia
Xiaoyong Wei, Xi'an Jiaotong University, Xi'an, China
Le He, Soochow University, Jiangsu, China

Local organizing committee

Prof. Vladimir Shur	Ekaterinburg, Russia
Mrs. Elena Pelegova	Ekaterinburg, Russia
Dr. Dmitry Pelegov	Ekaterinburg, Russia
Mrs. Yana Mayorova	Ekaterinburg, Russia
Dr. Ekaterina Shishkina	Ekaterinburg, Russia
Mr. Eduard Linker	Ekaterinburg, Russia
Dr. Andrei Ushakov	Ekaterinburg, Russia
Dr. Victoria Pryakhina	Ekaterinburg, Russia

ISBN 978-5-9500624-6-9

9 785950 062469

ББК 22.37

Ural Federal University
named after the first President
of Russia B.N. Yeltsin

MSN-2023 sponsors

MTEON Ltd.
https://www.mteon.ru/

TUTORIAL LECTURES

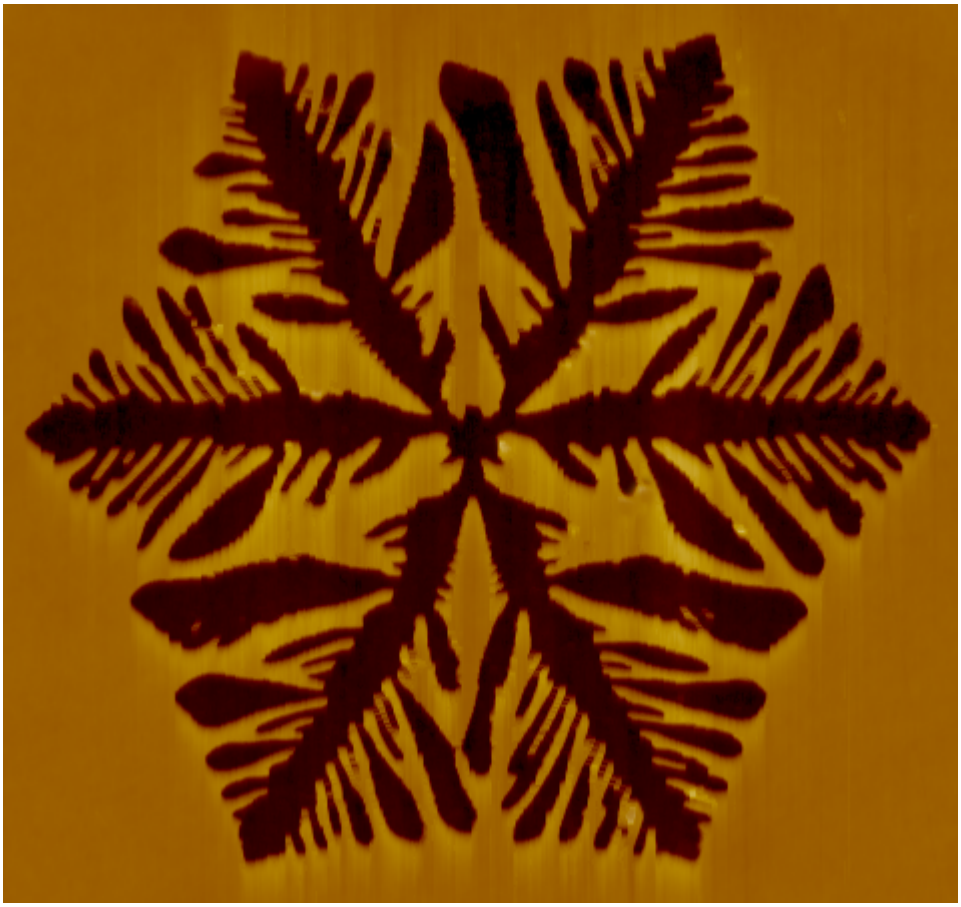

L1

Physics and application of ferroelectric domains

V.Ya. Shur

School of Natural Sciences and Mathematics, Ural Federal University, 620000 Ekaterinburg, Russia

vladimir.shur@urfu.ru

The difference between ferroelectric and magnetic domains, modern methods of domain imaging and the main stages of the domain kinetics are presented. Particular attention is paid to strongly nonequilibrium switching conditions. The results of systematic experimental study of the domain shape are considered. The explanation of obtained effects is based on the analogy between growth of domains and crystals from the liquid phase.

Ferroelectrics are often considered as the electric analog of ferromagnets thanks to existence of hysteresis loops, structural phase transitions and domain kinetics in the field. At the same time the screening of depolarizing fields in ferroelectrics which has no analogue in ferromagnets leads to stabilization of metastable domain structures, thus opening the way for domain engineering.

The evolution of domain structures during polarization reversal was studied in single crystals of various uniaxial ferroelectrics. It was shown that the convex polygonal domain shape with walls parallel to the main crystallographic directions were formed for effective screening only. The irregular polygons are formed if screening is ineffective. The rapid recovery of the polygonal shape after domain merging is due to the appearance of the ultrafast domain walls deviating from the main crystallographic directions. To explain the shape of growing domains, we considered: (a) stochastic step nucleation with an equiprobable position of nucleation centers leading to rounded domain shape, (b) determined step generation at the polygon vertices stimulating the shape defined by the crystal symmetry. Stochastic nucleation at the elevated temperature, due to increase of the bulk conductivity, opened the way to fractal and dendritic domains.

The evolution of self-assembled structures has been investigated by high resolution domain imaging and direct observation of domain kinetics. The kinetic approach was used for analysis of obtained results considering the decisive role of the residual depolarizing field caused by bulk screening delay. This field appeared behind a moving domain wall and slowed down the domain growth. The domain shape changes at highly nonequilibrium switching conditions leads to appearance of self-similar domain structures. The simulations of the shape change have been carried out.

The micro- and nano-domain engineering is an important step in the manufacturing of the electro-optical and nonlinear optical devices. The periodically poled crystals allowed to develop the light sources with record frequency conversion efficiency using the quasi-phase-matching effect. The prospects for domain engineering are very broad. The production of submicron-thick single-crystalline thin films of lithium niobate and lithium tantalate by ion cleavage, opens the possibility for creating nonlinear optical waveguides with submicron domain periods. The development of the domain wall control will be important for nanoelectronics with walls as the active elements.

L2

Basics of elastic domains

A. Roytburd[1], I. Lubomirsky[2]

[1]*University of Maryland, MD, USA*

[2]*Weizmann Institute of Science, Rehovot*

Similar to ferromagnetic and ferroelectric domains, elastic domains define the behavior of material under corresponding external field. The theory of elastic domains passed a long way from the interpretation of twinned structures of martensite phases [1] to the prediction of polydomain structures of epitaxial films [2]. At the end of 1980s, the possibility to produce defect free crystalline materials made the concept of elastic domains indispensable for modern functional materials [3-5].

The formation of elastic domains is an effective way to reduce internal stress in crystalline structures and it is currently considered as the mechanism of the stress relaxation. It has also been shown in ref [5] that besides the elastic domains, which decrease and, sometimes, completely relax the internal stress, there are also elastic domains, which may stabilize the internal stress, keeping it constant, during deformation of thin films. In this report, we present an outline of the theory supporting this phenomenon for the transformations in crystals and rods.

As an example of polydomain structure evolutions under stress and strain, we present the analysis of a tetragonal to orthorhombic transformation. It is shown that different transformation self-strain produce either “eutectic-like or “peritectic-like temperature-strain and temperature-stress diagrams describing the formation of equilibrium polydomain structures. The elastic anisotropy of the product phase may result in the formation of additional polydomain structures: “eutectic-like” case produces additional “peritectic” transformations and “peritectic-like” case produces additional “eutectic-like” transformations.

1. A.L. Roitburd, Domain structure of crystals formed in solid phase, *Sov. Phys. Solid State* **10**, 2870 (1969).
2. A.L. Roitburd, Equilibrium structure of epitaxial layers, *Phys. Status Solidi A* **37**, 329 (1976).
3. A.L. Roytburd, Elastic domains and polydomain phases in solids, *Phase Transit.* **45**, 1 (1993).
4. A.K. Tagantsev, L.E. Cross, J. Fousek, Domains in ferroic crystals and thin films. In Domains in ferroic crystals and thin films (Springer: Berlin, 2010).
5. A.L. Roytburd, J. Ouyang, A. Artemev, Polydomain structures in ferroelectric and ferroelastic epitaxial films, *J. Phys. Condens. Mat.* **29**, 163001 (2017).

L3

Magnetic nanomaterials for biomedical sensoric: selected examples and requests

G. Kurlyandskaya

Ural Federal University named after the First President of Russia B.N. Yeltsin, 620002, Ekaterinburg, RF
galinakurlyandskaya@urfu.ru

Many traditional nanomaterials and composites are not suitable for the increasingly complex requirements of the fast-growing number of microsystems designed for environmental control, biosensing, biomedical applications, drug delivery and others. The need for micro- and nanoscale sensors continues to challenge the materials science community to develop novel magnetic and composite materials that are suitable for such purposes. Magnetic nanomaterials were extensively studied for the last 30 years. There are of different types of nanostructured magnetic materials suitable for different sensor applications.

Recently special attention was paid for the design and development of magnetic biosensors. A magnetic sensor is a device, which measures changes in a magnetic field: a magnetic transducer converts a magnetic field variation into a change of frequency, current, voltage, light intensity etc. A magnetic biosensor is a compact analytical device incorporating a biological, a biomimetic or a biologically derived material associated with either physicochemical magnetic transducer or transducing microsystem [1-2]. Different effects have a capacity to support magnetic biosensor development: search coil, Hall effect, fluxgate, superconducting quantum interference device (SQUID), magnetoresistance, optical pumping, magnetoelastic resonance, magnetoimpedance (MI) and some others [2-5]. MI shows an advantage of the possibility of magnetic noise reduction, thin film designs up to simple point-of-care compact devices and sensitivity at room temperature comparable with potential sensitivity of a SQUID [6-8]. There were works describing MI prototypes adapted to microfluidic technologies, lab-on-a-chip packaging and sensor array design.

Magnetic nanomaterials have been studied for use in biosensors both as the sensitive element and in the form of microbeads, which work as biomolecular labels or magnetic carriers. Although the properties of the individual particle are the most important parameters, it is also essential to test the processes of the particles' accumulation in conditions as close as possible to those which might obtain in a device. Measurements of the properties of an individual magnetic particle enable us to avoid difficulties in interpreting the data derived from assemblies where dipolar interactions between the particles can play important roles and must be taken into account. Magnetic particles in biosensors play a double role: they work as labels and as the carriers of the attached biological molecule. The improvement of the detection limit supposes not only the achievement of the optimal functional characteristics for each part of the device separately but also the development of pairs of best performance adapted to the conditions of the particular test. Here we will discuss the possible use of nanostructured materials as the basis for a new generation of sensors for electronics, biology, chemistry, drug delivery and medicine.

This work was supported by the Russian Science Foundation (grant №23-29-00025,https://rscf.ru/project/2329-00025/).

1. N.J. Darton, A. Ionescu, J. Llandro, *Magnetic nanoparticles in biosensing and medicine*, CUP, 172 (2019).

2. D.R. Baselt, G.U. Lee, M. Natesan, et al., *Biosens. Bioelectr.* **13**, 731 (1998).

3. T. Uchiyama, K. Mohri, Sh. Nakayama, et al. *IEEE Trans. Magn*. **47**, 3070 (2011).

4. G.V. Kurlyandskaya, D. de Cos, S.O. Volchkov, *Rus. J. Nondestr. Test*. **45**, 377 (2009).

5. A. Kumar, S. Mohapatra, V. Fal-Miyar, et al., *Appl. Phys. Lett.* **91**, 143902 (2007).

6. G.V. Kurlyandskaya, F.A. Blyakhman, E.B. Makarova, et al., *AIP Advances* **10**, 125128 (2020).

7. N.A. Buznikov, A.P. Safronov, I. Orue, et al. *Biosens. Bioelectr*. **117**, 366 (2018).

8. G.Yu. Melnikov, V.N. Lepalovskij, A.V. Svalov, et al. *Sensors* **21**, 3621 (2021).

L4

Introduction to SAXS (Small-Angle X-ray Scattering) characterization of nanomaterials

P. Zelenovskii

School of Natural Sciences and Mathematics, Ural Federal University, 620000 Ekaterinburg, Russia

Department of Chemistry and CICECO−Aveiro Institute of Materials, University of Aveiro, 3810-193 Aveiro, Portugal

zelenovskiy@urfu.ru

Small-Angle X-ray Scattering, widely known as SAXS, is one of the most universal methods for the characterization of nanomaterials. It can be applied to solids, powders, gels, and colloids. The studied materials can be amorphous or crystalline. In contrast to typical powder or single crystal X-ray diffraction, SAXS is a low-resolution method. Instead of the information on the crystal structure and atomic positions, SAXS provides information on the size and shape of the particles, volume and specific surface area, molecular weight, and many others.

This tutorial aims to introduce the audience to the basic principles of SAXS measurements and familiarize them with the main instrumental blocks and modern equipment. A practical part is devoted to the examples of SAXS data analysis and interpretation.

INVITED
PRESENTATIONS

I1

Shape and orientation of the domain walls in uniaxial ferroelectrics

V.Ya. Shur

School of Natural Sciences and Mathematics, Ural Federal University, 620000, Ekaterinburg, Russia
vladimir.shur@urfu.ru

The variety of the domain shapes and domain wall orientations appeared in uniaxial ferroelectric crystals during polarization reversal in uniform electric field will be presented, classified, and described. The revealed dependence of the domain wall orientation on the switching conditions will be considered in terms of kinetic approach to domain structure evolution based on analogy of domain and crystal growth.

The domain structure evolution has been studied experimentally in wide temperature and field range using various complimentary methods of domain imaging at the surface and in the bulk including optical microscopy, scanning electron microscopy, piezoresponse force microscopy and Cherenkov-type confocal Second Harmonic Generation (CSHG). The main attention was paid to results of *in situ* optical imaging of domain growth with high temporal resolution and bulk domain imaging using CSHG. The single crystals of uniaxial high-quality lithium niobate $LiNbO_3$ and lithium tantalate $LiTaO_3$ family have been studied as the model materials.

It is important to point out that the classical theoretical approach predicted the random orientation of the 180-degree domain walls in uniaxial ferroelectrics [1,2]. The formation and growth of convex polygonal domains with wall orientation along main crystallographic axis were obtained in classical experiments. Our detail experimental study allows to reveal that the wall orientation and domain shape can be widely controlled by variation of the temperature and parameters of the applied electric field pulses [3,4].

The domain wall motion has been considered because of the generation of elementary steps with pair of charged kinks and kink motion along the wall. The step generation rate and kink motion velocity are proportional to the excess over the thresholds of the local value of the electric field produced by applied voltage and partially screened depolarization field. The effect of the retardation of the bulk screening on the wall orientation was demonstrated. It was shown that the straight domain walls appeared for determined step generation at fixed points (vertexes of the polygonal domains) and anisotropic kink motion in directions determined by crystal symmetry, whereas the stochastic step generation realized at the elevated temperatures leads to curved domain walls [4,5].

The determined step generation at the domain vertices stimulated formation of the convex polygonal domains with walls parallel to the main crystallographic axis which shapes match to the crystal symmetry. The wall deviation and formation of the irregular polygons and stars are caused by screening retardation [4,5].

The fast restoration of the initial wall orientation after domain merging is due to arising of the short-lived superfast domain walls [6,7]. The measured giant velocity increase of the deviated domain walls was attributed to increase of the kink concentration.

The equipment of the Ural Center for Shared Use “Modern nanotechnology” Ural Federal University (Reg.№ 2968) which is supported by the Ministry of Science and Higher Education RF (Project № 075-15-2021-677) was used. The research was made possible by Russian Science Foundation (Project № 19-12-00210).

1. I.S. Zheludev, L.A. Shuvalov, *Kristallografiya* **1**, 681 (1956).
2. J. Fousek, V. Janovec, *J. Appl. Phys.* **40**, 135 (1969).
3. V.Ya. Shur, A.R. Akhmatkhanov, *Phil. Trans. R. Soc. A.* **376**, 20170204 (2018)**.**
4. V.Ya. Shur, E.V. Pelegova, M.S. Kosobokov, *Ferroelectrics* **569**, 251 **(**2020**)**.
5. A.A. Esin, A.R. Akhmatkhanov, V.Ya. Shur, *Appl. Phys. Lett.* 114, 092901 (2019).
6. V.Ya. Shur, A.A. Esin, M.A. Alam, et al, *Appl. Phys. Lett.* **111**, 152907 (2017).
7. A.A. Esin, A.R. Akhmatkhanov, V.Ya. Shur, *Appl. Phys. Lett.* **114**,192902 (2019).

I2

New quantum technologies of ultrashort-pulse laser nanoinscription in bulk dielectrics

S.I. Kudryashov[1,2], M.S. Kosobokov[1], A.R. Akhmakhanov[1], P.A. Danilov[2], V.Y. Shur[1]

[1]*School of Natural Sciences and Mathematics, Ural Federal University, 620000, Ekaterinburg, Russia sikudryashov@urfu.ru, kudryashovsi@lebedev.ru*

[2]*Lebedev Physical Institute, 119991, Moscow, Russia*

In our studies, tightly focused (numerical aperture NA = 0.25÷0.65) ultrashort laser pulses with a central wavelength of 1030 or 1050 nm and a duration of 0.2÷3 ps produced in a self-consistent manner in the filamentation mode (peak powers = 5÷50 MW) in the volume of amorphous and crystalline dielectrics (amorphous fused quartz, crystalline lithium niobate, calcium fluoride, and diamond) extended microscale tracks of a uniformly modified material, characterized by dark field optical microscopy inside the sample, scanning electron microscopy and atomic force microscopy in the sample cross section after polishing. Along with a homogeneous modification, the tracks include ordered arrays of nanocavities with periods on the order of a wavelength, which form a high-contrast Bragg grating. Their spectral response is dominated by near-wavelength periodical modulation of the laser induced supercontinuum, peaked at the central pump wavelength of 1030 or 1050 nm. The plasmonic mechanism of formation of an array of nanocavities along a continuum plasma microchannel of filamentation nature is discussed.

This research was funded by the Ministry of Science and Higher Education of the Russian Federation (Ural Federal University Program of Development within the Priority-2030 Program).

I3

Ferroics in strong THz fields

E.D. Mishina, K.A. Brekhov, N.E. Sherstyuk

MIREA – Russian Technological University,119454, Moscow, Russia
mishina_elena57@mail.ru

Terahertz radiation and the effects induced by it can have great potential for practical application both for the development of new generation photonic and electronic devices and for fundamental research aimed at revealing new properties of well-known functional materials. For ferroelectric materials, the advantage of using THz radiation lies in the possibility of an electrodeless application of an electric field to a ferroelectric and thus affecting its polarization in the pico(femto)second time range.

Changes in the polarization state of the material caused by a picosecond THz pulses were investigated by time resolved X-ray diffraction and optical methods (pump-probe techniques). X-ray techniques directly prove shift of the ion sublattice in a crystal under electric field of THz pulse. Among optical techniques, the second harmonic generation method is the most adequate to study transient shifts of ions which result in dielectric polarization modulation or dynamic polarization switching. On the other hand, SHG intensity dependence on electric field may have pure electronic nature, such as in semiconductors at low fields (electric field induced SHG or EFISH). Thus, a direct prove of ion movements is extremely important for the SHG results interpretation. However, a time resolved XRD is available mostly at synchrotron sources. On the contrary, SHG provides a much less expensive, but very fast and informative method for studying the polarization behavior. This includes information on the dielectric polarization (re-)orientation (switching) under the action of ultrashort electric field pulse due to the general proportionality of the SH field to the ferroelectric polarization vector.

Over the past decade, a large number of ferroelectric materials under THz pulse excitation have been studied, including model crystals ($SrTiO_3$ [1], $BaTiO_3$ [2]) and technological materials as well ($BaSrTiO_3$ films [3], $PbTiO_3/SrTiO_3$ heterostructures [4], BST/PZT ferroelectric photonic crystals [5]). In THz scheme, electric field is applied in-plane. Such configuration is used while considering modulators, phase shifters, tunable filters, phased antenna arrays, sensors, and several kinds of memory elements. Nevertheless, domain structures with a polarization vector lying in the plane of the film have been little studied, despite the fact that they can potentially be useful in optical devices in which domains with vertical domain walls can be manipulated optically.

In this work, we report the results of experimental studies of polarization modulation induced by strong picosecond THz pulse in several ferroelectric materials: Si:PbGeO and TGS crystals, $BaSrTiO_3$ and $Bi_4Ti_3O_{12}$ films on different substrate. SHG as a measure of polarization is used. The dependences of the SHG intensity on the THz field, as well as polarization hysteresis loops, are discussed. Criterion is introduced for estimating the fraction of polarization involved in modulation.

The work is supported by Russian Science Foundation, Grant #22-12-00334.

1. X. Li, T. Qui, J. Zhang, et al, *Science* **364**, 1079 (2019).
2. F. Chen, Y. Zhu, S. Liu, et al, *Phys. Rev. B* **94**, 180104 (R) (2016).
3. V. Bilyk, N. Ilyin, E. Mishina, et al, *Scripta Materiala* **214**, 114687 (2022).
4. J. Ji, S. Zhou, J. Zhang, et al, *Sci. Rep.* **8**, 2682 (2018).
5. J. Zeng, W. Wang, F. Ling, J. Yao, *Phot. Research* **8**, 1002 (2020).

I4

Soft mode “puzzle” in relaxor ferroelectrics

S.G. Lushnikov[1], N.K. Derets[1], A.I. Fedoseev[1], R.S. Katiyar[2], J.-H. Ko[3]

[1]*Ioffe institute, 194021 St. Petersnurg, Russia*
sergey.lushnikov@mail.ioffe.ru
[2]*University of Puerto Rico, PR 110007, San Juan, USA*
[3]*Hallym University, 24252, Chuncheon, Korea*

Relaxor ferroelectrics (relaxors) with the perovskite structure have been a challenge to the scientific community in the last 60 years, since the first reports of observed anomalies of physical properties. The unique dielectric and piezoelectric characteristics of relaxors have been widely demanded by the industry, and their nature is still the subject of wide discussion. The broad, frequency-dependent permittivity anomaly is not associated with a structural phase transition, which makes it difficult to consider the classical lattice dynamics in the framework of a soft-mode approach in these compounds. The analysis of possible mechanisms of the dielectric response anomaly in relaxors was considered in detail in [1], but no unified concept has appeared. The existence of the contribution of relaxation mechanisms associated with polar nanoregions has been experimentally shown, but this was not enough to correctly describe the behavior of the dielectric response with temperature changes. Studies of the low-frequency region of the vibrational spectrum using vibrational spectroscopy indicate the appearance of a soft mode in the high-temperature region [2, 3]. A detailed analysis of its behavior with a decrease in temperature left more questions than answers. Starting with how many soft modes are observed in experiments and ending with the question of a theoretical model describing the dynamics of the crystal lattice of relaxors. This motivated us to return to the question of the soft-mode dynamics of relaxors and build a general picture of the behavior of soft optical modes in the vicinity of the Γ-point of Brillouin zone. $PbMg_{1/3}Nb_{2/3}O_3$ (PMN) is chosen as an example on which we will consider the behavior of long-wave optical phonons, the studies of which are most complete.

The PMN crystal is a model object in studying the lattice dynamics of relaxors. The symmetry of the crystal remains cubic up to helium temperatures, while a wide maximum of the dielectric constant is observed near $T_m \approx 270$ K. In the dynamics of the PMN lattice, another characteristic temperature $T^* \approx 400$ K is distinguished, at which many physical properties experience anomalies, but the nature of these anomalies remains unclear. Studies of soft modes in the PMN vibrational spectrum, which could be responsible for the anomalies of the dielectric response near Tm, have been going on for many years, and the results of experiments on neutron scattering, IR spectroscopy, hyper-Raman scattering do not always agree with each other. This report contains the published results of studies of the soft–mode dynamics of the PMN crystal by various methods, which are supplemented by the results of our measurements of Raman scattering of light in a wide temperature range (100÷1150 K). The behavior of the main phonon modes and quasi-elastic light scattering was analyzed in the scattering spectra of polarized light. Temperature dependences of intensity, frequency and width of phonon modes are constructed. It is shown that in the region of 950 K there is a reversible disappearance of the Raman spectra of the first order and quasi-elastic scattering. PMN cooling does not lead to anomalies in the frequency and half-width of phonon modes near the Burns temperature ($T_B \approx 640$ K). A “softening” observed at $T > 400$ K and a “tightening” at $T < 350$ K were found in the temperature dependences of the frequency of low-lying modes. The comparison of the obtained results showed good agreement with the literature data on neutron, IR and hyper-Raman spectroscopy, complementing the general picture of the temperature evolution of the low-frequency vibrational spectrum PMN. The discussion of the behavior of low-frequency optical phonons in PMN will be conducted within the framework of modern ideas about the physics of relaxors.

1. A.A. Bokov, Z.-G. Ye *J. Adv. Diel.* **2**, 1241010 (2012).
2. R.A. Cowley, et.al. *Adv. Phys.*, **60**, 229 (2011).
3. S. Kamba, *APL Mater*. **9**, 020704 (2021).

I5

Investigations of magnetic thin film nanostructures in the M.N.Mikheev Institute of Metal Physics of Ural Branch of Russian Academy of Sciences

A.P. Nosov

M.N. Mikheev Institute of Metal Physics of Ural Branch of Russian Academy of Sciences, 620118, Ekaterinburg, Russian Federation
nossov@imp.uran.ru

Spintronics, also known as spin electronics, is the field of modern physics aimed at investigations of numerous phenomena originating from the existence of intrinsic property of spin of the electron and its associated magnetic moment, in addition to its fundamental electronic charge, which is widely exploited in contemporary solid-state devices.

Utilization of spin degree of freedom except for the charge one at least eliminates the Joule heating in physical phenomena involving electron transport. It can be used to boost the efficiency of next generation devices for data storage, manipulation, and transfer.

Spintronic phenomena are most prominent in nanostructures – artificial thin film-layered structures consisting of materials with different magnetic and/or conductive properties. Typical thickness of individual layers can vary from fractions to tens of nanometers. The exact value being critical for realization of such physical mechanisms as interlayer exchange coupling, spin polarized tunneling, direct and inverse spin Hall effect and others.

Depending on the magnetic properties of materials used, one can distinguish ferromagnetic (FM) [1] and antiferromagnetic (AFM) [2] spintronics.

In the field of ferromagnetic metallic spintronics the classical 3d metallic ferromagnetic materials and their alloys are used. The activities in the IMP in this area are concentrated on metallic-based nanostructures and multilayers in which the giant magnetoresistance effect (GMR) can be realized. The nanostructures are prepared by magnetron sputtering. Such structures as spin valves and multilayers can be prepared. The unique properties of the obtained nanostructures are due to the choice of the optimal composition and the use of original magnetic and non-magnetic alloys in them. Exchange-coupled metallic CoFeNi/CuIn superlattices have been developed that exceed the foreign analogs in terms of magnetoresistance, minimal hysteresis, and high magnetic field linearity and are the best in their class of magnetically sensitive nanomaterials. Such nanostructures are resistant to high temperatures up to T=300°C and can serve as initial magnetically sensitive media for creating magnetic sensors for various applications. Their transport, optical and high frequency properties are extensively studied.

In the field of antiferromagnetic spintronics the activities in the IMP are concentrated on nanostructures with such materials as $YFeO_3$, Fe_2O_3, NiO. They can be used for realization of such interesting spin dependent phenomena as spin transfer torque, direct and inverse spin Hall effect, spin accumulation and others in which the relativistic spin–orbit coupling plays the primary role. The investigations are aimed at growth of high quality single crystalline films in which both FM and AFM resonances with the frequencies in the sub-terahertz frequency range can be observed. This frequency range is of primary importance for development of 5G telecommunication systems and devices. The AFM films can be used in the investigations of ultrafast magnetization reversal for development of next-generation data storage technologies. Complex investigations of their transport, optical and high frequency properties are carried out.

The research was carried out within the state assignment of Ministry of Science and Higher Education of the Russian Federation (theme “Function” No. 122021000035-6).

1. C. Chappert, A. Fert, F. van Dau, *Nature materials* **6**, 813 (2007).
2. T. Jungwirth, X. Marti, P. Wadley, *Nature nanotechnology* **11**, 231 (2016).

I6

On the origin of non-classical electrostriction in ion conductors

I. Lubomirsky

Dept. of Molecular Chemistry and Materials Science, Weizmann Institute of Science

Electrostriction is a second order electromechanical response observable in all solid dielectrics. According to the scaling law presented more than two decades ago by Prof. R. Newnham (Penn State), the electrostriction polarization coefficient for a wide range of classical electrostrictors scales with the ratio of the elastic compliance to the dielectric constant.

In 2012, Gd-doped ceria, one of the most studied oxygen ion conductors, was reported to exhibit an unusually large electrostriction. This first report was followed by reports on non-classical electrostriction (NCES) in other aliovalent-doped ceria, on (Nb,Y)-stabilized cubic Bi_2O_3 and acceptor-doped, hydrated barium zirconate, suggesting that strong electrostriction may be an inherent property of superionics. At room temperature, these ceramics exhibit a longitudinal electrostriction strain coefficient $|M_{33}| > 10^{-17} m^2/V^2$. However, with elastic modulus >80 GPa and dielectric constant <100, the experimental Q-coefficients of these materials are at least 100 times larger than values predicted by the classical scaling law. Of the three ceramics, aliovalent-doped ceria is the most studied. Below 1 Hz, $|M_{33}|$ for 10 mol% Sm- or Gd-doped ceria reaches 10^{-16} m^2/V^2 relaxing to $<10^{-18}$ m^2/V^2 above 100 Hz. Aliovalent lanthanide dopants with smaller ionic radii than that of Gd, such as Lu or Yb, raise $|M_{33}|$ at 100 Hz to $\approx 10^{-17} m^2/V^2$.

Acceptor-doped $BaZr_{1-x}X_xO_{3-x/2+\delta}H_{2\delta}$ proton-conducting ceramics, where X= Ga, Sc, In, Y or Eu, and $0.05 \leq x \leq 0.2$, exhibit non-classical electrostrictive strain for all dopants in both the dry and hydrated states: $|M_{33}| = (1\text{-}7)\cdot 10^{-16} m^2/V^2$ below, and $\approx 10^{-18}\text{-}10^{-17} m^2/V^2$ above, the Debye-type relaxation frequency. Hydration does not significantly affect M_{33}, but raises the relaxation frequency by a factor of 10 to 100, indicating that proton-based elastic dipoles can respond more quickly than those based on oxygen vacancies.

According to our current understanding, NCES emerges from electric field-induced rearrangement of highly polarizable elastic dipoles induced by point defects: oxygen vacancies or proton interstitials. In this model, elastic and dielectric properties are largely defined by the host lattice, while electrostrictive strain is controlled by the strength of the elastic dipoles. We suggest that non-classical electrostriction may be a common feature for crystalline dielectrics containing mobile point defects.

I7

Nanocrystalline state and nanomaterials. The state-of-the-art - advances and challenges.

A.Ye. Yermakov, M.A. Uimin, A.S. Minin, Yu.S. Ponosov, I.V. Byzov, E.A. Kravtsov, Yu.A. Salamatov, A.S. Konev

M.N. Mikheev lnstitute of Metal Physics of Ural Branch of Russian Academy of Sciences, 620137, Yekaterinburg, Russia
yermakov.anatoly@gmail.com

In the talk the nanocrystalline state, synthesis of nanocrystalline materials and different applications will be discussed. Special attention will be paid on the recent advances and perspectives in this area (novel nanomaterials, including metal and compounds with carbon and graphene coating; medicine applications and so on). But the most important point of the lecture we will try to underline and to consider the main problems and challenges in this field.

The research was carried out within the state assignment of Ministry of Science and Higher Education of the Russian Federation (theme “Magnet” No. 122021000034-9)

I8

Dynamic susceptibility of ferrogels

A.Yu. Zubarev

Ural Federal University, 620000, Ekaterinburg, Russia
A.J.Zubarev@urfu.ru

Ferrogels are smart composite materials, consisting of a host polymer gel and embedded magnetic nano particles. These systems attract considerable interest of researchers and engineers due to rich set of unique physical properties valuable for many industrial and bio-medical applications. Dynamic reaction of magnetic composites on alternating magnetic fields is one of the most interesting, from the point of view of basic research, and important, from the viewpoint of high-tech applications, characteristics of these materials. One of the most perspective bio-medical applications of magnetic gels is magneto-hyperthermia (MH) method of therapy of cancer diseases. The key idea of this method is in injection of magnetic nanoparticles into the region with the diagnostic tumor. The ill cells anchor these particles. Then the tumor region is placed in an alternating magnetic field, which heats the particles and, therefore, the tumor cells. If temperature of this cell exceeds some threshold one, usually estimated as 42^oC, the tumor cell dies. At the same time the healthy cells remain uninjured till $52\div55^oC$.

There are two main mechanisms of the heat production by the magnetic nanoparticles in a surrounding medium. The first one is rotation of the particles and energy loss because of the viscous friction between the particles and the medium. The second one is internal (Neel) remagnetization. Experiments show that magnetic nanoparticles, being embedded into biological cells, as a rule, are tightly bounded with the tissue and, therefore, they are immobilized. Therefore, the Neel mechanism must be dominating for the particles in biological tissues; for example, at organization of the MH therapy.

The classical theoretical investigations of dynamic remagnetization of ferromagnetic nanoparticles deal with the simplest system of non-interacting particles ("ideal gas" approximation) which means that their concentration is very small. However magnetic reaction of composites with low concentration of the particles is too weak for many practical applications. Increase of the particle's concentration leads to enhance of effect of their magnetic interaction. At the same time numerous experiments show that ferroparticles, injected in a biological tissue for the MH therapy, very often conglomerate to various structures where the "ideal gas" approximation cannot be used in principle.

We present results of theoretical study of effect of magnetic interparticle interaction on dynamic magnetic susceptibility and magnetic hyperthermia in systems of single-domain ferromagnetic particles, immobilized in a host medium. These systems can model ferrogels, solid magnetic nanocomposites, biological tissues with embedded particles and other similar materials.

Two kinds of the systems are considered – the ones with homogeneous (gas-like) spatial distribution of the particles and, secondly, composites with the simplest heterogeneous internal structures (dimers, consisting of two particles). It is supposed that energy of the internal magnetic anisotropy of the particles is significantly more than the thermal energy of the system. This is typical, for instant, for the magnetite particles with diameter about and more than $17\div18$nm, which can provide significant response of the system on an alternating magnetic field.

Analysis is based on the solution of the Fokker-Planck equation for the distribution function (density of probability) of a given orientation of magnetic moments of the interacting ferroparticles. For the systems with gas-like spatial distribution of the particles, this equation has been solved in the frames of the well-known pair approximation. As a result, simple linear differential equations for the statistically mean (measurable) magnetic moment of the particle have been obtained. Note that these equations differ from the phenomenological Debye equations, very often used for the analysis of the relaxation phenomena.

One of the most important characteristics of the dynamic reaction of the systems on the external field are statistical susceptibility of the composite and time of magnetization relaxation to the alternating field. Our results show that increase of the field amplitude decreases the characteristic time of the Neel remagnetization of the particles.

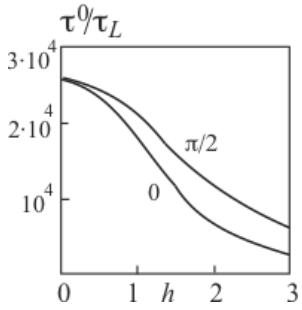

Figure 1. Relaxation time $\tau^0(\alpha)$ of the single particle remagnetization vs. dimensionless magnetic field amplitude h for two angles between the applied field and the particle axis of easy magnetization. τ_L is the Larmor damping time.

If the field amplitude is small ($h < 1$), magnetic interparticle interaction increases time of the particle moment relaxation. For the homogeneous spatial distribution of the magnetite particles with the diameter 17÷18 nm, this increase is about 20÷30%. For the clusters of the particles this increase can achieve 2÷4 orders of magnitude. This means that the clustered particles will be excluded from the dynamic response of the systems on the fields oscillating with the period, comparable with the time of relaxation of the single particle.

In the opposite case of the strong external field, this interaction decreases this relaxation time (about a few tens of per cent for the particles with volume concentration about several per cent). Thus, effect of the interparticle interaction on the rate of the remagnetization is determined by the applied field amplitude.

The equilibrium mean (measured) magnetic moment of the particle increases due to the interparticle interaction both for the clustered and homogeneously distributed particles. Effect of these factors on the intensity of the heat production under the oscillating magnetic field (magnetic hyperthermia) is discussed.

I9

Theory of localized shear-thickness resonances in quartz microbalance sensors

P.V. Yudin[1,2], A. Dejneka[1]

[1]*Institute of Physics of the Academy of Science of the Czech Republic, 18221, Prague, the Czech Republic yudin@fzu.cz*

[2]*Kutateladze institute of thermophysics SB RAS, 630090, Novosibirsk, Russia*

Quartz crystal microbalance (QCM) is widely used in biology, chemistry, and material science to detect small amounts of matter attaching to a surface. The device uses a piezoelectrically excited shear-thickness acoustic wave confined in a quartz plate, whereas a mass attached to the plate surface effectively changes the resonator thickness and therefore shifts its frequency peaks. Current understanding of mass sensitivity of QCM sensors not often goes beyond a one-dimensional model in the direction normal to the quartz plate. However real devices use the principle of acoustic lenses, where the oscillations are confined in a small area with a bell-shaped amplitude profile. Here we focus on the distribution of oscillation amplitude along the lateral coordinates and trace its effect on the resonant frequencies and losses.

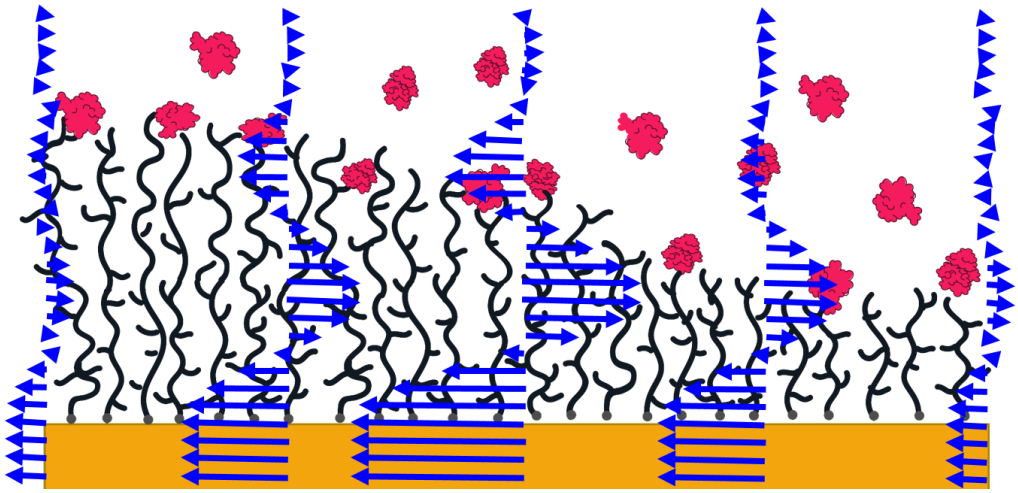

Figure 1. Schematic for a QCM biosensor with distributed properties. Blue arrows show local vibratory displacements. Black is a polymeric brush grown on the surface ofattached to a golden electrode of the resonator. Red particles are the proteins or bacteria to be detected

We start with a simple 2D model to elucidate the effect of vibrational energy trapping, which occurs in a finite number of modes, characterised with their frequencies and amplitude profiles. These are most often enabled by the added mass of electrodes on top of flat quartz crystal plates. Similarly, a point mass locally added on the resonator surface slightly perturbs the amplitude profile and shifts the frequency of the resonance. Analytical expressions are obtained for the frequency shift due to mass loading. These are generalized to a universal expression covering the case of a QCM sensor with distributed parameters, such as a biosensor having a polymeric coating operating in a fluid cell (Fig. 1). Along the existing theories, the presence of a viscous fluid and a viscoelastic polymeric brush is described by an evanescent wave with implications for both the frequency and the dissipation factor.

Further a widespread case of QCM resonators with circular electrodes is analytically described. The resonance modes form a three-dimensional array with wave-numbers $\alpha(n,m,l)$, where n, 2m, and l are the numbers of nodes of the corresponding oscillation amplitude profile along the three cylindrical coordinates. The frequencies of the resonances are found and compared to the results of experimental tests. The analysis shows that the approximation of in-plane elastic isotropy, used in the model is sufficient to describe the ground modes, usually used for the mass detection. A perturbation theory is developed to accurately describe higher-order oscillatory modes and their eigen-frequencies.

I10

Scanning probe microscopy and spectroscopy for investigations of structures and properties of nanostructures

V.A. Bykov, An.V. Bykov, A.A. Bykov, Yu.A. Bobrov, V.V. Kotov, S.I. Leesment, V.V. Polyakov, S.V. Timofeev

NT-MDT Company, Moscow, Russia

Scanning probe microscopy emerged in the early 1980s. Today SPM include a number of different methods named modes – different topographies, magnetic contrasts, conductivities registrations, Kelvin modes – registrations of surface electric potential, distributions of electric capacity between cantilever and surface structures, hardness distributions, distributions of adhesin interactions, piezoelectric properties registrations and not only. It is possible induce of modification of surface structures to create of single active elements. In a combination with spectroscopies methods and laser technic it is possible greatly increase of investigations power of systems.

Significant development of the SPM market began after the invention of scanning with a cantilever vibrating at a resonant frequency - the "tapping" mode. In recent years, adaptive logic systems have been developed that make it possible to create devices with elements of artificial intelligence, which significantly reduces the requirements for the level of the device user. Already at present, the functions of the devices have been introduced with the ability to quickly, automatically select scanning parameters in the "Tapping" mode, which makes our company's atomic force microscopes accessible to technologists, materials scientists and even schoolchildren, makes it possible to obtain a high-quality image of the surface topography.

Modern models of our NT-MDT AFMs allow fully automatic adjustment of scanning parameters in a semi-contact AFM (ScanTronic module): cantilever oscillation amplitude, value of the operating oscillation amplitude, feedback gain, scanning speed.

To study fragments of integrated circuits, a powerful system has been created - a scanning probe microscope VEGA, which allows you to work with objects with an area of 200×200 mm^2 and at the same time obtain atomic resolution, efficiently and repeatedly study fragments of an integrated circuit in various parts of the plate.

Figure 1. Scanning probe microscope VEGA – for complex investigations of samples with the size up to 200x200 mm^2 with return to the testing points with accuracy up to 1 micrometer.

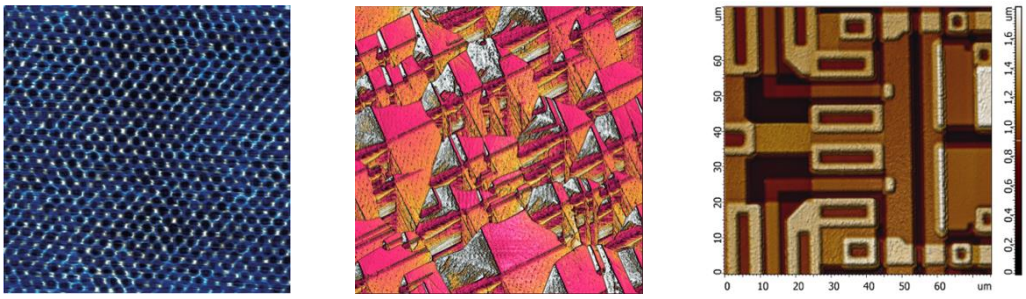

Figure 2. SPM VEGA scanning results: atomic resolutions at HOPG 6×6 nm^2 (left), “BLACK” Si, 30×30 μm^2 and integral scheme fragment in ScanTronicsTM mode with automatic parameter scan in Tapping mode.

It can be confidently stated that by now Russia has developed and organized the production of an almost complete set of instruments and methods for studying micro and nanostructures using scanning probe microscopes, with the exception of ultrahigh vacuum SPMs. For laboratories - devices of the NTEGRA line were created, for the education system in schools and colleges - budgetary, but rather powerful NANOEDUCators and SOLVER-NANO, and for research work - devices briefly described in this article. It should be noted that the development of nanoelectronics, the creation of a new element base make it possible to further improve devices, more and more introduce artificial intelligence systems into software with the disclosure of the capabilities of the developing element base of controllers, the obsolescence of which today is about 5 years.

I11

Current limited domain wall motion during local switching in uniaxial ferroelectrics

A.R. Akhmatkhanov[1], A.P. Turygin[1], V.A. Shikhova[1], M.S. Kosobokov[1], E.V. Shishkina[1], E.V. Pelegova[1], O.N. Sergeeva[2], P.V. Yudin[3,4], V.Ya. Shur[1]

[1]*School of Natural Sciences and Mathematics, Ural Federal University, 620000, Ekaterinburg, Russia andrey.akhmatkhanov@urfu.ru*

[2]*Tver State University,170100, Tver, Russia*

[3]*Physics Institute, Czech Academy of Sciences, 18221, Prague, Czech Republic*

[4]*Kutateladze Institute of Thermophysics, 630090 Novosibirsk, Russia*

The influence of humidity on the domain growth during local switching by a biased tip of a scanning probe microscope (SPM) has attracted considerable attention during recent years. It was demonstrated that the external screening processes related to the existence of adsorbed water surface layer strongly influences the domain wall kinetics during local switching [1,2]. However, the detailed study of this phenomenon is not presented yet.

We have studied the domain wall motion during local polarization reversal under controllable humidity conditions in single crystals of Rb-doped potassium titanyl phosphate $KTiOPO_4$ (Rb:KTP) (C_{2v} symmetry) and deuterated triglycine sulphate $(NH_2CH_2COOH)_3H_2SO_4$ (DTGS) (C_2 symmetry). It should be noted that the threshold fields in these crystals differ by two orders of magnitude. Qualitative change of domain structure evolution during local polarization reversal in a high humidity atmosphere as compared to switching in a dry atmosphere has been revealed.

The field application in DTGS crystals using a biased SPM tip in a dry atmosphere resulted in formation of partially switched area, strongly elongated in ***c*** crystallographic direction. At the same time, switching at high humidity led to a circular shape of the area [3]. The effect was attributed to the change in the governing screening mechanism from anisotropic bulk conductivity to isotropic surface conductivity through an adsorbed water layer [3].

The increase of humidity during local switching in Rb:KTP resulted in the change of the isolated domain shape from regular hexagonal to elongated hexagonal. The domain length/width ratio in this case increases with pulse duration and reaches 3.5 for 10 s duration and decreases to unit for longer pulse durations [4]. The effect was explained by the difference of velocities of "slow" walls oriented in [010] crystallographic direction and "fast" walls oriented in [110] direction [4]. The domain elongation is realized by the motion of fast walls, and the domain widening - by the motion of slow walls. We have shown that the motion of fast wall is limited by the external screening current through the adsorbed water layer, while the motion of slow wall is limited by its mobility.

The research was made possible by the Russian Foundation for Basic Research (project no. 21-72-10160). The equipment of the Ural Center for Shared Use "Modern nanotechnology" Ural Federal University (Reg.№ 2968) which is supported by the Ministry of Science and Higher Education RF (Project № 075-15-2021-677) was used.

1. C. Blaser, P. Paruch, *New J. Phys.* **17**, 013002 (2015).
2. A. Brugère, S. Gidon, B. Gautier, *J. Appl. Phys.* **110**, 052016 (2011).
3. A.P. Turygin, V.A. Shikhova, M.S. Kosobokov, et al., *ACS Appl. Electron. Mater.* **4**, 5215 (2022).
4. E.V. Shishkina, E.V. Pelegova, M.S. Kosobokov, et al., *ACS Appl. Electron. Mater.* **3**, 260 (2021).

I12

Room-temperature optical and magnetoelectric response in A and B site co-doped layer structured Aurivillius ceramics

M.S. Alkathy[1], F.L. Zabotto[1], M.H. Lente[2], E.B. Araujo[3], I.A. dos Santos[4], J.A. Eiras[1]

[1]*Physics Department, Federal University of São Carlos, 13565-905, São Carlos/SP, Brazil*
eiras@df.ufscar.br

[2]*Inst. de Ciência e Tecnologia, Universidade Federal de São Paulo,12231-280, São José dos Campos/SP, Brazil*

[3]*Depto. Física, Universidade Estadual de São Paulo, 15385-000, Ilha Solteira /SP, Brazil*

[4]*Depto. Física, Universidade Estadual de Maringá, 87020-900, Maringá/ PR, Brazil*

The mutual control of the (anti)ferromagnetic and ferroelectric orders by electric and magnetic fields, respectively, based fundamentally on the magnetoelectric (ME) coupling, is essential for the fabrication of new multifunctional devices. In a broad context, for example, it refers to the possibilities of creating non-volatile memories with magnetic reading and electrical writing operations, among countless other potential applications. The existence and nature of the magnetoelectric coupling at room temperature in solid solutions is still debated and is not well established experimentally. Despite the high technological interest generated by magnetoelectric (ME) multiferroic materials, there are few single-phase materials that exhibit magnetoelectric coupling at room temperature. Typical approaches to induce multiferroic state in ferroelectrics, as well as to tune other physical properties (dielectric, piezoelectric, optical, magnetic, …), is to use specific processing procedures and/or specific dopants.

In this work single phase layer structured Aurivillius bulk ceramics (bismuth titanate-BIT based ceramics), with A and B site co-doped ($Bi_{3.25}A_{0.75}Ti_{3-x}(Co, Fe)_{x/2}O_{12}$, where A=La, Nd or Sm x = 0, 0.1, 0.2, 0.3, 0.4), were prepared through the conventional oxide mixture process. The influence of the iso- and heterovalent doping in the structural, dielectric, ferroelectric, magnetic and optical absorption have been investigated. The experimental results, that show changes in the band gap (red shift) and in the room temperature multiferroic state, are discussed correlating with changes in the electronic structure, octahedral tilting angles, bond lengths, octahedral distortions, and oxygen vacancies formation, still maintaining a ferroelectric spontaneous polarization.

Acknowledgments:

The authors gratefully acknowledge the Brazilian funding agencies CNPq and FAPESP.

I13

Novel multiferroics for Magneto Electric – Spin Orbit - like devices

Z.V. Gareeva[1,2], N.V. Shulga[1], K.A. Zvezdin[2,3], A.K. Zvezdin[2,3]

[1]*Institute of Molecule and Crystal Physics, Subdivision of the Ufa Federal Research Centre of the Russian Academy of Sciences, 450075, Ufa, Russia*

[2]*"New Spintronic Technologies" LLC, Skolkovo, 121205, Moscow, Russia*

[3]*Prokhorov General Physics Institute of the Russian Academy of Sciences, 119991, Moscow, Russia*

zukhragzv@yandex.ru, k.zvezdin@nst.tech

The development of new computing technologies and energy - consuming devices requires the implementation of high-tech multiferroic materials. The use of multiferroics allows the realization of competitive energy efficient scalable logic and storage devices as an alternative to traditional CMOS technology. The low power consumption in Magneto Electric – Spin Orbit (MESO) logics [1] and MRAM components is provided by magnetoelectric switching in multiferroic-based systems by a low-energy electric field. A significant decrease in the dissipation energy of the order of 1–100 μJ/cm2, demonstrated recently in BiFeO3 – heterostructures, indicates their potential advantage and the need to search for multiferroic materials with strong magnetoelectric effect and high ferroelectric and magnetic response.

Our work concerns the modelling of the magnetoelectric (ME) - spin orbit (SO) logics with a focus on the ME component responsible for low power consumption. We consider the principle of operations of MESO-based logic devices; discuss the physical mechanisms, responsible for converting charge into spin in ME input and spin to charge in SO output; and simulate magnetization reversal processes in ME component of MESO.

To address this, we develop a model of magnetization switching in ME heterostructures, which leverage multiferroics (MF) to control magnetic states in a ferromagnetic (FM) layer via electric field. As an example, we take well - studied multilayers, combining such FMs as metals (Co, CoFe, Ni and permalloy), half metals (e.g. Fe_3O_4) and insulators (iron garnets, $BaTiO_3$,) coupled with MFs ($BiFeO_3$, Cr_2O_3, Ruddlesden – Popper structures) [2]. Representing the system in a form FM(1)-FM(2)-MF with a top layer of a soft ferromagnet FM(1) and a bottom layer of multiferroics (MF) separated by a pinning layer FM(2), we explore the magnetic states in the top FM (1) at different ME states in MF [3]. The ME states in a perovskite – like MFs (e.g. $BiFeO_3$) are determined by the pairwise perpendicular vectors ***P, L, M***, where ***P*** is an electric polarization, ***L*** is an antiferromagnetic vector, ***M*** is a weak ferromagnetic vector. Exchange coupling between antiferromagnetic MF and FM leads to emergence of the unidirectional anisotropy in a pinning layer FM(2), which affects the magnetization states in the top FM(1). Unidirectional anisotropy axis (UAA) is associated with vector ***L*** coupled with spontaneous polarization ***P***. Reorientation of polarization ***P*** induced by electric field or strains affect orientation of UAA and as a consequence magnetic states in the top FM layer.

The ability to incorporate a number of factors (such as the geometry and dimensions of the system, the presence of several phases, interfacial interactions and energy-efficient external influences) makes developed approach promising for studying ME heterostructures and their compatibility with spin-orbit switching schemes. Hybrid magnetoelectric – spin orbit (MESO – like) systems play an important role in pursuit of low - energy consuming devices and expected to provide ultra-fast dynamics and ultra-low power consumption.

Z.V. Gareeva, N.V. Shulga acknowledge the support by the Russian Science Foundation No. 23-22-00225, K.A. Zvezdin, A.K. Zvezdin acknowledge the support by the Ministry of Science and Higher Education of the Russian Federation, Agreement № 075-11-2022-046.

1. S. Manipatruni, et al., *Nature* **565**, 35 (2019).
2. E. Gradauskaite, P. Meisenheimer, M. Müller, J. Heron, M. Trassin, *Phys. Sci. Rev*. **6**, 20190072 (2020).
3. M.D. Davydova, K.A.Zvezdin, A.A. Mukhin, A.K. Zvezdin, *Phys. Sci. Rev*. **5**, (2020).

I14

Phase transitions in multiferroics ferroborates with huntite structure

A.S. Krylov

Kirensky Institute of Physics FRC KSC SB RAS, 660036, Krasnoyarsk, Russia
shusy@iph.krasn.ru

The ferroborates with the huntite structure with the general formula of $LnMe_3(BO_3)_4$ (Ln = rare-earth cation, Me = Fe, Ga) are the objects of many studies due to the wide range of promising physical properties. They are multiferroic, combining the mutual influence of magnetic and electrical subsystems, where transition points may be varied by substituting as rare earth element as a magnetic ion [1]. We present the Raman spectroscopy result of the investigation of single crystals and a solid solution.

Temperature measurements were performed in the temperature range 10÷400 K. This study aims to investigate the possible existence of a soft mode related to structural order parameter and effects of magnetic transitions on Raman spectra. Analysis of the experimental Raman spectra, temperature dependences of the provisions of the centers of lines, their width and relative intensity was carried out, as well as theoretical temperature approximation for some lines. Some anomalies in the temperature dependences of the spectral lines associated with the occurrence of magnetic order. It was found that significant changes are observed in the spectrum of low-frequency range (below 100 cm^{-1}) - there is a mode corresponding to two-magnon scattering. The structural phase transition accompanied condensation of soft mode [2].

The phase diagram Temperature – Composition (Fig. 1) has been acquired for several systems. Structural transitions manifest clearly by soft mode restoration, and abnormal changes of line position indicate a temperature of magnetic ordering [3].

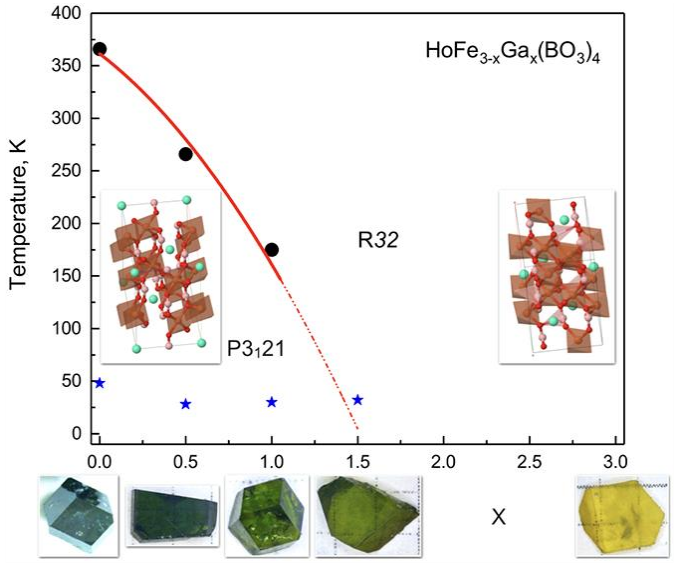

Figure 1. Phase diagram of Composition−Temperature of the $HoFe_{3-x}Ga_x(BO_3)_4$ crystals. (●) The points of structural phase transitions. (★) The points of magnetic phase transitions.

The phase diagram Pressure-Temperature has been acquired for several systems. Stability of R32 phase is increase with increasing temperature and pressure. There are no new phases found during investigations.

RFBR funded the reported study according to the research project № 21-52-12018.

1. A.S. Krylov et al. *Solid State Commun.* **174**, 26 (2013).
2. E. Moshkina et al. *Cryst. Growth. Des.* **16**, 6915 (2016).
3. E. Moshkina et al. *Cryst. Growth. Des.* **20**, 1058 (2020).

I15

Multiferroic ordering and cross coupling effects in 2D magnetic materials

A.P. Pyatakov, A.S. Kaminskiy, N.V. Myasnikov

M.V. Lomonosov Moscow State University, 119991, Moscow, Russia
pyatakov@physics.msu.ru

The advent of 2D magnets [1], and 2D multiferroics [2] in particular, provides a new prospective for study of cross-coupling effects between magnetic, ferroelectric and mechanical subsystems of crystals. Due to their geometry the 2D materials are naturally prone to bending deformation [3] as well as electric field application without screening effects [2].

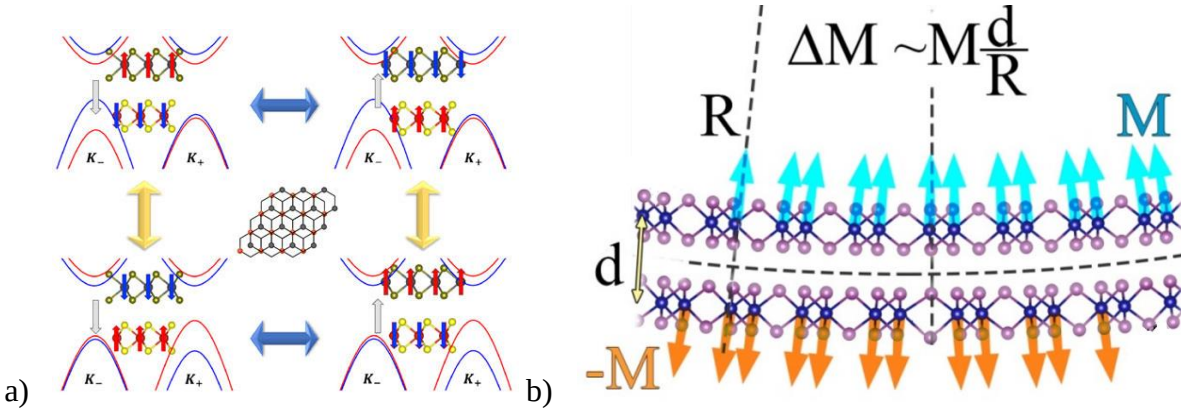

Figure 1. (a) the ferrovalley-mediated multiferroic ordering in VS_2 bilayer (the gray arrows are electric polarization, the red and the blue arrows are Vanadium spins, $\boldsymbol{K}^{\pm}$ are critical points in Brillouin zone corresponding to two valleys) [4], (b) the strain-induced magnetization ΔM in CrI_3 bilayer (***M*** is one-layer magnetization, ***R*** is curvature radius, ***d*** is the interlayer distance).

The graphene-like materials have another electron degree of freedom, the valley one. In VS_2 bilayer the valley polarization plays the role of the mediator between the electric polarization and the antiferromagnetic ordering (Fig. 1a) providing the new type of magnetoelectric coupling in crystals [4].

The coupling between mechanical and ferroelectric subsystems in 2D materials manifest itself in flexoelectric effect since the strain gradient induces polar direction in crystal. The nontrivial consequence of bending can be flexomagnetism, i.e. the appearance of decompensated magnetization in antiferromagnetically coupled bilayers (Fig. 1b).

The enhanced magnetoelectric and flexomagnetic effects in 2D magnetic materials are not only of fundamental interest, but also of practical importance for spintronics and straintronics.

The support of Theoretical Physics and Mathematics Advancement Foundation “BASIS” (The Junior Leader Program) is acknowledged.

1. B. Huang, G. Clark, E. Navarro-Moratalla et al, *Nature* **546**, 270 (2017).
2. Sh. Liang et al, *Nature Electronics* **6**, 199 (2023)
3. A. Edström, D. Amoroso, S. Picozzi et al, *Phys. Rev. Lett.* **128**, 177202 (2022).
4. X. Liu, A.P. Pyatakov, W. Ren, *Phys. Rev. Lett.* **125**, 247601 (2020).

I16

Investigations of high-conductivity interfaces of heterostructures ferroelectric/dielectric

R.F. Mamin

Zavoisky Physical-Technical Institute, FRC Kazan Scientific Center of RAS, 420029, Kazan, Russia
mamin@kfti.knc.ru

Unique properties of functional materials are achieved due to the effects associated with the complex composition of the interface structure. The creation of quasi-two-dimensional electron gas at the interface and the ability to control such states by magnetic and electric fields is impossible without the use of new design interfaces. A high-mobility electron gas is observed at the interface of heterostructure $LaAlO_3$ and $SrTiO_3$ when the number of $LaAlO_3$ layers is larger than three [1, 2]. Such a system undergoes a transition to a superconducting state at temperature 300 mK [2]. We have studied heterostructures based on ferroelectric and dielectric oxides with the $BaTiO_3/LaMnO_3$ and $BaTiO_3/La_2CuO_4$ type structures, and, using calculations from the first observations, we have modeled the electronic and magnetic properties of this heterostructure. It was found that, as a result of the destruction of the $BaTiO_3/LaMnO_3$ and $BaTiO_3/La_2CuO_4$ heterostructures, the band gap in the region of disappearance is forbidden, and the system is established in a state with metallic conductivity at the interface. In this work, we investigated the properties of the interface between ferroelectric oxide and insulating oxide in heterostructures $BaTiO_3/LaMnO_3$ on $LaMnO_3$ single crystal and in heterostructures $Ba_{0.8}Sr_{0.2}TiO_3/LaMnO_3/Ba_{0.8}Sr_{0.2}TiO_3$ and $LaMnO_3/Bi_4Ti_3O_{12}/Ba_{0,4}Sr_{0,6}TiO_3$ on MgO substrate and the effect of illumination on the properties of this heterostructures.

Previously the numerical simulations of the structural and electronic characteristics of the $BaTiO_3/LaMnO_3$ interface have been performed. The conductivity and photoconductivity properties had been studied for these heterostructures. For both of heterostructures it was found experimentally that in the samples with polarization of ferroelectric film directed perpendicular to the surface, below certain temperature the electrical resistance exhibits metallic-like behavior. Thus, the evidence of a transition to the state with 2DEG at the interface is demonstrated. The effect of a light on $Ba_{0.8}Sr_{0.2}TiO_3/LaMnO_3$and on $LaMnO_3/Bi_4Ti_3O_{12}$ interface had been investigated. The resistivity properties of the interface $Ba_{0.8}Sr_{0.2}TiO_3/LaMnO_3$ and $LaMnO_3/Bi_4Ti_3O_{12}$ interfaces greatly change under uniform illumination incident on the surface of the ferroelectric film, exhibiting negative photoconductive properties. The effect of metallic conductivity is explained by the discontinuity of ferroelectric polarization. Negative photoconductive can be associated with partial screening of the ferroelectric polarization by photogenerated charge carriers causes the reduction of the carrier concentration at the interface. Measurements in the Kelvin mode of atomic force microscopy showed that illumination has a similar effect on the surface charge concentration, which confirms our hypothesis.

The reported study was funded by Russian Scientific Foundation, research project No. 21-12-00179.

1. A. Ohtomo, H. Ywang, *Nature* **427**, 6973 (2004).
2. N. Reyren, S. Thiel, A. D. Caviglia, et al., *Science* **317**, 1196 (2007).

I17

Low-temperature phase transitions in ANLT4.5 ceramics

A. N. Vtyurin[1,2], A. S. Krylov[1], S. N. Krylova[1], E. M. Roginskii[3], J. Li[4], Y. Tian[4], X. Wei[4]

[1]*Kirensky Institute of Physics SB RAS, 660036, Krasnoyarsk, Russia*
vtyurin@iph. krasn.ru
[2]*Siberian Federal University, 660041, Krasnoyarsk, Russia*
[3]*Ioffe Physical-Technical Institute RAS, 194021, St. Petersburg, Russia*
[4]*Intl. Center for Dielectric Research, Xi'an Jiaotong University, 710049, Xi'an, China*

Silver niobate and lithium tantalate are functional materials belonging to the perovskite family. In particular, $AgNbO_3$ was shown earlier [1,2] to be promising as an active medium in energy storage systems, however, the disadvantage of this material is its instability in stronger electric fields. It was shown in [3,4] that tantalum and lithium additives stabilize this material and increase its energetic capacity.

Several authors have observed up to six phase transitions in single crystals, polycrystals, and ceramics of silver niobate, but most of them were found at higher temperatures. More interesting for practical applications, the region near and below room temperatures has been little studied.

In mixed compositions at room temperature, the most promising for practical applications wide hysteresis loop with full saturation was found in ceramics $0.955\ AgNbO_3–0.045\ LiTaO_3$ [5], and, therefore, this composition was studied in this work.

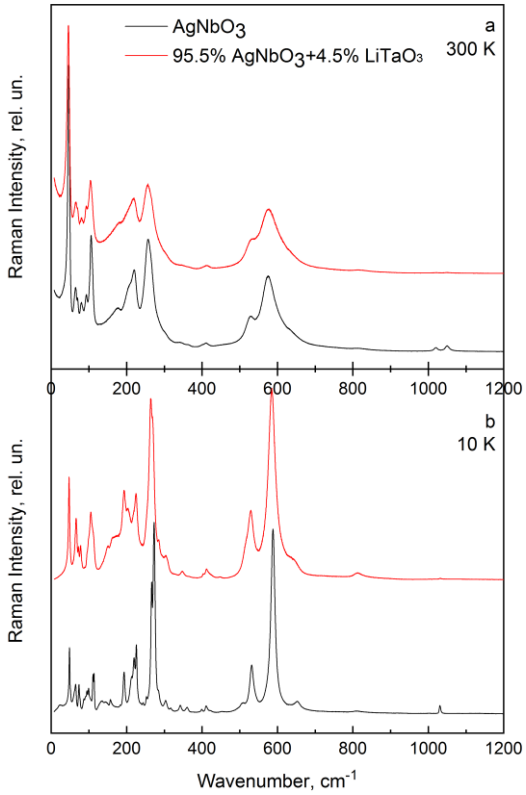

Raman spectra of $AgNbO_3$ (black) and $0.955\ AgNbO_3–0.045\ LiTaO_3$ (red) ceramics: a –300 K, b – 10 K.

In this work, the Raman scattering method was used to study ceramics In this work, the Raman scattering method was used to study $0.955\ AgNbO_3–0.045\ LiTaO_3$ and $AgNbO_3$ ceramics in the temperature range 10÷415 K. For their interpretation, DFT simulation of the lattice dynamics was performed using the PBE (GGA), PBEsol (GGA) functionals. In $AgNbO_3$ ceramics in the region of 320–350 K, a soft mode was observed, apparently related to the known ferroelectric phase transition *Pbcm* – *Pmc*2$_1$. A similar anomaly is also observed in $0.955\ AgNbO_3–0.045\ LiTaO_3$ ceramics 30 K below (T_c = 310 K).

In the region of 50–120 K, the spectrum of $AgNbO_3$ shows the appearance of new lines in the region of low (130–150, 160 cm^{-1}, Ag and O vibrations) and medium (515 cm^{-1}, O vibrations) frequencies. Presumably, this is due to another phase transition in the region of 120 K.

Partial substitution of Nb for Ta leads to the disappearance of the 22 cm^{-1} line in the spectrum of $0.955\ AgNbO_3–0.045\ LiTaO_3$; this vibration corresponds to movements of Nb/Ta ions in the layer. As the temperature decreases, this composition also exhibits a phase transition in the region (120÷150 K).

1. Y. Tian, L. Jin, H. Zhang, et al., *J. Mater. Chem. A* **4**, 17279 (2016).
2. Y. Tian, P. Song, G. Viola, et al., *J. Mater. Chem. A* **10**, 14747 (2022).
3. A. Niewiadomski, A. Kania, G. E. Kugel, et al., *Mater. Res. Bull.* **65**, 123 (2015).
4. S. Li, H. Nie, G. Wang, et al., *J. Mater. Chem. C* **7**, 4403 (2019).
5. T. Lu, Y. Tian, A. Studer, et al., *IUCrJ* **6**, 740 (2019).

I18

Hafnium oxide films for the implementation of ferroelectric field effect transistors and ferroelectric tunnel junctions

A.A. Chouprik, V.V. Mikheev, I.G. Margolin

Moscow Institute of Physics and Technology, 141700, Dolgoprudny, Russia
chouprik.aa@mipt.ru

Doped (or alloyed) HfO_2-based thin polycrystalline ferroelectric films have emerged as viable candidates for nonvolatile ferroelectric memories [1] because of their full compatibility with modern silicon microelectronics technology. Many efforts have been focused on the development of three known types of ferroelectric memories based on HfO_2: ferroelectric random-access memory (FeRAM), ferroelectric field-effect transistors (FeFETs) and ferroelectric tunnel junctions (FTJ). While the performances of HfO_2-based FeRAM are excellent (except for their retention issues), the benefit of using of this material in FeFET and FTJ is not yet obvious due to poor performances [2]. This is caused by the specific properties of hafnium oxide films. This talk will discuss the advantages and disadvantages of this material (compared to perovskite ferroelectrics) for FeFET and FTJ memory implementations, and will also make a general comparison using hafnium for FeRAM.

A common feature of FeFET and FTJ is the origin of the informative signal — the readout signal (the current flowing during the read procedure either through a semiconductor inversion channel or across an ultrathin ferroelectric layer) is determined by the average value of the surface charge of spontaneous polarization. On the one hand, this feature of both memory concepts provides a non-destructive readout procedure, which can potentially improve the memory endurance. On the other hand, it induces a number of implementation challenges compared to FeRAM. For example, this is the cause of faster retention loss. Indeed, in all HfO_2-based ferroelectric memory devices the retention loss originates from the imprint effect, which consists in the emergence of a built-in field that increases logarithmically with time [3]. In FeFET and FTJ, it causes a proportional decrease in the informative current signal, whereas in FeRAM it causes another temporal dependence of the polarization loss, which can be much slower than the logarithmic one. Other challenges are related to the polymorphic structural phase composition of the hafnia film, the domain structure and its transformation, charging interface traps and surface states as well as with the dielectric interlayer. All these parasitic issues play a more crucial role than in FeRAM. To overcome these challenges, the material and interface engineering of functional structures is currently underway, and there are already a number of promising results that will be overviewed in the talk.

Implementation of HfO_2-based FTJ memory is more challenging than FeFET. Additional parasitic factors contribute significantly to the performance of FTJs and ferroelectric memristors. Among these are the minimal critical thickness of film (4 nm) [5], leakage current along the grain boundaries and through the grains of the paraelectric phase [6] and the mobile charge migrating across the ferroelectric film [7]. In this talk, technological approaches to minimize these effects and scientific methods for their differentiation will be described and discussed.

The work was financially supported by the Ministry of Science and Higher Education of the Russian Federation (agreement No. 075-03-2023-106, project No. FSMG-2022-0031.

1. T.S. Böscke, J. Müller, D. Brauhaus, et al., *Appl. Phys. Lett.* **99**, 102903 (2011).
2. A. Chouprik, D. Negrov, Y. Tsymbal, A. Zenkevich, Nanoscale **13**, 11635 (2021).
3. A.K. Tagantsev, I. Stolichnov, N. Setter, J.S. Cross, *J. Appl. Phys*. **96**, 6616 (2004).
4. V. Mikheev, E. Kondratyuk, A. Chouprik, *Phys. Rev. Applied* **18**, 064084 (2022).
5. V. Mikheev, A. Chouprik, Yu. Lebedinskii, et al., *Nanotechnology* **31**, 215205 (2020).
6. A. Chouprik, A. Chernikova, A.M. Markeev, et al., *Microelectron. Eng.* **178**, 250 (2017).
7. V. Mikheev, A. Chouprik, Yu. Lebedinskii, et al., *ACS Appl. Mater. Interfaces* **11**, 32108 (2019).

I19

Ultrahigh electrostrictive effect in Sm^{3+}-doped $Pb(Mg_{1/3}Nb_{2/3})O_3$-$PbTiO_3$ ferroelectrics ceramics

Yunyao Huang, Li Jin

Electronic Materials Research Laboratory, Key Laboratory of the Ministry of Education, School of Electronic Science and Engineering, Xi'an Jiaotong University, Xi'an 710049, China
ljin@mail.xjtu.edu.cn

Rare-earth Sm^{3+}-doped $Pb(Mg_{1/3}Nb_{2/3})O_3$-0.25$PbTiO_3$ (PMN-0.25PT) ferroelectric ceramics with doping amount between 0–3% were developed via a conventional solid-state method. The doping effect of Sm^{3+} ions on the PMN-0.25PT matrix was systematically investigated on the basis of the phase structure, temperature-dependent dielectric, ferroelectric and electrotechnical properties. Due to the disruption of long-range ferroelectric order, the addition of Sm^{3+} ions effectively lowers the T_m (temperature corresponding to maximum permittivity) of the samples, leading to enhanced relaxor ferroelectric (RFE) characteristic and superior electric field-induced strain (electrostrain) properties at room temperature. Intriguingly, a considerable large-signal equivalent piezoelectric coefficient d_{33}^* of 2376 pm/V and a very small hysteresis were attained in the PMN-0.25PT component doped with 2.5 mol.% Sm^{3+}. The findings of piezoelectric force microscopy indicate that the addition of Sm^{3+} increases the local structural heterogeneity of the PMN-0.25PT matrix, and that the enhanced electromechanical performance is due to the dynamic behavior of polar nanoregions. Importantly, strong temperature-dependent electrostrain and electrostrictive coefficient Q_{33} are observed in the critical region around T_m in all Sm^{3+}-modified PMN-0.25PT ceramic samples studied. This work elucidates the phase transition behavior of Sm^{3+}-doped PMN-0.25PT and reveals a critical region where electrostrictive properties can be greatly improved due to a strong temperature-dependent characteristic.

I20

Characterization of structure, microstructure and functional properties of modified lead-free perovskite ceramics

E.D. Politova[1], G.M. Kaleva[1], S.A. Ivanov[2], A.V. Mosunov[2], S.Yu. Stefanovich[2], N.V. Sadovskaya[3], D.A. Kiselev[4], T.S. Ilina[4], V.Y. Shur[5], A.D. Ushakov[5], M.Z. Faizullin[6]

[1]*N.N. Semenov Federal Research Center for Chemical Physics RAS, 119991, Moscow, Russia*
politova@nifhi.ru

[2]*Lomonosov Moscow State University, 119991, Moscow, Russia*
[3]*SRC «Crystallography and Photonics» RAS, 119333, Moscow, Russia*
[4]*National University of Science and Technology "MISiS", 119049, Moscow, Russia*
[5]*School of Natural Sciences and Mathematics, Ural Federal University 620000, Ekaterinburg, Russia*
[6]*Institute of Thermal Physics, Ural Branch RAS, 620016, Ekaterinburg, Russia*

Lead-free perovskite oxides promising for development of materials for various applications based on perovskites $(K_{0.5}Na_{0.5})NbO_3$ (KNN), $BaTiO_3$ (BT), $BaZrO_3$ (BZ), $NaNbO_3$ (NN), $(K_{0.5}Bi_{0.5})TiO_3$ (KBT) and $(Na_{0.5}Bi_{0.5})TiO_3$ (NBT) were intensively studied last years in order to replace the widely used Pb-based ones.

We studied influence of cation substitutions and preparation conditions on phase content, structure, microstructure, dielectric, ferroelectric, and local piezoelectric properties of compositions from Morphotropic Phase Boundaries (MPB) in the KNN, NBT and NN oxides modified by BT, KBT and BZ up to 10 mol %.

Ceramic samples were prepared by the two-step solid-state reaction method at temperatures up to 1450 K and characterized using X-ray Diffraction (XRD), Scanning Electron Microscopy (SEM), Second Harmonic Generation (SHG), Dielectric Spectroscopy (DS) and Piezoresponse Force Microscopy (PFM) methods. Polarization switching current and dielectric hysteresis loops were also measured.

The unit cell volume changes and crystallite size distributions were observed by the XRD method in ceramics prepared. In NBT-BT samples modified by KBT increase of the volume-weighted crystallite size distribution function was observed with KBT additive increasing indicating to changes in relative content of polar nanoregions in tetragonal nonpolar matrix.

Ferroelectric phase transitions at ~ 400 – 700 K were confirmed by polarization measurements and using the DS and SHG methods. Decrease in temperatures of phase transitions was observed in the NBT, NN, and KNN-based samples with amounts of additives increasing. In NBT-based ceramics additional effects of dielectric relaxation were observed at temperatures > 800K caused by formation of oxygen vacancies in compositions with aliovalent substitutions.

The observed increase in polarization and energy storage performance confirmed positive influence of BZ dopants on functional properties of the NN- and KNN-based ceramics.

Using the PFM method increase in effective d_{33} piezoelectric coefficient in some ceramics studied correlated with increase in dielectric permittivity and spontaneous polarization values at the room temperature was observed thus confirming improvement of functional properties and prospects of new lead-free piezoelectric and electrocaloric materials development on the base of modified KNN, NN and NBT-based compositions.

The work was supported by the Russian Foundation for Basic Research (grant 21-53-12005) and by the Ministry of Higher Education and Science of the Russian Federation in the framework of State assignments "Nanostructured systems of a new generation and unique functional properties" (registration number 122040500071-0)**,** and within the state assignment FSRC "Crystallography and Photonics" RAS.

PFM studies were performed at Center for Shared Use "Material Science and Metallurgy" at the National University of Science and Technology "MISiS" and were supported by the Ministry of Science and Higher Education of the Russian Federation (Project No. 075-15-2021-696).

The equipment of the Ural Center for Shared Use "Modern nanotechnology" Ural Federal University (registration number 2968) was used funded by the Ministry of Science and Higher Education of the Russian Federation (grant 075-15-2021-677).

I21

Evolution of the dipole moment in crystals and films of strontium barium niobate

A.M. Pugachev, A.A. Sokolov

Institute of authomation and electrometry RAS, 630090, Novosibirsk, Russia
apg@iae.nsk.su

The subject of research is the polar states in films of strontium barium niobate ($Sr_{1-x}Ba_xNbO_6$ hereinafter referred to as SBN-x). In the low-temperature ferroelectric phase, this is spontaneous polarization, and in the centrosymmetric paraelectric phase, it is electric fields in local polar regions ("polar nanoregions") that appear in the centrosymmetric phase, and upon cooling up to the phase transition, their size and concentration change. The temperature evolution of dipole moments depends on various factors, such as local mechanical stresses, the chemical composition of the film, the type of substrate, the growth method, etc. The nature of the influence of various factors remains unexplored at present and requires additional systematic studies.

Our aim is a study of the nature of dipole moments in thin ferroelectric films as a function of temperature, local mechanical stresses, the chemical composition of the film, substrate, and other factors that are important in the growth and operation of products based on ferroelectric films. In this study, spectroscopic methods are used: optical second harmonic generation (SHG), Raman scattering (RS), IR spectroscopy. These methods are non-contact and non-destructive, but also make it possible to study the properties of thin films that are difficult or impossible to study by "traditional" methods (X-ray diffraction studies, dielectric spectroscopy, pyroelectric effect, etc.).

The SBN films of various thicknesses were obtained by rf sputtering on various substrates with various electrodes.

Special attention is paid to the pyroelectric effect in thin films. Film pyroelectric sensors are sensitive in a wide spectral range, have high sensitivity and can operate without cooling. The authors found an exceptionally high sensitivity of special SBN films. An explanation for the observed phenomenon is proposed with the help of the emergence of moving elements in the system "substrate – bottom electrode – ferroelectric – top electrode" . As an example, the detachment of the upper electrode from the ferroelectric or the detachment of the lower electrode from the substrate under the additional assumption of the presence of local conduction channels in the sample.

The work was supported by the State Assignments of the IA&E SB RAS FWNG-2021-0004 and FWNG-2021-0014. Some of experiments were carried out at the High-Resolution Spectroscopy of Gases and Condensed Matter Center of Multiple Access in the Institute of authomation and electrometry of the Siberian Branch of the Russian Academy of Sciences (Novosibirsk, Russia).

I22

2D Nanocomposite for the photocatalytic degradation of various pollutants: Textile dyes, Heavy metal ions, Antibiotics

M. Khanuja

Centre for Nanoscience and Nanotechnology, Jamia Millia Islamia, New Delhi, 110025

The release of untreated noxious pollutant into the water bodies are causing irreversible damage to the ecosystem. The widespread increase in population leading to unacceptable concentrations of waste pollutants in water poses threats to human and ecosystem. Here, various 2D nanocomposite including WS_2, $MoSe_2$, g-C_3N_4, and their composites with Polyaniline (PANI), Polypyrrole (PPY), and Metal Organic Framework (MOF) has been synthesized via hydrothermal method followed by in situ polymerization. The synthesized nanocomposite was characterized by several techniques such as High-resolution transmission electron microscope (HRTEM), Field emission scanning electron microscope (FESEM) Energy-dispersive X-ray (EDX) spectroscopy, X-ray diffractogram (XRD), Fourier transform infrared (FTIR) spectroscopy, Zeta potential, Tauc's plot, Photoluminescence (PL) spectroscopy, Time-Resolved Photoluminescence **(**TRPL), and BET. The 2D nanocomposite showed excellent photocatalytic activity for the photodegradation of various pollutants such as textile dyes: Anionic (Methyl orange, Congo red, Direct red), Cationic (Methylene blue, Malachite green, Crystal violet); Heavy metal ions (Chromium VI) and Antibiotics (Nitrofurantoin, Tetracycline, Metronidazole). A scavenger experiment was also done to confirm the formation of photoinduced reactive oxygen species (•OH and $O_2^{\bullet-}$). Further, photocatalytic results revealed that all the nanocomposites exhibited significantly enhanced photocatalytic activity with 100% degradation efficiency. The enhanced photocatalytic activity was attributed to the improved separation of photo-induced electron-hole pairs and surface area.

I23

Exotic water structures and diffusion in peptide nanochannels

P. Zelenovskii[1,2], P. Brandão[1], V.S. Bystrov[3], F. Figueiredo[4], L. Mafra[1], A. Kholkin[2,4]

[1]*Department of Chemistry and CICECO−Aveiro Institute of Materials, University of Aveiro, 3810-193 Aveiro, Portugal*

[2]*School of Natural Sciences and Mathematics, Ural Federal University, 620000 Ekaterinburg, Russia*

[3]*Institute of Mathematical Problems of Biology, Keldysh Institute of Applied Mathematics, RAS, 142290 Pushchino, Russia*

[4]*Department of Physics and CICECO−Aveiro Institute of Materials, University of Aveiro, 3810-193 Aveiro, Portugal*

zelenovskiy@urfu.ru

Water confined in nanochannels possesses various unique properties essentially different from those in a macroscopic bulk state. Most studies are focused on water within carbon nanotubes, which are hydrophobic and weakly interact with water molecules. In contrast, nanochannels made of organic species form strong hydrogen bonds with water thus completely determining its behavior and biasing the properties. Therefore, the study of such systems is of great fundamental and practical importance.

In this work, we analyzed the structure and dynamic behavior of water confined in the nanochannels made of different dipeptides, such as dileucine (Leu-Leu, LL), alanine-valine (Ala-Val, AV), and diphenylalanine (Phe-Phe, FF). These dipeptides self-assemble into microporous crystals consisting of nanochannels with the pore size below 1 nm. The molecular structure of the water confined in the channels was determined by X-ray diffraction and confirmed by computer modeling, and its dynamic behavior was analyzed by ^{2}H solid-state nuclear magnetic resonance method (ss-NMR) and the dynamic vapor sorption (DVS) measurements.

Water molecules captured in the nanochannels actively form hydrogen bonds with the ionic functional groups at the peptide shell, which dictates water the spatial organization and the behavior. Depending on the shell configuration and the pore size, the linear chains, single and double spirals of water molecules were observed. The analysis of ^{2}H NMR spectra allowed distinguishing crystallographically inequivalent water molecules in the nanochannels, whereas the determined spin-spin relaxation times indicate the mode of their diffusion. Direct DVS measurements were used to derive the coefficients of self-diffusion for different types of water.

The obtained results demonstrate a great potential for peptide nanotubes usage for the transportation of water and other small molecules in various micro- and nanofluidic devices.

This work was developed within the scope of the project CICECO-Aveiro Institute of Materials, UIDB/50011/2020, UIDP/50011/2020, and LA/P/0006/2020, and the project UniRCell (SAICTPAC/0032/2015, POCI-01-0145-FEEDER-016422) financed by national funds through the FCT/MEC (PIDDAC). NMR spectrometers are part of the National NMR Network (PTNMR) and are partially supported by the Infrastructure Project 022161 (cofinanced by FEDER through COMPETE 2020, POCI and PORL and FCT through PIDDAC). This work has received funding from the European Research Council (ERC) under the European Union's Horizon 2020 research and innovation program (Grant Agreement 865974).

ORAL
PRESENTATIONS

O1

Directional motion of domain walls in iron garnet crystals

S.E. Pamyatnykh, M.S. Lysov, L.A. Pamyatnykh, G.A. Shmatov

Ural Federal University, 620026, Ekaterinburg, Russia
Pamyatnykh.Sergey@urfu.ru

Domain walls (DWs) control (control of the parameters and position of the DWs) is a topical problem both from the point of view of fundamental science and possible technical applications [1]. The motion of the DW system as a whole (DW drift) is related to the motion of topological defects – magnetic dislocations (MDs) [2], which originate in certain nucleation centers – local regions of the sample with reduced values of the material constants. The intensity of the MD nucleation center (I_{MD}) is the number of MDs that originate in this center per second.

The results of study of the drift of stripe domains lattice in the direction perpendicular to the DW plane in iron garnet crystals with different types of magnetic anisotropy in a harmonic magnetic field $H = H_0\sin(2\pi ft)$ (f = 3÷1000 Hz, H_0 up to $2{,}2\cdot10^4$ A/m), which was applied perpendicular to the sample plane, are presented. Dynamic DS was visualized using the magnetooptic Faraday effect and recorded with a high-speed digital camera (frame rate up to 2000 fps) using a stroboscopic installation based on a pulsed laser with a wavelength of 532 nm and a pulse duration of 10 ns.

A change of the direction of the DW drift in $(TbErGd)_3(FeAl)_5O_{12}$ iron garnet (110) plate with anisotropy of shape with an increase of the amplitude of alternating harmonic magnetic field has been experimentally established. The DW drift velocities (Fig.1a) and intensities of MD nucleation centers (curves 1, 2 and 3 in Fig. 1b) were measured. The change of direction of DWs drift (Fig. 1a) is related to the sharp increase of the intensity of the MD nucleation center E (Fig. 1b). At the external magnetic field frequency f = 100 Hz the drift velocity changes sign with increase of the field amplitude at $H_0 = 10{,}35\cdot10^3$ A/m, while the intensity of the center E increases sharply from 0 to 400 MD/s.

It is proposed that the reason for the change of the direction of the DW drift is a change of the direction of the gradient of demagnetizing fields in the sample with an increase of the external field amplitude. The change in the configuration of the internal magnetic field is indicated by an experimentally established change in the activity of the centers of MD nucleation with an increase of the amplitude of the external field. A model is proposed in which the direction and velocity of the DW drift are determined by the gradient of the magnetic field in the sample [3].

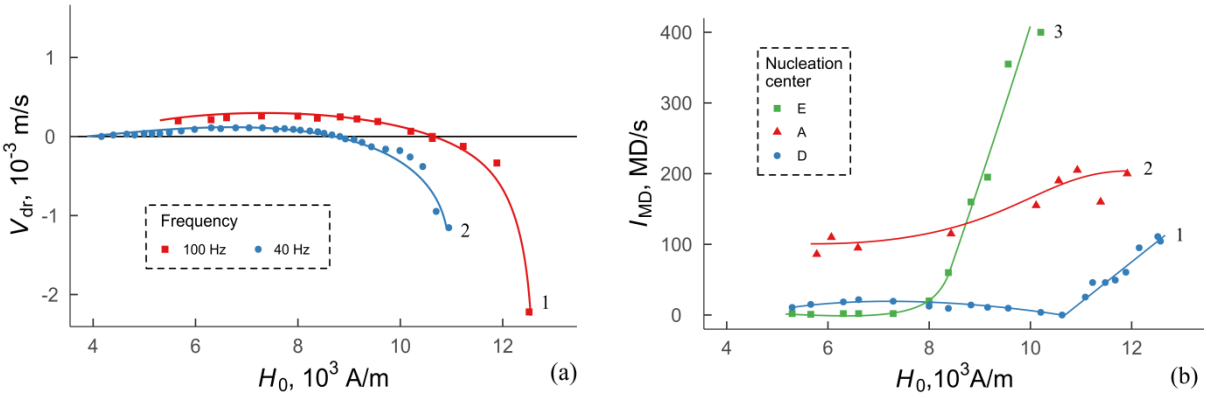

Figure 1. (a) Dependences of DW drift velocity V_{dr} on harmonic magnetic field amplitude. Curves 1 and 2 are DW drift velocities at f = 100 Hz and f = 40 Hz. (b) Dependences of intensity of MD nucleation centers E, A, D on harmonic magnetic field amplitude at frequency f = 100 Hz.

This work was performed within the framework of the state assignment of the Ministry of Science and Higher Education of the Russian Federation (Project FEUZ 2023-0020).

1. D. Kumar, T. Jin, R. Sbiaa et al., *Phys. Rep.* **958**, 1 (2022).
2. L.A. Pamyatnykh, B.N. Filippov, L.Y. Agafonov and M.S. Lysov, *Sci. Rep.* **7**, 18084 (2017).
3. L. Pamyatnykh, M. Lysov, S. Pamyatnykh and G. Shmatov, *JMMM* **542**, 168561 (2022).

O2

Structural and ferroelectric properties of hafnia in presence of an electric field: first-principle and experimental insight

I.G. Margolin, E.V. Korostylev, E.B. Kalika, D.V. Negrov, A.A. Chouprik

Moscow Institute of Physics and Technology (Research Institute), 141700, Dolgoprudny, Russia
margolin.ig@phystech.edu

Because of its compatibility with semiconductor-based technologies, HfO_2 is today's most promising ferroelectric (FE) material for applications in memory devices. Nevertheless, understanding of the ferroic and electromechanical properties of this all-important compound is still lacking [1]. Even the origin of ferroelectricity in HfO_2 thin films remains debated [2-5].

One of the white spots in the knowledge about this material is the influence on the structural and ferroelectric properties of the built-in electric field [5, 6], which is always present, whether due to the presence of a contact potential difference, or due to oxygen vacancies at the HfO_2-metal electrode interface or due to other mechanisms. Here we demonstrate a deeper insight into how the presence of a built-in homogeneous electric field in a FE HfO_2 affects its structural and ferroelectric properties.

Ideally, owing to the symmetry, the two states of polarization up and down should correspond to the same lattice constants. Precisely because of the symmetry, in the absence of an electric field, there are only even degrees in the decomposition of free energy by degrees of polarization

$$F = F_0 + \alpha P^2 + \beta P^4, \quad (1)$$

where F is free energy and P is polarization (see the phenomenological theory of ferroelectricity [7]). Therefore, two states of spontaneous polarization $-P_0$ and P_0 correspond to the same ground state energy. But in the presence of an electric field, an odd term $-EP$ appears in the decomposition of free energy

$$F = F_0 + \alpha P^2 + \beta P^4 - EP, \quad (2)$$

here E is an electric field. In this case, two equilibrium states of polarization up and down correspond to different ground state energies and may well correspond to different lattice constants.

Indeed, using X-ray microdiffractometry on the DESY synchrotron research facility, we have shown that when switching polarization, structural properties change: lattice constants and, as a consequence, the interplane distance. Moreover, there is a drift of the interplane distance with cycling of the structure. We assume this behavior is related to the presence of a built-in electric field, which leads to the appearance of vertical asymmetry. Based on first-principles calculations, we present a confirmation and an explanation of how the existence of a built-in homogeneous electric field leads to a difference in the structural properties of HfO_2 for the two polarization states. Furthermore, based on calculations, it is possible to say which mechanism of the built-in electric field dominates in the appearance of structural differences for the two polarizations.

The work was financially supported by the Russian Science Foundation (Project No. 20-19-00370, https://rscf.ru/en/project/20-19-00370/).

1. S. Dutta, P. Buragohain, S. Glinsek et al., *Nat. Commun.* **12**, 7301 (2021).
2. T. Shiraishi, K. Katayama, T. Yokouchi et al., *Appl. Phys. Lett.* **108**, 262904 (2016).
3. T. Schenk, C.M. Fancher, M.H. Park et al., *Adv. Electr. Mater.* **5**, 1900303 (2019).
4. M.D. Glinchuk, A.N. Morozovska, A. Lukowiak et al., *J. Alloys Compd.* **830**, 153628 (2020).
5. V. Lenzi, J.P. Silva, B. Šmíd et al., *Energy Environ. Mater.* e12500 (2023).
6. A. Chouprik, D. Negrov, E.Y. Tsymbal, A. Zenkevich, *Nanoscale* **13**, 11635 (2021).
7. V.L. Ginzburg, *Usp. Fiz. Nauk.* **38**, 490 (1949).

O3

Shape evolution of the hysteresis loops in relaxor ferroelectric PMN-0.28PT

A.D. Ushakov[1], M.S. Kosobokov[1], Q. Hu[2], X. Liu[2], Z. Xu[2], X. Wei[2], V.Ya. Shur[1]

[1]*School of Natural Sciences and Mathematics, Ural Federal University, 620000, Ekaterinburg, Russia*
bddah@ya.ru

[2]*Electronic Materials Research Laboratory, Key Laboratory of the Ministry of Education and International Center for Dielectric Research, Xi'an Jiaotong University, 710049, Xi'an, China*

This research conducts an in-depth analysis of the dielectric hysteresis loop transformations throughout the heating process in single-domain PMN-0.28PT plates, initially in the rhombohedral phase at room temperature. The typical ferroelectric hysteresis loop changes to a triple loop at 102°C, lasting until 124°C, at which point it transforms into a double-loop one. A slim hysteresis loop is present beyond 150°C (Fig. 1a). These observations can be interpreted as the effect of internal bias fields, generated by bound charges at the phase borders during the relaxor state.

The emergence of the triple hysteresis loop beyond the freezing temperature is linked to the emergence of nonpolar inclusions within the polar matrix, which expand with the temperature rise. The internal bias fields, induced by local depolarization fields near the interfaces, are responsible for the modification of the hysteresis loop shapes [1, 2].

The abrupt transition of the loop shape from a triple to a typical for relaxors double configuration at 126°C [3, 4] can be explained by the percolation transition from a polar matrix with nonpolar inclusions to a nonpolar matrix embedded with polar polydomain clusters [1]. The gradual reduction in cluster size with temperature coincides with the emergence of single-domain polar regions (polar nanoregions), exhibiting switching without hysteresis.

Support for our proposed model comes from Finite Element Method (FEM) simulations of the hysteresis loops in the crystal with the bias fields caused by nonpolar inclusions (Fig. 1b).

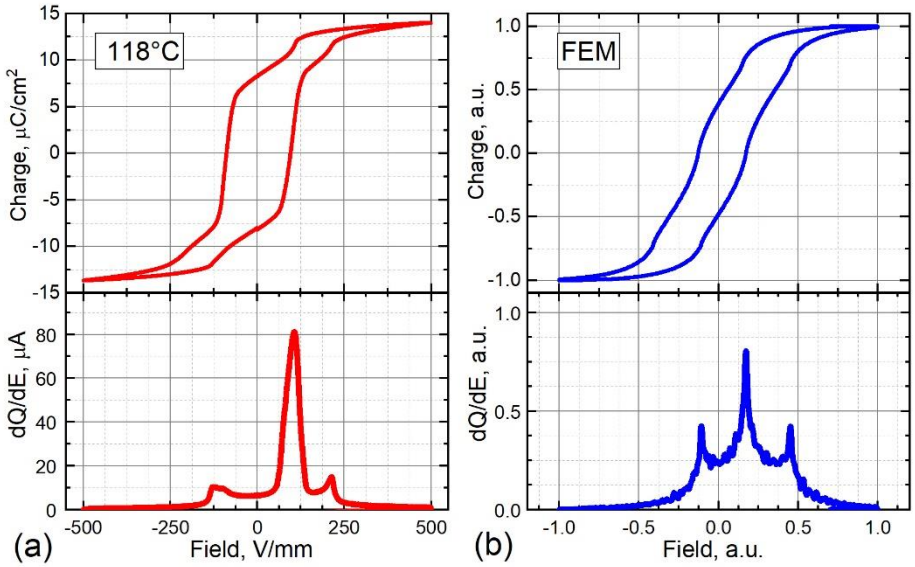

Figure 1. Triple hysteresis loop (upper images) and the corresponding charge derivative (bottom images) obtained (a) in PMN-0.28PT single crystal at 118°C, (b) by FEM simulations of proposed model.

The research was supported by the Ministry of Science and Higher Education of the Russian Federation (project no. 075-15-2021-1387) and the National Key R&D Program of China (grant no. 2021YFE0115000). The work was performed using the equipment of the Ural Center for Shared Use "Modern Nanotechnologies" UrFU (reg. No. 2968).

1. V.Ya. Shur, *Phase Transitions* **65**, 49 (1998).
2. V.A. Shikhova, V.Ya. Shur, D.V. Pelegov, et al., *Ferroelectrics* **398**, 115 (2010).
3. C.H. Hong, H. Guo, X. Tan, et al., *J. Mater.* **5**, 634 (2019).
4. V.Ya. Shur, in *Handb. Adv. Dielectr. Piezoelectric Ferroelectr. Mater.*, edited by Z.-G. Ye (Elsevier, 2008), pp. 622–669.

O4

Study of dielectric and polarization responses in relaxor ferroelectrics $PbB'B''O_3$ (B'= Fe, Ni, Co; B''= Nb, Ta) single crystals

V.G. Zalesskii, A.A. Levin, T.A. Smirnova, S.G. Lushnikov

Ioffe Institute RAS, 194021, Saint Petersburg
vg.zalessky@gmail.com

The family of complex perovskites with the general chemical formula $PbB'B''O_3$ and their solid solutions demonstrate a wide range of physical states: ferroelectrics, relaxor ferroelectrics, antiferroelectrics, etc. [1]. Of particular interest are compounds that have magnetically active ions of variable valence in one of the B-positions. Some compounds of this family are multiferroics and some exhibit phase separation [2].

The talk presents results of a study of the structure, dielectric permittivity, conductivity, and polarization of $PbB'B''O_3$ (B'= Fe, Ni, Co; B''= Nb, Ta) single crystals. According to previously published data [1], all the above compounds exhibit the broad and frequency-dependent maxima on the temperature dependence of complex dielectric permittivity. This gave the reason to include the crystals into the family of relaxor ferroelectrics. However, the study of the polarization properties of some crystals was accompanied by contradictory results in which the dielectric hysteresis loops differed significantly from those for typical ferroelectrics and ferroelectric relaxors. For example, the E-P- loops close to saturation were observed only in an extreme electric field at temperature of liquid nitrogen. Moreover, the dependence of the polarization on the field became linear when the crystals were cooled down to helium temperatures, despite an application of intense field up to the breakdown value. For some crystals of this family, there are even fewer published data on dielectric and polarization properties. Therefore, the temperature response of the dielectric and polarization behavior of the crystals requires detailed studies.

The talk presents the results of studies of the crystal structure using X-ray powder diffraction, the temperature dependences of the complex permittivity in the frequency range from 12 Hz to 100 kHz, and ac/dc- conductivity in the temperature range of 77÷700 K. The remanent polarization was studied by method of thermally stimulated depolarization (TSD).

As a result, the following data have been obtained for $PbB'B''O_3$ (B'= Fe, Ni, Co; B''= Nb, Ta) single crystals:

1) Crystal structure and crystal cell parameter.

2) The magnitude of the maximum on the temperature dependence of the complex permittivity, its temperature, width, and frequency dependence.

3) Values of ac- and dc- conductivity, their temperature dependence, and activation energy of charge carriers.

4) The magnitude and temperature range of existence of the remanent polarization induced by an external field.

A comparative analysis of the data obtained for different compounds makes it possible to determine the effect of certain ions on the relaxor state and other physical properties of the complex perovskites. The research results are discussed in terms of the phase separation model previously proposed for the related $PbCo_{1/3}Nb_{2/3}O_3$ crystal [2].

1. G.A. Smolensky, *Ferroelectrics and Related Materials*, (NY: Academic Press) (1981).
2. B.Kh. Khannanov et al., *JETP* **130**, 439 (2020).

O5

Jahn-Teller magnets with charge transfer

A.S. Moskvin

Ural Federal University, 620083, Ekaterinburg, Russia
alexander.moskvin@urfu.ru

By Jahn-Teller (JT) magnets we include compounds based on Jahn-Teller 3d- and 4d-ions with configurations of the $t_{2g}^{n1}e_g^{n2}$ type in a highly symmetrical octahedral, cubic, or tetrahedral environment and with ground state orbital *E*-doublet. These are compounds based on tetra-complexes with the configuration d^1 (Ti^{3+}, V^{4+}, Cr^{5+}), low-spin (LS) configuration d^3 (V^{2+}, Cr^{3+}, Mn^{4+}), and high-spin (HS) configuration d^6 (Fe^{2+}, Co^{3+}), octa-complexes with HS-configuration d^4 (Cr^{2+}, Mn^{3+}, Fe^{4+}, Ru^{4+}), low-spin configuration d^7 (Co^{2+}, Ni^{3+}, Pd^{3+}), as well as octa-complexes with configuration d^9 (Cu^{2+}, Ni^{1+}, Pd^{1+}, Ag^{2+}). The class of JT-magnets includes a large number of promising materials that are the focus of modern condensed matter physics, such as β-Sr_2VO_4, $(Sr,Ba)_3Cr_2O_8$, CrO, CrF_2, manganites $RMnO_3$, oxoferrates $(Ca,Sr)_2FeO_4$ $(Ca,Sr)FeO_3$, $(Ca,Sr)_3Fe_2O_7$, ruthenates RuO2, $(Ca,Sr)_2RuO_4$ $(Ca,Sr)RuO_3$, $(Ca,Sr)_3Ru_2O_7$, a wide range of ferropnictides (FePn) and ferrochalcogenides (FeCh), Na_5CoO_4, 3D nickelates $RNiO_3$, $(Li,Na,Ag)NiO_2$, cuprates CuO, CuF_2, K_2CuF_4, $KCuF_3$, 2D cuprates (La_2CuO_4, ...) and nickelates $RNiO_2$, silver-based compounds AgO, AgF_2, $KAgF_3$, Cs_2AgF_4. These materials have a rich spectrum of unique properties from various types of magnetic and charge ordering to metal-insulator transitions and superconductivity.

The lifting of the orbital *E*-degeneracy in the high-symmetry "progenitor" JT-magnets can be associated both with the specifics of the crystal structure, as, for example, in "apex-free" 2D cuprates (Nd_2CuO_4) and $RNiO_2$ nickelates, and with the conventional Jahn-Teller effect, which, as a rule, leads to the formation of a low-symmetry insulating antiferromagnetic (La_2CuO_4, $KCuF_3$, $LaMnO_3$) or ferromagnetic (K_2CuF_4) phase with orbital order. A competing mechanism for removing orbital degeneracy in JT magnets considered above is "anti-Jahn-Teller", "symmetric" *d*-*d*-disproportionation according to the scheme $d^n + d^n \rightarrow d^{n+1} + d^{n-1}$, assuming the formation of a system of bound or relatively free electronic d^{n+1} and hole d^{n-1} centers, differing by a pair of electrons/holes [1]. Formally, an electron/hole center can be represented as a hole/electron center with a pair of electrons/holes $d^2/\underline{d}^2$ localized at the center. In other words, a disproportionate system can be formally represented as a system of effective local spin-singlet or spin-triplet composite electron/hole bosons "moving" in the lattice of hole/electron centers. Note that in frames of the toy model the disproportionation energy Δ_{dd} formally coincides with the energy of local correlations U_{dd}, which gives reason to associate symmetric *d*-*d*-disproportionation with the negative-*U* phenomenon. We argue that the unusual properties of a wide class of JT-magnets with different crystal and electronic structures, with an unusual charge and magnetic order can be explained within a unified scenario [1,2]. Anti-JT disproportionation in all these JT-magnets leads to the formation of a system of effective local composite spin-singlet or spin-triplet, electron or hole S-type bosons “moving” on magnetic or nonmagnetic lattice, which can be found in various localized or delocalized, magnetic or nonmagnetic phase states, including unconventional charge or spin-charge orders, spin-singlet (cuprates, nickelates) or spin-triplet (manganites, FePn/Ch, ruthenates) superconducting state.

In the talk we consider in more detail all the peculiarities of the anti-JT disproportionation in different JT magnets, spin and orbital structure of the effective composite bosons, effective spin-charge hamiltonians for single- and two-band JT magnets. A review of the electronic structure and phase diagrams of a wide class of JT magnets will be given.

1. A.S. Moskvin, *J. Phys.: Cond. Matter* **25**, 085601 (2013).
2. A.S. Moskvin, Yu.D. Panov, *JMMM* **550**, 169004 (2022).

O6

Ab initio characterization of magnetoelectric coupling in ferromagnet/ferroelectric heterostructures

K.V. Evseev[1], I.I. Piyanzina[1,2], R.F. Mamin[1,2]

[1]*Institute of Physics, Kazan Federal University, 420008 Kazan, Russia*
ekv97@mail.ru
[2]*Zavoisky Physical-Technical Institute, FRC Kazan Scientific Center of RAS, 420029 Kazan, Russia;*

Today multimode tunable flexible spintronics based on ferromagnet (FM)/ferroelectric (FE) oxide heterostructures is of particular interest due to higher speed, smaller size, and more efficient energy than their traditional current-controlled counterparts [1, 2].

In this work, Fe/$BaTiO_3$, Fe/$SrTiO_3$ (STO), Co/$BaTiO_3$, and Co/$SrTiO_3$ film heterostructures were studied using density functional theory (DFT) calculations. The choice of the listed components of the heterostructure is motivated by the fact that Fe and $BaTiO_3$ are two "classical" ferroic materials with well-known bulk properties. In addition, bcc Fe and $BaTiO_3$ have a very good lattice constant match (the mismatch is only about 1.4%), which allows to carry out the layer-by-layer epitaxial growth of Fe = $BaTiO_3$ multilayers without significant misfit dislocations, as well as to simulate the heterostructure on a computer. Further, since the Fe/BTO heterostructure was deeply studied earlier [3-5], in this work we present a comparison with heterostructures based on similar compounds: ferromagnetic Co and quantum paraelectric $SrTiO_3$ (potential ferroelectric), in which the ferroelectric phase transition is suppressed by quantum fluctuations.

Ab initio calculations were carried out on the basis of the density functional theory. Exchange and correlation effects were taken into account using the generalized gradient approximation (GGA) using the PBE functionals (Perdue, Burke, and Ernzerhoff parameterization). The Kohn-Sham equations were solved using projectively extended wave potentials and wave functions. All calculations were carried out using the VASP (Vienna ab-initio Simulation Package) program built into the MedeA computational software [6].

In this work, the cells of heterostructures were modeled in such a way (Fig. 1) that six atomic layers of Fe accounted for twelve atomic layers of BTO (or STO). A vacuum region of 20 Å thick was also added to avoid interaction of the surfaces with their periodic images. To simulate substrate conditions, the bottom (right side in Fig. 1) four atomic layers were "frozen" during the optimization procedure (their atomic positions were not changed).

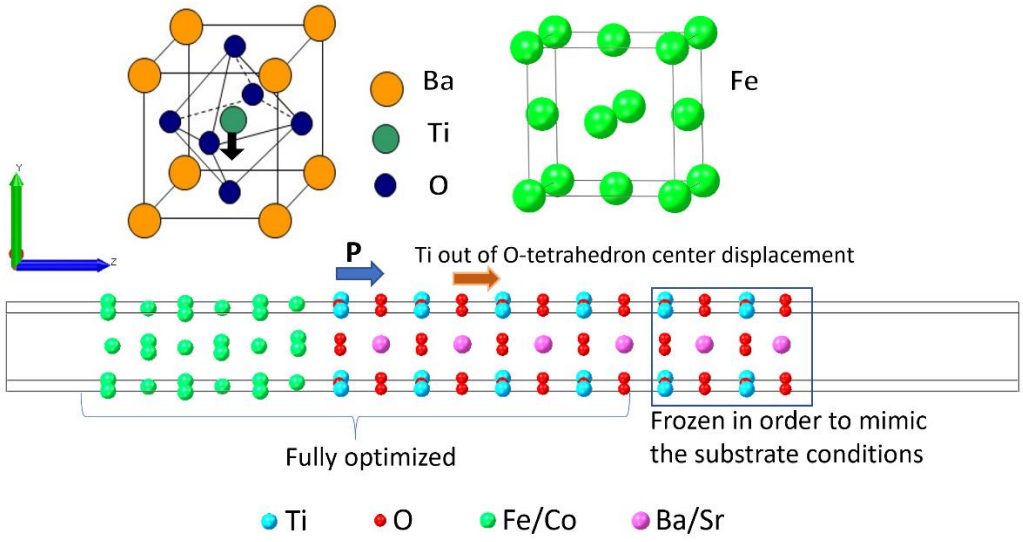

Figure 1. The unit cells of BaTiO3 in the tetragonal phase and bcc Fe; and the heterostructures Ba(Sr)TiO_3/Fe (Co) used for simulations with arrows showing the displacement of Ti from the center of oxygen octahedra and corresponding ferroelectric polarization in BTO. z-axis

The structural, electronic, and magnetic properties of ferromagnet/ferroelectric heterostructures were studied for Fe/$BaTiO_3$, Fe/$SrTiO_3$, Co/$BaTiO_3$, Co/$SrTiO_3$. It was found that the structural

properties depend on the type of ferroelectric used in the heterostructure, for example, cobalt causes strong structural distortions associated with the displacement of barium and titanium. Taken together, these distortions lead to the appearance of polarization directed from the interface towards the ferroelectric substrate. It was shown that the magnetic properties of the heterostructures are also different for different ferromagnetic films used: while in the heterostructures with cobalt the magnetic moments are uniformly distributed over the thickness of the ferromagnet, the BTO/Fe and STO/Fe heterostructures have a nontrivial and different distribution.

1. S.S. Won, H. Seo, M. Kawahara, et al., *Nano Energy* **55**, 182 (2019).
2. J. Yao, X. Song, X. Gao, et al., *ACS nano* **12**, 6767 (2018).
3. P.V. Leksin, N.N. Garif'yanov, I.A. Garifullin, et al., *Appl. Phys. Lett.* ***97***, 102505 (2010).
4. C.G. Duan, E.Y. Tsymbal, S.S. Jaswal, , *Phys. Rev. Lett.* **97**, 047201 (2006).
5. Y. Zhao, R. Peng, Y. Guo,et al., *Adv. Funct. Mater.* **31**, 2009376 (2021).
6. MedeA version 3.6; MedeA is a registered trademark of Materials Design, Inc., San Diego, USA.

O7

About determination of effective coupled temperature coefficients of nanostructured pyropiezoelectric composites by effective moduli and finite element methods

A.V. Nasedkin

Southern Federal University, 344090, Rostov-on-Don, Russia
nasedkin@math,sfedu.ru

To determine the effective moduli of nanostructured pyropiezoelectric (thermoelectroelastic) composites, static boundary problems are considered, in which the scale factor is taken into account according to the generalized Gurtin-Murdoch theory by introducing surface thermoelectroelastic fields at interface boundaries. In this model, surface moduli significantly affect the macrocharacteristics, if only the inclusions or pores are nanosized.

As is known, the effective moduli of piezoelectric nanostructured composites without temperature fields can be found from solutions to homogenization problems, when linear essential or constant natural boundary conditions are accepted at the external boundary of the representative volume element of the composite [1]. Then, from the conditions of the energy balance between the composite and the comparison medium, the effective moduli are expressed in terms of the averaged stress or strain fields and electric induction or electric field strength. In this case, when surface effects are taken into account, averaging is carried out both by integration over a representative volume, as well as by integration over interface boundaries [2].

Here, in order to find the complete set of effective moduli, it is necessary to solve, in the general case, nine boundary-value homogenization problems, when individual mechanical or electrical external influences are not equal to zero. To solve these problems, it is convenient to use the finite element method and algorithms for the formation of representative volumes, which describe the main features of the internal structure of the composite.

The paper shows that the effective temperature coupled coefficients can be determined in a similar way if the effective material moduli of the composite without temperature fields are known in advance. Thus, the effective moduli of temperature stresses are found from solutions of boundary value problems for certain nonzero mechanical external influences on the outer boundary of a representative volume and for a constant nonzero temperature field inside the volume, while effective pyroelectric constants are calculated from solutions of boundary value problems for given nonzero electrical external influences on the outer boundary and again at a constant nonzero temperature field in the volume. The corresponding formulas for the effective temperature coupling moduli here are also obtained from the energy balance equations.

The results of numerical experiments made it possible to analyze the dependences of effective moduli on the choice of essential or natural boundary conditions, on the percentage and nanosize of inclusions or pores, and on the relative areas of interface boundaries.

Note that due to the well-known analogy between the problems of thermoelasticity and poroelasticity, it is possible to determine effective moduli of porous-piezoelectric composites (fluid-saturated porous piezoelectric media), including those with interface effects, similarly to how it was described in [3] for poroelastic nanostructured composites.

Author acknowledges the support of the Russian Science Foundation (grant number No. 22-11-00302), https://rscf.ru/project/22-11-00302/, at the Southern Federal University.

1. A.V. Nasedkin, M.S. Shevtsova, *Ferroelectrics and superconductors: Properties and applications*. Ed. I.A. Parinov. (Nova Science Publishers, N.-Y.), 231 (2011).
2. A. Nasedkin, *Ferroelectrics* **509**, 57 (2017).
3. M. Chebakov, M. Datcheva, A. Nasedkin, A. Nasedkina, R. Iankov, *Numerical Methods and Applications. 10th Int. Conf. NMA 2022, Borovets, Bulgaria, August 22–26, 2022, Proc.* *Lecture Notes in Computer Science* **13858**, 114 (2023).

O8

Properties of Hydroxyapatite with various substitutions

V.S. Bystrov[1], E.V. Paramonova[1], L.A. Avakyan[2], S.V. Makarova[3], N.V. Bulina[3]

[1]*Institute of Mathematical Problems of Biology, Keldysh Institute of Applied Mathematics, RAS, 142290 Pushchino, Russia, vsbys@mail.ru*

[2]*Physics Faculty, Southern Federal University, 344090 Rostov-on-Don, Russia*

[3]*Institute of Solid State Chemistry and Mechanochemistry, Siberian Branch of RAS, 630128 Novosibirsk, Russia*

Hydroxyapatite (HAP) is a widely used biomaterial in medical applications due to its biocompatibility with human bone tissues, being the main mineral component of human bones and teeth. In the bone structure, HAP crystallizes in the form of platelet nanocrystals (2÷3 nm thick and ~25÷45 nm in size) in the interstices of tropocollagen fibrils, forming and strengthening the bone structure [1]. HAP has many useful properties, including piezoelectric properties, which are important for bone tissue remodeling processes. However, the mechanical properties of synthetic HAP are noticeably lower than those of human cortical bone—pure HAP turns out to be a rather brittle material. Therefore, such HAP is actively used as thin ceramic coatings on more durable titanium implants - here it ensures the survival of the implant. At the same time, biological HAP is also distinguished by the presence of a significant amount of various impurities, ions and molecular ionic groups [1]. Therefore, to improve the properties of biocompatibility, synthetic HAP is usually modified by introducing similar additives and substitutions of atoms into it. Experimentally it is quite laborious to carry out a series of various substitutions in HAP. Therefore, one of the effective ways to study structural changes and substitutions in HAP is computer modeling and numerical studies, especially with the help of modern methods of density functional theory (DFT) [1-3]. The formation and properties of bone tissue are also significantly affected by other ions: F, Sr, Mn, and others, but Magnesium is still the most important in maintaining bone strength and remodeling. Previously, we have already performed DFT calculations of the structure and properties of HAP modified with Sr, Mg, Fe, etc. Our results showed that Fe imparted magnetic properties to HAP [3], while Sr, Mg changed the piezoelectric properties of HAP [4].

In this work, we present the results of modeling and DFT calculations for the substitution of Ca by Mg and Mn ions at different concentrations. Here we continue and develop our numerical studies based on the HAP super-cell model (352 atoms and 8 elementary hexagonal cells of 44 atoms each). The relaxation of the HAP-Mg lattice by DFT methods is carried out according to the technique developed by us [1-3] in 2 stages: 1) optimization with the PBE functional, 2) calculations with the hybrid HSE functional (as an option, here a point calculation is performed for already optimized structures). This makes it possible to obtain highly accurate and correct values of both the cell parameters and the band gap. Currently, the main DFT calculations are carried out on Quantum ESPRESSO. We modeled the relaxation of the HAP-Mg structure by substituting Ca atoms for Mg atoms in different Ca1 and Ca2 positions with different numbers of substituting Mg atoms: nMg/Ca1, nMg/Ca2 at n = 1, 2, 4, 8, 12, 16 in the supercell HAP of 352 atoms, in which there are 80 Ca atoms, which corresponds to 1.25; 2.5; 5; 10; 15; 20% Mg.

The results obtained show a decrease in the cell parameters with an increase in the amount of Mg, in good agreement with the experimental data. In this case, differences are observed in the substitutions of Mg in the Ca1 and Ca2 positions, and characteristic and different changes occur in the distances between the Ca-O, Mg-O, and Ca-H atoms. Narrowing of the HAP OH channel is noted, and it is noticeably asymmetric for Mg/Ca2 substitutions. There is also a change in the band gap, which also has a different character for the nMg/Ca1 and nMg/Ca2 substitutions. The resulting dependence of the formation energy Ef of substitutions is ~ 0.095 - 0.115 eV/f.u. and has a different character for nMg/Ca1 and nMg/Ca2, a critical point at 10% Mg. These works are ongoing to refine these results. The obtained results of DFT calculations were analyzed in comparison with various experimental data. The work was supported by the Russian Science Foundation grant No. 21-12-00251.

1. V. Bystrov, E. Paramonova, L. Avakyan, et al., *Nanomaterials* **11**, 2752 (2021).
2. N.V. Bulina, S.V. Makarova, et al., *Minerals* **11**, 1310 (2021).
3. L. Avakyan, E. Paramonova, V. Bystrov, et al., *Nanomaterials* **11**, 2978 (2021).
4. V.S. Bystrov, E.V. Paramonova, A.V. Bystrova, et al., *Ferroelectrics* **590**, 41- 48 (2022).

O9

Characterization of the polyimide doped with carbon-based nanostructures

N.V. Kamanina[1,2,3]

[1]*Lab for Photophysics of Media with Nanoobjects at Vavilov State Optical Institute, St.-Petersburg, Russia*
[2]*St.-Petersburg Electrotechnical University ("LETI"), 197376 St.-Petersburg, Russia*
[3]*Petersburg Nuclear Physics Institute, National Research Center «Kurchatov Institute», Gatchina, Russia*
nvkamanina@mail.ru

Among different optoelectronic materials the organic ones can be considered as the good matrix for the sensitization [1]. It should be mentioned that at the present time the doping process of the organic materials (such as the polyvinyl carbazole, polyaniline, pyridine, polyimide, etc.) using namely the perspective nanostructures occupies the specific place in order to reveal the change of the basic physical-chemical properties of these materials. Moreover, after extensive use of the laser tools in the study of the doped organics the refractive characteristics can be considered as the main ones [2]. It is due to the reason that the refractive parameters change is connected with structural, spectral and photoconductive features modifications. The perspective dopant agents such as: the fullerenes, carbon nanotubes (CNTs), graphene oxides (GrO), shungites (Sh), etc. carbon-based nanoparticles can be used for this aim.

In the current research the polyimide photosensitive materials doped with the large groups of the carbon-based sensitizers are investigated. The unique optical limiting, high-frequency Kerr effects, UV treatment of the doped polyimide are discussed. In order to explain the efficiently of the doping process the intermolecular charge transfer complex formation is taken into account.

The basic photorefractive characteristics were studied using the four-wave mixing technique. The second harmonic of the nanosecond pulsed Nd-laser operated at the wavelength of 532 nm was used. The energy density was chosen in the range of 0,1-0,9 J×cm^{-2}. The amplitude-phase thin gratings were recorded under the Raman-Nath diffraction conditions at the spatial frequency (Λ) of 90, 100 and 150 mm^{-1}. Indeed, the condition for the thin amplitude-phase holograms recording under the Raman-Nath conditions was implemented, when the thickness of the medium under the test is less than the period of the formed lattice. It should be remembered that the photorefractive parameters were revealed not only for the nanosensitized polyimide films, but for the pure ones too, for the comparison. Some experimental and calculated results are shown in Table 1 [3-5].

Table 1. Comparative data of laser-induced change of the refractive index Δn_i for the currently studied and investigated before polyimide materials at the wavelength of 532 nm.

Studied structure	Dopant content, wt.%	Energy density, J×cm^{-2}	Λ, mm^{-1}	Laser pulse width, ns	Δn_i	References
Pure PI	0	0.6	90	20	10^{-4}-10^{-5}	[3]
PI+C_{60}	0.2	0.5-0.6	90	10-20	4.2×10^{-3}	[3]
PI +C_{70}	0.2	0.6	90	10-20	4.68×10^{-3}	[3]
PI +Shungite	0.1	0.5	100	20	4.1×10^{-3}	current
PI + Shungite	0.15	0.5	90	10-20	5.2×10^{-3}	current
PI + Shungite	0.2	0.5	100	20	5.5×10^{-3}	current
PI + Shungite	0.2	0.6	150	20	5.3×10^{-3}	[4,5]
PI +CNTs	0.1	0.5-0.8	90	10-20	5.7×10^{-3}	[3]
PI +CNTs	0.2	0.6	100	20	5.5×10^{-3}	current
PI +GrO	0.1	0.1	100	20	7.5×10^{-3}	current
PI +GrO	0.2	0.3	100	20	7.7×10^{-3}	current
PI + GrO	0.1	0.1	150	20	6.5×10^{-3}	current

The author would like to thank her Lab colleagues at Vavilov State Optical Institute and other Scientific Centers for their partial help in this study. Some results have been shown and discussed at the Applied Optics conference (Saint-Petersburg, December 2022).

1. F. Gutman, L.E. Lyons, *Organic Semiconductors*, J. Wiley & Sons, New York, 858 p., 1967.
2. N.V. Kamanina, *Materials (MDPI)* **15**, 2153 (2022).
3. N.V. Kamanina, D.P. Uskokovic, *Mater. Manuf. Process.* **23**, 552 (2008).
4. N.V. Kamanina, S.V. Serov, N.A. Shurpo, N.N. Rozhkova, *Tech. Phys. Lett.* **37**, 949 (2011).
5. N.V. Kamanina, S.V. Serov, Y. Bretonniere, Ch. Andraud, *J. Nanomaterials* **2015**, 278902 (2015).

O10

The impact of various factors on the surface of X-cut lithium niobate and properties of proton-exchange waveguides

A.V. Sosunov[1], I.V. Petukhov[1], V.I. Kichigin[1], R.S. Ponomarev[1], A.A. Mololkin[2], M. Kuneva[3]

[1]*Perm State University, 614990 Perm, Russia*

[2]*Fomos-Materials, 107023, Moscow, Russia*

[3]*Institute of Solid State Physics, Bulgarian Academy of Sciences, 1784 Sofia, Bulgaria*

alexeisosunov@gmail.com

Lithium niobate (LN) is an excellent optical material and not without reason is referred to as 'silicon of photonics'. It stands out among other optical crystals owing to its unique physicochemical and electro-optical properties. Due to these properties, waveguide and domain structures can be formed on the LN surface for various photonic applications.

It is well known that LN is anisotropic crystal, and each cut has its peculiar properties. The ferroelectric properties of different surface planes were described [1]. X-cut is non-polar and technologically simple. This allows one to form the electrodes of simpler topology on the X-cut surface for broadband optical modulators. On the other hand, X-cut LN surface has perpendicular orientation to the crystal cleavage planes [2]. This results in better permeability of X-cut for hydrogen; thus, the X-cut surface is prone to damage, defect formation, and larger strains during PE [3,4].

The aim of this work is to perform the complex analysis of the effect of various impacts (thermal, plasma, chemical) on the lithium niobate X-cut surface on the structure and optical characteristics of proton-exchanged (PE) waveguides made thereafter.

Congruent lithium niobate crystals, X cut (Fomos-Materials, Russia) were used for study. Impact on LN sample before PE was carried out by one of the following procedures: (1) annealing in air at 500°C for 4 hours; (2) argon plasma treatment in an X-ray photoelectron spectroscopy K-Alpha+ system (Thermo Fisher Scientific) with built-in equipment for plasma treatment. The treatment was carried out in two successive stages with duration of 3 min, beam power was 3 keV; (3) exposure of the samples to various acid solutions sulfuric acid and hydrogen peroxide (30 wt.%) with mixing ratio 4:1 at 60^{o}C for 10 min, or to a mixture (2:1) of concentrated nitric acid and hydrofluoric acid at 22°C for 10 min.

Proton exchange was done in leak-free zirconium reactor in molten benzoic acid at 210°C for 2 h. After proton exchange, the samples were annealed in air at 370°C for 7.5 h. X-ray diffraction, XPS, prism coupling method, optical microscopy and profilometry, as well as computed tomography were used as research methods.

Pre-annealing of lithium niobate in the optimum temperature regime 500°C reduces the structural inhomogeneity of the crystal and improves properties of PE waveguides. As a result of pre-annealing, [Li]/[Nb] ratio on the LN surface approaches the congruent value.

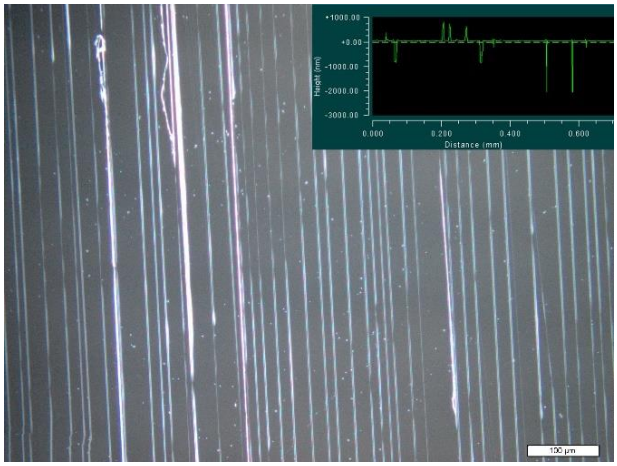

Figure 1. LN surface after treatment with Ar-plasma and proton exchange. Surface profile – inset in the upper right corner.

Argon plasma treatment has a pronounced effect on the phase composition of PE layers and lattice strains during PE. As a result of plasma treatment, strip defects up to 500 nm in height are formed after proton exchange (Fig. 1). The strip defects are detected also on LN samples after pre-annealing; however, in that case the defects are much smaller.

XPS results suggest that immersion in a H_2SO_4 + H_2O_2 solution decreases the Li concentration and increases oxygen content on the LN surface. Immersion in a HNO_3 + HF mixture decreases the [Nb]/[O] ratio. These changes in surface chemistry affect the adsorption of benzoic acid on lithium niobate and transfer of protons across the lithium niobate/benzoic acid melt interface. As opposed to plasma treatment, acid solutions do not affect the structure of PE phases. Nevertheless, the pre-exposure to acid mixtures influences the refractive index in annealed PE waveguides (Fig. 2).

In summary, different factors (pre-annealing, plasma treatment, exposure to acids) can manifest themselves in different ways when the waveguides for integrated optical devices are manufactured. A combination of factors can have a considerable effect on proton exchange, structure and characteristics of the waveguides. The results are of importance for improving stability of proton-exchanged waveguides in integrated optical circuits for various systems in instrument making industry.

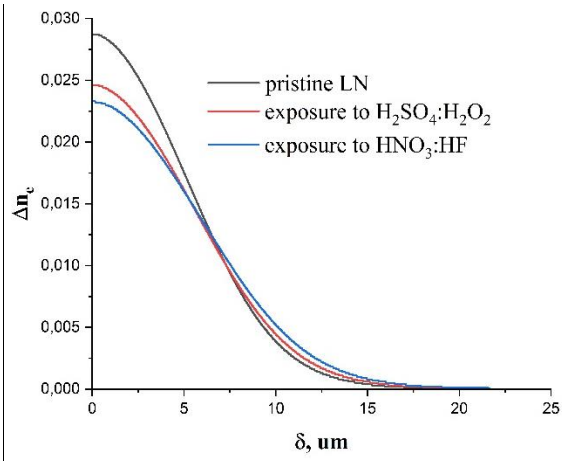

Figure 2. Profiles of waveguides during different chemical exposure of surface LN

This work was funded by RFBR and Perm Region [grant number 20-42-596001]

1. S. Sanna, W.G. Schmidt, *J. Phys. Condens. Matter*. **29**, 413001 (2017).
2. P. Nekvindová et al., *Opt. Mater.* **19**, 245 (2002).
3. S.M. Kostritskii et al., *J. Eur. Opt. Soc. Rapid Publ.* **9**, 14055 (2014).
4. A.V. Sosunov et al., *Ferroelectrics.* **506**, 24 (2017).

O11

Degenerate anisotropic Bragg diffraction on the regular domain structure in lithium tantalate crystal

A.V. Dubikov[1], S.M. Shandarov[1], N.I. Burimov[1], E.N. Savchenkov[1], A.R. Akhmatkhanov[2], M.A. Chuvakova[2], V.Ya. Shur[2]

[1]*Tomsk State University of Control Systems and Radioelectronics, Tomsk, Russia, rossler@mail.ru*
[2]*School of Natural Sciences and Mathematics, Ural Federal University, Ekaterinburg, Russia*

Degenerate anisotropic Bragg diffraction on the acoustic waves was described in [1]. Herein, we study the degenerate anisotropic Bragg diffraction on the regular domain structure (RDS) in lithium tantalate, which has been observed for two temperature segments within the range between 10 and 100ºC. The examined RDS with spatial period of Λ = 7.99 μm was formed in a stoichiometric 1%MgO:$LiTaO_3$ sample with sizes of 1×2×6 mm^3 along the *X*, *Y*, and Z axes, respectively, by electric poling method. The used experimental setup is schematically shown in Figure 1.

The vector diagrams for degenerate anisotropic Bragg diffraction on RDS in 1%MgO:$LiTaO_3$ crystal at two temperatures when first of them is below the isotropic point whereas the second one lies above of this point are illustrated by Figures 2a and 2b, respectively.

Both types of these degenerate anisotropic Bragg diffraction were realized in the experiments, as are shown in Figures 3 and 4. In the case of low segment of temperature the extraodinary polarizated probe beam is directed along the Y-axis of the sample. We have observed by the temperature about 42ºC two simmetrical Bragg diffracted odinary polarizated output beams on the screen spaced at the distance of 1 m from the crysnal, as it is shown in the photo (Fig. 4).

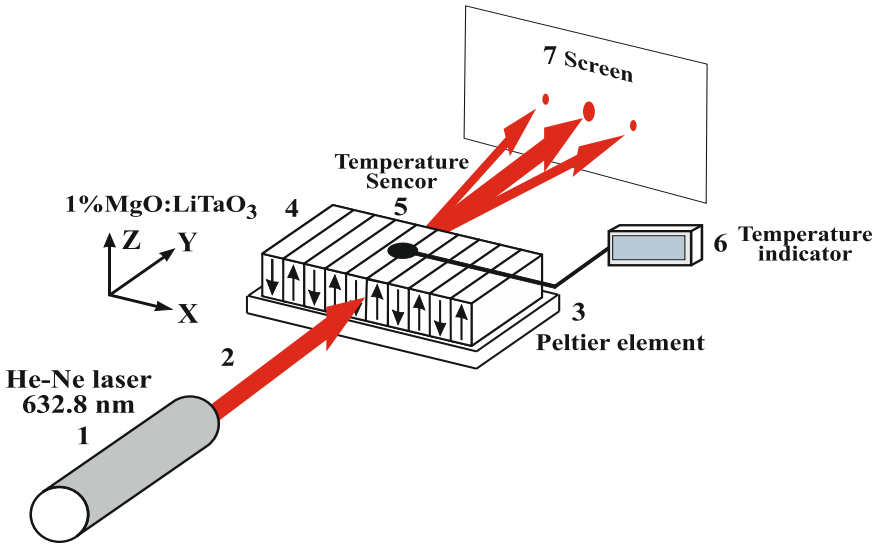

Figure 1. Schematic illustration of degenerate anisotropic Bragg diffraction on RDS.

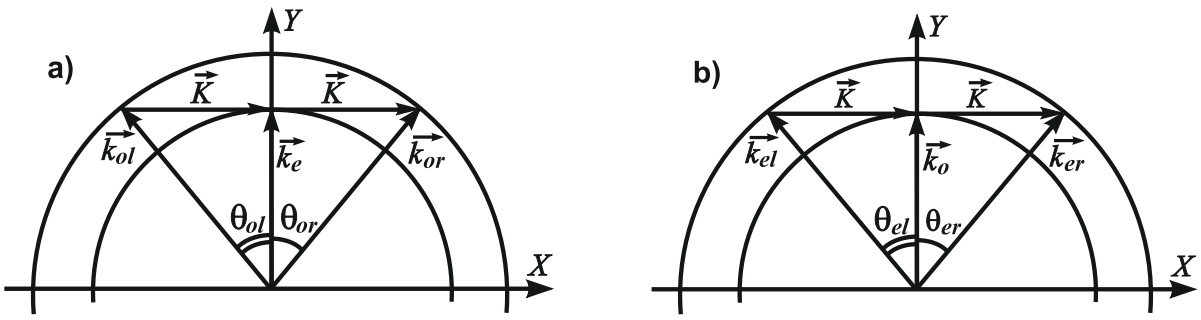

Figure 2. Vectors diagrams of degenerate anisotropic Bragg diffraction on RDS in 1%MgO:$LiTaO_3$ crystal. (a) at low temperature, (b) at high temperature. $\vec{K}$ – RDS grating vectors, $\vec{k}$ – wave vectors for "*o*"/"*e*" – ordinary/extraordinary polarized waves, "*l*"/"*r*" – left/right, θ – angles of diffraction.

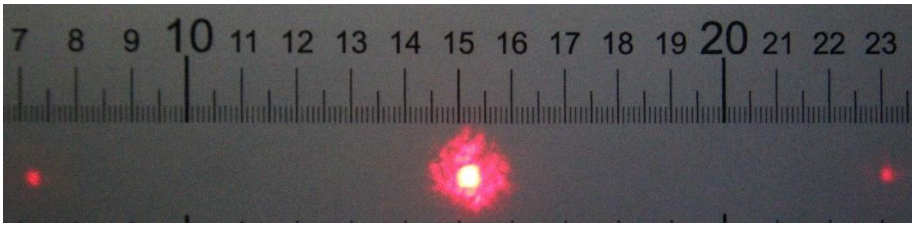

Figure 3. Degenerate anisotropic Bragg diffraction for the extraodinary polarizated probe beam (in the middle) into two simmetrically located odinary polarizated output beams, which is observed at the temperature about 42ºC at the distance of 1 m from the crystal.

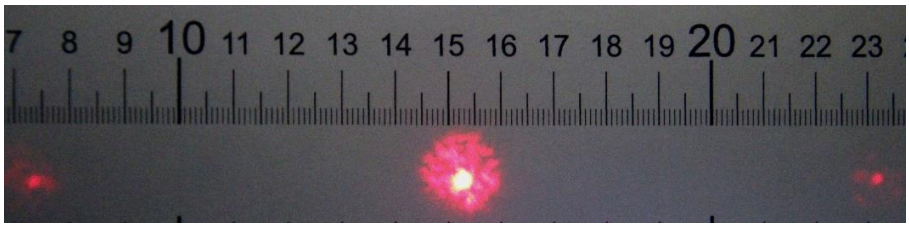

Figure 4. Degenerate anisotropic Bragg diffraction for the odinary polarizated probe beam (in the middle) into two simmetrically located extraodinary polarizated output beams, which is observed at the temperature about 90ºC at the distance of 1 m from the crystal.

One can see in Fig. 5 the same effect for odinary polarizated probe beam at the temperature about 90ºC where two output light beams have extraodinary polarization.

Temperature dependences of diffraction efficiency for left (▲) and right (◆) diffraction maxima pointed in Figs. 4 and 5 are shown in Fig. 6 both for extraordinary (a) and ordinary (b) polarized probe beams.

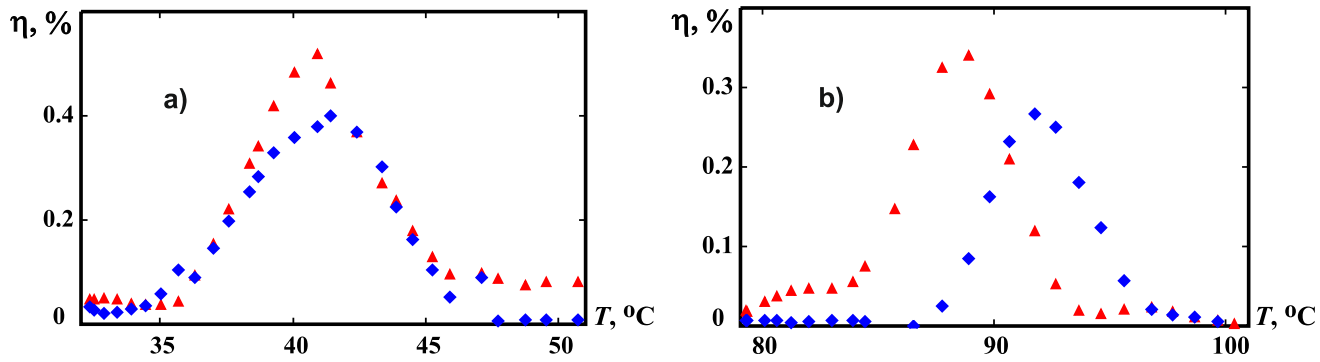

Figure 5. Diffraction efficiency for the degenerate anisotropic Bragg diffraction vs. the temperature for (a) extraodinary and (b) extraodinary polarizated probe light beam. ▲– left maximum, ◆ – right maximum.

This study was funded by the Ministry of Science and Higher Education of the Russian Federation in the framework of the state assignment for 2023-2025 (job-order FEWM-2023-0012). The study was performed using the equipment provided by Ural Common Use Center ”Modern Nanotechnologies“ Ural Federal University (Reg. No. 2968) supported by the Ministry of Science and Higher Education of the Russian Federation (project 075-15-2021-677).

1. J. Xu, R. Stroud, *Acousto-optic devices: principles, design, and applications* (Wiley), 1992.

O12

Atomic structure at middle range order of La_2O_3-Nb_2O_5-B_2O_3 glass

L.A. Avakyan[1], R.O. Alexeev[2], G.Yu. Shakhgildyan[2], J.A. Firsova[2,3], V.N. Sigaev[2], G.B. Sukharina[1], L.A. Bugaev[1]

[1]*Southern Federal University (SFedU), 344090, Rostov-on-Don, Russia*
laavakyan@sfedu.ru

[2]*Mendeleev University of Chemical Technology of Russia (MUCTR), 125047, Moscow, Russia*

[3]*Corporation «Lytkarino Optical Glass Plant» (LZOS), 140080, Lytkarino, Russia*

The non-silica oxide glass are studied as a perspective high-refraction index materials which does not contain lead [1,2] . The lanthanum and niobium oxides are promising high refraction index materials, but their glass-forming ability is weak, so that glass can be formed only in extreme conditions. i. e. using containerless processing technology in aerodynamic levitation furnaces [3,4] , which is not suitable for industry. The addition of boron oxide allows [5] to produce La_2O_3-Nb_2O_5-B_2O_3 (in the following – LNB) glass with refraction index using convenient glass-production technologies. The obtained samples are transparent and have refraction index of 1.71–1.98 (depending on the boron oxide concentration) which is lower than in binary glass system (2.25), but higher than in silica or phosphate glass (~ 1.5). Despite of the practical importance of such glass systems, their atomic structure is not well established. In particular, the spatial arrangement of NbO_6 octahedra in glass systems is debated. Masuno et al [3] proposed that NbO_n polyhedra are connected by corners and by edges in the glass, while the last is not expected in low-density glass structures. Iordanova *et al* [6] states that both octahedral NbO_6 and tetrahedral NbO_4 groups are present in amorphous framework. Aronne *et al* [7] insisted on the high static disorder of the first coordination shell Nb-O ($N_{Nb\text{-}O}$ ~ 6, $R_{Nb\text{-}O}$ ~ 1.9-2.1 Å) with no NbO_4 groups.

In order to reveal the atomic structure of the obtained LNB samples we applied the IR, Nb K- and La L_3- XAFS spectroscopy methods and X-ray total scattering (PDF). The studied LNB glass samples have the nominal composition of $22.5La_2O_3$, xNb_2O_5 and $(77.5 - x)B_2O_3$ with x = 5 ... 30, which are denoted in the following as 5LNB, ... 30LNB.

Here we focus the consideration on the pair distribution function analysis. The experimental scattering patterns were obtained at beamline P02.1 within the rapid access program 2021A of PETRA III (DESY, Hamburg). The scattering patterns were processed using GSAS-II [8] and PDFgui [9] codes.

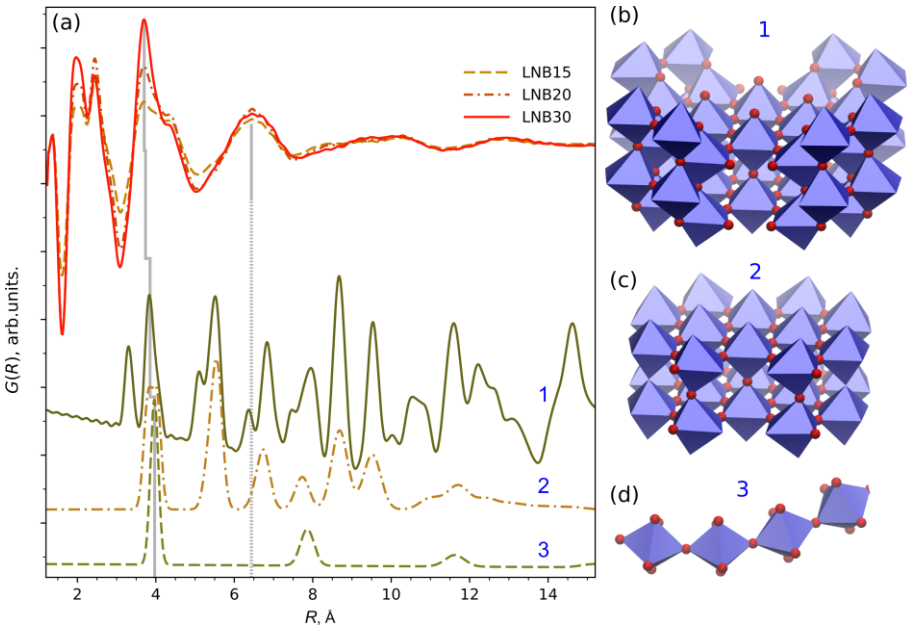

Figure 1. (a) The comparison of experimental PDFs for LNB samples with theoretical ones obtained from model structures. (b-d) Illustration of model structures cut from bulk Nb_2O_5 oxide. Color notation at right panels: blue – Nb, red – oxygen.

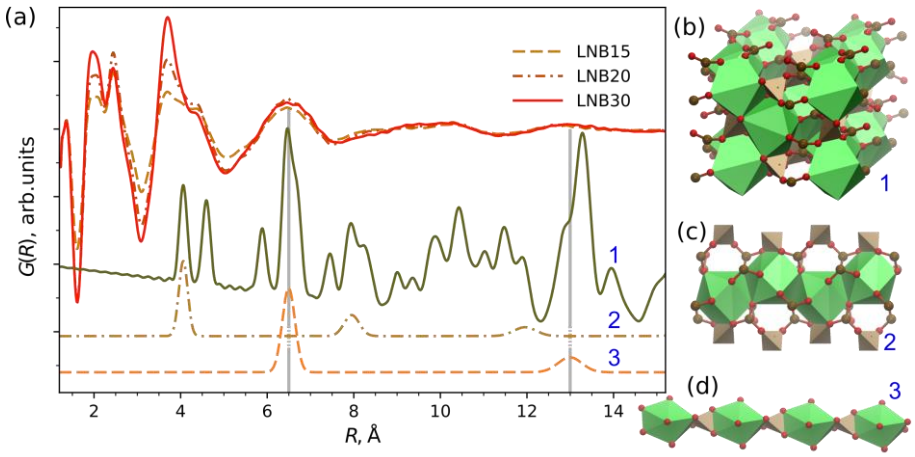

Figure 2. (a) The comparison of experimental PDFs for LNB samples with theoretical ones obtained from model structures. (b-d) Illustration of model structures cut from bulk La_2O_3 oxide. Color notation at right panels: green – La, red – oxygen, gray – boron.

Figures 1 and 2 compares the obtained experimental pair distributions functions $G(R)$ for LNB samples with the theoretical functions, calculated for different atomic structures, which are generated from the crystal structures of bulk Nb_2O_5 (I4/mmm, COD ID 1528723, see Fig. 1) and LaB_3O_6, (I12/a1, COD ID 1510925, see Fig. 2) oxides [10]. The full crystals are denoted with number 1, while structures modified by fragments removal – with numbers 2 and 3.

The $G(R)$ peaks at low distances (< 3 Å) are correspond to B-O, Nb-O and La-O bond lengths and are in a good agreement with reference data and the results of our XAFS analysis [5]. However, the nature of middle-range order distance peaks (< 10 Å) is not clear. The $G(R)$ peak at ~ 4 Å can be formed both by La – La and Nb – Nb correlations bridged by oxygen. While peaks at ~ 6.5 and 13 Å are owing to the presence of LaB_3O_6 phase.

The PDF analysis of the considered samples allows to conclude that:

i. NbO_6 octahedra are connected only by corners with the average length of the chain below 0.5 nm; The study of glass of another system, i. e. $BaO\text{-}Nb_2O_5\text{-}P_2O_5$, lead to similar distribution of Nb ions;

ii. LaO_8 polyhedra are dominately connected through borate groups;

iii. The length of LaO_8 polyhedra chains extends above 1 nm.

The work was financially supported by a Russian Science Foundation, grant # 22-12-00106.

1. T.T. Fernandez, S. Gross, K. Privat, et al., *Adv. Func. Mater.* **32**, 2103103 (2021).
2. T. Komatsu, T. Honma, T. Tasheva, V. Dimitrov, *J. Non-Cryst. Solids* **581**, 121414 (2022).
3. A. Masuno, S. Kohara, A. C. Hannon, et al., *Chem. Mater*. **25**, 3056 (2013).
4. A. Masuno, H. Inoue, K. Yoshimoto, Y. Watanabe, *Opt. Mater. Express* **4**, 710 (2014).
5. R. Alekseev, L. Avakyan, G. Shakhgildyan, et al., *J. Alloy Compd.* **917**, 165357 (2022).
6. R. Iordanova, M. Milanova, L. Aleksandrov, et al., *J. Non-Cryst. Solids* **543**, 120132 (2020).
7. A. Aronne, E. Fanelli, P. Pernice, et al., *J. Non-Cryst. Solids* **357**, 1218 (2011).
8. B.H. Toby, R.B. von Dreele, *J. Appl. Crystallogr*. **46**, 544 (2013).
9. C.L. Farrow, P. Juhas, J.W. Liu, et al., *J. Phys.: Condens. Matter* **19**, 335219 (2007).
10. S. Gražulis, A. Daškevič, A. Merkys, et al., *Nucleic Acids Res.* **40**, D420 (2012).

O13

Influence of raw material pretreatment methods on macro responses in $BaTiO_3$–$BaZrO_3$ solid solutions

D.V. Volkov[1], L.A. Dykina[1], A.Yu. Malykhin[1], A.A. Martynenko[1], A.A. Pavelko[2]

[1]*Southern Federal University, Institute of High Technologies and Piezotechnics, 344090, Rostov-on-Don, Russia*

dvvolkov@sfedu.ru

[2]*Southern Federal University, Research Institute of Physics, 344090, Rostov-on-Don, Russia*

Much attention is paid to the development of new and improvement of existing materials for the electronic component base. Important criteria include reducing the size of end devices, environmental friendliness, as well as the need for high energy efficiency. In the matter of energy efficiency, it can be noted that there are quite a wide range different concepts and solutions related to the creation of compact and efficient energy sources. One of these solutions are dielectric capacitors, in some cases superior in power, compactness and efficiency to other devices for storing and delivering electricity. However, they also require the development of a new component base for their modernization. They have a set of distinctive physical characteristics, are effective when exposed to strong electric and magnetic fields and can both maintain and predictably change its properties in a wide range of temperatures. However, most high-performance ferroelectric materials are lead-containing compounds. The release of lead-containing ceramics into the environment leads to its contamination and harms human health, and the processing of lead-containing ceramics is still a challenge.

One of the interesting lead-free ferroelectric materials is $BaTiO_3$, it has a high dielectric constant, distinctive pyroelectric activity, and low dielectric loss factor. Barium titanate based solid solutions are widely used in multilayer capacitors, pulse generation devices, converters, [1,2]. The high efficiency, energy density and significant breakdown voltage achieved in the systems $BaTiO_3$–$BaZrO_3$ [3,4], $BaZrO_3$–$BaCaO_3$–$BaTiO_3$ [5-7], and $BaZrO_3$–$BaTiO_3$–$BiNaTiO_3$ [8] are high.

In this paper, we consider the effect of precursors mechanical activation to optimize the technological process of obtaining solid solutions of the $BaZr_xTi_{1-x}O_3$ system, while maintaining optimal electrophysical properties.

Earlier it was found that this system of solid solutions, in addition to the ferroelectric phase, has a region of a diffusion phase transition, a wide region in which relaxor properties are manifested, and can also pass into the state of dipole glass. Also, $BaZr_xTi_{1-x}O_3$ ceramics have a higher dielectric constant at $x \geq 0.15$, and, therefore, exhibit higher piezoelectric and electrostrictive coefficients than $BaTiO_3$. However, to obtain solid solutions, $BaZr_xTi_{1-x}O_3$ high quality is required: much attention should be paid to the preparation of raw materials, a long holding time at high temperatures of 1773÷1973 K and the application of pressure up to 1500 bar. One of the ways to reduce the cost while maintaining the properties can be the use of various methods of preparing raw materials. For example, using the method of mechanical activation, it is possible to increase the reactivity of the synthesis components, which leads to an increase in the completeness of sintering and a decrease in the temperature required for it.

In this study two groups of solid solutions $BaZr_xTi_{1-x}O_3$ prototypes where x = 0, 0.1, 0.15, 0.2, 0.25, 0.3, 0.45 by the method of two-stage solid-phase synthesis were obtained. Before sintering, the objects were divided into two groups, one of which was processed in a mechanical activation chamber for 20 minutes, followed by its sintering carried out at T=1733 K, t=2 hours. $BaCO_3$ (99%), ZrO_2 (99%) were used as feedstock, TiO_2 (99%). The phase composition and completeness of the synthesis were controlled using X-ray diffraction at the CoKα wavelength, using a DRON-3 diffractometer. At each stage of the technological process, a step-by-step optimization of the conditions for the formation of solid solutions carried out. Determination of the experimental and relative density of the samples was carried out by hydrostatic weighing in n-octane. The dielectric constant was measured over a wide range of temperatures (T=80÷500 K) and frequencies (f=10-10^6 Hz).

It has been established that both groups of solid solutions are not homogeneous and at room temperature. Two phases with similar parameters of the unit cell are coexist in them. It is shown that the use of mechanical activation leads to a significant increase in the density of solid solutions. A nonlinear

change in density in the regions of morphotropic phase transitions for two groups of solid solutions was found. The study of the dielectric constant indicated the concentrations at which there is a gradual decrease in the Curie temperature and in the region of the unstable ferroelectric state for both groups of solid solutions. The paper also discusses changes in piezoelectric properties and other macroresponses that could be caused by mechanical activation.

The research was carried out with the financial support of the Ministry of Science and Higher Education of the Russian Federation, state task in the field of scientific activity, project No. FENW-2022-0033.

1. S. Song, et al., *Ceram. Int*. **48**, 10789 (2022).
2. T. Maiti, R. Guo, A.S. Bhalla, *J. Am. Cer. Soc.* **91**, 1769 (2008).
3. K. Nitish, et al., *Appl. Phys. Lett.* **106**, 252901 (2015).
4. L. Zhongshuai, et al., *Mater. Chem. A* **6**, 12291 (2018).
5. V.S. Puli, et al., *J. Phys. D: Appl. Phys.* **44**, 395403 (2011).
6. V.S. Puli, et al., *J. Mater. Sci.* **48**, 2151 (2013).
7. V.S. Puli, et al., *Ferroelectrics* **157**, 139 (2014).
8. J. Qian, et al., *ACS Appl. Mater. Interfaces* **14**, 54012 (2022).

O14

Lattice dynamics of the $BaMg_{1/3}Ta_{2/3}O_3$ complex perovskite

S.N. Krylova[1], E.A. Popova[2], Y.E. Kitaev[2], S.G. Lushnikov[2]

[1] *Kirensky Institute of Physics Federal Research Center KSC SB RAS,660036, Krasnoyarsk, Russia slanky@iph.krasn.ru*

[2]*Ioffe Institute, Polytekhnicheskaya 26, 194021, St. Petersburg, Russia*

$BaMg_{1/3}Ta_{2/3}O_3$ (BMT) belongs to the complex perovskites with the general formula AB′ B″ O (A = Ba, B′ = Mg, B″ = Ta). It is known that BMT possesses s the high product of frequency (f) and Q (Q_f ~ 430000 GHz), moderate dielectric constant (ε_r ~ 24) [1, 2]. BMT can be used as dielectric resonators, filters, or oscillators. Some experimental articles have been devoted to lattice dynamics. For example, articles on Raman spectroscopy [3, 4], neutron scattering [5], micro-Brillouin scattering [6], infrared absorption [7], and inelastic X-ray scattering [8] have been published before. The theoretical first-principal studies have been performed to study the order-disorder phenomena of the B-site cations in BMT and to explain vibrational spectra in other complex perovskites. Thus, it became necessary to explain the accumulated experimental data using a theoretical calculation of the lattice dynamics.

$BaMg_{1/3}Ta_{2/3}O_3$ has an ordered trigonal phase as well as a disordered cubic phase depending on the preparation temperature [9]. This work is devoted to studying lattice dynamics, vibrational spectra, and electronic band structure of the BMT in the trigonal phase. The theoretical calculation was performed within the framework of the plane-wave basis based on the density functional theory in the CASTEP software package. The experimental data were taken as initial data (lattice parameters, atomic positions). The cell geometry was optimized by minimizing the total energy. To minimize the energy, we used the Broyden-Fletcher-Goldfarb-Shanno (BFGS) algorithm. The $E_{cu}t$ has been chosen to be 990 eV. A Monkrost-Pack 3x3x2 k-point grid was applied. The convergence of the total energy was $1x10^{-7}$ eV/atom. We have used norm-conserving potentials for all atoms. Then the lattice dynamics was calculated in Γ, A, H, K, M, L highly symmetrical points of the Brillouin zone. The DFT calculations show the trigonal phase of the BMT is stable. The calculation results were analyzed in comparison with the experiments. The calculations are in good agreement with the experimental data.

Krylova S. N. thanks the Russian Foundation for Basic Research and DFG project number No 21-52-12018 for partial financial support.

1. R. Guo, A.S. Bhalla, L.E. Cross, *J. Appl. Phys.* **75**, 4704 (1994).
2. H.F. Cheng, Y.C. Chen, G. Wang, et al., *J. Eur. Cer. Soc.* **23**, 2667 (2003).
3. R. Tao, et al., *J. Raman spectrosc.* **27**, 873 (1996).
4. D. Grebennikov, P. Mascher, *J. Mater. Res.* **26**, 1116 (2011).
5. S.N. Gvasaliya, B. Roessli, D. Sheptyakov, *Eur. Phys. J. B-Cond. Matter and Complex Syst.* **40**, 235 (2004).
6. J.H. Ko, S. Kojima, S.G. Lushnikov, *Appl. Phys. Lett.* **82**, 4128 (2003).
7. D.A. Sagala, S. Koyasu, *J. Am. Cer. Soc.* **76**, 2433 (1993).
8. A. Cervellino, et al. *Phys. Rev. B* **86**, 104107 (2012).
9. S. Janaswamy, G.S. Murthy, E.D. Dias, V.R.K. Murthy, *Mater. Lett.* **55**, 414 (2002).

O15

Non-steady-state photo-EMF for studying the effect of photoinduced conductivity in a periodically poled 5%MgO:$LiNbO_3$ crystal

M.A. Bryushinin[1], V.V. Kulikov[1], I.A. Sokolov[1], E.N. Savchenkov[2], N.I. Burimov[2], S.M. Shandarov[2], A.R. Akhmatkhanov[3], M.A. Chuvakova[3], V.Ya. Shur[3]

[1]*Ioffe Institute, St. Petersburg, Russia*
[2]*Tomsk State University of Control Systems and Radioelectronics, Tomsk, Russia*
rossler@mail.ru
[3]*School of Natural Sciences and Mathematics, Ural Federal University, Ekaterinburg, Russia*

The effects of photoinduced conductivity during sub-bandgap illumination for the Bragg electrooptical diffraction on periodic domain structures (PDS) in 5%MgO:$LiNbO_3$ crystal with the walls inclined to the its polar axis at the angle $\alpha = \pm 0.31°$ has recently been demonstrated [1]. In this report, we present the direct method of non-steady-state photo-EMF for studying of photoconductive parameters of the above-mentioned PDS, which is based on registration of alternating current occurring in a photoconductive material illuminated by an oscillating interference pattern [2].

The schematic configuration for experimental observation of the non-steady-state photo-EMF is shown in Figure 1. The single-frequency laser beam with wavelength of $\lambda = 457$ nm and power of $P_{out} = 200$ mW is split into two beams, one of which is phase-modulated with amplitude $\Delta = 0.36$ using an electro-optical modulator. The beams are forwarded at a specified angle to the crystal with PDS, where an interference pattern is formed with average intensity I_0, contrast $m = 0.26$ and spatial frequency K. The laser emission has the polarization vector along the X axes that is perpendicular to the incidence plane. The current occurring in the crystal creates the voltage drop on load resistor $R_L = 1.0$ MΩ (or 100 kΩ for a frequency range up to 150 kHz). This voltage drop is amplified and then measured by selective voltmeter.

In the experiments we have studied the same PDS in the crystal 5%MgO:$LiNbO_3$ as in [1] with inclined walls and a period of 8.79 μm. Specimen dimensions are 8.0×2.0×1.0 mm^3 along the X, Y, and Z axes, respectively. Electrodes are applied to the sides (8.0×2.0 mm^2) using silver paste. The recorded grating vector and excited transient holographic current are parallel to the polar axis of the crystal.

In the experiment on the identification of the phase of registered signal it was established that this PDS is characterized by n-type of conductivity. Dependencies of non-steady-state photo-EMF amplitude on the modulation frequency f, which is also interference pattern oscillation frequency, are shown in Figure 2.

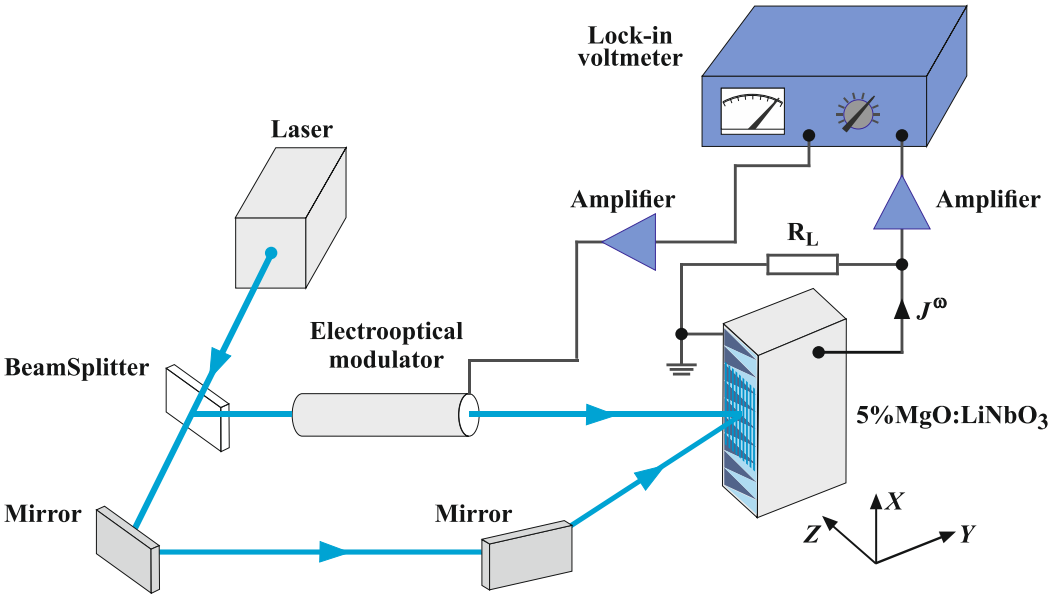

Figure 1. Non-steady-state photo-EMF effect experimentsl setup for 5%MgO:$LiNbO_3$ crystal

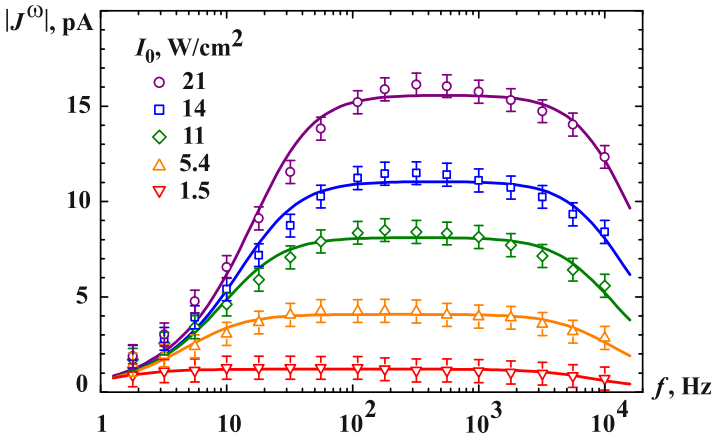

Figure 2. Frequency dependencies of non-steady-state photo-EMF amplitude measured for different light intensities $K = 1.6$ μm^{-1}

It can be seen that the experimental data (points) for non-steady-state photo-EMF current J^{ω} are in good agreement with its theoretical dependences (solid lines) on the modulation frequency [3, 4]:

$$J^{\omega} = \frac{-Sm^2(\Delta/2)\sigma_0 E_D i\omega\tau_M}{1-\omega^2\tau\tau_M + i\omega\left(\tau+\tau_M\left(1+K^2L_D^2\right)\right)}, \quad (1)$$

where S is the electrode area, σ_0 is the specific photoconductivity of the material, E_D is diffusion field, $\tau_M = \varepsilon\varepsilon_0/\sigma_0$ is the Maxwell relaxation time, τ and L_D is the electron lifetime and diffusion length, $\varepsilon = 30$ is the permittivity, ε_0 is the electric constant.

The dependencies of the signal amplitude versus the intensity and spatial frequency of the interference pattern were also studied. The analysis of these dependences allows determining the following effective photoelectric parameters of the materials of PDS in 5%MgO:LiNbO$_3$: $L_D = 0.32$ μm, $\tau_M = 8.0$ ms and $\tau = 22$ μs. Specific photoconductivity is estimated as $\sigma_0 = 3.3 \cdot 10^{-10}$ Ω^{-1}cm^{-1} at light intensity $I_0 = 21$W/cm^2.

In summary, excitation of non-steady-state photo-EMF in the PDS on the base of 5%MgO:LiNbO$_3$ crystal was performed. The registered signal demonstrated the behavior typycal for the diffusion mode of light-induced space-charge recording. Photoelectric parameters of the PDS in 5%MgO:LiNbO$_3$ crystal were determined for the light wavelength of 457 nm.

This study was funded by the Ministry of Science and Higher Education of the Russian Federation in the framework of the state assignment for 2023-2025 (job-order FEWM-2023-0012). The study was performed using the equipment provided by Ural Common Use Center ”Modern Nanotechnologies“ Ural Federal University (Reg. No. 2968) supported by the Ministry of Science and Higher Education of the Russian Federation (project 075-15-2021-677).

1. E.N. Savchenkov, et al., *Opt. Mater.* **122**, 11813 (2021).
2. M.P. Petrov, I.A. Sokolov, S.I. Stepanov, G.S. Trofimov, *J. Appl. Phys.* **68**, 2216 (1990).
3. S. Stepanov, *Academic Press, Burlington* **2**, 205 (2001).
4. I.A. Sokolov, M.A. Bryushinin, *Nova Science Publishers, Inc., New York*., 229, (2017).

O16

Investigation of the oxygen vacancies distribution in non-stoichiometric PMN- based solid solutions

A.R. Lebedinskaya1, A.G. Rudskaya[2]

[1]*Academy of Architecture and Arts, Southern Federal University, 344090, Rostov-on-Don, Russia*
lebed1989@rambler.ru

[2]*The Department of Physics, Southern Federal University, 344090, Rostov-on-Don, Russia*

The wide application of relaxor ferroelectrics in modern electronic sensors, converters and other electronic devices [1,2] is due to a set of unique properties observed in these materials and explains the constant interest in studying and improving the design of the properties of these materials. An intensive study of the physical properties of relaxor ferroelectrics has not yet provided an unambiguous relationship between the observed physical properties and the structure of these materials. The main factors explaining the observed relaxor properties are the compositional substitutional disorder in the positions of cations in the *A*- and *B*- sublattices and various defects and vacancies in the crystal lattice, in particular, the resulting oxygen vacancies [3].

It has been found that oxygen vacancies in relaxor ferroelectrics with the formula $A(B'B'')O_3$ affect their physical properties, while the perovskite structure is retained even at a high concentration of these oxygen vacancies [4]. The loss of negative oxygen charges in the presence of a vacancy, possibly for the preservation of electrical neutrality, includes a compensatory mechanism that causes redistribution of cations in the *A*- and *B*- sublattices. Changing the concentration and distribution of oxygen vacancies can open up an effective way to control the relaxor properties of these materials, which is the reason for the purpose of their study in this work.

In this work, the objects of study were ferroelectric ceramic samples, in which initially there was an oxygen deficiency and the ratio of cations in the *B*-sublattice was set to 1:1, which violated the electrical neutrality. Ceramics were synthesized from a mixture of *PbO*, *MgO*, and Nb_2O_5 oxides selected in appropriate proportions, corresponding to compositions: $(1-x)PbMg_{1/3}Nb_{2/3}O_3 - xPbMg_{1/2}Nb_{1/2}O_{2.75}$, where *x* varied from 0 to 1 with a step of 0.1 [5].

For all values of the parameter *x* in these samples, the perovskite structure was retained, the cell remained cubic, but a nonlinear dependence of the cell parameter *a(x)* was found.

The dielectric parameters ε and $tg\delta$ were measured, which also showed a nonlinear dependence on the parameter x: the highest values were observed at $x = 0.5 \div 0.6$. As noted by other researchers, vacancies tend to accumulate near any inhomogeneities, surfaces, and interfaces, since the energy of vacancy formation in such places can be much lower than in a homogeneous volume [6]. In places where vacancies accumulate, they can create sufficiently strong fields, which in turn can lead to the appearance of new phases in relaxors, for example, polar (ferroelectric) phases.

Further, in the work, a model analysis of the distribution of cations in the *B*-sublattice was made depending on the concentration of oxygen vacancies due to the composition of the sample. Based on the results obtained, it can be assumed that the transition to the ferroelectric phase can be caused in the relaxor by the influence of oxygen vacancies, which are elastic dipoles at some sufficiently high concentration of vacancies.

1. S. Pandya, J. Wilbur, J. Kim, et al., *Nature Materials* **17**, 432 (2018).
2. L.E. Cross, *Mater. Chem. Phys*. **43**, 108 (1996).
3. M.D. Glinchuk, E.A. Eliseev, G. Li, et al., *Phys. Rev. B* **98**, 094102 (2018).
4. S. Steinsvik, R. Bugge, J. Gjonnes, et al., *J. Phys. Chem. Solids* **58**, 969 (1997)
5. A. Lebedinskaya, *AIP Conf. Proc.* **2533**, 020046 (2022).
6. F. Wang, Z. Pang, L. Lin, et al., *Phys. Rev. B* **80**, 144424 (2009).

O17

Controlled growth of 2D nanodomain structures during switching at elevated temperatures in CLN with dielectric layer

I.A. Kipenko, M.A. Chuvakova, A.R. Akhmatkhanov, V.Ya. Shur

Institute of Natural Sciences and Mathematics, Ural Federal University, 620002, Ekaterinburg, Russia
ilya.kipenko@urfu.ru

The development of methods of self-organized formation of domain structures during polarization reversal in nonequilibrium switching conditions is an important branch of domain engineering, a field of knowledge related to creating the ferroelectric domain structures with a given geometry for various practical applications.

Lithium niobate ($LiNbO_3$, LN) is widely used for applications in nonlinear optics due to its large electro-optical and nonlinear optical coefficients. Domain engineering techniques in LN allow to create devices for light frequency conversion with record efficiency based on quasi-phase-matching effect [1].

This paper represents study of formation of quasi-regular stripe domain structures in LN single crystals during polarization reversal from initial state, consists of the 2D matrix of hexagonal domains, arranged in square or hexagonal lattices. We have studied the evolution of the domain structure during polarization reversal (1) at room temperature with free polar surface and (2) at elevated temperature with polar surface covered by an artificial dielectric layer for investigation the influence of retardation of bulk screening on domain kinetics.

In case of switching without the artificial dielectric layer in samples with a square lattice, isolated domains stretch along one of the Y crystallographic directions coinciding with the lattice basis vector of the 2D structure [2]. It is shown that the velocities of the domain walls in samples with 2D structure exceed the velocities of domain walls with the same orientation in monodomain samples by orders of magnitude [3,4].

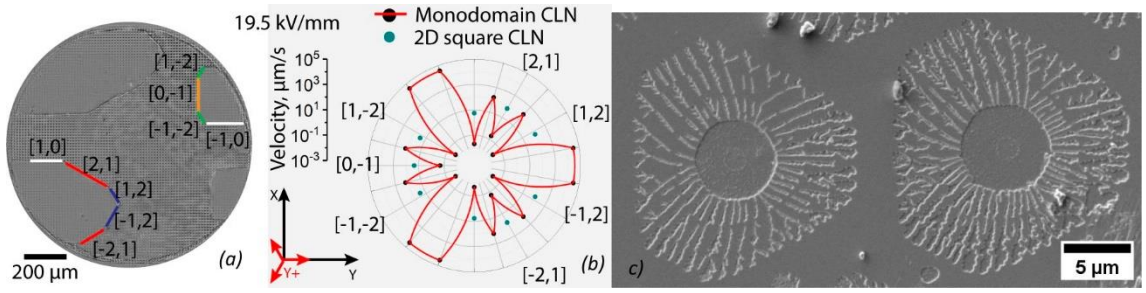

Figure 1. (a)-(b) Domain walls, observed in CLN with square matrix of domains during switching in room temperature (E_{ex} = 19.5 kV/mm): (a) main types of domain walls; (b) comparison of Wulff plots (angular dependences of domain wall velocity) for square matrix CLN and monodomain CLN; (c) SEM images of domain structure revealed by selective chemical etching in CLN with hexagonal domain matrix covered by dielectric layer after switching at 300°C.

During polarization reversal in LN with an artificial dielectric layer at 300°C, submicron domain rays with a width of about 300 nm and a period about 800 nm are formed at the domain walls of hexagonal domains. The rays are oriented mainly along Y crystallographic directions. A branching process was observed at a ray spacing of more than 1 µm. It is shown that the quasi-regular structure is formed in the near-surface layer with a thickness of about 15 µm.

The equipment of the Ural Center for Shared Use “Modern Nanotechnology” UrFU was used. The research funding from Russian Science Foundation (21-72-10160) is gratefully acknowledged.

1. V.Ya. Shur, A.R. Akhmatkhanov and I.S. Baturin, *Appl. Phys. Rev.* **2**, 040604 (2015).
2. I.A. Kipenko et al., *Ferroelectrics* **604**, 40 (2023).
3. A.A. Esin, A.R. Akhmatkhanov, V.Ya. Shur, *Appl. Phys. Lett.* **114**, 192902 (2019).
4. A.R. Akhmatkhanov et al., *Appl. Phys. Lett*. **117**, 022903 (2020).

O18

Domain growth in the bulk in lithium tantalate with charged domain wall

E.D. Greshnyakov, M.A. Chuvakova, A.D. Ushakov, A.R. Akhmatkhanov,

M.S. Kosobokov, V.I. Pryakhina, M.S. Nebogatikov, V.Ya. Shur

School of Natural Sciences and Mathematics, Ural Federal University, 620000, Ekaterinburg, Russia
Corresponding author e-mail: evgeny.greshnyakov@urfu.ru

The experimental observation of polarization reversal in the bulk lithium tantalate ($LiTaO_3$, LT) plate with a charged domain wall in uniform electric field was demonstrated.

Congruent crystals LT (CLT) grown by the Czochralski method have a deviation of Li concentration (c_{Li}) about 1.5 mol.% compared the stoichiometric composition (SLT, c_{Li} = 50 mol.%) [1]. Postgrowth annealing of z-cut CLT plate in Li-rich powder (60 mol.% Li_2CO_3 + 40 mol.% Ta_2O_5) at 1100-1300 ℃ was used for change c_{Li} in the bulk along polar direction [2]. The dependence of $c_{Li}(z)$ was measured by confocal Raman microscopy [2].

Annealing was performed at a temperature above Curie temperature thus during cooling a ferroelectric phase transition occurred. As a result, in the absence of an external field, a charged domain wall (CDW) is formed at the place where the composition gradient changes sign, since this gradient acts as an internal bias field [2].

The static domain structure (DS) was imaged using optical microscopy after selective chemical etching in HF for 3–5 min. DS imaging in the bulk was carried out by the Cherenkov-type second harmonic generation microscopy [3].

Transparent indium tin oxide electrodes were deposited on the polar surfaces of the sample by ion-plasma sputtering. The polarization reversal was carried out in a constant field at elevated temperature (350℃). Rectangular field pulses with an amplitude of 1–2 kV/mm and a duration of 10 – 40 s were applied. *In situ* imaging of the DS evolution at the polar surface was carried out in transmitted polarized light with an image recording frequency of 500 to 1000 frames/s.

The first experimental study of the polarization reversal in uniaxial ferroelectric with a CDW by formation and forward growth in the bulk of ledges at the wall. An analysis of the time dependence of the area fraction occupied by domains on the polar surface was realized using modification of Kolmogorov-Avrami approach. The main stages of the DS evolution on the polar surface during the decay of a CDW including formation of a domain maze have been revealed. The obtained results are attributed to the spatially inhomogeneous decrease in the screening efficiency of the depolarization field during shift of the CDW in the applied field. It was shown by COMSOL simulations that the local values of residual depolarization field increase with increase of the local curvature of the CDW. This fact allows to explain the formation of ledges at the tops of the teeth of a real CDW, which leads to appearance of isolated domains on the polar surface.

The equipment of the Ural Center for Shared Use “Modern nanotechnology” Ural Federal University (Reg. no. 2968), which is supported by the Ministry of Science and Higher Education RF (Project no. 075-15-2021-677), was used.

1. D.S. Hum, et al., J. *Appl. Phys.* **101**, 093108 (2007).

2. E.D. Greshnyakov, et al., *Ferroelectrics* **604**, 31 (2023).

3. Y. Sheng, et al., *Optics Express* **18**, 16539 (2010).

O19

Hierarchical nanopatterns inscribed by femtosecond laser pulses in lithium niobate

M. Kosobokov[1], S. Kudryashov[1,2], A. Rupasov[2], A. Akhmatkhanov[1], G. Krasin[2], P. Danilov[1,2], B. Lisjikh[1], A. Turygin[1], A. Abramov[1], E. Greshnyakov[1], E. Kuzmin[2], M. Kovalev[1,2], A. Efimov[1], V. Shur[1]

[1]*School of Natural Sciences and Mathematics, Ural Federal University, 620000 Ekaterinburg, Russia*
[2]*Lebedev Physical Institute, 119991 Moscow, Russia*
mihail.kosobokov@urfu.ru

The ultrafast interaction of tightly focused femtosecond laser pulses with bulk ferroelectric media in direct laser writing (inscription) regimes is known to proceed via complex multi-scale light, plasma and material modification nanopatterns, which are challenging for exploration owing to their mesoscopic, transient and buried character.

In this study, we report on the experimental demonstration and analysis of hierarchical multi-period coupled longitudinal and transverse microtracks and nanogratings in bulk lithium niobate inscribed in the focal region by 1030 nm, 300 fs laser pulses in the recently proposed sub-filamentary laser inscription regime [1]. The longitudinal Bragg-like topography nanogratings, possessing the laser-intensity-dependent periods ≈ 400 nm, consist of transverse birefringent nanogratings, which are perpendicular to the laser polarization and exhibit much smaller periods ≈ 160 nm. Near nanostructured microtracks ferroelectric nanodomains were formed in the bulk [2]. The microtracks and related nanodomains were imaged by optical, scanning probe and confocal second-harmonic generation microscopy methods. The nanoscale material sub-structure in the microtracks was visualized in the sample cross-sections by atomic force microscopy (AFM). The piezoresponce force microscopy (PFM) revealed sub-100 nm ferroelectric domains formed in the vicinity of the embedded microtrack seeds, indicating a promising opportunity to arrange nanodomains in the bulk ferroelectric crystal in on-demand positions. Our analysis and modeling support the photonic origin of the longitudinal nanogratings, appearing as prompt electromagnetic and corresponding ionization standing waves in the pre-focal region due to interference of the incident and plasma-reflected laser pulse parts. The transverse nanogratings could be assigned to the nanoscale material modification by interfacial plasmons, excited and interfered in the resulting longitudinal array of the plasma sheets in the bulk dielectric material. Our experimental findings provide strong support for our previously proposed mechanism of such hierarchical laser nanopatterning in bulk dielectrics, giving important insights into its crucial parameters and opening the way for directional harnessing of this technology.

This research was funded by the Ministry of Science and Higher Education of the Russian Federation (Ural Federal University Program of Development within the Priority-2030 Program). The equipment of the Ural Center for Shared Use “Modern nanotechnology” Ural Federal University (Reg. no. 2968), which is supported by the Ministry of Science and Higher Education RF (Project no. 075-15-2021-677), was used.

1. S. Kudryashov, et al., *Nanomaterials* **12**, 4303, (2022).

2. S. Kudryashov, et al., *Nanomaterials* **12**, 4147, (2022)

O20

Formation of ferroelectric domains in MgO-doped lithium niobate by femtosecond laser irradiation

B.I. Lisjikh, M.S. Kosobokov, A.V. Efimov, D.K. Kuznetsov, V.Ya. Shur

School of Natural Sciences and Mathematics, Ural Federal University, 620002, Ekaterinburg, Russia
boris.lisikh@urfu.ru

The interest of ferroelectrics using is related with possibilities of development of microresonators [1], and laser frequency convertors [2] and piezoactuators [3] due to the creating of stable micro- and nanodomain patterns which is a field of domain engineering. Creating of domains because of ultrashort laser pulses influence represents a perspective method of domain engineering allowing realization of polarization reversal in the bulk and creating of three-dimensional domain structures.

Lithium niobate crystals are widely applied in photonics, due to the outstanding nonlinear-optical and electrooptical properties. MgO-doped lithium niobate (MgO:LN) owing less polarization switching fields and higher optical damage threshold comparing to congruent LN has been chosen as a studying material.

1-mm thick single-domain MgO:LN plates cut perpendicular to the polar axis were fixed at the motorized table for local laser inscription. Yb-fiber system TETA-10 (Avesta Project, Russia) emitting irradiation at the wavelength of 1030 nm, 240 fs pulse duration, 100 kHz frequency and pulse energies 2.7-12 μJ was used as source of laser irradiation. Laser beam propagated along polar axis and was focused by the microobjective (50x, NA = 0.65) at depths 200 – 800 μm.

To visualize microtracks and domains in the bulk and on the surface three methods were used: 1) optical microscopy (Olympus BX-61, Olympus, Japan), 2) Cherenkov-type second harmonic generation confocal microscopy (Ntegra Spectra, NT-MDT, Russia), 3) scanning electron microscopy (EVO LS 10, Carl Zeiss, Germany) after selective chemical etching.

It was shown that microtracks representing modified crystal areas with length about 50 μm formatted in the bulk because of focused laser irradiation action. Using optimal values of focusing depth and pulses energy allowed to realize ferroelectric domains growth from microtracks. Domains grown to the surface had typical for LN crystals hexagonal shape.

Domain growth and formation were attributed to the action of spatial nonuniform pyroelectric field, emerging during the cooling after the local heating by laser pulses [4,5].

The results represent the great interest for domain engineering methods development and using them in photonics due to the allowing to realize creating of periodical domain structures without using of external electric field.

1. J Lin., Y. Xu, M. Wang, et al., *Sci. Rep.* **5**, 8072 (2015).
2. X. Chen, P. Karpinski, V. Shvedov, et al., *Opt. Lett.* **41**, 2410 (2016).
3. E.D. Greshnyakov, V.I. Pryakhina, B.I. Lisjikh, et al., *Ferroelectrics* **592**, 26 (2022).
4. V.Ya. Shur, M.S. Kosobokov, A.V. Makaev, et al., *Acta Materialia* **219**, 117270 (2021).
5. B.I. Lisjikh, M.S. Kosobokov, A.V. Efimov, et al., *Ferroelectrics* **604**, 47 (2023).

O21

Self-organization of magnetic domain structures under the action of an alternating magnetic field

D.S. Mekhonoshin, L.A. Pamyatnykh

[1]*Ural Federal University, 620026, Ekaterinburg, Russia*
dmitry.mehonoshin@urfu.ru

Magnetic domain structures in thin films have gained importance because of the promise of new types of spintronic devices [1]. The formation of ordered structures from initially disordered domain patterns is known as self-organization of magnetic domains. The spontaneous nucleation of dynamic spiral domains (Fig. 1a) from a labyrinthine domain pattern in iron garnet films subjected to an alternating magnetic field is one of the most impressive examples of such self-organization processes [2]. Chains of magnetic spiral domains (Fig. 1b) are formed by simultaneous action of homogeneous oscillating field and constant gradient magnetic field [3].

The spontaneous nucleation of spiral domains has been studied experimentally and by numerical simulation. The phase field model [4-5] was used to numerically simulate the dynamics of the domain structure of a thin magnetic film. The scalar continuous 2D variable $\varphi(\mathbf{r})$ represents a normal component of the reduced magnetization of the film. The Hamiltonian of the model has the form

$$H = \int \left(\frac{a}{2} |\nabla \varphi(\mathbf{r})|^2 - \frac{k}{2} \varphi(\mathbf{r})^2 - h(t)\varphi(\mathbf{r}) + \int \varphi(\mathbf{r})\, \varphi(\mathbf{r}') G(\mathbf{r}, \mathbf{r}') d\mathbf{r}' \right) d\,\mathbf{r}\,,$$

where each of the terms is related to the exchange interaction, the perpendicular magnetic anisotropy, the interaction with an external magnetic field and the magnetostatic interaction, respectively. The equation of the model dynamics is

$$\frac{\partial \varphi}{\partial t} = (1 - \varphi(\mathbf{r})^2) B,$$

where the effective magnetic field is $B = -\delta H / \delta \varphi$.

In the simulation, a disordered labyrinthine domain structure was obtained from a bubble phase as a consequence of a series of shape instabilities. The dynamic spiral domain (Fig. 1c) was formed under the action of an alternating magnetic field. The formation of topologically different dynamic domain structures was revealed within the framework of a 2D scalar phase field model.

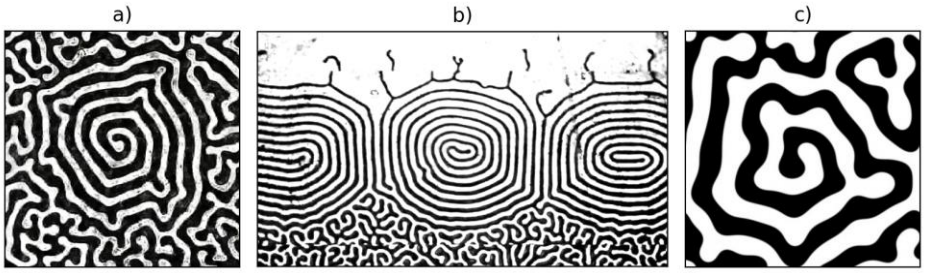

Figure 1. (a) The dynamic spiral domain in iron garnet $(YLuBi)_3(FeGa)_5O_{12}$ film in uniform oscillating magnetic field with frequency f = 2400 Hz and amplitude $H_0 = 40$ Oe. (b) The chain of dynamic spiral domain in iron garnet $(YLuBi)_3(FeGa)_5O_{12}$ film in an oscillating magnetic field (f = 5000 Hz, $H_0 = 30$ Oe) and constant gradient magnetic field ($\mathrm{grad}\, \boldsymbol{H} = 710$ Oe/cm). (c) The snapshot of the simulated domain pattern. The parameters of the model: $a = 8 \cdot 10^{-4}$, $k = 2.5$, $h(t) = h_0 \sin(\omega t)$, $h_0 = 0.55, \omega = 4.2 \cdot 10^{-3}$.

This work was performed within the framework of the state assignment of the Ministry of Science and Higher Education of the Russian Federation (Project FEUZ 2023-0020).

1. D. Kumar, T. Jin, R. Sbiaa et al., *Phys. Rep.* **958**, 1 (2022).
2. G.S. Kandaurova, *Phys.-Usp.* **45**, 1051 (2002).
3. A.G. Pashko, et al., *Solid State Phenom.* **168**, 227 (2011).
4. E.A. Jagla, *Phys. Rev. B* **72**, 094406 (2005).
5. D. Andelman, R.E. Rosensweig, *J. Phys. Chem. B* **113**, 3785 (2009).

O22

Field induced domain kinetics in calcium orthovanadate crystals with charged domain walls

V.V. Yuzhakov[1], E.V. Shishkina[1], M.A. Chuvakova[1], A.R. Akhmatkhanov[1],

M.S. Nebogatikov[1], E.A. Linker[1], L.I. Ivleva [2], V.Ya. Shur[1]

[1]*School of Natural Sciences and Mathematics, Ural Federal University, 620000 Ekaterinburg, Russia vladimir.juzhakov@urfu.ru*

[2]*Prokhorov General Physics Institute, Russian Academy of Sciences, 119991 Moscow, Russia*

Calcium orthovanadate $Ca_3(VO_4)_2$ (CVO) is a high-temperature ferroelectric with Curie temperature T_C=1110±10°C and spontaneous polarization value $68*10^{-2}$ C/m^2 [1]. Nominally pure and doped with rare earth elements, CVO single crystals possess the nonlinear optical properties, which make them promising materials for second harmonic generation [2, 3]. The creation of a periodic domain structure can significantly improve the efficiency of radiation frequency converters, which makes it important to study the polarization reversal in CVO.

The investigated CVO plates 0.4 mm thick were cut perpendicular to the polar axis. The polarization was switched at an elevated temperature by series of electric field pulses with strength up to 5 kV/mm and duration from 20 to 500 μs. Domain kinetics was *in situ* optically visualized with simultaneous recording of the switching current. Confocal Raman microscopy and Cherenkov-type second harmonic generation microscopy were used for domain structure visualization in the bulk.

Polarization reversal in CVO with the initial domain structure consisting of isolated domains with charged domain walls (CDWs) located in the bulk proceeded via formation of the ledges on the CDW and their growth in the polar direction. The shape and size of isolated domains appeared on the polar surface remained constant upon further switching.

The most surprising feature of the obtained domain kinetics is that the domain appearance at the surface continues for minutes after termination of the field pulse application [4]. This fact can be attributed to the CDW unstable state formed as a result of application of the field pulses series. The stability of CDW at the initial state is due to effective bulk screening of the depolarization field. Application of the field pulses series leads to oscillation of the wall, decreasing of the screening efficiency and growth of ledges under the action of partially screened depolarization field [5].

Thus, in CVO crystals, the domain kinetics upon polarization reversal was experimentally studied by applying a series of electric field pulses at an elevated temperature. The observed features indicated the formation of stable domains with neutral vertical walls as a result of ledge formation at the CDW and growth to the polar surface. An anomalous discrete switching was observed for the first time after termination of the field pulses application.

The reported study was done under financial support of the Ministry of Science Higher Education of the Russian Federation (state task FEUZ-2023-0017). The equipment of the Ural Center for Shared Use “Modern nanotechnology” Ural Federal University (Reg.№ 2968) was used with the financial support of the Ministry of Science and Higher Education of the Russian Federation (Project № 075-15-2021-677).

1. A.M. Glass et al., *Ferroelectrics* **17**, 579 (1978).
2. P.S. Bechthold, J. Liebertz, *Opt. Commun.* **27**, 393 (1978).
3. I.S. Voronina, V.V. Voronov, E.E. Dunaeva et al., *J. Cryst. Growth* **555**, 125965 (2021).
4. V.V. Yuzhakov, M.A. Chuvakova, E.V. Shishkina et al., *Ferroelectrics* **604**, 99 (2023).
5. E.V. Shishkina, M.A. Chuvakova, V.V. Yuzhakov et al., *J. Appl. Phys.* **132**, 184101 (2022).

O23

Characterization of the magnetoelectric coupling in (1-x)Pb(Zr,Ti)O_3-xPb($Fe_{1/2}Nb_{1/2}$)O_3 ceramics

M.H. Lente[1], F.L. Zabotto[2], V.F. Barbosa[2], A.C.S. Pereira[1], F.R. Estrada[3], J.A. Eiras[2], V.R. Mastelaro[4]

[1]*Federal University of São Paulo, ZIP code 12231-280, São José dos Campos, Brazil*
mlente@unifesp.br

[2]*Federal University of São Carlos , ZIP code 13565-905, São Carlos, Brazil*

[3]*Brazilian Synchrotron Light Laboratory , ZIP code 3085-970, Campinas, Brazil*

[4]*University of SãoPaulo , ZIP code 13563-120, São Carlos, Brazil*

Single phase magnetoelectric multiferroic materials are a prominent class of compounds due to their high potential impact on the developing of novel multifunctional devices such as sensors, non-volatile memories and transducers [1]. Besides scare single phase multiferroic compounds at room temperature, up to now it is not clear why there are so few magnetoelectric multiferroic materials at room temperature and satisfactory models. In this work, a systematic production, characterization and phenomenological analyses of the physical properties of single phase (1-x)Pb(Zr,Ti)O_3-xPb($Fe_{1/2}Nb_{1/2}$)O_3 ceramics (PZT-xPFN), with $0.10 \leq x \leq 0.35$ is reported. The results revealed an intriguing dependence of the magnetoelectric coupling at room temperature on the composition. For x=0.10 higher magnetic order and magnetoelectric coupling were observed at room temperature, followed by very week ones for x=0.30 and 0.35. On the other hand, within compositional range $0.10 < x < 0.30$ the samples presented neither magnetic order nor magnetoelectric coupling. The obtained results are discussed on the light of the most know theoretical models proposed in the literature.

1. Y. Lu, R. Fei, X. Lu, et al., *ACS Appl. Mater. Interfaces* **12**, 6243 (2020).
2. M.D. Glinchuk, E.A. Eliseev, A.N. Morozovska, *J. Appl. Phys.* **116**, 054101 (2014).

O24

Thermal magnetization switching in rectangular submicron Ni particles on Lithium Triborate

D.A. Bizyaev, A.A. Bukharaev, N.I. Nurgazizov, A.P. Chuklanov

Zavoisky Physical-Technical Institute, FRC Kazan Scientific Center, Russian Academy of Sciences, 420029, Kazan, Russia
a.chuklanov@gmail.com

In 2020, for the first time it was experimentally observed in our lab that it is possible to control the magnetization structure in planar multidomain square CoNi microparticles deposited on Lithium Niobate ($LiNbO_3$) single-crystal substrate when heating or cooling sample [1]. The rearrangement of the magnetization in such microparticles occurred when the sample was heated or cooled due to the thermally induced magnetoelastic effect. Since the thermal expansion coefficients of $LiNbO_3$ single crystal are significantly different along mutually perpendicular axes, a change of sample temperature by only a few tens of degrees leads to the induction of uniaxial magnetoelastic anisotropy in ferromagnetic microparticles. This made it possible to form a quasi-homogeneous magnetization in a lower external magnetic field and to significant decrease of the switching field [2].

Changing the temperature of the sample is used in Heat-Assisted Magnetic Recording (HAMR). In this case, it is necessary that, after magnetization reversal, the quasi-homogeneous state of microparticle magnetization with new orientation be stable after the external magnetic field was turned off and temperature is lowered to the initial value [3]. For these purposes, a submicron single-domain particles with configurational shape anisotropy are suitable [4]. It is possible to rotate the quasi-homogeneous magnetization in it by 180º by heating the heterostructure and applying external magnetic field to it. Obviously, the ferromagnetic metals and alloys with a large value of the magnetostriction constant should give a stronger thermally induced magnetoelastic effect. In addition, there should also be a small saturation magnetization. When compared CoNi and alloys of common ferromagnetic metals, the nickel is most suitable choice [5]. For increasing the effect, substrates with bigger difference in the thermal expansion coefficients along mutually perpendicular axes in compare to $LiNbO_3$ single-crystal are needed. As an alternative, a Lithium Triborate (LiB_3O_5) single crystal can be used as substrate.

In this work, the Ni particles of size 900×300×30 nm were formed on the surface of optically polished LiB_3O_5 single crystal (by HG Optronics). According to manufacturer's data, the temperature expansion coefficients along different axes of the single crystal differ by a factor of 3 (for $LiNbO_3$ the factor is 2). A solid Ti film 5 nm thick was preliminarily deposited onto the LiB_3O_5 surface. To remove the electrostatic charge during the experiments, this film was grounded. The deposition of solid Ni film on LiB_3O_5 with Ti cover was carried out at 32 ºC in ultrahigh vacuum in an Omicron Multiprobe P. The Ni particles were engraved from the continuous film by scanning probe lithography. The Ntegra Scanning Probe Microscope and a D300 diamond probe (SCDprobes) was used for these purposes. 18 particles were made.

The image from atomic-force microscope (AFM) of 5 of 18 Ni particles is shown on Fig. 1a. During registration in magnetic force microscope (MFM), it was possible to set and maintain the sample temperature and apply in-plane constant external magnetic. On all MFM images, all the 18 particles were recorded simultaneously. The magnetic field was directed along the long side of the particles. MFM measurements were carried out using a single-pass technique. This made it possible to reduce the influence of probe on the magnetization distribution in particles. At the initial state, the particles were magnetized by a field of -20 mT. The obtained MFM image corresponded to single-domain particles (Fig. 1b) magnetized in one direction. Next, the magnetic field was increased stepwise in the opposite direction from 0 to +20 mT. A series of experiments was carried out at sample temperatures of 25, 35 and 45 ºC. The switching of the magnetization of a particle was detected by a change in its MFM image, when the magnetic contrast was rotated by 180º (Fig. 1*c*).

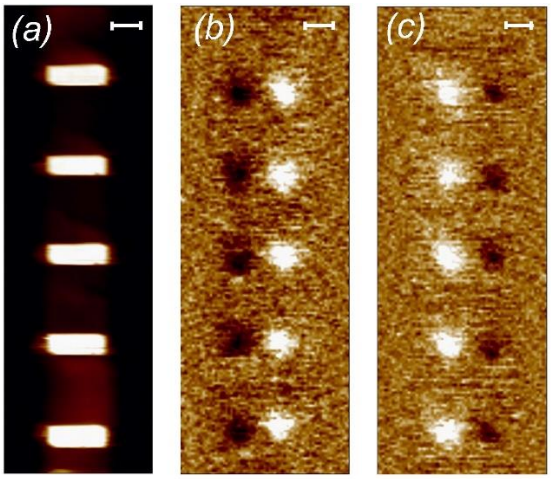

Figure 1. AFM image of 5 out of 18 Ni particles – (a), MFM images of the particles at the initial state – (b) and after magnetization reversal – (c). Scale bar is 500 nm. The range of contrast for (a) is 45 nm, (b) and (c) is 1º.

The number of particles that changed its magnetization orientation to the opposite was determined from MFM images. The graphs of the increase in the number of remagnetized particles with an increase of external magnetic field at certain temperature are shown on Figure 2. Since the Ni particles had certain deviations in size and shape, the values of their switching fields have a spread. From the dependences, one can make a conclusion about the influence of temperature on the switching field. The average value of this parameter is determined as field at which the maximum amount of particles is switched into new magnetization orientation. It is decreased with increasing temperature and is 12, 10 and 8 mT at 25, 35 and 45 ºC, respectively.

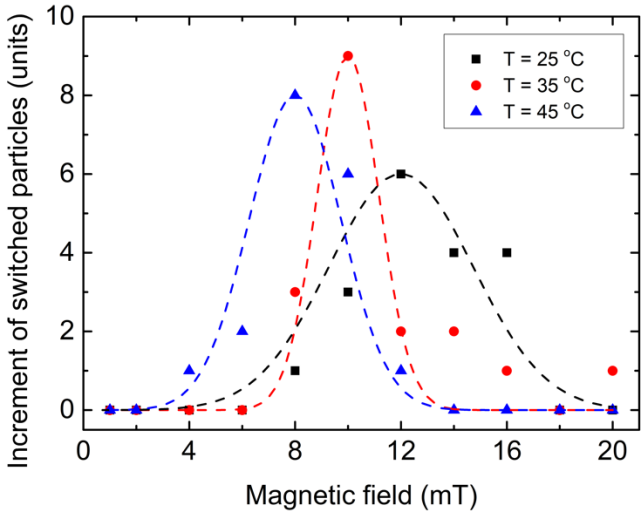

Figure 2. Increasing the number of remagnetized Ni particles as a function of external magnetic field at different sample temperature. The dashed lines are gauss-approximation curves, it used for determination of average switching field for each temperature.

When the magnetization reversal of the entire particles took place, the heating of sample and the external magnetic field were successively switched off. After that, the particles held their new magnetization direction due to the shape anisotropy.

The work supported by RSF (grant № 23-29-00085).

1. D.A. Bizyaev, A.A. Bukharaev, A.P. Chuklanov, et al., *Phys. Status Solidi - RRL* **14**, 2000256 (2020).
2. D.A. Bizyaev, N.I. Nurgazizov, A.A. Bukharaev, V.Ya. Shur, et al., *Phys. Solid State* **63**, 1427 (2021).
3. W.-H. Hsu, R.H. Victora, *J. Magn. Magn. Mater.* **563**, 169973 (2022).
4. A.A. Bukharaev, A.K. Zvezdin, A.P. Pyatakov, Y.K. Fetisov, *Phys. – Usp.* **61**, 1175 (2018).
5. N.I. Nurgazizov, D.A. Bizyaev, A.P. Chuklanov, V.Ya. Shur, et al., *Phys. Solid State*, **64**, 1305 (2022).

O25

Linking exchange bias with the formation of the antiferromagnetic phase in thin films with Cr-Mn

M.E. Moskalev[1], A.A. Feshchenko[1], E.A. Kravtsov[2,3], E.V. Kudyukov[1], V.N. Lepalovskij[1], V.O. Vas'kovskiy[1,2]

[1]*Institute of Natural Sciences and Mathematics, Ural Federal University, 620026, Ekaterinburg, Russia*
mikhail.moskalev@urfu.ru

[2]*Institute of Metal Physics, Ural Branch of the Russian Academy of Sciences, 620066, Ekaterinburg, Russia*

[3]*Institute of Fundamental Education, Ural Federal University, 620062, Ekaterinburg, Russia*

Widely believed to be the most abundant class of magnetically ordered materials, antiferromagnets, unlike ferromagnets, for a long time have not received proper scientific attention, and as such, have been left out of most research. All that despite the fact, that antiferromagnets have been extensively used in a variety of industrial products, such as magnetic storage devices, and a multitude of different sensors [1]. The reason for that is the ability of antiferromagnets to pin the magnetization of adjacent ferromagnetic layers in thin films, effectively displacing their hysteresis loops, thus giving rise for the exchange bias effect. Much as with the search for rare-earth-free materials for permanent magnets, there is an on-going search for antiferromagnets, that do not contain platinum-group metals [2]. One of such candidates is the antiferromagnetic Cr-Mn alloys, in bulk format displaying the Néel temperature of up to 700 K [3].

In this work we study the antiferromagnetic Cr-Mn alloys in thin magnetron-sputtered films with focus on their ability to provide the exchange bias effect. We employ a variety of X-ray diffractometry measuring geometries to thoroughly study the crystal structure of Ta/Cr-Mn/Ta films. By analyzing these results, we are able to construct a room-temperature phase diagram of Cr-Mn in magnetron sputtered films (Fig.1), assess its lattice constant and mean grain size, and draw some conclusions on the principles of its growth. We then study the magnetic properties of Ta/Cr-Mn/$Fe_{20}Ni_{80}$/Ta films, emphasizing those in which the exchange bias effect is present. Based on the results of temperature measurements, including those obtained in accordance with a specialized measurement protocol, we establish that the high value of the maximum blocking temperature, of up to 540 K, and the assessed value of the effective anisotropy constant of Cr-Mn, suggest that Cr-Mn can be considered for industrial use as a pinning layer in film heterostructures with exchange bias.

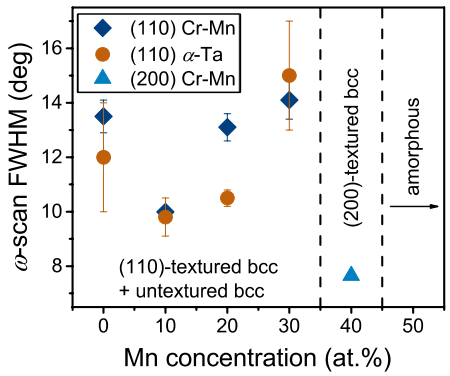

Figure 1. Manganese-concentration dependence of ω-scan FWHM and RT Cr-Mn phase diagram for Ta/Cr-Mn/Ta films.

This work was financially supported by the Russian Science Foundation, project No. 22-22-0814.

1. B. Lim, et al., *APL Mater.* **10**, 051108 (2022).
2. A. Hirohata, et al., *J. Phys. D: Appl. Phys.* **50**, 443001 (2017).
3. S. Maki, K. Adachi, *J. Phys. Soc. Jap.* **46**, 1131 (1979).

O26

Using ferroelectrics to tune the electronic and magnetic properties of heterostructures

I.I. Piyanzina[1], A.A. Evseev[1], K.V. Evseev[2], R.F. Mamin[2]

[1]*Institute of Physics, KFU, Kazan, 420008, Russia*
i.piyanzina@gmail.com

[2]*Zavoisky Physical-Technical Institute, FRC Kazan Scientific Center of RAS, Kazan, 420029, Russia*

The presence of ferroelectric as a component of heterostructure gives us new outstanding functionality which can be used in possible electronic devises based on it. Thanks to the presence of spontaneous polarization in the ferroelectric thin film, the two-dimensional gas (2DEG) can occur at the interface [1]. The electronic properties of arising state can be tuned by an external field through the ferroelectric dipoles' direction change. Besides, the presence of electrostatic field along the ferroelectric field is favorable in the possible structures with spin-orbit (SO) splitting. The control of SO splitting by ferroelectric polarization is a desirable property for spintronic applications. Natural materials demonstrating both gigantic and ideal states of Rashba are extremely rare, so computer simulations could help in this problem [2-5].

Another property which can be useful for electronic application is magnetoelectric coupling. This property is associated with possibility of controlling the ferromagnetic ordering at the interface due to interactions of spins through conduction electrons and with arising of multiferroic properties of all heterostructure. Multiferroic materials are compounds where at least two order parameters coexist in the same phase. One very important but extremely rare group is ferroelectric ferromagnets, which have recently stimulated an increasing number of research activities for their scientific uniqueness and application in the novel multifunctional devices. Magnetoelectric materials are mainly interesting due to the possibility to control magnetic properties by an external electric field. Due to the extraordinary challenge of creating multiferroic compounds, it was essential to create superlattice multicomponent materials as more efficient [6].

So, the present research dedicated to the *ab initio* study within the DFT approach [7] of heterostructures having a ferroelectric as one of the components. The aim is to investigate the possibilities of controlling the interfacial properties (2DEG, Rushba effect, ME coupling) via ferroelectric polarization.

1. V.V. Kabanov, I.I. Piyanzina, Yu.V. Lysogorskiy et al., *Mater.Res.Express* **7**, 5 (2020).
2. M. Chen, F. Liu, et al., *Natl. Sci. Rev.* **8** (2021).
3. E.I. Rashba, V.I. Sheka, *Fiz. Tverd. Tela – Collected Papers* (Leningrad) II, 162 (1959) [in Russian].
4. Yu.A. Bychkov, E.I. Rashba, *Sov. Phys. - JETP Lett.* **39**, 78 (1984) [in Russian].
5. A.D. Caviglia, M. Gabay, S. Gariglio et al., *Phys. Rev. Lett.* **104**, 126803 (2010).
6. I.I. Piyanzina, R.F. Mamin, *J. Mater. Sci.* **57**, 21620 (2022).
7. G. Kresse, J. Furthmüller, *Phys. Rev. B* **54**, 11169 (1996).

O27

Spatially-resolved study of the electronic transport and resistive switching in polycrystalline bismuth ferrite

A. Abramov, B. Slautin, V. Pryakhina, V. Shur, A. Kholkin, D. Alikin

School of Natural Sciences and Mathematics, Ural Federal University, 620000, Ekaterinburg, Russia
alexander.abramov@urfu.ru

Ferroelectric materials attract much attention for applications in resistive memory devices due to the large current difference between insulating and conductive states and the possibility of carefully controlling electronic transport via the polarization set-up [1]. Bismuth ferrite films are of special interest due to the combination of high spontaneous polarization and antiferromagnetism, implying the possibility to provide multiple physical mechanisms for data storage and operations [2]. Macroscopic conductivity measurements are often hampered to unambiguously characterize the electric transport, because of the strong influence of the diverse material microstructure.

Here, we studied the electronic transport and resistive switching phenomena in polycrystalline bismuth ferrite using advanced conductive atomic force microscopy (CAFM) at different temperatures (Fig. 1) and electric fields [3]. The new approach to the CAFM spectroscopy and corresponding data analysis are proposed, which allow deep insight into the material band structure at high lateral resolution. Contrary to many studies via macroscopic methods, postulating electromigration of the oxygen vacancies, we demonstrate resistive switching to be caused by the pure electronic processes of trapping/releasing electrons and injection of the electrons by the scanning probe microscopy tip. The electronic transport was shown to be comprehensively described by the combination of the space charge limited current model, while a Schottky barrier at the interface is less important due to the presence of the built-in subsurface charge.

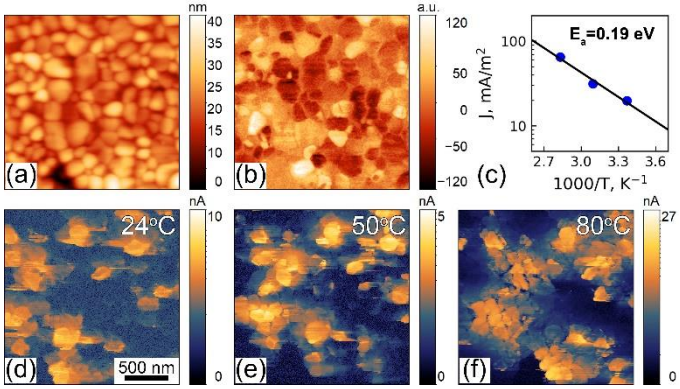

Figure 1. BFO thin film: (a) Topography, (b) out-of-plane PFM, (c) dependence of C-AFM current density (J) on reverse temperature, (d)-(f) CAFM in BFO thin film in dependence on temperature: (d) RT, (e) 50 °C, (f) 80 °C.

The equipment of the Ural Center for Shared Use "Modern nanotechnology" Ural Federal University (Reg. no. 2968), which is supported by the Ministry of Science and Higher Education RF (Project no. 075-15-2021-677), was used. The research funding from the Ministry of Science and Higher Education of the Russian Federation (Ural Federal University Program of Development within the Priority-2030 Program) is gratefully acknowledged.

1. R. Waser, M. Aono, *Nanoscience and Technology: A Collection of Reviews from Nature Journals* (World Scientific Publishing Co., Co-Published with Macmillan Publishers Ltd), pp. 158–165 (2009).

2. A. Sawa, *Mater. Today* **11**, 28 (2008).

3. A. Abramov, et al., *Sensors* **23**, 526 (2023).

O28

Superconducting spin valve Fe1/Cu/Fe2/Cu/Pb on a piezoelectric substrate PMN-PT

A.A. Kamashev, N.N. Garif'yanov, A.A. Validov, R.F. Mamin, I.A. Garifullin

[1]*Zavoisky Physical-Technical Institute, FRC Kazan Scientific Center of RAS, 420029, Kazan, Russia*
kamandi@mail.ru

The properties of a superconducting spin valve Fe1/Cu/Fe2/Cu/Pb on a piezoelectric substrate PMN-PT substrate ($[Pb(Mg_{1/3}Nb_{2/3})O_3]_{1-x}$ - $[PbTiO_3]_x$) under the influence of an electric and magnetic field have been studied. The magnitude of the shift of the superconducting transition temperature in the magnetic field H = 1 kOe equal to 150 mK was detected, while the full superconducting spin valve effect was demonstrated. Abnormal behavior of superconducting transition temperature was shown, which manifests itself in the maximum values of superconducting transition temperature with orthogonal orientation of the magnetization vectors of ferromagnetic layers, when studying the angular dependence of superconducting transition temperature in an external magnetic field (Fig. 1). This may indirectly indicate the fixation of the magnetization vector of the Fe1-layer on a PMN-PT piezoelectric substrate. It was found that with an increase in the magnitude of the applied electric field to the PMN-PT substrate, the shift in superconducting transition temperature of the Fe1/Cu/Fe2/Cu/Pb heterostructure increases. The maximum shift was 10 mK when an electric field of 1 kV/cm was applied (Fig. 2).

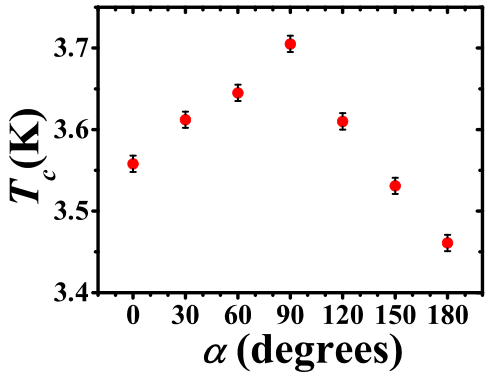

Figure 1. Dependence of T_c on the angle α between the direction of the cooling field used to fix the direction of the magnetization of the Fe1 layer and the applied magnetic field H = 1 kOe that rotates the magnetization of the Fe2 layer.

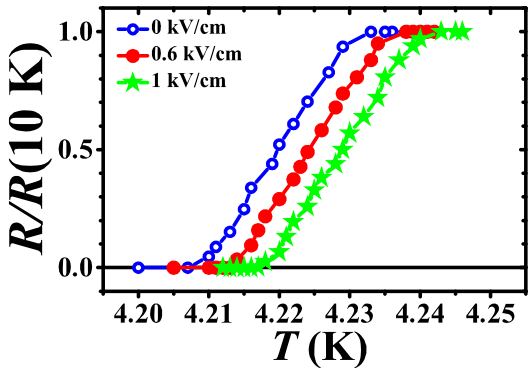

Figure 2. Superconducting transitions curves for the sample for the sample PMN-PT/Fe1(3nm)/Cu(4nm)/Fe2(1nm)/Cu(1.2nm)/Pb(60nm)/Si_3N_4 when applying an electric field to PMN-PT substrate: shift of T_c is 5 mK when applying an electric field 0.6 kV/cm; shift of T_c is 10 mK when applying an electric field 1 kV/cm. The error of the experiment corresponds to the size of the characters.

The reported study was funded by Russian Science Foundation according to the research project No. 21-72-10178.

O29

Phase evolution and relaxor to ferroelectric phase transition boosting ultrahigh electrostrains in (1-*x*)($Bi_{1/2}Na_{1/2}$)TiO_3-*x*($Bi_{1/2}K_{1/2}$)TiO_3 solid solutions

R.Y. Jing, X.Y. Wei, L. Jin

Electronic Materials Research Laboratory, Key Laboratory of the Ministry of Education & International Center for Dielectric Research, School of Electronic Science and Engineering, Faculty of Electronic and Information Engineering, Xi'an Jiaotong University, Xi'an, 710049, China
ryjing@xjtu.edu.cn

Owing to the complex composition architecture of these solid solutions, some fundamental issues of the classical (1−*x*)$Bi_{1/2}Na_{1/2}TiO_3$-*x*$Bi_{1/2}K_{1/2}TiO_3$ (BNT-*x*BKT) binary system, such as details of phase evolution and optimal Na/K ratio associated with the highest strain responses, remain unresolved. In this work, we systematically investigated the phase evolution of the BNT-*x*BKT binary solid solution with *x* ranging from 0.12 to 0.24 using not only routine X-ray diffraction and weak-signal dielectric characterization, but also temperature-dependent polarization versus electric field (*P*–*E*) and current versus electric field (*I*–*E*) curves. Our results indicate an optimal Na/K ratio of 81/19 based on high-field polarization and electrostrain characterizations. As the temperature increased above 100 °C, the *x* = 0.19 composition produces ultrahigh electrostrains (> 0.5%) with high thermal stability. The ultrahigh and stable electrostrains were primarily due to the combined effect of electric-field-induced relaxor-to-ferroelectric phase transition and ferroelectric-to-relaxor diffuse phase transition during heating. More specifically, we revealed the relationship between phase evolution and electrostrain responses based on the characteristic temperatures determined by both weak-field dielectric and high-field ferroelectric/electromechanical property characterizations (Fig. 1). This work not only clarifies the phase evolution in BNT-*x*BKT binary solid solution, but also paves the way for future strain enhancement through doping strategies.

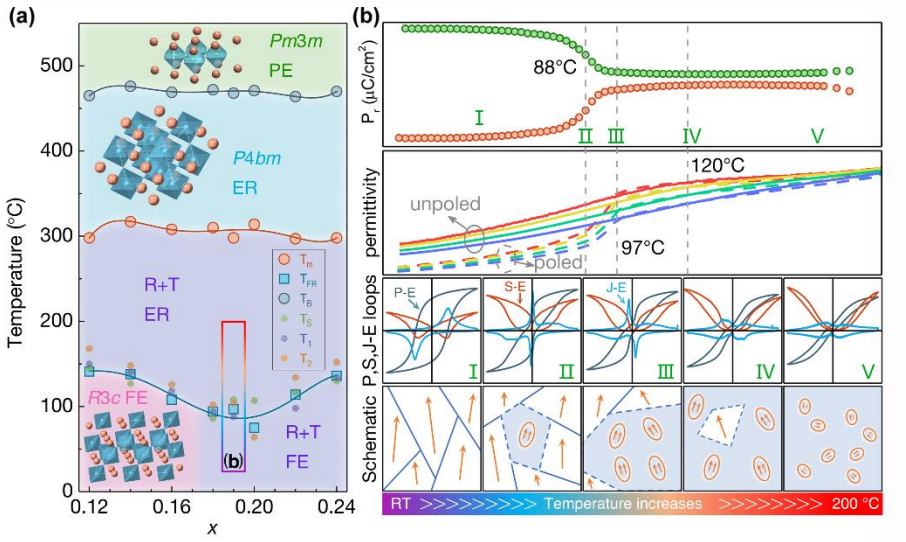

Figure 1. (a) A schematic phase diagram of BNT-*x*BKT ceramics. (b) Positive and negative remnant polarization (P_r), permittivity of the sample before and after poling as a function of temperature for BNT-0.19BKT ceramic. Corresponding the polarization versus electric field (*P*–*E*), strain versus electric field (*S*–*E*) and current density versus electric field (*J*–*E*) curves and schematic diagrams of the domain growth and reorientation under electric field at some characteristic temperatures for BNT-0.19BKT ceramic.

O30

Luminescent $MgAl_2O_4$ optical nanoceramics doped with carbon particles

A.N. Kiryakov[1], A.S. Kocyh[1], T.V. Dyachkova[2], A.P. Tyutyunnik[2]

[1]*Ural Federal University, 620002, Ekaterinburg, Russia*
arseny.kiriakov@urfu.ru

[2]*Institute of Solid State Chemistry UD of RAS, 620108, Ekaterinburg, Russia*

The current pace of development dictates the need to create promising phosphors with improved radiative characteristics. Recent advances in the field of creation and functionalization of carbon nanodots show the promise of this type of nanoparticles as a photoluminescent material for sensors, sensors, and various types of detectors [1]. The key problem in this case was and remains the task of creating bulk structures whose photoluminescent properties are determined by stabilized quantum dots. In most cases, the peculiarity of creating such materials is the need to use aggressive media to obtain a volumetric transparent medium. In this regard, the purpose of this work is the thermobaric synthesis and certification of optically transparent $MgAl_2O_4$ nanoceramics doped with carbon nanoparticles.

$MgAl_2O_4$ nanopowders synthesized by co-precipitation from a solution of aluminum and magnesium nitrates were used as the starting material. Subsequently, this powder was used to form an optical medium for carbon particles. Carbon was introduced into the nanopowder in two ways. The first one consisted in the mechanical grinding of spinel nanopowder with a graphene additive in a sapphire mortar (to exclude additional impurities due to the strong abrasive properties of spinel). The second method consisted in the synthesis of carbon nanoparticles by the wet chemistry method and subsequent impregnation of the spinel nanopowder with this solution. A mixture of spinel powders and carbon particles was subjected to quasi-hydrostatic compression at 6 GPa for 10 min and a temperature of 600 oC. As a result of thermobaric treatment, transparent $MgAl_2O_4$:C nanoceramics were formed (Fig. 1).

Figure 1. Photo of $MgAl_2O_4$:C nanoceramics.

It has been established that the mechanical milling of graphene in spinel nanopowder makes it possible to form additional PL centers, previously assigned to graphene quantum dots, characterized by a wide distribution of geometric parameters. A complex structural analysis was carried out using XRF, Raman, optical and EPR spectroscopy. Graphene nanoparticles are characterized by pronounced edge vibrations, mode D', which is apparently due to nanosized graphene inclusions [1] (Fig. 2).

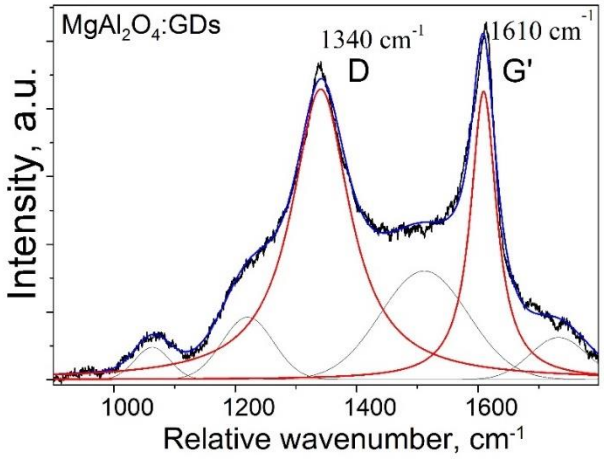

Figure 2. Raman spectrum of ceramics doped with graphene particles.

Optical ceramics with nanoparticles synthesized by wet chemistry methods also provide a wide spectral range of photoluminescence, which is not inherent in pure nanoceramics. However, the signal strength is much lower than expected. Apparently, the implemented technological process, in which the necessary operations are carried out, is not applicable for such objects and its improvements are required. more research is needed.

1. J. Liu, R. Li, B. Yang, *ACS Central Sci.* **6**, 2179 (2020).
2. L.G. Cancado et al., *Phys. Rev. Lett.* **93**, 247401 (2004).

O31

Crystallization and recrystallization of spherulite thin PZT films

I.P. Pronin

Ioffe Institute, 194021, St. Petersburg Russia,
Petrovich@mail.ioffe.ru

The physical properties of thin ferroelectric films differ significantly from the properties of their macroscopic analogues - ferroelectric single crystals or ceramic (polycrystalline) samples. To a large extent, this is due to the action of mechanical stresses caused by the difference in the temperature coefficients of linear expansion of the thin film and substrate, and in the case of epitaxial growth, with an additional contribution to mechanical stresses due to the difference in their lattice parameters. An important role is also played by the level of thin-film fabrication technology used, which makes it possible to form single-phase structures. At present, thin lead zirconate titanate films (PZT) hold absolute primacy in practical applications, and the main microelectronic substrate is silicon covered by electrodes of platinum group metals.

This paper reviews experimental studies on the features of crystallization and recrystallization of thin PZT films fabricated by RF magnetron sputtering on platinized silicon substrates ($PZT/Pt/TiO_2/SiO_2/Si$). The microstructure of the films was perovskite spherulites either with stepped (Fig. 1) or radiant growth (Fig. 2) [1,2]. The microstructure and films composition were analyzed using scanning electron microscopy, atomic force microscopy, and nonlinear optical microscopy. The results of a study of the ferroelectric properties with a change in the synthesis temperature of the perovskite phase are presented, the mechanisms of formation (growth) of spherulite islands, and the role of pores in the process of crystallization (recrystallization) of the perovskite phase are discussed. The features of the piezoelectric response of the spherulite structure and the signal of the second optical harmonic are presented and discussed.

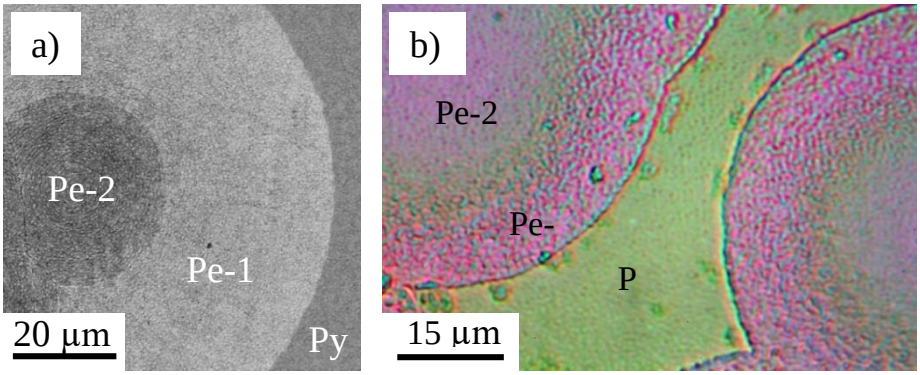

Figure 1. SEM images of spherulite crystallization and recrystallization with a stepped growth microstructure characterized by different porosity in thin PZT films .

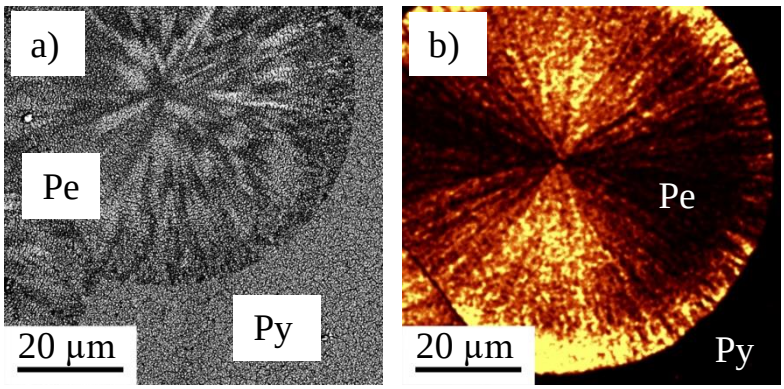

Figure 2. SEM and SHG images of radiant spherulite perovskite islands in pyrochlore matrix of PZT thin films.

1. V.P. Pronin, S.V. Senkevich, E.Yu. Kaptelov, I.P. Pronin, *J. Surf. Invest. X-ray* **4**, 703 (2010).
2. A.S. Elshin, I.P. Pronin, S.V. Senkevich, E.D. Mishina, *Tech. Phys. Lett.* **46**, 385 (2020).

O32

Synthesis of graphene on Ni and Al_2O_3 nanoparticles by chemical vapor deposition

Yu.A. Salamatov, E.A. Kravtsov, Yu.V. Korkh, Yu.S. Ponosov, A.Ye. Yermakov, M.A. Uimin, T.V. Kuznetsova

[1]*Institute of Metal Physics UB RAS, 620108, Ekaterinburg, Russia*
salamatov@imp.uran.ru

Studies of graphene (Gr), a two–dimensional allotropic modification of carbon with a thickness of one to several atomic monolayers, are currently being conducted very widely, motivated by the unique properties of graphene and the possibilities of its wide application in various fields. By present time, the synthesis of graphene by the CVD method on bulk metal (Pt, Cu, Fe, Ni) substrates is well mastered. As a novel composites and substrates, the nanopowders consisting of graphene-coated metal and dielectric nanoparticles have been of great interest, due to their unique physicochemical properties and the possibility of their wide application in various fields from catalysis to the production of biomedical materials. However, the obtaining such nanopowders is a complex and not fully solved task, and so far, researchers have managed to synthesize a small number of such systems.

In this paper, we report for the first time on the successful synthesis of Ni@Gr and Al_2O_3@Gr nanopowders. Ni and Al_2O_3 nanopowders were produced by gas condensation (flow levitation) synthesis [1]. Particle size was in (15-25) nm interval. Ni nanoparticles were covered with NiO shell as a result of passivation in air. Powders or tablets with a diameter of 4-5 mm and a thickness of 1 mm were used as initial objects. Graphene synthesis was carried out at a CVD facility using methane as a carbon source. The control of the number of deposited graphene monolayers and the degree of its defectness was carried out using Raman spectroscopy.

During the synthesis of Ni@Gr nanopowders prepared in tablet form, a reference graphene sample was simultaneously synthesized on Ni foil. Initially, the samples were annealed in a reactor at a temperature of 1075°C for 30 minutes in a hydrogen atmosphere (the gas flow was 120 cm^3/min at a pressure of 10 Torr). Graphene synthesis was carried out for 10 minutes at a temperature of 1035°C when a mixture of hydrogen and methane was fed into the reactor (flows of 120 cm^3/min and 5 cm^3/min, respectively, pressure of 10 Torr). Cooling was carried out in a flow of 200 cm^3/min of pure hydrogen at a pressure of 10 Torr.

Figures 1a and 1b show the Raman spectra measured for the foil and nanopowder at various points of the sample surface. Multilayer graphene was formed on the reference sample of nickel foil (intensity ratio $I_{2D}/I_G < 1$, the number of layers is more than 3). When synthesized on the tablet from the pressed nanocrystalline Ni-NiO powder, a complete reduction of NiO occurred with the formation of Ni@Gr nanopowders. As can be seen from the Raman spectrum in Fig. 1b, regions with two-layer ($I_{2D}/I_G > 1$) and regions with single-layer ($I_{2D}/I_G > 2$) graphene were formed. Graphite is present at some points of the sample. There are no D peaks in all Raman spectra of both samples, which indicates the absence of disorder, deformations and defects in the crystal structure of graphene.

During the synthesis, partial sintering of Ni@Gr nanopowder was detected, which can be avoided by using a mixture of Ni-NiO nanoparticles with Al_2O_3 nanoparticles. Figure 1c shows the Raman spectrum for for mix of Ni-NiO and Al_2O_3 nanopowders (1:3 mass parts) after graphene synthesis. The ratios of the heights of the 2D and G peaks in the presented spectra (Fig. 1c) correspond mainly to the two-layer graphene. At some points, the number of layers reaches 4-5. Unlike the previous samples of pure nickel, a weak D peak (~1350 cm^{-1}) appears here, which indicates the presence of minor defects in the atomic lattice of graphene. Thus, the addition of Al_2O_3 nanoparticles slightly degrades the quality of graphene and slightly increases the number of layers, but at the same time protects the Ni@Gr nanopowder from sintering.

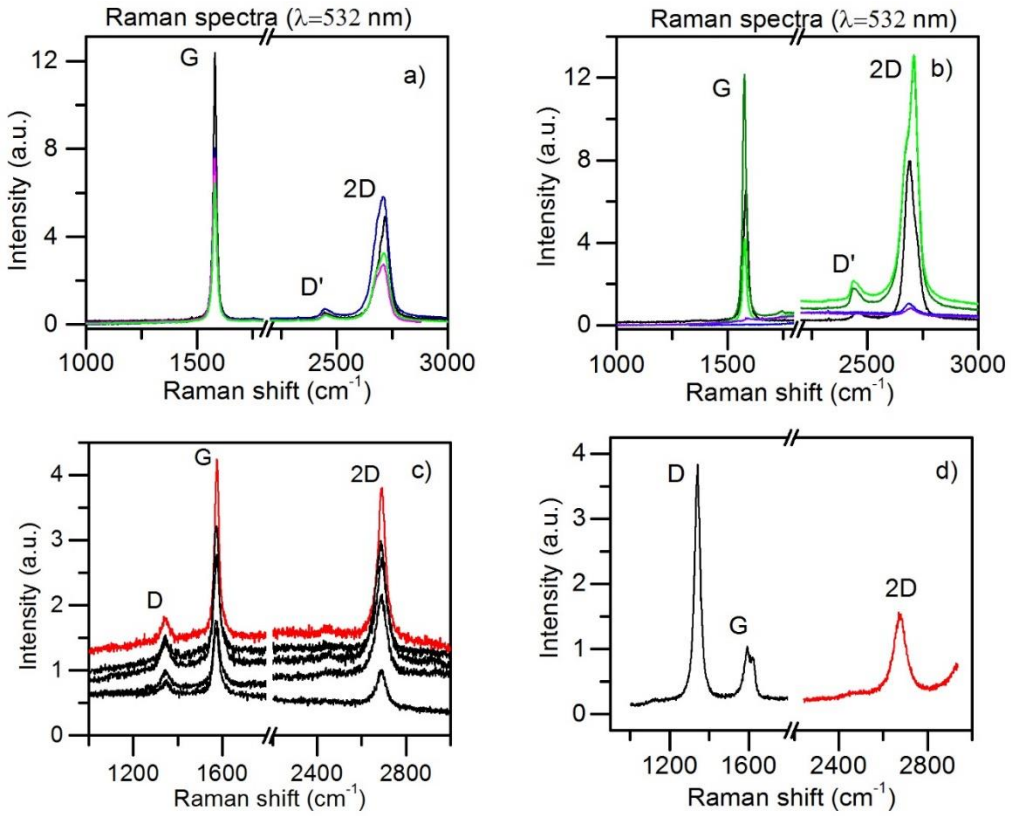

Figure 1. Raman spectra measured at various points of the samples: (a) Ni foil; (b) Ni-NiO nanopowder in the tablet form; (c) a mixture of Ni-NiO+Al_2O_3 nanopowders in the tablet form; (d) Al_2O_3 nanopowder in the tablet form.

Changing the gas flows (reducing the hydrogen flow to 50 cm^3/min and increasing methane flow to 15 cm^3/min) and increasing the exposure time (90 minutes), it is possible to obtain graphene-coated Al_2O_3 nanoparticles with a thickness of 1-2 monolayers, the Raman spectra of which are shown in Fig. 1d. The ratio of peak intensities G and 2D (Fig. 1d) indicates the presence of 1-2 layers of graphene. The large half-width of the peaks, the high peak D and the appearance of the peak D´ (next to the peak G) are due to a large number of defects. Similar results were obtained in [1].

Thus, in this work, Ni@Gr and Al_2O_3@Gr nanopowders were synthesized for the first time by chemical vapor deposition. When using Ni-NiO nanoparticles, Ni-O is completely reduced with the formation of Ni@Gr nanopowders, where the thickness of graphene is 1-2 monolayers and its defect is completely absent. Partial sintering of nanoparticles is observed, which can be avoided if a mixture of these nanoparticles with Al_2O_3 nanoparticles is used. Using larger gas flows and an extended exposure time, it is possible to obtain a graphene coating with a thickness of 1-2 monolayers on the Al_2O_3 nanoparticles, however, in this case, a significant graphene defectness is observed.

The research was carried out within the state assignment of Ministry of Science and Higher Education of the Russian Federation (theme “Spin” No. 122021000036-3, theme “Magnet” No. 122021000034-9).

1. H.J. Song, et al., *Nanoscale* **4**, 3050 (2012).

2. M.A. Uimin, et al., *Phys. Metals Metallogr.* **122** (2021).

O33

Magnetoelectric core-shell nanoparticles based on biocompatible $MnFe_2O_4$ and $Ba_{0.9}Ca_{0.1}Ti_{0.9}Zr_{0.1}O_3$ for biomedical applications

R.V. Chernozem, P.V. Chernozem, M.A. Surmeneva, A.L. Kholkin*, A.G. Pershina, R.A. Surmenev

Tomsk Polytechnic University, 634050, Tomsk, Russia

r.chernozem@mail.ru, holkin_al@tpu.ru; rsurmenev@mail.ru.

The magnetoelectric (ME) nanoparticles (NPs) are considered the most promising materials for the targeted drug delivery, theranostics, and regenerative medicine due to their unique possibility of the provision of noninvasive precise locomotion and electrical stimulation [1-2]. However, there are two important challenges, such as the usage of potentially toxic materials and sophisticated synthesis technology, which arise numerous challenges for clinical application of ME NPs as follows: biocompatibility, reproducibility, biodistribution, *etc*. Thus, the present study aims to design novel biocompatible ME NPs for biomedical applications using simple and cost-effective technology.

ME core-shell NPs were formed via microwave-assisted hydrothermal synthesis. First, to avoid NPs agglomeration, an *in-situ* synthesis of biocompatible magnetic $MnFe_2O_4$ (MFO) cores with their surface functionalization using citric acid was performed at 175°C for 30 min. Second, the biocompatible perovskite $Ba_{0.9}Ca_{0.1}Ti_{0.9}Zr_{0.1}O_3$ (BCZT) shell was fabricated at 225°C for 3h. To exclude non-magnetic phases, all NPs after the formation was washed out using magnetic separation. The morphology, structure, composition and physical properties of ME NPs was characterized using transmission electron microscopy, Raman spectroscopy, X-ray photoelectron spectroscopy, magnetometer and atomic force microscopy (AFM). The cytotoxicity of NPs was studied using MTT-test.

The analysis of the morphology and internal structure confirmed the formation of quasi-spherical ME core-shell NPs with BCZT shell thickness of ~20 nm on the surface of MFO cores with the size of 38.5±16.2 nm. The structural analysis revealed the formation of the typical spinel and perovskite structure for MFO and BCZT, respectively. The phase ratio between MFO and BCZT in ME NPs was 39%/61%, respectively. The formation of the BCZT shell resulted in the reduced average magnetization and increased coercivity force of MFO cores from 41.4±1.2 emu/g to 6.1±0.2 emu/g and from 46±3 Oe to 69±5 Oe, respectively. MTT-test demonstrated the absence of the toxicity of the developed ME NPs on the cells, such as fibroblasts and cancer cells.

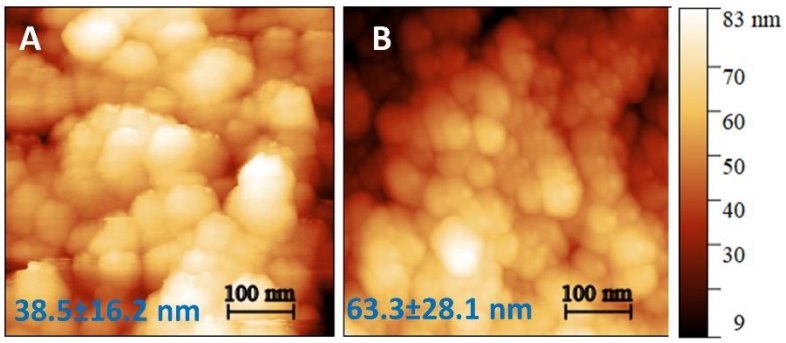

Figure 1. AFM images of (A) MFO and (B) ME core-shell MFO@BCZT NPs.

The developed novel biocompatible ME NPs can be considered as a promising platform for the theranostics and other biomedical applications.

The work was financially supported by the Ministry of Science and Higher Education (#075-15-2021-588 from 1.06.2021) and Russian Science Foundation (project #23-23-00511). Authors thank Dr. D.V. Wagner and Dr. K.N. Romanyuk for the assistance with the NPs characterization.

1. X.Z. Chen, et al., *Adv. Mater.* **29**, 8 (2017).
2. F. Mushtaq, et al., *Adv. Func. Mater.* **29**, 12 (2019).

POSTER

PRESENTATIONS

P1

Thermophysical properties of relaxor ceramics $PbFe_{0.5}Nb_{0.5}O_3$

S.N. Kallaev, A.G. Bakmaev, Z.M. Omarov

Institute of Physics, Dagestan Federal Research Center, Russian Academy of Sciences, Makhachkala, Russia
bakmaev@mail.ru

In recent years, a class of materials - ferroelectrics-relaxors, in which a magnetic structure (multiferroics) is realized, has attracted considerable interest from researchers. They have both magnetic and electrical ordering and are promising materials for solid-state electronics. One of the classic model objects for studying such materials is lead ferroniobate $PbFe_{0.5}Nb_{0.5}O_3$ (PFN) perovskites. $PbFe_{0.5}Nb_{0.5}O3$ ceramic samples were obtained using conventional ceramic technology. X-ray diffraction measurements at room temperature showed that the samples are single-phase and have a cubic (space group Pm3m) perovskite structure.

The thermophysical properties of the $PbFe_{0.5}Nb_{0.5}O_3$ ferroelectric in the temperature range of 300÷800 K are studied. As can be seen from the figures, in the temperature dependences of the heat capacity of PFN in the temperature range T_c≈380K, an anomaly of the ferroelectric phase transition is observed, which has a "smeared" character characteristic of relaxors. At high temperatures of 670 K, the dependences $C_p(T)$ of PFN exhibit an anomalous behavior characteristic of phase transformations. Possibly, nanopolar regions begin to appear in the PFN relaxor ceramics in this temperature range. Those. at T_d≈670 K, a phase transition occurs, which leads to rhombohedral lattice distortion in local nanoscale regions and the appearance of polarization in them. However, the correlation length of such regions is very small and no macroscopic polarization occurs. In our case, the anomalous behavior of the heat capacity of PFN, which begins to be observed experimentally in the region of 670 K, is really close to the Burns temperature T_d≈603÷690 K, determined on the basis of structural and acoustic studies of PFN [1-5].

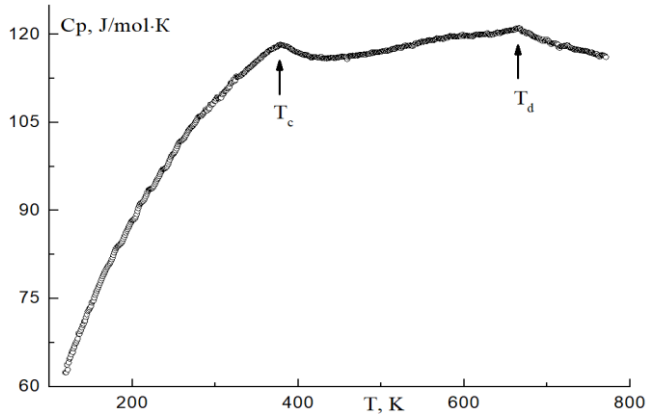

Figure 1. Temperature dependence of the heat capacity Cp of the ferroelectric $PbFe_{0.5}Nb_{0.5}O_3$.

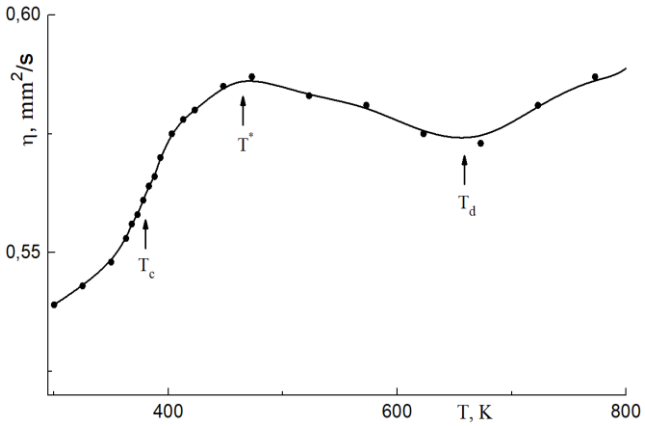

Figure 2. Temperature dependence of thermal diffusion of ferroelectric $PbFe_{0.5}Nb_{0.5}O_3$.

Figures 2 and 3 show the temperature dependences of thermal diffusion η and thermal conductivity λ of PFN samples in the temperature range 300÷800 K. The dependences η(T) and λ(T) exhibit anomalous behavior, as well as the dependences $C_p(T)$, in the temperature range of the diffuse ferroelectric transition of the phase transition T_c ≈380 K and T_d ≈ 670 K. An additional anomaly is observed in the dependence η(T) in the temperature range T≈470 K. It is possible that at this temperature T*≈470 K, the nanopolar regions merge into larger and long-lived dipole regions (nanoscale phase transition associated with random fields), because in many known relaxor ferroelectrics based on Pb, the temperature T* is in the temperature range 450÷570 K [1, 3].

As can be seen from Figures 2 and 3, in the temperature range of the diffuse ferroelectric transition Troom < T < T* (T*> T_c), when PFN is heated, a slight increase in thermal diffusion and thermal conductivity is observed, which is usually characteristic of amorphous and glassy bodies. It can be assumed that such a behavior of the thermal conductivity coefficient in the region of 300÷470 K is explained by the decay of ferrodomains into disordered dipoles (i.e., the formation of a dipole glass), which can be considered as defects in the crystal lattice and on which the phonons involved in the process of heat transfer are scattered.

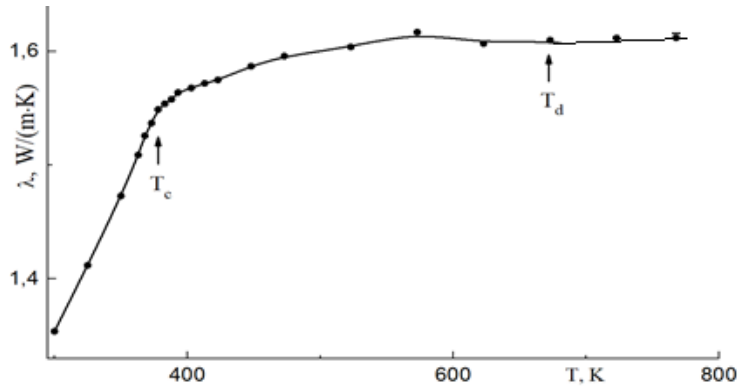

Figure 3. Temperature dependence of the thermal conductivity λ of the ferroelectric $PbFe_{0.5}Nb_{0.5}O_3$.

As can be seen from Figure 2, in the temperature range T_c <T< T_d, when PFN is heated, first an increase to a temperature T* ≈ 470 K is observed, and then a slight decrease in thermal diffusion to T_d, which may be due to an increase in the decay above T* of long-lived static polar regions into smaller dynamic nanopolar regions with increasing temperature, which leads to an increase in phonon scattering centers. At T > T_d ≈650 K, nanopolar regions disappear (i.e., polar shifts of ferroactive Pb^{2+} and Nb^{5+} cations), which leads to a significant decrease in lattice distortions; scattering centers, and, accordingly, a noticeable increase in thermal diffusion in the region T > T_d (Fig. 2).

The results of the studies and their analysis indicate that the main mechanism of phonon scattering in a relaxor PFN is local distortions of the crystal lattice caused by polar shifts of Pb^{2+} and Nb^{5+} cations and displacement of oxygen from their initial positions and the resulting nanopolar regions and glass dipole phase. On the temperature dependences of heat capacity, thermal diffusion and thermal conductivity, anomalies characteristic of phase transitions of the ferroelectric at T_c≈ 380 K, "nanoscale" at T*≈470 and Burns at T_d ≈ 670 K. It is shown that studies of thermophysical properties make it possible to determine all temperatures characteristic of ferroelectric relaxors associated with the appearance and temperature evolution of a nanopolar structure.

1. E. Dul'kin, A. Kania, M. Roth, *Mat. Res. Exp.* **1**, 016105 (2014).
2. B. Mihailova, B. Maier, C. Paulmann, et al., *Phys. Rev. B* **77**, 174106 (2008).
3. B. Dkhil, P. Gemeiner, A. Al-Barakaty, et al., *Phys. Rev. B* **80**, 064103 (2009).
4. M. Roth, E. Mojaev, E. Dul'kin, et al., *Phys. Rev. Lett.* **98**, 265701 (2007).
5. J. Toulouse, *Ferroelectrics* **369,** 203 (2008).

P2

Multiplexing in sandwich magnonic crystal/ferroelectric/ferromagnetic

V.V. Balayeva, O.V. Matveyev, M.A. Morozova
Saratov State University named after N.G.Chernyshevsky, 410012, Saratov, Russia
vkonda2000@mail.ru

Layered structures of the type based on ferroelectric and ferromagnetic layers are artificial multiferroics and exhibit properties characteristic of both ferromagnets and ferroelectrics separately, as well as completely new properties associated with the interaction of magnetic and electrical subsystems. This advantage opens up wide opportunities for the use of such structures as basic elements in a number of functional devices of microwave electronics [1].

In this paper, the features of the propagation of hybrid electromagnetic spin waves in a sandwich structure based on a ferromagnetic film with a periodic system of grooves (a magnonic crystal), a ferroelectric layer and a ferromagnetic film without grooves are investigated (Fig. 1a).

A pecularity of periodic structures is the presence of bragg resonances, which cause band gaps – non-transmission bands - appear in the spectrum of propagating waves [2, 3]. A feature of the coupled structures is the pumping of power, however, in the periodic structure, the signal supplied to the ferromagnetic film at the band gap frequency is not pumped between the layers.

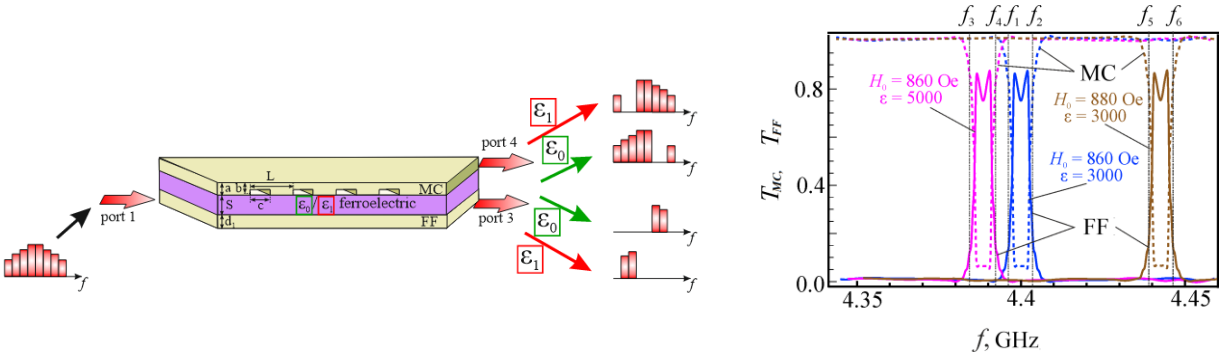

(a) (b)

Figure 1. (a) The structure scheme and the principle of demultiplexing. (b) The dependence of the transmittance coefficients of the ferromagnetic film and the magnonic crystal on the frequency at different values of the external magnetic field and the permittivity of the ferroelectric.

This feature allows to implement the function of demultiplexing based on the structure investigated. Depending on the frequency, the signal exits through different output ports of the structure (Fig. 1a), i.e. the structure under study allows for frequency channel separation - demultiplexing. The frequency range coming out to this port is determined by the value of the dielectric permittivity of the ferroelectric (the value of the electric field applied to the ferroelectric) and the value of the magnetic field applied to the ferromagnetic layers.

The research was supported by Russian Science Foundation (grant № 23-79-30027).

1. A.P. Pyatakov, A.K. Zvezdin, *Phys.-Usp.* **55**, 557 (2012).
2. A. Barman, G. Gubbiotti, S. Ladak, et al., *J. Phys.: Cond. Matter* **33**, 413001 (2021).
3. A.A. Nikitin, A.V. Kondrashov, A.B. Ustinov, et al., *J. Appl. Phys.* **122**, 153903 (2017).

P3

Effect of mechanical strain on ferroelectric and dielectric properties of HfO_2: theoretical study

E.B. Kalika, V.V. Mikheev, I.G. Margolin, A.A. Chouprik

Moscow Institute of Physics and Technology (Research Institute), 141700, Dolgoprudny, Russia
kalika.eb@phystech.edu

Today hafnium oxide (HfO_2) is considered one of the most promising materials for electronics application, as it has several advantages compared to standard perovskite-based ferroelectric materials. Orthorhombic phase HfO_2 films demonstrate ferroelectricity in nanometer-scale thickness, which allows to minimize the size of ferroelectric-material-based nonvolatile memories [1]. They are also convenient due to their compatibility with CMOS complementary metal-oxide semiconductor standard processing conditions [2]. However, the origin of ferroelectric properties in HfO_2 is still not understood well. It is particularly debated how mechanical stress affects the ferroelectric properties of the material.

Several studies are confirming that mechanical deformation influences ferroelectricity in HfO_2. First of all, the metastable orthorhombic phase in hafnia is usually stabilized by the following procedure: amorphous HfO_2-based thin films deposited on Si substrate with bottom electrode are crystallized by rapid thermal processing after the deposition of the top electrode [3,4]. On the other hand, orthorhombic phase was barely observed for films that were thermally processed without top electrodes [5]. Therefore, it is considered that the ferroelectric phase may originate from mechanical stress created by the different thermal expansion coefficients for film and substrate. It was also shown that lanthanium-doped HfO_2 exhibits large remanent polarization. It is likely that in this case in-plane strain impacts the formation of the ferroelectric phase during annealing [6]. Furthermore, Dutta et. al. has demonstrated that piezoelectric response in hafnia varies greatly depending on the film thickness, which regulates the mechanical stress of the film [7].

Current research reveals that mechanical stress in HfO_2 films impacts the ferroelectric properties. Moreover, using density functional theory with Perdew-Burke-Ernzerhof potential for solids (PBEsol) [8] and Berry phase approach [9, 10], we demonstrated that by varying the mechanical strain it is possible to control the ferroelectric and dielectric properties of HfO_2 film, particularly its spontaneous polarization, band gap and dielectric permittivity. This result was not only theoretically predicted, but we were also able to create an experiment, which demonstrated the possibility to vary the properties of the $Hf_{0.5}Zr_{0.5}O_2$ film due to its mechanical deformation.

The work was financially supported by the Russian Science Foundation (Project No. 20-19-00370, https://rscf.ru/en/project/20-19-00370/).

1. M.H. Park, H.J. Kim, Y.J. Kim, et al., *Appl. Phys. Lett.* **102**, 242905 (2016).
2. S. Clima, D.J. Wouters, C. Adelmann, et al., *Appl. Phys. Lett.* **104**, 092906 (2014).
3. U. Schröder, E. Yurchuk, J. Müller, et al., *Jap. J. Appl. Phys.* **53**, 08LE02 (2014).
4. P.D. Lomenzo, Q. Takmeel, C. Zhou, et al., *Appl. Phys. Lett.* **107**, 242903 (2015).
5. J. Müller, T.S. Böscke, U. Schröder, et al., *Nano Lett.* **12**, 4318 (2012).
6. T. Schenk, C.M. Fancher, M.H. Park, et al., *Adv. Electr. Mater.* **5**, 1900303 (2019).
7. S. Dutta, P. Buragohain, S. Glinsek, et al., *Nature Commun.* **12**, 7301 (2021).
8. J.P. Perdew, A. Ruzsinszky, G.I. Csonka, et al., *Phys.l Rev. Lett.* **100**, 136406 (2008).
9. R.D. King-Smith, D. Vanderbilt, *Phys. Rev. B* **47**, 1651 (1993).
10. R. Resta, *Ferroelectrics* **136**, 51 (1992).

P4

Magnetic structure and macroscopic magnetic properties of R-Co thin films

E.V. Kudyukov[1], A.N. Nizaev[1], A.N. Gor'kovenko[1], V.N. Lepalovskij[1], V.O. Vas'kovskiy[1,2]

[1]*School of Natural Sciences and Mathematics, Ural Federal University, 620002, Yekaterinburg, Russia*
e.v.kudyukov@urfu.ru

[2]*Institute of Metal Physics, UB RAS, 620137, Yekaterinburg, Russia*

Films of alloys of the R-T type attract the interest of researchers due to the presence in them of a wide range of functional properties that provide a huge potential for technical applications in the field of magnetomicroelectronics. Thus, the presence of magnetostriction in these systems allows us to consider them as components of composite multiferroics [1]. Films of R-T alloys are also of fundamental interest due to the observation of non-collinear magnetic structures in them, such as speromagnetism, asperomagnetism, and helical magnetic structures. Understanding the features and mechanisms of formation of such structures is important for the development of promising scientific and technical areas, in particular, chiral spintronics [2, 3]. At present, alloys with a high content of the T-element have been widely considered due to the manifestation of various magnetic properties at room temperature. However, insufficient attention has been paid to R-riched alloys, which can be of no less important fundamental and applied importance. Thus, this work is devoted to the study of the magnetic properties of films of the R-Co type (R=Gd,Tb,Dy,Ho) in a wide concentration range (from 0 to 100 at.% of the R-element).

All film samples were obtained on an AJA ORION-8 magnetron sputtering unit in the presence of a magnetic field of 200 Oe in the substrate plane. The films were deposited on Corning cover glass 22×22 mm. The deposition was carried out in an argon atmosphere with a working pressure of $1 \cdot 10^{-3}$ Torr. A PANAlytical diffractometer was used to certify the structural properties of the films. The magnetic properties were studied using a SQUID magnetometer and a PPMS complex in fields up to 70 kOe and a temperature range from 5 to 350 K.

In this work, the characteristics of the magnetic structure and macroscopic magnetic properties of thin films of alloys of the R-Co type are obtained in a wide range of composition, temperature, and magnetic fields. It is shown that in a number of systems with a high content of the R-element in the nanocrystalline state, there is a strong frustration of the exchange interaction and magnetic anisotropy, leading to the appearance of a noncollinear magnetic structure. For all systems under study, a magnetic phase diagram has been constructed, an example of which is shown in Figure 1.

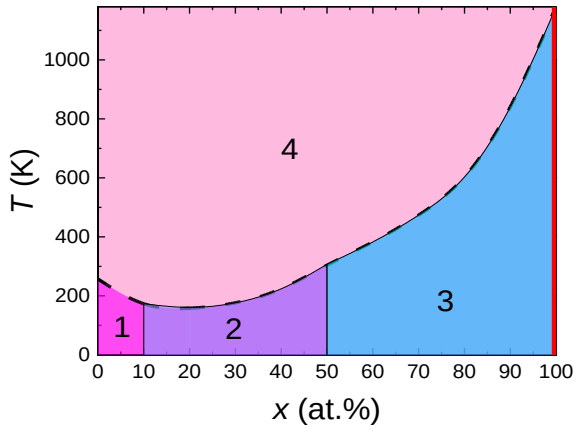

Figure 1. Magnetic phase diagram in T-x coordinates of Gd-Co films. 1 – asperomagnetic, 2 – ferromagnetic, 3 – ferrimagnetic, 4 – paramagnetic states. The dash line on the picture represents T_c of Gd-Co films including pure Gd and Co. The bold red line represents ferromagnetic state for pure Co.

1. Z.M. Hu, Y. Su, J. Li, *Int. J. Solids and Structures* **212**, 96 (2021).
2. C. Holzmann, A. Ullrich, O.-T. Ciubotariu, M. Albrecht, *ACS Appl. Nano Mater.* **5**, 1023 (2022).
3. D. Chen, Y. Xu, et al., *Phys. Rev. Mater.* **6**, 014402 (2022).

P5

Formation of Bragg resonances in a multilayer structure of magnon crystals with different periods

N.D. Lobanov, O.V. Matveev, D.V. Romanenko, M. A. Morozova

Saratov State University, 410071 Astrakhanskaya 83, Saratov, Russia
nl_17@mail.ru

At present, there is a rapid development of radio engineering and electronics, but the reduction of classical semiconductor devices to nanometer sizes inevitably leads to quantum limitations. In this regard, the development of quantum electronics, in particular such a field as magnonics, has started.

Magnonics is a science that studies the magnetic properties of materials and ways to control them by means of spin wave propagation [1-3]. Spin waves arise when the spins of electrons oscillate along a certain direction in a magnetic material, resulting in oscillations of magnetic moments around that direction. These oscillations of magnetic moments result in the propagation of a spin wave along the material. Note in this case the higher speed of signal transmission and energy efficiency compared to classical electronics. Magnonics ideas are used to create new types of microelectronic devices, such as magnetic transistors, magnetic memory, signal generators, magnetic filters.

This paper investigates a structure consisting of two magnon crystals separated by a dielectric interlayer. Magnon crystals are ferromagnetic films with a periodic system of grooves. The grooves are etched in this case on ferromagnetic films of iron- yttrium garnet. In this kind of periodic structures, it is interesting to study the formation of band gaps - Bragg resonances, i.e. areas, where the wave does not practically propagate [4, 5].

The transition from a single magnon crystal to coupled magnon crystals leads to splitting of the spin wave into two modes: symmetric and antisymmetric. Also due to inhomogeneities - periodic grooves - reverse symmetric and antisymmetric waves are formed. Thus, 4 types of waves appear in the structure and formation of up to 4 band gaps in the range of the first Bragg resonance is possible.

By changing the geometric and magnetic parameters it is possible to influence the formation of the band gaps. In the case of equal periods there are 2 band gaps. Varying the period for one of the magnon crystals results to the formation of 4 band gaps. Moreover, increasing the ratio of periods will significantly affect the width and position of only two band gaps, while the other two will change weakly. By keeping different periods locked and increasing the magnetization ratio of the ferromagnetic layers, initially one band gap disappears, and by further increasing the magnetization ratio, only 2 of the 4 band gaps remain.

It can be seen that structures based on coupled magnon crystals due to effective control of geometric and magnetic parameters can be used in microwave electronics as tunable microwave filters, phase shifters, delay lines.

This work was supported by the Russian Science Foundation (project № 19-79-20121).

1. S.A. Nikitov, et al., *Usp. Fiz. Nauk* **185**, 1099 (2015).
2. S. Vysotsckii, et al., *Acta Phys. Polonica* **133**, 508 (2018).
3. S.L. Vysotskii, et al., *IEEE Magn. Lett.* **8**, 3706104 (2017).
4. M.A. Morozova, et al., *J. Appl. Phys.* **120**, 223901 (2016).
5. A.V. Vashkovsky, V.S. Stalmahov, Y.P. Sharaevsky, *Magnetostatic waves in ultrahigh frequency electronics* (Saratov University Publishing), 311 (1993).

P6

High-coercivity state in nanostructured alloys of the Sm-Co system

V.E. Maltseva, S.V. Andreev, A.N. Urzhumtsev, A.S. Volegov

Ural Federal University, 620002, Ekaterinburg, Russia
viktoria.maltseva@urfu.ru

Hard magnetic materials and permanent magnets made of them are widely used in modern high-precision measuring systems, systems, used as functional and structural. Thus, the former are used in power engineering, space technology, household devices. Structural materials are widely used in nuclear power, gas and oil production.

Practical application of nanostructured alloys in these areas requires a detailed understanding of remagnetization processes, depending on which ways to achieve the high-coercivity state will differ. The issue of remagnetization processes in rapidly hardened alloys has been investigated many times; however, there is still no definitive unequivocal answer [1-3].

The aim of this work is to investigate the ways to achieve the high-coercivity state and the remagnetization mechanisms in the rapidly quenched nanostructured alloys of the Sm-Co system.

$SmCo_5$ system alloys of stoichiometric compositions were synthesized as samples. The alloys were obtained by induction melting in a quartz crucible of the initial components followed by casting on a copper disk with disk rotation speeds ranging from 20 m/s to 50 m/s (Fig. 1).

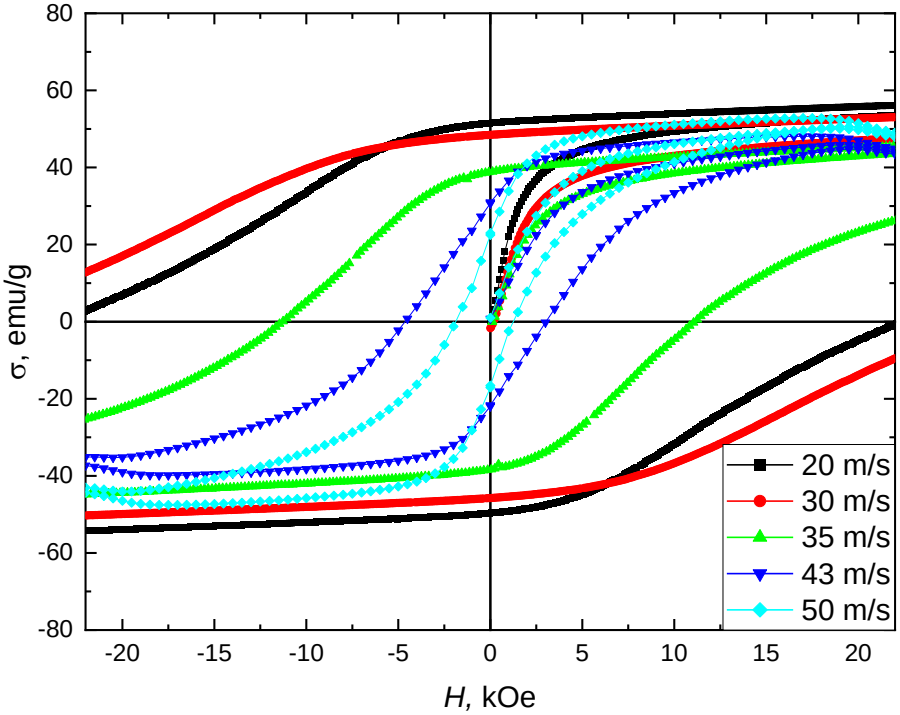

Figure 1. Magnetic hysteresis loops of the $SmCo_5$ system obtained at different rotational speeds of the quenching disk.

To determine the preliminary hysteresis properties and select the best samples for further studies, the obtained tapes were measured by means of a KVANS-1 vibromagnetometer at room temperature. Then, the tapes of the $SmCo_5$ system were annealed in vacuum at a temperature range of 600°C to 1050°C for 30 minutes and/or 1 hour to obtain the optimum magnetic properties (Fig. 2). Subsequent measurements of the magnetic hysteresis properties were carried out using a DynaCool 9 T measuring system in the temperature range from 2 K to 300 K.

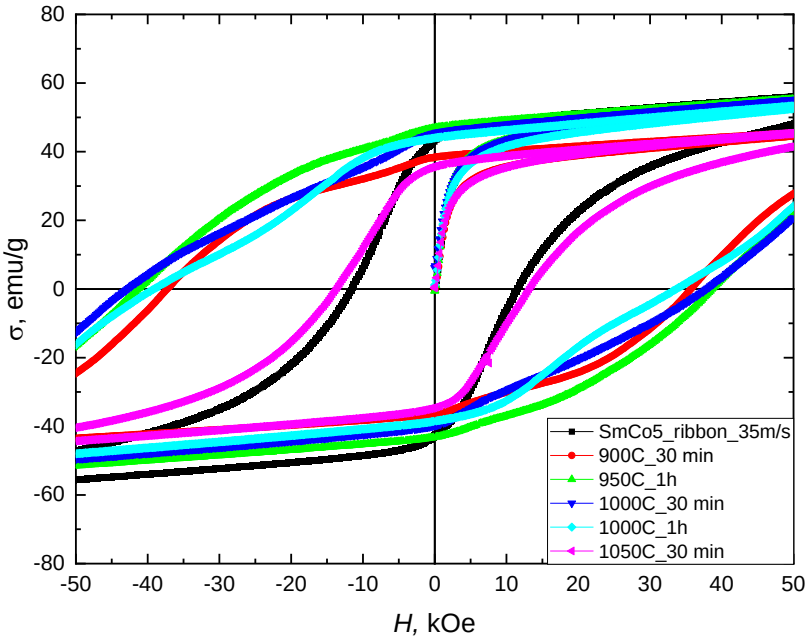

Figure 2. Magnetic hysteresis loops of the $SmCo_5$ system obtained at different temperatures and annealing times.

The best magnetic hysteresis properties are possessed by the tapes obtained at a quenching disk speed of 35 m/s and annealed at 1000C for 30 minutes. The coercive force for this sample is 44 kE, which is the best result presented in the literature. Presumably, nucleation is the prevailing mechanism of remagnetization for the Sm-Co system. The mechanisms of remagnetization and the results obtained will be described in more detail in the report. Figures should be embedded in the text. Size of the figure labels should not exceed 11 pt at the final figure size (not to be bigger than the text).

Support by grant RSF № 21-72-10104 is acknowledged.

1. A.S. Volegov, et.al., *Acta Materialia* **188**, 733 (2020).
2. E.F. Kneller, R. Hawig, *IEEE Transactions on Magnetics* **27**, 3588 (1991).
3. K.-T. Chu et. al., *J. Phys. D.: Appl. Phys.* **38**, 4009 (2005).

P7

Simulation of the charged spin-triplet boson system on the 2D square lattice by classical Monte Carlo Method

S.N. Nuzhin, V.A. Ulitko, Y.D. Panov, A.S. Moskvin

Institute of Natural Sciences and Mathematics of UrFU, 620026, Yekaterinburg, Russia Federation
nuzhin.stepan@urfu.ru

Simulation spin-triplet boson systems is currently relevant as it allows for thermodynamically describing classical and quantum systems and obtaining special phase states such as superfluidity, Bose-Einstein condensation, and supersolid. Systems that are naturally described by lattice boson models include an ultra-cold atomic gas in optical lattices, dimer antiferromagnets [1], non-traditional superconductors [2], and materials with charge disproportionation [3].

AgF_2 is considered as a potential unconventional superconductor, particularly due to its isostructural similarity to cuprates [4]. Therefore, there is a hypothesis that the charge disproportionation mechanism present in cuprates [3] is realized in silver compounds [2, 4]. Based on this, we simulation valence mixing (cationic disordering) by a system of spin-triplet charged bosons.

We consider bosons with spin *S=1*, which move from node to node of a square lattice. The basis is introduced at each node of the lattice $|n\ \sigma\rangle$, where n is the number of bosons and σ is the spin projection, includes 4 states: $|0\ 0\rangle$, $|1\ 1\rangle$, $|1\ 0\rangle$, $|1\ -1\rangle$. The Hamiltonian of this model,

$$\widehat{\mathcal{H}} = -t \sum_{<ij>\sigma} \left(B_{i\sigma}^{\dagger} B_{j\sigma} + B_{j\sigma}^{\dagger} B_{i\sigma}\right) + V \sum_{<ij>} \hat{n}_i \hat{n}_j + J \sum_{<ij>} \left(\vec{S}_i, \vec{S}_j\right) - \sum_{i} \left(\vec{h}, \vec{S}_i\right),$$

describes the transfer of (t) boson to the nearest node while conservation the spin projection, charge-charge correlations (V) that do not depend on the boson spin projections, antiferromagnetic isotropic exchange (J) between bosons in neighboring nodes and the interaction of bosons with a magnetic field $\vec{h}$.

We have implemented the classical Monte Carlo algorithm in which the density of bosons is conserved at each elementary step, and phase diagrams are calculated within the canonical and grand canonical ensembles. The paper discusses the peculiarities of the algorithm related to the need to organize an uniform sampling of states from the phase space and the possibility of organizing parallel computations. The obtained results are compared with the results of simulation within the grand canonical ensemble and with limit cases for a system of local (hard-core) bosons.

The work is supported by the FEUZ-2023-0017 project of the Ministry of Education and Science of the Russian Federation.

1. Th. Giamarchi, Ch. Rüegg, O. Tchernyshyov, *Nat. Phys.* **4**, 198 (2008).
2. J. Gawraczynski, et al., *Proc. Natl. Acad. Sci.* **116**, 1495 (2019).
3. A.S. Moskvin, *J. Phys. Condens. Matter* **25**, 085601 (2013).
4. J.P. Allen, D.O. Scanlon, G.W. Watson, *Phys. Rev. B* **84**, 115141 (2011).

P8

Correlation functions and properties of local distributions of frustrated phases in the ground state of a dilute Ising chain in a magnetic field

Y.D. Panov

Ural Federal University, 620002, Ekaterinburg, Russia
yuri.panov@urfu.ru

For low-dimensional and especially for the one-dimensional magnets, a characteristic feature is the presence of frustrated phases in the ground state. Frustrated states may be associated with various exotic properties of these systems, such as magnetization plateaus, quasi-phases or pseudo-transitions. The source of frustrations in magnets, in addition to the lattice geometry, can be impurities. The simplest model of such magnets is a dilute Ising chain. In a zero magnetic field, this model has an exact solution [1]. Accounting the magnetic field, the standard transfer matrix method allows us to study the thermodynamic properties of this model by numerically solving a system of nonlinear algebraic equations [2]. However, the properties of the ground state, especially the concentration dependences of various physical quantities, within the standard framework can only be investigated at a qualitative level from the analysis of the numerical solution at low temperatures.

Earlier [3], an analytical method was considered for calculating various physical properties of the ground state of a dilute Ising chain based on the principle of maximum residual entropy, the explicit expression for which is derived from the Markov property of the system [4]. In the present paper, correlation functions and properties of local distributions of frustrated phases of the ground state of an Ising chain diluted with non-magnetic interacting impurities in a longitudinal magnetic field are obtained and investigated.

An explicit form of dependences on the impurity concentration for impurity and spin correlation functions, as well as the average length and average length dispersion for various types of periodic sequences: spin ferromagnetic, spin antiferromagnetic, impurity and impurity-spin are found. It is shown that for the weakly diluted case, both the spin and impurity correlation length in the magnetic field is finite for the frustrated ferromagnetic and infinite for the frustrated antiferromagnetic phase. At the same time, from the point of view of the properties of local distributions these phases are equivalent. It is shown that the field-induced transition from the non-frustrated antiferromagnetic ground state to a frustrated one is accompanied by the appearance of charge ordering for non-magnetic impurities. The properties of the frustrated paramagnetic phase of the ground state, which is realized in the highly dilute case, are also investigated. The obtained characteristics are compared with the case of a zero magnetic field, for which the results of an exact solution are known [4].

1. B.Y. Balagurov, V.G. Vaks, R.O. Zaitsev, *Sov. Phys. Solid State* **16**, 1498 (1975).
2. A.V. Shadrin, Yu.D. Panov, *JMMM* **546**, 168804 (2022).
3. Y. Panov, *Phys. Rev. E* **106**, 054111 (2022).
4. Y.D. Panov, *JMMM* **514**, 167224 (2020).

P9

Structure and properties of Co-C nanocomposites

A.V. Sosunov[1], L.V. Spivak[1], K.B. Tsiberkin[1], G.I. Tselikov[2]

[1]*Perm State University, 614990 Perm, Russia*

[2]*Moscow Institute of Physics and Technology, 141701 Dolgoprudny, Russia*

alexeisosunov@gmail.com

Three-dimensional carbon nanocomposites with subnanometer channels, a high specific surface area with a defective outer shell, and a tuneable electronic structure differ significantly from carbon nanotubes and graphene. These structural and morphological characteristics make such fullerene-like materials a new platform for energy conversion and storage, photonics, medicine, and chemistry [1]. The development of this new platform is possible with the use of magnetic nanoparticles, expanding the functionality and properties of this family of composite materials. However, this requires investigation of their basic physical properties.

Such materials open up new approaches to the study of phase transformations in a matrix containing clusters of ferromagnetic metal nanoparticles isolated from each other, capable of first- and second-order phase transitions. This gives prospects for the emergence of a new scientific direction in solid state physics: phase transformations in matrix nanostructures.

The object of study is three-dimensional composite carbon nanocomposites, which are ferromagnetic Co nanoparticles coated with several layers of carbon (Co-C). Synthesis of an array of Co-C nanocomposites was carried out using pyrolysis in nitrogen atmosphere [2].

Morphological and structural properties of studied materials were characterized by the high-resolution transmission electron microscopy (HR-TEM) system (JEOL JEM 2010) operating at 200 kV with a Gatan Multiscan CCD in imaging and diffraction modes. Samples were prepared by dropping 2 μL of NPs solution onto a carbon-coated TEM copper grid and subsequent drying at ambient conditions. Analysis of selected area electron diffraction (SAED) pattern was performed using ProcessDiffraction v.8.7.1 software.

The results are presented in fig. 1. The structure of the samples has a homogeneous close-packed network of Co-C nanoparticles with a size of 3-5 nm.

The thermal properties of the studied samples were determined using an STA "Jupiter" 449 instrument (Netzsch Holding). Heating was carried out in an argon atmosphere at a rate of 5–40 K/min. The gas flow rate was 25-30 ml/min. The results are presented in fig. 2.

Comparison with the data obtained for the massive Co (mCo) [3] allows us to make the following generalizations: (1) polymorphic transformation during Co−C nanocomposites heating occurs at lower temperatures than in mCo; (2) the thermal effect of the transformation into Co−C nanocomposites (10 J/g) is by several times greater (3.4 J/g) than the values during the phase transformation into mCo; (3) the activation energy of phase transformations during heating in Co−C nanocomposites does not depend on heating cycles. In this case, it is significantly less than the values determined under similar conditions for mCo (230−370 kJ/mol); (4) Co−C nanocomposites reheating is characterized by transformation temperature shift towards higher temperatures compared to the initial heating and is accompanied by increase in the thermal effect of transformation.

Taking into account the very small size of Co-C particles and the relatively low phase transformation temperature and activation energy, it can be assumed that this transition occurs by a diffusionless massive mechanism.

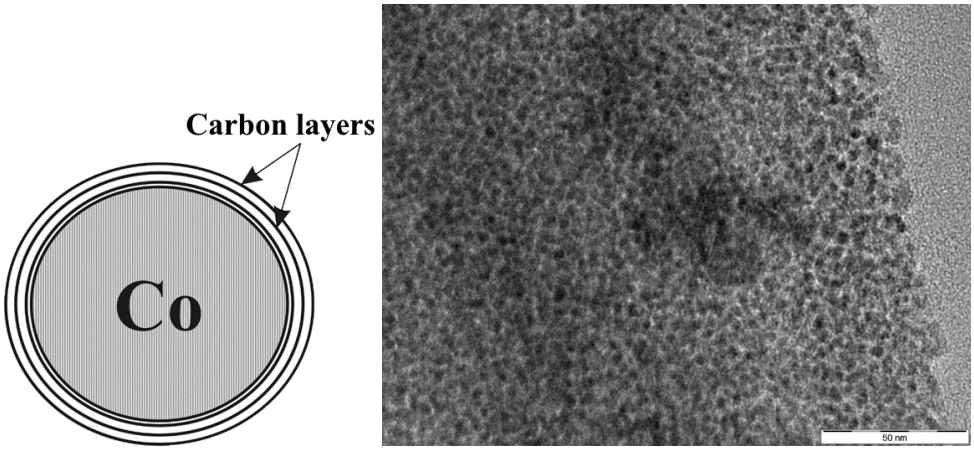

Figure 1. Co-C nanoparticle model (*left*); TEM image of Co-C nanocomposite (*right*).

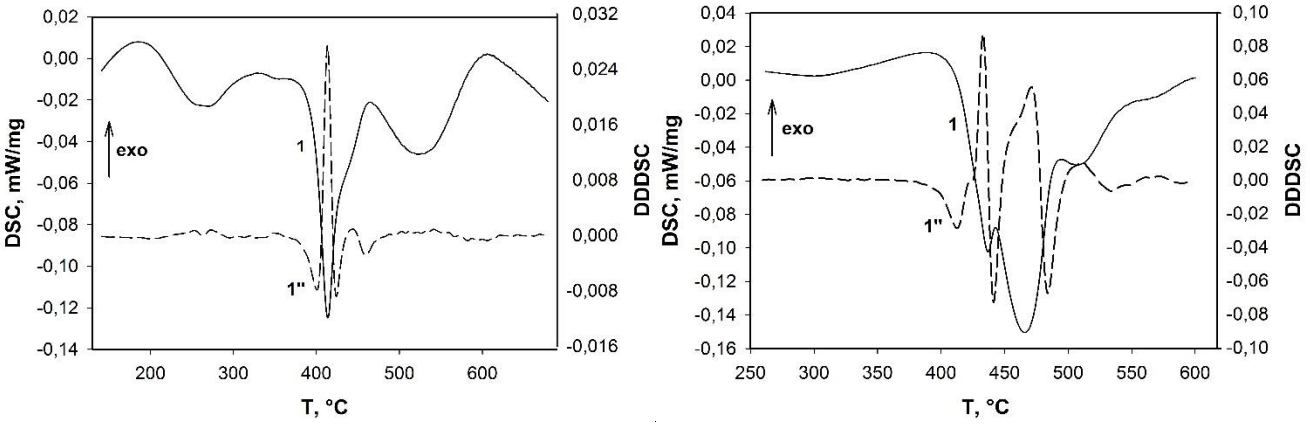

Figure 2. Change in the DSC (*solid line*) and DDDSC (*dashed line*) signals during heating of Co-C nanocomposite at a rate of 10 °C/min. First (*left*) and second (*right*) heatings.

The work was funded by state assignment no. 121101300016-2.

1. Z. Ma, F. Jing, Y. Fan, et al., *J. Alloys Compd.* **789**, 71 (2019).
2. G.A. Rudakov, A.V. Sosunov, R.S. Ponomarev, et al., *Phys. Sol. State.* **60**, 167 (2018).
3. L.V. Spivak, N.E. Shchepina, *Tech. Phys.* **67**, 478 (2022).

P10

The modelling of skyrmions in ferri- and ferromagnetic metallic nanostructures

V.D. Bessonov, V.S. Teplov, A.V. Telegin

IMP of UB of RAS, 620108, Yekaterinburg, Russia
bessonov@imp.uran.ru

Topology provides a framework for an understanding of emergent phenomena in various fields such as the appearance of new results in the field of spintronics [1]. The past decade has witnessed dramatic progress related to various aspects of emergent topological textures in HM/FM metal-oxide nanostructures displaying vortices and skyrmions, among others. The new emergent states of matter join together with exotic functional properties (such as chirality) that, along with their small size and ultrafast dynamical response, make them potential candidates in multifunctional devices provided the fertile background for the dawning of the skyrmions era.

This work addresses the micromagnetic modelling of chiral spin textures in heavy metal/ferri- and ferromagnetic (FM) metallic nanostructures.

As a main result of the work, the effect of interlayer indirect exchange coupling in multilayer structures on the topological structure and behavior of chiral spin textures was investigated by micromagnetic modeling methods, and the damping of spin texture dynamics depending on the magnitude and sign of the VDM under the influence of spin current was estimated.

Based on the simulation results the following conclusions were made about the stabilization and movement of the skyrmion under the action of current in a FM and ferrimagnetic (FIM) structure:

1) the region of magnetic parameters corresponding to the stable existence of the skyrmion is much wider in the case of FIM than in the case of FM. The depth of the potential pit limiting the stable state of the skyrmion in the case of FIM is much greater than in the case of FM, therefore the skyrmion in FIM is much more stable,

2) the speed of movement of the skyrmion in the case of FIM is two orders of magnitude higher than in the case of FM. Such an increase is associated with the tendency of the total topological charge of the skyrmion in the FIM to zero as it approaches the compensation state,

3) under the action of a spin-polarized current, the skyrmions in the FIM moves almost rectilinearly, due to the compensated action of the gyrotropic force.

The disadvantages of FIM include:

1) a high potential barrier preventing the destruction of the skyrmions. If in the case of FM the skyrmion can be obtained as a result of demagnetization, then it will require local external action for FIM,

2) the magnetic moment of the FIM strongly depends on the temperature, which means that the magnitude of the current will greatly change the properties of the skyrmions due to Joule heating. It imposes restrictions on the choice of FIM composition.

Support of the Russian Science Foundation № 21-72-20160 (https://rscf.ru/en/project/21-72-20160) is acknowledged.

1. A. Fert, et al., *Nature Rev. Mater.* **2**, 17031 (2017).

P11

Monte Carlo algorithm with charge conservation for simulation of a spin-pseudospin model

V.A. Ulitko, Yr.D. Panov

Ural Federal University, 620002 Ekaterinburg, Russia
vasiliy.ulitko@urfu.ru

Within the previously developed [1,2] pseudospin model of HTSC cuprates, CuO_2 planes are considered as a square lattice where nodes represent states of CuO_4clusters. Possible charge states |1,1⟩ for $[CuO_4]^{5-}$ and |1, -1⟩ for $[CuO_4]^{7-}$- are spin singlets, while the one-hole state |1,1⟩ for $[CuO_4]^{6-}$ s a spin $s = 1/2$ doublet. As a result, the basis | 1M; μ⟩ at each node consists of 4 states: {| 11; 00⟩, | 10; 1/2 1/2⟩, | 10; 1/2 -1/2⟩, | 1-1; 00⟩}. The effective pseudospin Hamiltonian of the model cuprate considers local and non-local charge correlations, three types of correlated single-particle transfer, two-particle transfer, and antiferromagnetic Heisenberg exchange interaction for $[CuO_4]^{6-}$ center states. The total charge of the system, counted from the charge of the lattice made up of $[CuO_4]^{6-}$ centers, corresponds to the degree of cuprate doping n. To calculate temperature-phase (T, n) diagrams, it is necessary to consider n constant. In terms of pseudospin operators, $n = 1/N \sum_i S_{zi}$, where for the S_z operator, the valence states of the CuO_4 cluster are eigenstates: S_z| 1M⟩ = M | 1M⟩.

In the standard approach, the constancy of n is ensured by introducing a term $-\mu \sum_i S_{zi}$ into the Hamiltonian, where μ is the chemical potential. However, in numerical modeling using the grand canonical ensemble, obtaining reliable (T, n) diagrams that describe the phase separation in the system is difficult due to the influence of metastable states. We consider a semiclassical algorithm, where the state at each node is defined by random complex coefficients of the wave function |1M⟩ = c_{+1}|11; 00⟩ + $c_{\uparrow}$| 10; 1/2 1/2⟩ + $c_{\downarrow}$| 10; 1/2 -1/2⟩ + c_{-1}| 1-1; 00⟩. The elementary Monte Carlo step involves changing the states of a pair of nodes while maintaining the total charge and ensuring homogeneity of the state sampling in the phase space for a given parameterization of the coefficients c_α.

The state selection algorithm for the quasi-classical Monte Carlo simulation that conserves the total charge consists of the following steps:

(i) calculation of the total charge $2n = n_{1,0} + n_{2,0}$ for the randomly selected pair of sites 1 and 2;

(ii) calculation of the value n_1 from equation $F_1(n_1|2n) = \gamma$, where $\gamma \in [0,1]$ is the uniformly distributed random value, and the function $F_1(n_1|2n)$ is the cumulative distribution function of the charge n_1 at the site 1 for the fixed pair charge $2n$;

(iii) calculation of the value $n_2 = 2n - n_1$;

(iv) calculation of values m_i, $i = 1,2$, from equations $F_2(m|n_i) = \gamma_i$, where $\gamma_i \in [0,1]$ is the uniformly distributed random value, the conditional distribution function $F_2(m|n_i)$ is defined by equation:

$$F_2(m|n_i) = \frac{\ln\left(m + \sqrt{m^2 - {n_i}^2}\right) - \ln|n_i|}{\ln\left(1 + \sqrt{1 - {n_i}^2}\right) - \ln|n_i|}, |n_i| \le m \le 1;$$

(v) calculation of ϕ_i, $i = 1,2$, from equations $\cos(2\phi_i) = n_i/m_i$;

(vi) calculation of θ_i, $i = 1,2$, from equations $\cos(2\theta_i) = m_i$;

(vii) generation of uniformly distributed random values ${\phi_k}^{(i)} \in [0,2\pi]$, $i = 1,2$, $k = +1, -1, \uparrow, \downarrow$ and $\psi_i \in [0, \pi/2]$,], $i = 1,2$.

The paper discusses the features of implementing the algorithm and compares the results with modeling within the grand canonical ensemble.

1. A.S. Moskvin, *Phys. Rev. B* **84**, 075116 (2011).
2. A.S. Moskvin, *J. Phys.: Cond. Matter* **25**, 085601 (2013).

P12

Influence of microstructure features on the mechanism of high-coercive state in Nd-Fe-B type permanent magnets

A.N. Urzhumtsev[1,2], V.E. Maltseva[1], A.S. Volegov[1]

[1]*Ural Federal University, 620002, Yekaterinburg, Russia*
andrei.urzhumtsev@urfu.ru

[2]*POZ-Progress Ltd., 624092, Verkhnyaya Pyshma, Russia*

Rare-earth permanent magnets (PM) of Nd-Fe-B type are necessary for modern industry, in particular for devices for electrical energy conversion. Their application is limited by the operating temperature within 150 °C in view of irreversible changes in their magnetic state. It is known that this class of magnets is characterized by a change in their coercivity mechanism from nucleation to pinning as the temperature increases [1]. This paper shows that such variations are also possible at room temperature, depending on the brand and microstructural features of this class of PM.

For today, the study of the processes of remagnetization and formation of high coercivity in hard magnetic materials as Nd-Fe-B and Sm(Co, Fe, Zr, Cu)$_z$ is based on the study of their microstructure using SEM and PEM microscopy, micromagnetic modeling, and magnetic measurements. This paper focuses on the interpretation of magnetic measurements with elements of structural analysis and modeling.

The most common textured sintered PM grades of the Nd-Fe-B type N35, N48 and N48SH based on the $Nd_2Fe_{14}B$ phase, provided by the enterprise POZ-Progress Ltd. were chosen for the study. Their microstructure was studied using SEM and EDX analysis on a Tescan Mira3 LMU microscope. Magnetic measurements were carried out on MPMS XL 7 measuring complexes in the range of fields ± 7 Tesla and DynaCool in the range ± 9 Tesla, respectively. Magnetization curves $\sigma(H)$ and $\sigma_r(H)$ from the thermodemagnetized state, reversible magnetic susceptibility curves $\chi(H)$ under an excitation alternating magnetic field $h\sim$ with an amplitude of 3.7 Oe and a frequency of 7 Hz, reversible magnetization contribution curves $(\sigma - \sigma_r)(H)$, and partial hysteresis loops were obtained and analyzed.

Figure 1 shows reversible magnetic susceptibility curves $\chi(H)$ in the DC magnetic field and in the state of residual magnetization $\chi(H = 0)$, after switching off of DC field.

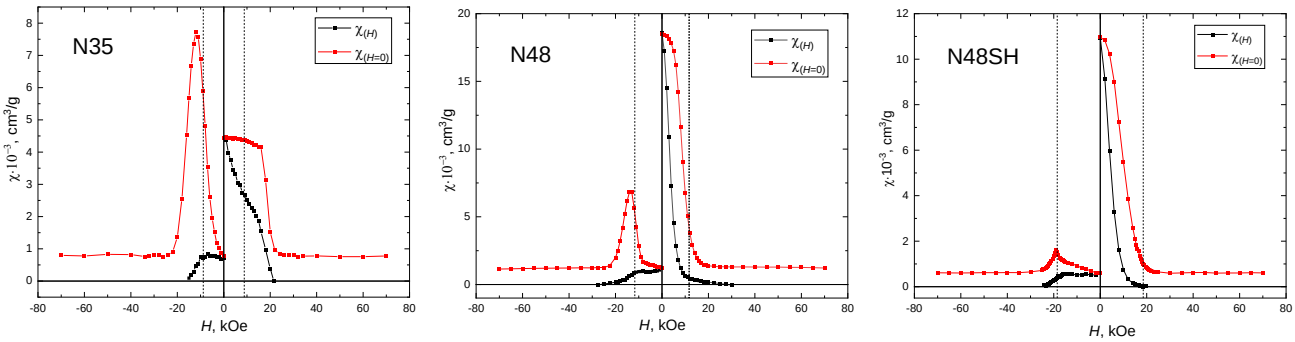

Figure 1. Dependences of reversible magnetic susceptibility χ(H) and magnetic susceptibility after switching off of the field χ(H = 0) of sintered microcrystalline material of N35, N48, N48SH grades.

Reduction of $\chi(H)$ level practically to zero is a consequence of sample reaching technical saturation. The figure shows that in the thermodemagnetized state, for all samples there is a non-zero level of susceptibility in the residual magnetization state $\chi(H = 0)$, which is a consequence of displacement of unfixed domain boundaries under the action of a weak AC magnetic field. This is also observed for sintered magnet samples such as Sm(Co, Fe, Zr, Cu)$_z$ type [2]. When approaching saturation, $\chi(H = 0)$ reaches a stable level maintained by the effect of rotating magnetic moments due to magnetic texture disorders. When N35 and N48 are demagnetized, there is a response from the displacement of loose domain walls, indicating the existence of many near-energy pinning centers, which is practically not observed in N48SH. The analysis of the angular dependences of the coercivity shows that the curves for N35 and N48 within the magnetostatic interactions approximation correspond

to the pinning model [3]. In N48SH, the remagnetization of the grains is predominantly irreversible, and the domain boundary passes through the entire grain volume almost without delay and is hard fixed on its boundary, which corresponds to the representations of the nucleation mechanism.

Figure 2 shows the curves of the reversible contribution to the magnetization $(\sigma - \sigma_r)(H)$ obtained during magnetization from the thermal demagnetized state and demagnetization from magnetically saturation.

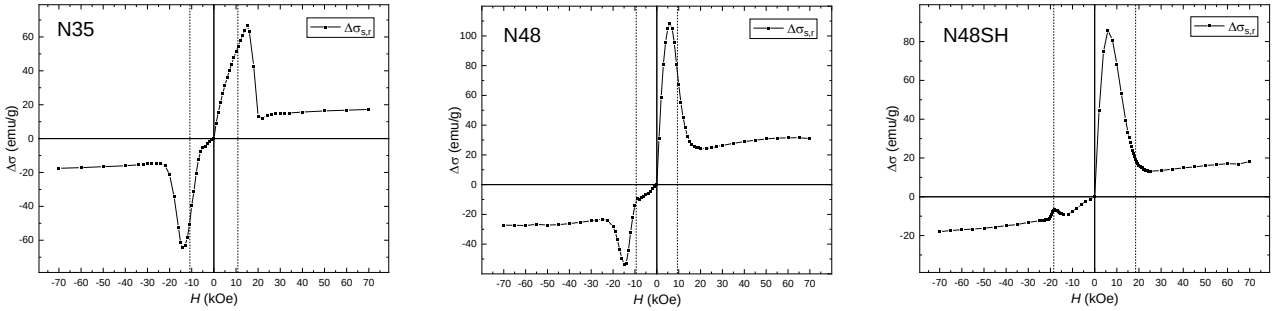

Figure 2. Curves of the reversible contribution to $(\sigma - \sigma_r)(H)$ magnetization.

During magnetization from the thermodemagnetized state, all the samples in Figure 2 firstly show an increase in $(\sigma - \sigma_r)(H)$, then a decrease. This is due to the process of leaving and fixing the domain walls beyond the grain boundaries of the main phase $Nd_2Fe_{14}B$. During demagnetization two situations are possible: anomalous growth or reduction of reversibility on $(\sigma - \sigma_r)(H)$. This behavior of the curves $(\sigma - \sigma_r)(H)$ is indirectly related to the mechanism of the high-coercivity state of this PM samples.

The paper shows that in PMs the presence of impurity phases based on rare-earth metals oxides both in the main phase $Nd_2Fe_{14}B$ of the magnet grains and in the intergranular boundaries, the basis of which is the $NdFe_4B_4$ phase, leads to the difficulty of magnetization to saturation from the thermal demagnetized state, while reducing the coercivity H_c.

The paper analyzes the results based on magnetometric techniques by which the role of the nucleation and pinning mechanism in the remagnetization processes of a wide range of Nd-Fe-B class PMs samples can be determined. The concept of the high-coercivity state mechanism for this hard magnetic material is presented. In the study presents a method for obtaining and interpreting the dependences of the reversible contribution to the magnetization $(\sigma - \sigma_r)(H)$ under an external field, which shows the influence of the local demagnetizing fields of grains on their nearest neighbors, in consequence of magnetostatic interactions. The results of this approach are consistent with the results for reversible magnetic susceptibility $\chi(H = 0)$.

The results show that within the same class of permanent magnets, depending on their microstructure, both the nucleation mechanism and the pinning mechanism may prevail. The hypothesis is presented that the presence of oxygen in the main phase of PMs grains forms local pinning centers and prevents easy magnetization, while the formation of oxides in the intergranular boundary phase reduces the nucleation energy of the domain walls, which reduces the maximum coercive force by almost 30 % and causes the predominance of the pinning mechanism over nucleation. It is shown that the superposition of the remagnetization mechanisms leads to a violation of the monotonicity on the partial hysteresis loops.

This work was financially supported by RSF grant № 21-72-10104.

1. Y. Matsuura, N. Kitai, R. Ishii, et al., *JMMM* **398**, 246 (2016).
2. A.N. Urzhumtsev, V.E. Maltseva, A.S. Volegov, *JMMM* **551**, 169143 (2022).
3. A.N. Urzhumtsev, V.E. Maltseva, V.Yu. Yarkov, A.S. Volegov, *Phys. Metals Metallogr.* **123**, 1054 (2022).

P13

Description of piezocomposite dielectric spectra using a new Havriliak-Negami equation-based model

A.V. Yudin[1,3], Y.I. Yurasov[1,2], V.V. Likhatsky[1,2], A.V. Nazarenko[1]

[1]*Federal Research Centre the Southern Scientific Centre of the Russian Academy of Sciences, 344006, Rostov-on-Don, Russia*

andryudin1997@gmail.com

[2]*Southern Federal University, Rostov- on-Don, Rostov- on-Don, Russia*

[3]*South-Russian State Technical University (NPI) of the M.I. Platov, Novocherkassk, Russia*

Piezocomposite manufacturing is one of the most promising technologies that leads to new developments in different industrial fields. The materials produced find its application in medicine, machinery, aerospace engineering, and electronic devices.

An exhaustive structural properties description is an important step of RnD process in material science. In the case of piezocomposite compounds the dielectric characteristics, such as permittivity ε, dielectric loss tangent tgδ and conductivity γ, among the parameters of interest. The iterative measurements under different external conditions lead to a data set formation. The latter is used to build a characteristic spectrum of the variables under consideration.

To fit the results and analyze a generalized structural response an approximation approaches are often applied. One of the most widely used is Havriliak-Negami model. In comparison with analogues, it combines simplicity, reliability and universality. It is applicable in different branches of science such as chemistry, medicine, hydrodynamics, geophysics, genetics, magnetism and so on. However, this leads to a disadvantage of parametric description that requires lots of experiments and observations.

To solve this issue in the field of electrical conductivity, a particular solution was developed and described in [1-4]. The model obtained allows the complex temperature-frequency response estimation for different materials and formulates as follows:

$$\gamma^* = \gamma_\infty + \sum_{n=1}^{\infty} \frac{\Delta\gamma_n}{\left(1+(i\omega\tau_n)^{1-\alpha}\right)^{\beta}} + \varepsilon_\infty''\omega\varepsilon_0 + i\varepsilon_\infty'\omega\varepsilon_0 \quad (1)$$

$$\alpha = \frac{kT}{E_a}\ln\left(Q_\infty\right) \quad (2)$$

where $\gamma^* = \gamma' + i\gamma''$ – total complex permittivity; ε'_∞, and ε''_∞ – real and imagery permittivity parts of ε* when $\omega\to\infty$; $\varepsilon''_\infty\omega\varepsilon_0$ – singular part responsible for conductivity values; $\varepsilon'_\infty\omega\varepsilon_0$ – additional part; $\Delta\gamma_n = \gamma_{Sn} - \gamma_{\infty n}$; n – number of relaxation process; $\gamma_{Sn} = \gamma_{\infty n-1}$; α, $\beta = 1 - \alpha$ – parameters of the temperature-frequency distribution of dielectric losses in piezocomposites ($0 \le \alpha \le 1$, $0 \le \beta \le 1$); $Q_\infty = \varepsilon'_\infty/\varepsilon''_\infty$– quality factor measured at high frequency ($\omega\to\infty$). The system is completed with M′ and M″ modulus calculation formulated as:

$$M' = \frac{\varepsilon'}{\varepsilon'^2+\varepsilon''^2},\ M'' = \frac{\varepsilon''}{\varepsilon'^2+\varepsilon''^2} \quad (3)$$

The system presented allows a high accuracy approximation of piezocomposite dielectric spectra. It was applied to analyze the structural characteristics of a lead-free polymer-containing compound (1-x)KNN-LTSN-xPVDF.

The results obtained are shown at the Figures 1, 2. The data presented shows a good agreement between experimental data and approximation curve. It demonstrates a great potential of the model in the field of piezoelectric materials description. The future research is concentrated at two-point measurement model that will allow significantly reduce the experimental costs.

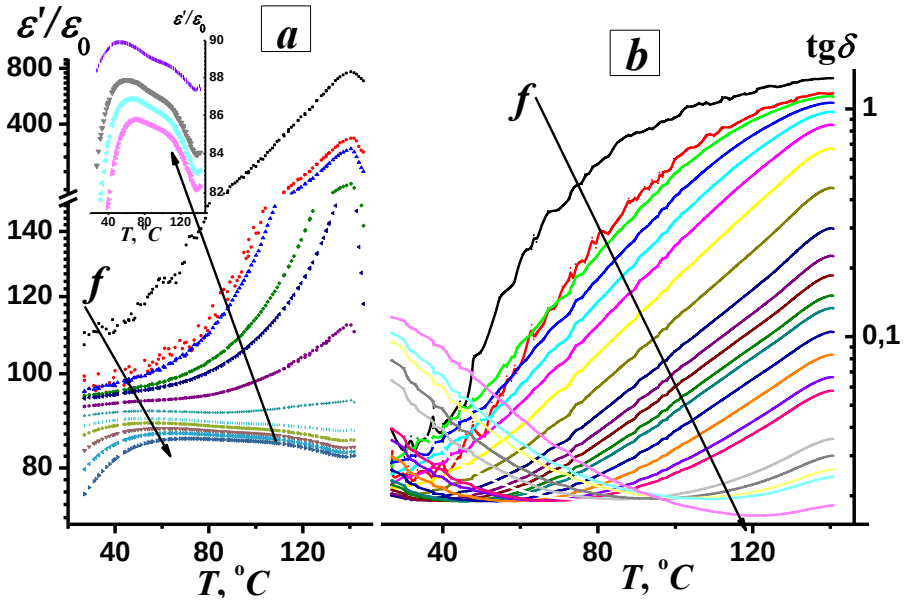

Figure 1. Temperature-frequency dependencies for piezocomposite (1-*x*)KNN-LTSN-*x*PVDF with *x* = 50 mol.%.

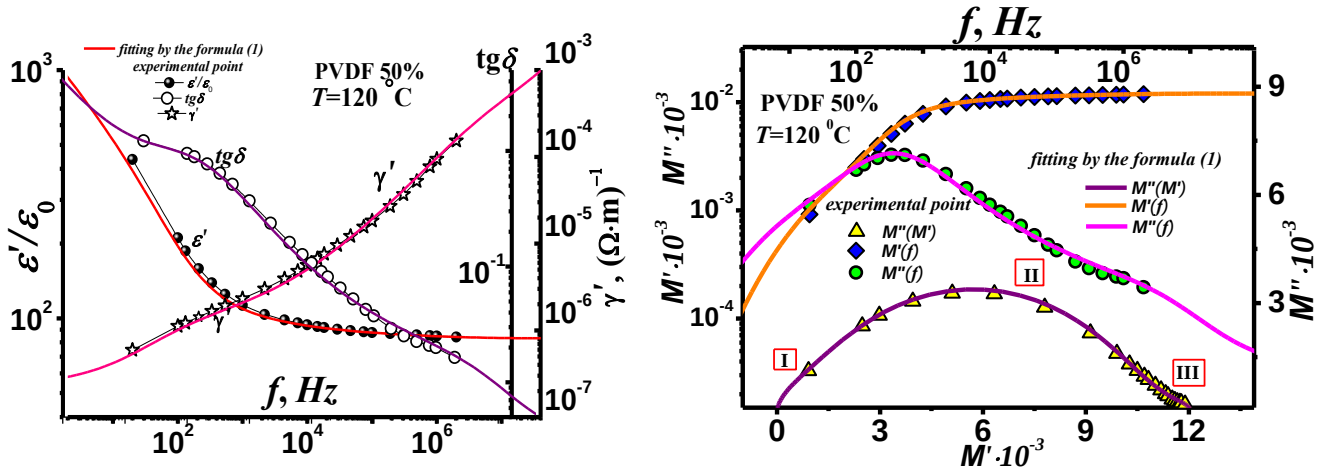

Figure 2. Behavior of $\varepsilon'/\varepsilon_0(f)$, $\mathrm{tg}\delta(f)$, $\gamma'(f)$ (a) and $M'(f)$, $M''(f)$, $M''(M')$ (b) for piezocomposite (1-*x*)KNN-LTSN-*x*PVDF with *x* = 50 mol.%. at 120°C.

This work was financially supported by the Ministry of Education and Science of the Russian Federation SSC RAS (No. 122020100254-3, 122020100352-6). On the equipment of the Central Collective Use Center of the SSC RAS No. 501994.

1. Y.I. Yurasov, A.V. Pavlenko, A.V. Nazarenko, *Program for PC* № 2019610938 (2019).
2. Y.I. Yurasov, A.V. Nazarenko, *Sci. South Russ.* **14**, 35 (2018).
3. Y.I. Yurasov, A.V. Nazarenko, *Sci. South Russ.* **15**, 31 (2019).
4. A.V. Nazarenko, A.V. Pavlenko, Yu.I. Yurasov, *J. Adv. Dielectr.* **12**, 2160013 (2022).
5. Y.I. Yurasov, A.V. Nazarenko, *J. Adv. Dielectr.* **10**, 2060006 (2020).
6. Y.I. Yurasov, M.I. Tolstunov, A.V. Nazarenko, et al., *J. Adv. Dielectr.* **11**, 2160015 (2021).

P14

Simulation of vacancy distribution in TiO_2 nanodots for memristive neuromorphic structure design

A.A. Avakyan[1], V.I. Avilov[1], I.L. Jityaev[1,2], V.A. Smirnov[1,2]

[1]*Southern Federal University, Institute of Nanotechnologies, Electronics and Electronic Equipment Engineering, Research Laboratory Neuroelectronics and Memristive Nanomaterials (NEUROMENA Lab), 347922, Taganrog, Russia*
izhityaev@sfedu.ru

[2]*Southern Federal University, Institute of Nanotechnologies, Electronics and Electronic Equipment Engineering, Department of Radioelectronics and Nanoelectronics, 347922, Taganrog, Russia*

This work reports on the study of distribution processes of electric field strength and conductive filaments in titanium oxide nanostructures (ONS) formed by the local anodic oxidation (LAO) method. Models that consider generation/recombination processes of oxygen vacancies and their migration under the action of an electric field in defect-free oxide structures.

Bottom electrode is a titanium film. The shape of the oxide nanostructure corresponds to LAO technology. The microscope probe is the top electrode. Such a structure is most often used in practice in local studies of nanoscale structures. The radius of the probe varied within 5÷50 nm. A decrease in the probe radius should contribute to an increase in the electric field strength at its tip and, accordingly, in the oxide in the interelectrode gap. In turn, the electric field strength affects the value of the energy barrier, which must be overcome to activate the processes of vacancy generation in the oxide nanostructure.

Figure 1a shows a general view of the model, where the probe (top electrode) is shown in pink, the oxide layer formed by the LAO is in yellow, the titanium layer (bottom electrode) is in violet, and the vacuum medium is blue.

The study of memristor oxide structures using a probe is accompanied by its local insertion into the near-surface region of the oxide. It follows from the simulation results (Fig. 1b) that this leads to the appearance of two points in the probe/oxide contact zone with the maximum electric field strength. Increasing the probe tip radius makes it possible to localize the maximum points farther apart, but at the same time contributes to the achievement of lower values of the electric field strength.

The oxide regions with the maximum electric field strength become centres where vacancies are generated in the oxide. Figure 1c shows the results of the formation of conductive filaments in the ONS with a rounding radius of the probe top of 50 nm. Areas with vacancies are shown in red; gradient contour lines show areas with the highest concentration of vacancies.

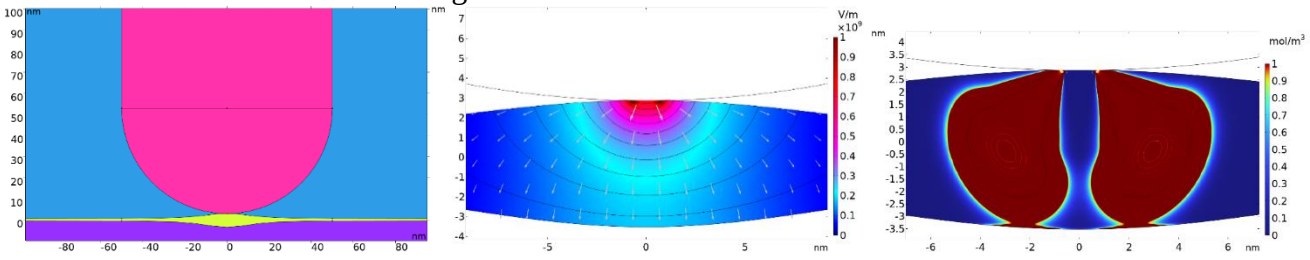

a) b) c)

Figure 1. Simulation results: a) general view; b) electric field strength distribution; c) vacancy distribution.

Studies have shown that the configuration of the probe affects the shape of the conductive filaments in the interelectrode gap of the ONS. It was found that four types of conducting filaments can form in the considered ONS during the generation and migration of vacancies: two unconnected filaments; two filaments connected at intermediate positions between the electrodes but reaching the bottom electrode by two conductive filaments; two joined filaments and reaching the bottom electrode with a single conductive filament; a single conducting filament in the entire interelectrode gap. The simulation results make it possible to understand the processes of conductive filament formation in ONS for the subsequent design of neuromorphic memristive devices.

The reported study was funded by the Russian Federation Government (Agreement No. 075-15-2022-1123).

P15

Using Atomic-Force Microscope for isolation a single upconversion luminescent nanoparticle

A.P. Chuklanov, N.I. Nurgazizov, E.O. Mityushkin, D.K. Zharkov, A.V. Leontiev, V.G. Nikiforov

Zavoisky Physical-Technical Institute, FRC Kazan Scientific Center, Russian Academy of Sciences, 420029, Kazan, Russia
a.chuklanov@gmail.com

Luminescent nanoparticles with an upconversion type of excitation (when two low-energy IR photons are absorbed and a visible spectrum photon is emitted) are used in many areas. In particular, due to the unambiguous dependence between the intensity of luminescent lines on temperature, such nanoparticles can be used as ultrasensitive thermometers with high spatial and time resolution [1]. If Upconversion Nanoparticles (UCNP) are used as temperature sensors, the measurement occurs by recording the ratio of line intensities in the spectrum of rare earth ions, which is the one of the simplest and most accurate method for remote measurement. One of the problems of using UCNP in applications is the strong variation of size and shape because of synthesis technology. This, in turn, leads to a noticeable difference in the luminescence spectra and to difficulties in calibration. To solve the problem described above, it is necessary to select UCNP by size. Therefore, in this work we propose the combined use of atomic force microscopy (AFM) and confocal optical microscopy (COM).

The synthesis of YVO_4 UCNP doped with Er^{3+} and Yb^{3+} was carried out by hydrothermal method [2]. Polished Si and glass plates with mechanically microscratch marks were used as the substrate. The width of the microscratches was selected in such a way that they could be visualized both AFM and COM. Thus, it is possible to compare AFM and COM data. To make manipulations with UCNP the Solver-Bio (NT-MDT) AFM combined with a conventional optical microscope was used. N11-A AlBS probes with hardness of 3 N/m and a resonant frequency of 60 kHz was used.

The UCNP manipulation algorithm consisted of several stages: (i) first, an appropriate place was chosen in the Solver-Bio optical microscope (near the intersections of marks-microscratches on substrate), (ii) an AFM image of the surface was recorded in the semi-contact mode with a large lateral scanning field (Fig. 1a), (iii) a suitable object was selected (for example, object A1 in Fig. 1a), (iv) the AFM was switched to contact mode and a series of scans were performed, the starting point, size and direction of which were chosen in such a way that as a result only one desired object remained in the field under study and (v) the results obtained were controlled in the semi-contact mode. Thus, the one UCNP was isolated on the glass substrate. It has a polarization in luminescence spectrum, that is not observed in spectra of UCNPs ensemble.

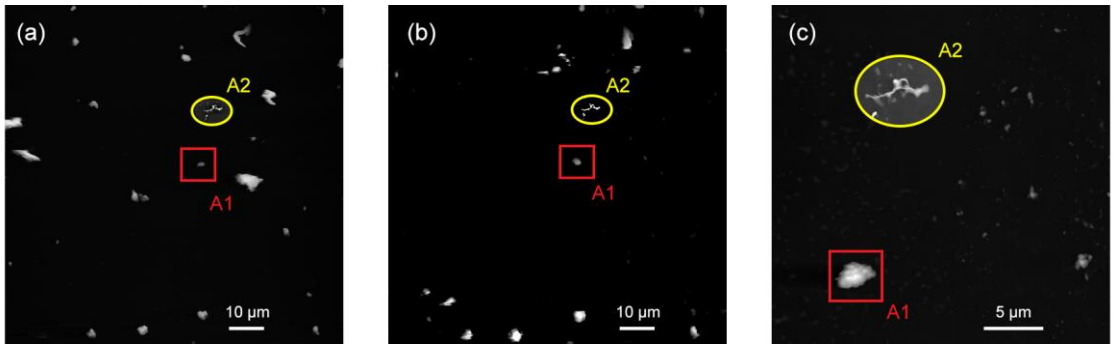

Figure 1. AFM images of surface with UCNP: (a) initial image; (b) after clearing by AFM; (c) after clearing, zoom. A1 is the region containing suitable object. A2 is a surface area with a characteristic shape defect that remained unchanged in the process of manipulating (the local contrast of the A2 area is increased for clarity).

The work supported by RSF (grant № 23-29-00516).

1. C. Zaldo, *Adv. Nanomat*. 335 (2018).
2. D.K. Zharkov, A.G. Shmelev, A.V. Leontyev, et al. *Laser Phys. Lett.* **17**, 075901 (2020).

P16

Triboelectric current generation by friction of AIIIBV and Si surfaces

M.S. Dunaevskiy, V.A. Sharov, D.A. Malykh, P.A. Alekseev

Ioffe Institute, Saint-Petersburg, Russia 194021
Mike.Dunaeffsky@mail.ioffe.ru

When a conducting contact is rubbed against the surface of a semiconductor substrate (without external electrical voltage) an electric current flows in the "movable electrode-substrate-external load" circuit [1]. This phenomenon is called triboelectric generation, which was previously demonstrated when the probe is rubbed against the surface of Si [2], GaAs [3], InP [4], and other semiconductor materials. The mechanism of triboelectric generation in semiconductor materials is debatable, and possible explanations include the tribovoltaic effect [5], tunneling of hot carriers through a natural surface oxide [6], flexoelectricity [7], and other models.

For the practical application of triboelectric generators, it is necessary to maximize their efficiency and achievable output power. One way to increase the output power is to increase the short circuit current. It has been shown in a number of works that an increase in the density of surface states leads to a significant increase in the short circuit current [2]. In III–V semiconductors, the density of surface states is several orders of magnitude higher than in Si, and high triboelectric current densities can be achieved during friction. The purpose of this work was to study triboelectric generation during friction of a conducting probe against a p- and n-GaAs surface and to discuss possible mechanisms that determine its efficiency.

The generation of a triboelectric current upon friction of a conducting probe against a GaAs surface with a natural oxide layer is studied. It is shown that the triboelectric current in GaAs is two orders of magnitude higher than the current in Si, and the current polarity is determined by the work function difference between the probe and the GaAs surface. An increase in the triboelectric current in GaAs compared to Si is due to the high density of amphoteric surface states and the tunneling of electrons from the probe to them during friction.

1. R. Yang, R. Xu, W. Dou, et al., *Nano Energy* **83**, 105849 (2021).
2. S. Lin, R. Shen, T. Yao, et al., *Adv. Sci.* **6**, 1901925 (2019).
3. M. Wang, J. Yang, S. Liu, et al., *Adv. Mater. Tech.* **8**, 2200677 (2023).
4. V.A. Sharov, P.A. Alekseev, B.R. Borodin, et al., *ACS Appl. Energy Mater.* **2**, 4395 (2019).
5. Z. Zhang, D. Jiang, J. Zhao, et al., *Adv. Energy Mater.* **10**, 1903713 (2020).
6. J. Liu, M. Miao, K. Jiang, et al., *Nano Energy* **48**, 320 (2018).
7. K.P. Olson, C.A. Mizzi, L.D. Marks, *Nano Lett.* **22**, 3914 (2022).

P17

Self-assembly of the dipeptide L-Alanyl-L-Phenylalanine under the action of methanol vapor with the formation of micro- and nanostructures

E.O. Kudryavtseva[1,2], A.S. Morozova[2], S.A. Ziganshina[1,2], M.A. Ziganshin[1], A.A. Bukharaev[2]

[1]*Kazan Federal University, Kazan, 420008 Russia*

elena.o.kudryavtseva@yandex.ru

[2]*Zavoisky Physical-Technical Institute, FRC Kazan Scientific Center, Russian Academy of Sciences, Kazan, 420029 Russia*

Molecular self-assembly is the spontaneous arrangement of molecules into ordered structures through non-covalent weak interactions. Short chain peptides (oligopeptides) have a number of advantages, such as simple synthesis, a variety of properties, the possibility of functionalization, and high biocompatibility [1]. Self-assembly makes it possible to create nanomaterials based on oligopeptides with a specific spatial structure. Depending on the chemical composition and external conditions, oligopeptides are able to form nanofibers, nanorods, nanovesicles, nanotubes, etc. [2]. Such structures are widely used in various fields, for example, in materials science, medicine, and energy. Despite the fact that various studies of nanostructures based on oligopeptides are currently being carried out, controlling the self-assembly of oligopeptide molecules in thin films and predicting the surface morphology and shape of the resulting crystals remains a difficult task.

In this work, we have proposed a method for obtaining amorphous films of the dipeptide L-alanyl-L-phenylalanine (Ala-Phe) from solutions in methanol and hexafluoroisopropanol on the surface of a silicon substrate. It is shown that the saturation of amorphous L-alanyl-L-phenylalanine films with methanol vapor results in the formation of micro- and nanosized structures on their surface. In this case, the type of structure and its shape depend both on the solvent used to obtain the film and on the time of its interaction with methanol vapor. The possibility of atomic force microscopy for determining amorphous and crystalline structures based on oligopeptides has been demonstrated.

The work was carried out within the framework of the state task of the Federal Research Center "Kazan Scientific Center of the Russian Academy of Sciences" (A.S. Morozova, E.O. Kudryavtseva, A.A. Bukharaev), as well as at the expense of the strategic academic leadership program of the Kazan (Volga Region) Federal University (Ziganshina S.A., Ziganshin M.A.)

AFM measurements were performed on the equipment Solver P47 Pro of the Central Collective Use Center of the Federal Research Center of the Kazan Science Center of the Russian Academy of Sciences.

1. S. Yang, M. Wang, T. Wang, et al., *Mater. Today Bio* 100644 (2023).
2. D. Mathur, H. Kaur, A. Dhall, et al., *Computers in Biology and Medicine* **133**, 104391 (2021).

P18

Improved hydrophilic properties of the aluminum surfaces structured by femtosecond laser irradiation

D.K. Kuznetsov, I.R. Kamalova, B.I. Lisjikh, V.Ya. Shur

School of Natural Sciences and Mathematics, Ural Federal University, 620002, Ekaterinburg, Russia
dimak@urfu.ru

Aluminum surfaces with superhydrophilic properties were produced by direct femtosecond laser micro- and nanostructuring. The created surfaces demonstrate excellent drop spreading performance at room temperature. The obtained effects highlight the potential of femtosecond laser structuring in controlling the wettability of metal surfaces for various applications.

The surfaces of 0.5-mm-thick aluminum substrates were treated by ytterbium laser system T-10W200K (OOO Femtonika, Troitsk, Russia) with a wavelength of 1035 nm and a pulse duration of 240 fs. The imaging of obtained surface structures was made by scanning electron microscope EVO LS 10 (Carl Zeiss). The surface wettability was characterized using the static contact angle. The contact angle was measured by a drop shape analyzer DSA25S (KRUSS, Germany) using the sessile drop technique.

The superhydrophilicity of structured surfaces is determined not only by strong surface oxidation after laser treatment, but also by a branched system of microcapillaries. The femtosecond laser treatment of aluminum surfaces leads to formation of periodical microchannels, the inner walls and outer edges of which are decorated with irregular shapes with sizes from several nanometers to several micrometers. Thus, because of processing by laser radiation, a micro- and nanoscale hierarchical structure is created on the surface of aluminum plates.

The developed surfaces were tested for wicking performance at room temperature. The tests show that the spreading is not uniform: in the direction of the microchannels, the water has spread much further and faster than in the perpendicular direction. After several iterations, the average drop spreading velocity decreased significantly. This effect was accompanied by an increase in the contact angle, which characterizes the surface transition from a hydrophilic state to a hydrophobic one.

The transition of laser-structured surfaces from a superhydrophilic to a hydrophobic and superhydrophobic state can be attributed to several contributions: partial decomposition of oxides on the surface [1], formation of hydrophobic functional groups on the surface [2], adsorption of hydrophobic hydrocarbons from ambient air where processed samples are stored [3]. In addition, the very process of measuring the contact angle can also affect the properties of the surface, since when measuring the contact angle, the interaction of the surface with water occurs, which can lead to an increase in some of the above effects.

1. F.M. Chang, S.L. Cheng, S.J. Hong, et al., *Appl. Phys. Lett.* **96**, 114101 (2010).
2. P. Bizi-bandoki, S. Valette, E. Audouard, S. Benayoun, *Appl. Surf. Sci.* **273**, 399 (2013).
3. K.M.T. Ahmmed, C. Grambow, A.-M. Kietzig, *Micromachines* **5**, 1219 (2014).

P19

Growth and characterization of physical properties of photovoltaic (K,Ba)(Ni,Nb)O_3 single crystals

M.H. Lente[1], Th.C. Fernandes[1], M.V. Gelfuso[2], D. Thomazini[2], J.A. Eiras[3]

[1]*Federal University of São Paulo, ZIP code 12231-280, São José dos Campos, Brazil*
mlente@unifesp.br

[2]*Federal University of Itajubá , ZIP code 37500-903, Itajubá, Brazil*

[2]*Federal University of São Carlos , ZIP code 13565-905, São Carlos, Brazil*

The increasing demand of the society for energies free from fossil fuels has demanded the development of new sources of green energy. In this context, photovoltaic devices are a well-known safety solution to convert solar energy into electricity. Concerning light absorber materials, ferroelectric oxides are promising candidates for substituting Si-based compounds in solar-energy conversion devices due to their relative low cost and the bulk photovoltaic effect instead of the classical p-n junction. In this work, (K,Na)(Nb,Ni)O_3 (KBNN) single crystal was grown by the Bridgman-Stockbarger method and their physical proprieties were characterized. Regarding the growth process, such as soaking time, temperature gradient at the liquid-solid interface and crystal growth rates, were chosen based on the thermal properties of the precursor oxides and theoretical heat transfer models proposed in the literature. Structural, chemical, and optical properties of the as-grown KBNN crystals were characterized. The results revealed a pure perovskite crystal structure and negligible compositional segregation. The optical data showed a red-shift of the absorption edge from the UV to the visible range due to the introduction of the Ni element into the ferroelectric host lattice.

1. I. Grinberg, D.V. West, M. Torres, et al., *Nature* **503**, 509 (2013).
2. R.C. Gennari, R. Lang, J.A. Eiras, M.H. Lente, *J. Amer. Ceram. Soc.* **102**, 3923 (2018).

P20

Characterization of single-walled carbon nanotubes by Raman spectroscopy

E.A. Levkevich[1,2], R.M. Zakalyukin[1,2]

[1]*Shubnikov Institute of Crystallography, Federal Scientific Research Centre «Crystallography and Photonics», Russian Academy of Sciences, 119333, Moscow, Russia*
levkevich.k@crys.ras.ru

[2]*MIREA – Russian Technological University, 119454, Moscow, Russia*

Single-walled carbon nanotubes (SWCNT) were studied by Raman spectroscopy using a 3D scanning laser Raman spectrometer Confotec NR500 using three lasers: green 532 nm (~2.33 eV), red 633 nm (~1.96 eV) and infrared 785 nm (~1.58 eV).

Several characteristic features can be observed in the spectra of single-walled carbon nanotubes (Fig. 1): first-order phonon modes – RBM (radial breathing mode ~100 – 300 cm $^{-1}$) and G (graphene mode ~1500 – 1600 cm^{-1}), second-order phonon modes – D (disorder induced mode ~1300 – 1350 cm^{-1}), 2D (second harmonic of the D mode ~2600 – 2700 cm^{-1}). As a rule, the G band is the most intense in the spectrum; however, one can observe that as the laser energy decreases, the relative intensity of the RBM band increases, and at 1.58 eV it becomes maximally intense. The intensity of the D band is about 5% of the intensity of the G band, which indicates the minimum number of defects in the sample.

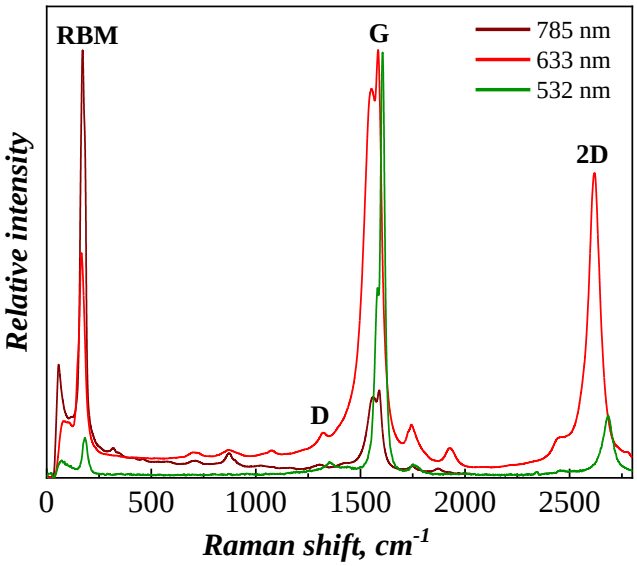

Figure 1. Raman spectroscopy of single-walled carbon nanotubes.

Of greater interest is a more thorough study of the RBM and G bands of the spectra. The former characterizes the distribution of SWCNT over diameters, while the latter characterize their electronic state. For this purpose, these spectral regions were studied with another diffraction grating (1800/500 instead of 300/600). An analysis of the RBM peaks positions indicates that SWCNT with diameters from 1.3 to 1.7 nm occur in the array of the studied nanotubes, with the predominant diameter being about 1.5 nm. As for the G bands, in the semiconducting resonance window (532 nm and partially 633 nm) there are three components (G+ or G_{LO}, G- or G_{TO}, G_{E2g}). When metallic SWCNT are in resonance (785 nm and partially 633 nm) G band has another three components: G+ or G_{LO}, G- or G_{TO}, G_{BWF}. The data obtained are consistent with the Kataura plot [1].

1. H. Kataura, et al., *AIP Conference Proceedings* **486**, 328 (1999).

P21

Characterization of carbon materials by Raman spectroscopy

E.A. Levkevich[1,2], R.M. Zakalyukin[1,2]

[1]*Shubnikov Institute of Crystallography, Federal Scientific Research Centre «Crystallography and Photonics», Russian Academy of Sciences, 119333, Moscow, Russia*
levkevich.k@crys.ras.ru

[2]*MIREA – Russian Technological University, 119454, Moscow, Russia*

Graphite, thermally expended graphite (TEG), oxidated graphite (OG), graphene, single-walled carbon nanotubes (SWCNT) were studied by Raman spectroscopy (Fig. 1) using a 3D scanning laser Raman spectrometer Confotec NR500 using green laser 532 nm (~2.33 eV).

All spectra contain characteristic features of carbon structures (Table 1):

G-band (graphite/graphene mode, ~1580 cm^{-1}) characterizes graphene/graphite in the plane of the sp^2 vibrational mode and displays the degree of the material crystallization. Unlike graphene/graphite, the G-band of carbon nanotubes consists of several peaks due to twisting effects. Two main components: G+ (oscillations of atoms parallel to the nanotube axis – LO phonon mode); G- (oscillations of atoms along the direction perpendicular to the nanotube axis tangentially to its wall – phonon mode TO). At a laser energy of ~2.33 eV SWCNTs of the semiconductor type are excited.

D-band, second-order mode (disorder-induced mode, ~1350 cm^{-1}) reflects the degree of structural disorder. The ratio of the Raman peaks intensities of the two bands (I_D/I_G) is used to calculate degree of material disorder.

2D (G')-band, second-order mode (~2700 cm^{-1}) – second harmonic of the D-mode. As applied to graphene, it is used to estimate the number of carbon layers if it is possible.

For SWCNT, due to their cylindrical geometric shape, there are features that are characteristic only for this type of structure. RBM-bands, first-order modes (radial breathing mode, ~120 – 350 cm^{-1}) correspond to radial vibrations of carbon atoms. It is possible to estimate the diameter distribution of SWCNTs from the positions of the peaks. Positions of the most intense peaks indicate that SWCNTs with a diameter of 1.8 – 2.2 nm predominate in the array of the studied carbon nanotubes.

Table 1. Comparison of the main bands of the Raman spectra of the studied carbon materials.

Material	D band, cm^{-1}	G band, cm^{-1}	I_D/I_G	2D band, cm^{-1}
graphite	1353.24	1581.19	0.081	2707.12
OG	1360.16	1580.63	0.013	2706.01
TEG	1350.67	1579.31	0.035	2706.17
graphene	1349.09	1577.90	0.044	2695.25
SWCNT	1345.71	G+ 1588.10 G- 1562.42	0.027	2670.61

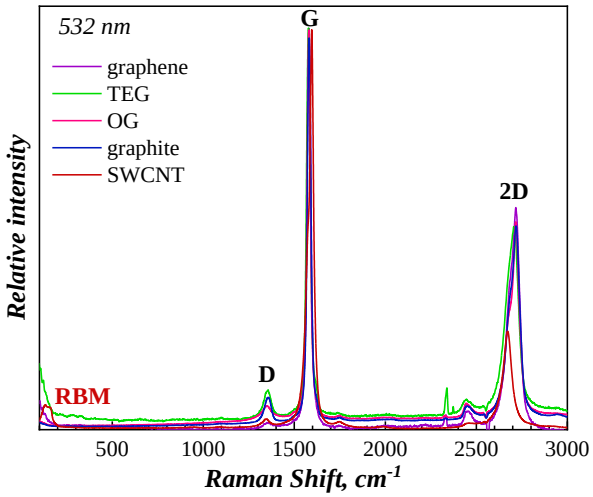

Figure 1. Raman spectroscopy of carbon materials.

P22

Overview and verification of the AFM cantilever stiffness calibration techniques

S.A. Melnikov, M.S. Kosobokov, L.V. Gimadeeva, D.K. Kuznetsov, V.Ya. Shur, D.O. Alikin

School of Natural Sciences and Mathematics, Ural Federal University, 620000, Ekaterinburg, Russia
mihail.kosobokov@urfu.ru

The determination of the atomic force microscopy (AFM) cantilever stiffness is everyday routine in the nanomechanical measurements and other techniques required quantification of the forces acting on the probe. Typically, manufacture provides a range of the values for cantilever stiffness, as the technological process involved in probe fabrication introduces variability that affects the probe's geometry, particularly its thickness. Therefore, it is often the user's responsibility to accurately calibrate the probes. Over the last few decades, reputable metrological institutions have proposed several highly accurate techniques for cantilever calibration, with an average error often below 3% [1,2]. However, many of these techniques present challenges in terms of implementation or require expensive external equipment, which is often not accessible to the average user. Fortunately, there are simpler and more widely available calibration techniques: analytical calculation the stiffness based on dimensional parameters or eigen frequencies, evaluation the stiffness from the parameters of the cantilever's constrained vibration (known as the Sader method) [3], or determination the stiffness through the measurement of thermal noise [4]. Another method involves performing quasistatic measurements of the cantilever stiffness by applying pressure against a reference cantilever with known parameters [5].

In this report, we compare the results obtained from these techniques with the measurement data from a Doppler vibrometer, which is provided by the probe manufacturer. Furthermore, we verify these results by conducting an in-depth analysis of the cantilever stiffness using finite element simulations, both in simplified and realistic geometries. We discovered that the values of cantilever stiffness obtained using the dimensional and dynamical methods require correction due to the distributed nature of the probe. These methods, along with the advanced Doppler vibrometer-based method, provide cantilever values that do not account for the stiffness of the probe. This omission can lead to significant errors in the force measurements with loaded beam end. To address this issue, we propose a novel algorithm for determining cantilever stiffness. This algorithm is based on finite element simulations of the probes in realistic geometries, and it optimizes the geometric parameters by fitting the cantilever eigen frequencies. The values obtained through this approach demonstrate the closest agreement with the results of thermal noise measurements, which also consider the stiffness of the probe. Therefore, a combination of complimentary thermal noise measurements and FEM simulations offers a robust approach to calibrate cantilever stiffness and sensitivity and avoid direct contact with the surface, thereby preserving the probe's integrity and preventing deformation.

The research funding from the Ministry of Science and Higher Education of the Russian Federation (Ural Federal University Program of Development within the Priority-2030 Program) is gratefully acknowledged. The equipment of the Ural Center for Shared Use “Modern nanotechnology” Ural Federal University (Reg. no. 2968), which is supported by the Ministry of Science and Higher Education RF (Project no. 075-15-2021-677), was used.

1. T.U. Ilmenau, P. Bundesanstalt, *IMEKO 23rd TC3, 13th TC5, 4th TC22 Int. Conf.*, Helsinki, Finl. (2017).
2. R.S. Gates, J.R. Pratt, *Nanotechnology* **37**, 375702 (2012).
3. J.E. Sader, J.A. Sanelli, at al., *Rev. Sci. Instrum.* **83**, 103705 (2012).
4. R. Proksch, T.E. Schäffer, at al., *Nanotechnology* **15**, 1344 (2004).
5. R.S. Gates, M.G. Reitsma, *Rev. Sci. Instrum.* **78**, 086101 (2007).

P23

Morphological and functional changes in Fe_2O_3 films under a thermal treatment at different temperatures

K.A. Merencova, V.V. Izyurov, M.S. Artemyev, I.A. Desyatnikov, S.S. Dubinin, A.P. Nosov

M.N. Mikheev IPM UB RAS, 620018, Ekaterinburg, Russia
merencovak@imp.uran.ru

α-Fe_2O_3 (hematite) is the oldest known iron oxide and is widely distributed in rocks and soils. This oxide has not only found wide applications in human life, but also are promising materials for such high-tech industries as micro- and optoelectronics, robotics, computer science [1], antiferromagnetic spintronics [2]. The hematite phase has a corundum crystallographic structure [3] with a bulk lattice constant of c=1.37489 nm. Hematite has unique magnetic properties: it is antiferromagnetic below the Morin temperature of 260 K and "weakly" ferromagnetic in the temperature range from 260 K to the Nel temperature of 950 K, above which it is paramagnetic. Hematite is a centrally symmetric antiferromagnet with an even principal axis of symmetry, in which the "weak" ferromagnetism is due to the symmetry of the magnetic sublattices [4] and the anisotropic superexchange interaction [5]. The main studies on the physical properties of hematite have been carried out on bulk materials (mono- and polycrystals). In recent years, however, modern applications of nanospintronics have mainly required thin films and nanoheterostructures based on them.

The phase composition of hematite α-Fe_2O_3 thin films (100 nm) on c-Al_2O_3 substrates prepared by magnetron sputtering followed by heat treatment in the temperature range of 673 - 1173 K in 50 K steps was investigated.

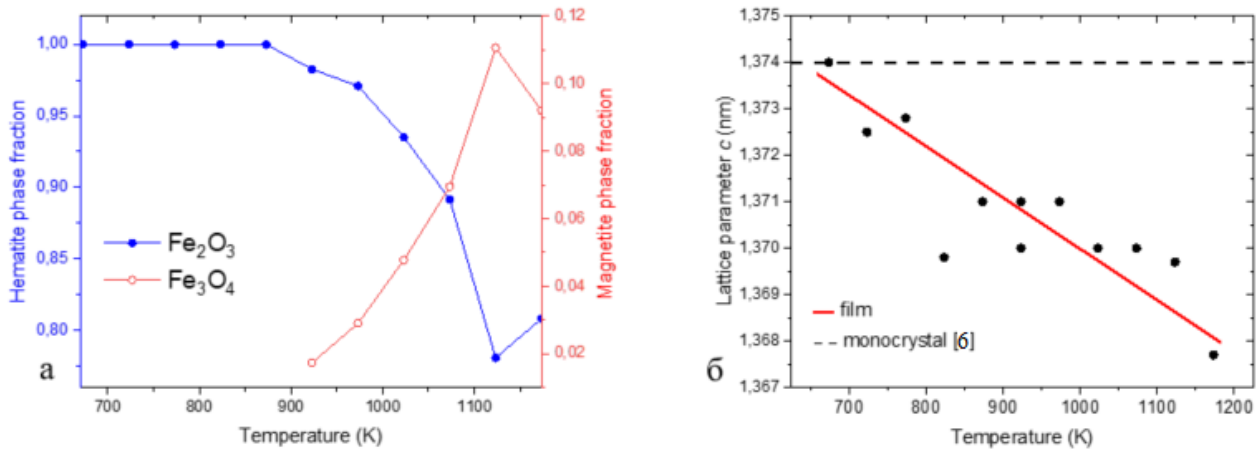

Figure 1. (a) Dependence of the phase composition of α-Fe_2O_3 films (100 nm) on the heat treatment temperature, (b) Dependence of the lattice parameter from the α-Fe_2O_3 phase on the heat treatment temperature. Dotted line is the value of c for the bulk single crystal [6].

According to the results of X-ray diffraction analysis (Fig. 1a), it was found that the samples are single-phase at the heat treatment temperatures up to 973 K. As the heat treatment temperature increases from 1023 K to 1173 K, the Fe3O4 magnetite phase is additionally formed in the films. The lattice parameter of the α-Fe2O3 phase for the films (Fig. 1b) has a lower value than for the bulk single crystal and systematically decreases with increasing heat treatment temperature.

This work was carried out within the framework of the state assignment of the Ministry of Science and Technology of the Russian Federation (subject "Function", state registration number 122021000035-6).

1. X. Liu, et al., *Sci. Rep.* **4**, 7452 (2015).
2. V. Baltz, A. Machnon, et al., *Rev. Mod. Phys*. **90**, 012002 (2018).
3. H. Wang, et al., *Phys. Rev. Lett*. **127**, 117202 (2021).
4. I. Dzyaloshinsky, *JETP* **32**, 1547 (1957).
5. T. Moriya, *Phys. Rev*. **120**, 91 (1960).
6. https://materials.springer.com/isp/crystallographic/docs/sd_054573

P24

Effect of heat treatment on the phase composition of α-Fe_2O_3 thin films: analysis by Raman spectroscopy

K.A. Merencova[1], Yu.V. Korkh[1], T.V. Kuznetsova[1,2], A.P. Nosov[1]

[1]*M.N. Mikheev IPM UB RAS, 620018, Ekaterinburg, Russia*

[2] *Ural Federal University, 620002, Yekaterinburg, Russia*

merencovak@imp.uran.ru

In recent decades, science and industry have focused their attention on the development of new materials with unique properties that can find wide applications in various fields. One such material of particular interest is hematite (α-Fe_2O_3).

Hematite is one of the most common iron oxides in nature. This material has found its application in various fields, including catalysis, photocatalysis, solar cells, sorbents [1], electrochemical devices, and magnetic materials. Its unique properties, such as high chemical stability, excellent electrical conductivity, and ability to be used in various environmental conditions, make it very attractive for many technological applications. In modern science and technology, thin films and nanoheterostructures based on them are most in demand.

One important aspect of the study of hematite is its structural and phase stability under various conditions. The dynamics of phase transformations in thin film systems based on Fe-O has not been studied sufficiently. Heat treatment of hematite thin films in a certain temperature range can lead, in general, to more complex phase transformations as compared to bulk materials.

Thin films of α-Fe_2O_3 on c-Al_2O_3 substrates, were obtained by AC magnetron sputtering of a polycrystalline target of stoichiometric composition in an atmosphere of 90%Ar + 10%O_2. During the sputtering process, the substrate temperature was 200 °C. Sputtering occurred at a rate of 0.43 nm/min. After sputtering the obtained films with characteristic sizes 15*11 mm were cut into samples of size ≈4.5×4.5 mm^2, each of which was heat-treated in air for 3 hours in the temperature range 400÷900 °C. The phase composition was controlled by X-ray diffraction analysis. According to the data obtained the samples heat-treated at temperatures up to 700 °C is a single phase (only hematite phase is present), and from 750 °C the additional phase of magnetite appears.

Also the phase composition of the obtained samples was studied by Raman spectroscopy [2] using a microscope Confotec MR200 (manufacturer - SOL Instruments). In the Raman spectra of all α-Fe_2O_3 films obtained at different power of excitation laser radiation, there are spectral lines characteristic of hematite phase. As the temperature of post-growth heat treatment increased, the intensity of all Raman peaks was observed. For a more detailed comparative analysis of the shape of the Raman lines, the decomposition into components using the Voigt function was carried out. The parameters of the individual components were determined, including the wavelength corresponding to the maximum λ_0. Then the dependences of λ_0 of different lines in the spectra on the temperature of heat treatment were plotted. The results are shown in Figure 1.

At temperatures of 450, 550 and 600 °C in the spectra of α-Fe_2O_3 films there are lines at 603 and 653 cm^{-1}, typical for the phase α-Fe_2O_3 [3]. At heat treatment temperatures of 650 and 700 °C the lines corresponding to hematite phase α-Fe_2O_3 are shifted towards lower wavelengths, which is characteristic of crystal lattice deformation. At temperatures of 750 °C and above the line of 603 cm^{-1} shifts towards longer wavelengths, but there is a third oscillation at a frequency of 660 cm^{-1}, characteristic of the Fe_3O_4 magnetite phase [4]. At 850 °C the line corresponding to the Fe_3O_4 phase shifts significantly towards longer wavelengths, apparently indicating improved crystallographic perfection of the magnetite phase (and possibly also a decrease in the size of magnetite nanocrystallites).

At a heat treatment temperature of 900 °C a significant shift towards lower wavelengths of 603 and 653 cm^{-1} vibration frequencies corresponding to the hematite phase α-Fe_2O_3 is observed, indicating a significant deformation of the crystal lattice of the hematite phase.

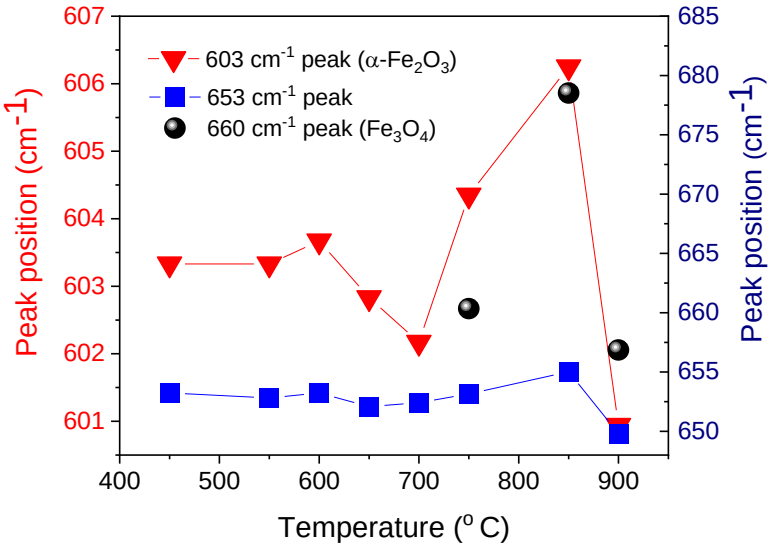

Figure 1. Positions of detected peaks in the range 600-680 cm^{-1} for the studied samples of α-Fe_2O_3 films as a function of heat treatment temperature

Thus, from the analysis of Raman spectra we can confirm the conclusion of X-ray studies that in the temperature range of 400-700 ^oC, the samples are single-phase (hematite phase α-Fe_2O_3) and are characterized by antiferromagnetic properties. At temperatures of heat treatment above 750 ^oC the formation of an additional ferromagnetic phase of magnetite Fe_3O_4.

This work was carried out within the framework of the state assignment of the Ministry of Science and Technology of the Russian Federation (subject "Function", state registration number 122021000035-6).

1. P. Sangaiya, R. Jayaprakash, *J. Supercond. Nov. Magn.* **31**, 3397 (2018).
2. H.G. Edwards, *J. Raman Spectrosc.* **36**, 210 (2005).
3. M. Giarola, G. Mariotto, *J. Raman Spectrosc.* **43**, 556 (2012).
4. C. Guo, Y. Hu, et al., *Mater. Charact.* **62**, 148 (2010).

P25

Numerical analysis of plano-concave circular transducer made of non-uniformly polarized porous piezoceramics

A.V. Nasedkin, A.A. Nasedkina, A.N. Rybyanets

Southern Federal University, 344090, Rostov-on-Don, Russia
nasedkin@math,sfedu.ru

Despite the widespread use of piezoelectric transducers in modern science-intensive industry, the tasks of improving their efficiency remain extremely important to this day. Thus, flextensional Moonie and Cymbal piezoelectric transducers were developed, demonstrating a greater coupling of planar and thickness vibrations. The standard types of the most common Cymbal transducers consist of a thickness-polarized piezoceramic disk with thin plate-shaped metal pads glued to the end surfaces of the disk. This shape of the Cymbal transducer contributes to the successful conversion of the radial oscillations of the disc into the thickness oscillations of the cymbals, and also provides sufficiently low-frequency thickness oscillations of the entire system. Another way to increase the efficiency of transducers is to use composite piezoceramic materials. In particular, porous piezoceramics have found application in hydroacoustic transducers, sensors, medical ultrasound devices, and renewable energy generators. Here, the prospects for its use are due to its lower acoustic impedance of porous piezoceramics compared to dense ones, as well as high values of piezosensitivity and hydrostatic quality indicators for both low-porous and high-porous piezoceramic materials.

Here, following [1], a combined version of the transducer is considered, including a special shape of a piezoelectric disk with one plano-concave surface and the use of porous piezoceramics as its active material. Modeling and analysis of the efficiency of such a transducer is carried out by the finite element method based on the ANSYS software package.

For this, programs in the APDL ANSYS command language were developed, which allow one to build their solid-state and finite element models with the required mesh density, perform static analysis with the calculation of the effective values of the piezoelectric moduli, determine the frequencies of electrical resonances and antiresonances, find the electromechanical coupling coefficients, obtain amplitude-frequency characteristics when applying a potential difference or electric current to the electrodes and determine various important characteristics of the transducer.

In this case, an important task of the study is to analyze the effect of the porosity of the ceramic material on the efficiency of the transducer, and the use of materials of dense piezoceramics, porous uniformly polarized piezoceramics, and inhomogeneously polarized piezoceramics with averaged moduli found by the methodology described in [2] is compared.

Numerous calculations were carried out, which made it possible to evaluate the effect of porosity and models of polarization inhomogeneity on the effective values of the piezoelectric moduli, electromechanical coupling coefficients, and on the displacements of radiating surfaces. The results obtained make it possible to recommend the considered type of transducer as an emitter and receiver of acoustic waves. By varying the radius of the concavity, the porosity of the piezoceramic, and the clamping conditions, it is possible to provide optimal transducer performance for a variety of acoustic applications.

This study was supported by the Russian Science Foundation, grant number No. 22-11-00302, https://rscf.ru/project/22-11-00302/, at the Southern Federal University.

1. A.V. Nasedkin, A.A. Nasedkina, A.N. Rybyanets, *Russ. J. Nondestructive Testing* **54**, 400 (2018).
2. T.E. Gerasimenko, N.V. Kurbatova, D.K. Nadolin, et al., *Adv. Struct. Mater.* **109**, 113 (2019).

P26

Raman spectra interpretation for $Li_4Ti_5O_{12}$ with a spinel structure

A.A. Nikiforov[1], A.S. Krylov[2], D.V. Pelegov[1]

[1]*School of Natural Sciences and Mathematics, Ural Federal University, 620002, Ekaterinburg, Russia*
alexey.nikiforov@urfu.ru

[2]*L.V. Kirensky Institute of Physics SB RAS, 660036, Krasnoyarsk, Russia*

Raman spectroscopy (RS) is an effective method, studying the composition and structure of substances by identifying the vibrational states (phonons) of atoms in a crystal lattice. The number of Raman-active modes can be determined using symmetry analysis, but sometimes the calculated number doesn't coincide with experimental data, and this can greatly complicate the quantitative analysis of experimental Raman spectra.

In this paper, we investigated lithium titanate $Li_4Ti_5O_{12}$ (LTO), a popular anode material for lithium-ion batteries. LTO has a spinel structure, for which theory predicts only six Raman-active vibrational modes. However, in practice, it is difficult to accurately describe the experimental Raman spectra for LTO with only six peaks and this makes LTO an interesting candidate to study such a discrepancy between theory and practice. Perhaps the additional bands are observed due to the fact that LTO has the structure of a defective spinel $Li[Li_{1/6}Ti_{5/6}]_2O_4$, where part of the lithium is in the position of titanium. Such irregularity can lead to the removal of degeneracy and an increase in the Raman-active vibrational modes.

In order to determine the exact number of characteristic bands to approximate the Raman spectrum for LTO, we have carried out a series of temperature measurements of powders and individual particles. The analysis of the temperature dependences allowed us to conclude that six peaks are not enough for an accurate deconvolution of the spectra, and it is necessary to use from seven to eleven peaks, each of which must correspond to its own vibrational mode.

We also carried out a series of measurements for different powers of exciting laser radiation, the comparison of which with temperature measurements allowed us to expand our recommendations for measuring and analyzing the Raman spectra for lithium titanate.

The research was carried out at the expense of a grant from the Russian Science Foundation (No 22-22-00350, https://rscf.ru/project/22-22-00350).

P27

Investigation of resistive switching of transparent memristor structures based on TiO_2 for neuromorphic systems

A.V. Saenko, V.V. Zheits, N.V. Polupanov, V.A. Smirnov

Institute of Nanotechnologies, Electronics, and Equipment Engineering, Southern Federal University, 347922, Taganrog, Russia
avsaenko@sfedu.ru

Titanium oxide (TiO_2) is the most studied wide-gap semiconductor with high transparency in the visible range of electromagnetic radiation, which opens up wide prospects for its application in transparent and flexible electronics, including machine vision. Machine vision is an important part of artificial intelligence technology. Photoelectric memristors can not only respond directly to light stimuli but also perform temporary memory and real-time processing of visual information and sensory data, providing a promising hardware foundation for the development of artificial vision systems [1, 2].

Memristor structures can switch between a high resistance state (HRS) and a low resistance state (LRS) when an appropriate voltage is applied to the electrodes. Such a change in resistance is mainly associated with the formation and breakage of conductive channels (filaments) in the oxide layer. At present, the development of memristor structures, which makes it possible to fabricate structures with controlled parameters, and the study of the resistive switching mechanism depending on the processes occurring at the boundaries between layers in the structure, is still an important task. Currently, most of the work is related to thin crystalline films of metal oxides, which are deposited on substrates at high temperatures. Such deposition methods have some drawbacks, in particular, a higher substrate temperature, which is unacceptable when creating a flexible resistive memory, as well as difficulties in improving the stability of memristors based on the filament model. Instead, amorphous TiO_2 films have the advantages of a low temperature deposition process, better oxide film uniformity observed from cell to cell, and higher stability [3].

This work is devoted to the creation and study of resistive switching in memristor structures based on TiO_2 films obtained by magnetron sputtering at room temperature (25 °C) in an oxygen-free environment on glass substrates for use in neuromorphic systems, including machine vision.

Glass/ITO/TiO_2/Ti memristor structure were formed as follows. The glass substrates were preliminarily cleaned with acetone, isopropanol and distilled water in an ultrasonic bath for 15 min respectively. A continuous thin layer of the lower ITO electrode with a thickness of about 200 nm was deposited on a cleaned glass substrate by magnetron sputtering in a pulsed mode with a frequency of 100 kHz (MF) at room temperature in an oxygen-free environment on a VSE-PVD-DESK-PRO system (AcademVak) [4]. Next, thin TiO_2 oxide layers were deposited on a continuous layer of the lower electrode, leaving a place for the lower contact using a mask. Thin films of TiO_2 were deposited when the magnetron was operating in the RF mode (frequency 13.56 MHz) at room temperature in an oxygen-free environment. The sputtered TiO_2 ceramic target (purity 99.99 %) had a diameter of 50.8 mm and a thickness of 4 mm. The sputtering power was 75 W and the operating pressure of argon was $5 \cdot 10^{-3}$ mbar. The deposition time was 15 min, which corresponded to a TiO_2 layer thickness of about 30 nm. At the final stage, the upper Ti electrode 100 nm thick and 0.453 mm^2 in area was deposited on the surface of the oxide film using a special mask using MF magnetron sputtering at room temperature in an argon atmosphere.

The film thicknesses were measured using an Alpha-Step D-100 profilometer (KLA-Tencor). The surface roughness was studied by atomic force microscopy (AFM) in the semi-contact mode at the NTEGRA nanolaboratory (NT-MDT). AFM images were processed using the Nova Image Analysis software package. Electrical measurements were carried out using a Keithley 4200-SCS (Keilhley) semiconductor measurement system and an EM-6070A submicron probing setup with tungsten probes.

Analysis of the AFM images (Fig. 1) showed that the TiO_2 films obtained by RF magnetron sputtering at room temperature in an oxygen-free environment have an amorphous structure. At the same time, TiO_2 films have a smooth surface with a fine microstructure without cracks and voids with an average roughness value of 0.7 ± 0.1 nm.

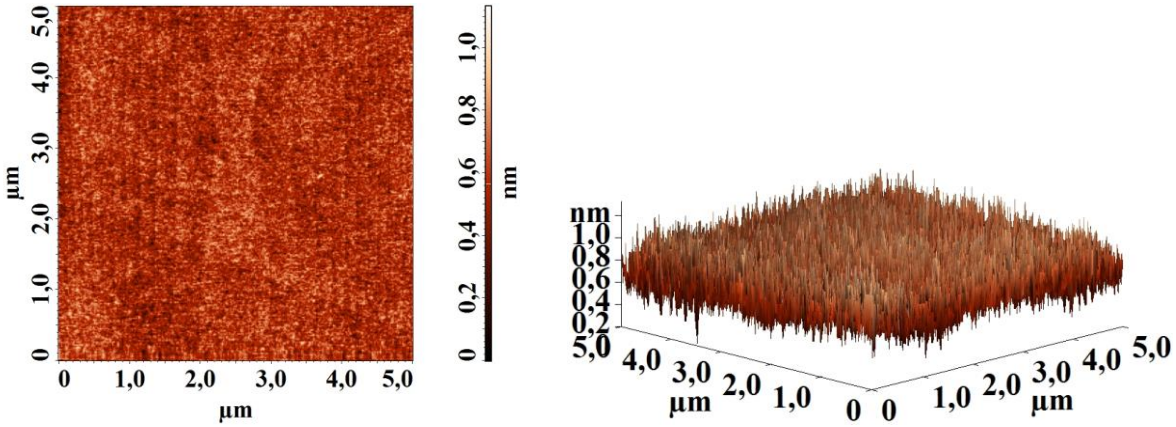

Figure 1. AFM image of the TiO_2 film surface.

During the measurement of current-voltage characteristics, a bias voltage was applied to the top Ti electrode, while the bottom ITO electrode was grounded. Figure 2a shows logarithmic current-voltage characteristics of the Glass/ITO/TiO_2/Ti memristor structure, which show the behavior of bipolar resistive switching without the initial electroforming process. Figure 2b shows the dependence of the TiO_2 film resistance on the number of switching cycles (endurance for LRS and HRS).

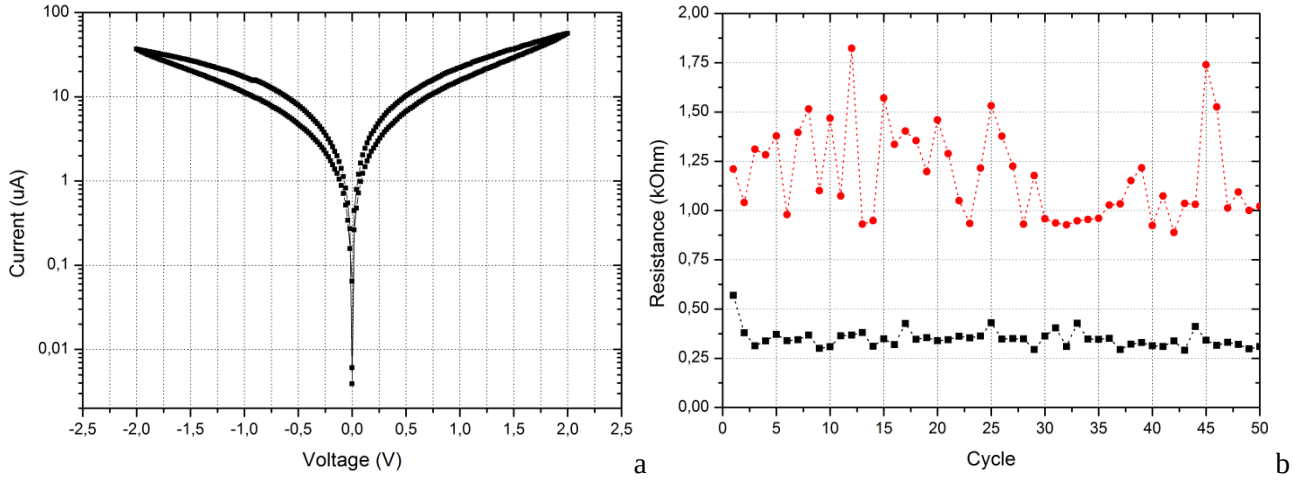

Figure 2. (a) Current-voltage characteristics and (b) resistive switching of the Glass/ITO/TiO_2/Ti memristor structure.

An analysis of the obtained results of measuring the current-voltage characteristic and studying the resistive switching of the memristor structure showed that the change in resistance from the HRS state to the LRS state occurs at 1.7 ± 0.3 V and from LRS to HRS at -1.9 ± 0.1 V, the switching current is 36.7 µA. It is shown that HRS is equal to 1.179 ± 0.233 kΩ and LRS is equal to 0.348 ± 0.047 kΩ, the resistance ratio in states is HRS/LRS = 3.38 at a read voltage of 0.005 V. A study of the dependence of HRS and LRS on the number of switching cycles showed that the state of HRS varies from 0.888 kΩ to 1.832 kΩ and LRS varies from 0.29 kΩ to 0.569 kΩ.

Thus, the possibility of creating transparent memristor structures based on TiO_2 films by magnetron sputtering at room temperature in an oxygen-free environment on glass substrates has been shown. The results obtained can be used in the manufacture of memristor structures on glass and flexible substrates for use in neuromorphic systems, including machine vision.

The reported study was funded by the Russian Federation Government (Agreement № 075-15-2022-1123) (in part of memristor structures resistive switching investigation). The fabrication of metal oxide thin films by magnetron sputtering were supported by a grant from the Russian Science Foundation № 23-29-00827, https://rscf.ru/project/23-29-00827/, at Southern Federal University.

1. Ch. Yang, B. Sun, G. Zhou, et al., *ACS Materials Letters* **5**, 2 (2023).
2. V.I. Avilov, R.V. Tominov, Z.E. Vakulov, et al., *Nano Res.* **16**, 10222 (2023).
3. H. Li, W. Dong, X. Wu, et al., *Mater. Res. Bull.* **84** (2016).
4. R.V. Tominov, Z.E. Vakulov, N.V. Polupanov, et al., *Nanomaterials* **12** (2022).

P28

New functional materials based on aluminum and gallium nitride polar structures for IR arrays

O.A. Shustova[1], I. Zezyanov[1], A.V. Solnishkin[1], O.N. Sergeeva[1], Sh. Sharofidinov[2], E.N. Mochov[2], I.P. Pronin[2], E.Yu. Kaptelov[2]

[1]*Tver State University, 170002, Tver, Russia*
o_n_sergeeva@mail.ru

[2]*Ioffe Institute, S.-Petersburg, Russia*

The presence of a spontaneously polarized state in crystals of wide-gap semiconductors of aluminum nitrides (AlN) and gallium (GaN) makes it possible to use them as functional materials for pyroelectric applications [1-3]. This paper presents the results of polar properties study of thin films, single crystals, and multilayer structures based on aluminum and gallium nitrides.

The dielectric properties were studied using an E7-30 immittance meter in the frequency range 10 Hz – 3 MHz. Pyroelectric responses were studied by the dynamic method using rectangular modulation of the heat flux in the frequency range 1÷1000 Hz.

It is shown that in thin single-crystal films of aluminum nitride and in single crystals grown by chloride hybrid gas-phase epitaxy on SiC/Si(111) substrates, and also in single crystals grown by the sublimation sandwich method [1], there is practically no dispersion of the pyroelectric current, starting from 10 Hz. Sufficiently high pyroelectric coefficient ($9\div17\times10^{-6}$ C/m^{2}K) and low dielectric constant (10÷30) provide high quality factors characterizing the operation of pyroelectric converters in a wide temperature range.

The formation of alternating layers of aluminum and gallium nitride (Fig. 1a) can lead to special dielectric and pyroelectric properties due to the formation of heterojunctions with a system of space charges. Figure 1b shows the dispersion dependences of the pyroelectric current (in the inset, the permittivity) for the AlN/AlGaN multilayer structure.ls should not exceed 11 pt at the final figure size (not to be bigger than the text).

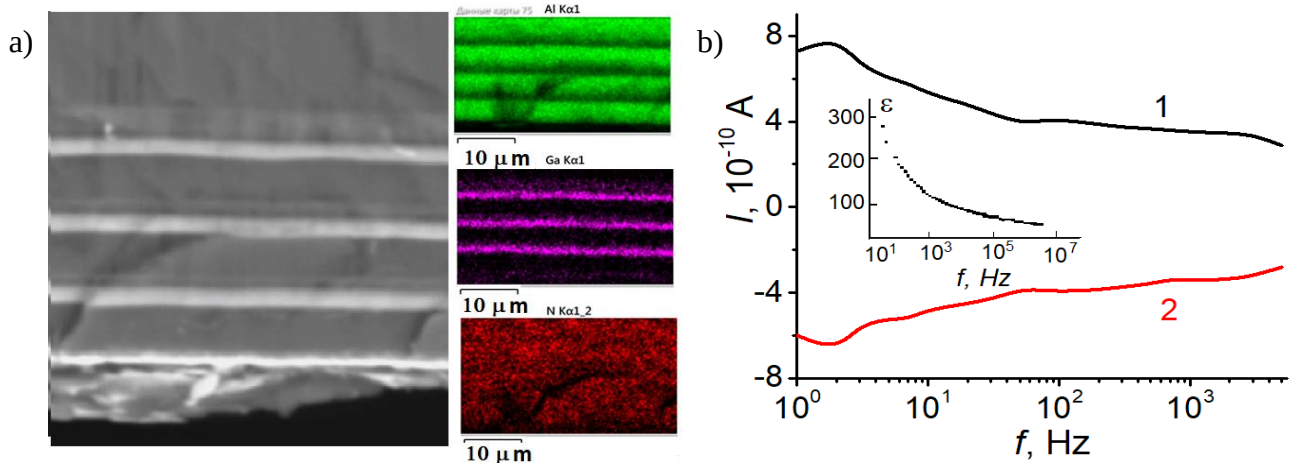

Figure 1. (a) SEM image of AlN/GaN periodic structure. (b) Frequency dependences of the pyrocurrent (1 - during heating, 2 - during cooling) and permittivity (inset) for the AlN/GaN structure.

The strongly pronounced dispersion of the permittivity indicates the contribution of the interfaces between the aluminum nitride and gallium nitride layers to the dielectric response. However, the analysis of the frequency dependences of the pyrocurrents (during heating (curve 1) and cooling (curve 2), Fig. 1) allows us to conclude that the polarization distribution over the thickness of the structure is quite uniform, which makes structures based on aluminum nitride promising functional materials for pyroelectric sensors.

1. P. Muralt, *Rep. Progr. Phys.* **64**, 1339 (2001).
2. O.N. Sergeeva, A.V. Solnyshkin, D.A. Kiselev, et al., *Phys. Solid State* **61**, 2386 (2019).
3. Sh.Sh. Sharofidinov, S.A. Kukushkin, M.V. Staritsyn, et al., *Phys. Solid State* **64**, 500 (2022).

P29

Piezoelectric hysteresis and relaxation process in ferroelectric ceramics in a weak electric field

I.A. Shvetsov, N.A. Shvetsova, E.I. Petrova, A.N. Reznichenko, A.N. Rybyanets

Southern Federal University, 344090, Rostov-on-Don, Russia
e-mail: wbeg@mail.ru

The study of domain orientation processes in ferroelectric ceramics and crystals under the influence of a dc electric field is extremely important both for the assessment of the material properties and for the practical use of these materials in ultrasonic transducers, piezoelectric sensors, and actuators. Standard methods for studying the field dependences of the properties of ferroelectric materials (measurement of hysteresis and current loops, reverse dielectric permittivity etc.) are widely used to estimate spontaneous and residual polarization, as well as to study domain orientation process in strong electric fields. These methods fail clearly when used for studying of transient processes and relaxation phenomena in ferroelectric ceramics under the influence of weak dc electric fields. Besides, these methods do not allowing estimation of complex parameters of ferroelectric ceramics responsible for the out of phase response of the material to external influences, as well as their electric field dependences. In our previous paper [1], we have proposed a new method for studying relaxation and transient processes in ferroelectric ceramics under external influences, based on the measurement and analysis of impedance spectra. Successive precision measurements and analysis of the piezoelectric resonance spectra for the thickness and radial extensional mode of vibrations of thin piezoceramic disks have provided the time and field dependences of the complex dielectric parameters of the ferroelectric ceramics under the influence of weak dc electric fields.

In this work, the piezoelectric hysteresis effect and relaxation process induced by a weak dc electric field in ferroelectric ceramics were studied using the impedance spectroscopy method and piezoelectric resonance analysis program (PRAP). The dc field and time dependences of the complex elastic, electromechanical, and dielectric parameters of ferroelectric ceramics were measured for the radial and thickness extensional modes of vibrations of thin piezoceramic disks. Successive precision measurements and analysis of the piezoelectric resonance spectra under a dc bias were made using Agilent 4294A impedance analyzer with integrated dc voltage (± 40 V) modulus. The PRAP data acquisition moduli for bias and time scan under a dc electric field was used to obtain and analyze the piezoelectric resonance spectra. The measurements were carried out in the region of weak dc electric fields (± 40 V), much smaller than the coercive field. The bias step was set at 20 V and number of cycles at 5. The sampling time of the impedance spectra was equal to 3 sec. PZT-type piezoelectric ceramics of the composition $Pb_{0.95}Sr_{0.05}Ti_{0.47}Zr_{0.53}O_3$ + 1% Nb_2O_5 were chosen as the object of the study. Thin discs of hot-pressed piezoceramics (diam. 10 mm and thickness 0.25 mm) were used for the experiments. Piezoceramic elements were polarized in air by applying to silver electrodes dc electric field (~1 kV/cm) at heating above Curie temperature (~340°C) and cooling to a room temperature.

It was shown that the obtained dc field dependences of the complex parameters of polarized ferroelectric ceramics are caused mainly by the reversible 90°- domains rotations. As a result of the studies, it was found that the relaxation nature of the time dependences of the complex parameters of the studied piezoceramics under the influence of a weak dc electric field is caused by the reversible 90°-domains rotations as well as the space charge transformations. A comparison of various methods for characterization of ferroelectric ceramics under external influences showed that the developed method based on the piezoelectric resonance analysis of impedance spectra allows obtaining more accurate data and clarifying mechanisms of relaxation and transient processes in ferroelectric ceramics taking into account the non-phase response of the material to external influences.

The work was financially supported by the Ministry of Science and Higher Education of the Russian Federation [State assignment in the field of scientific activity, Southern Federal University, 2023, Project No. FENW-2023-0015/(GZ0110/23-08-IF)].

1. I.A. Shvetsov, M.A. Lugovaya, N.A. Shvetsova, et al., *Tech. Phys. Lett.* **46**, 368 (2020).

P30

Electromechanical and ferroelectric hysteresis in dense and porous PZT-type piezoceramics

N.A. Shvetsova, I.A. Shvetsov, E.I. Petrova, A.N. Rybyanets

Southern Federal University, 344090, Rostov-on-Don, Russia
nashvecova@sfedu.ru

Ferroelectrics are a technologically important class of materials that are used in sensors, actuators, and ultrasonic transducers. Except in some special applications, electromechanical hysteresis is undesired in high-precision sensor, actuator and capacitor applications. The control, description and understanding of the electromechanical and ferroelectric hysteresis is an important and difficult matter both from a practical and theoretical point of view. Thus, the study of hysteresis can provide valuable information about various physical processes occurring in ferroelectric materials, for example, space charge relaxation, domain orientation process, pinning of domain walls, and defect ordering.

The interest towards porous ceramics has grown rapidly in recent years with the increasing demand for specific properties and features that generally cannot be achieved by their dense counterparts. Porous ferroelectric ceramics possess usually remarkably less polarizability than dense ceramics; instead they display high tenability of various physical properties [1, 2]. However, the effect of porosity on the polarization switching behavior of ferroelectrics, which is the fundamental physical process determining their functional properties, remains poorly understood. In part, this is due to the complex effects of porous structure on the local electric field distributions within these materials.

In present work, particular aspects of the switching properties and electromechanical hysteresis of the PZT-type porous piezoceramics were investigated by comparison with the dense piezoceramics of the same composition. PZT type dense and porous piezoelectric ceramics of the composition $PbTi_{0.45}Zr_{0.53}(W_{½}Cd_{½})_{0.02}O_3$ with relative porosity from 0 up to 40% and average pore size of 10÷30 μm were chosen as the object of the study. Porous PZT samples were fabricated using the pore former burning-out method. A dense PZT samples with the same chemical composition were fabricated by conventional sintering method.

Ferroelectric polarization and strain loops were recorded at the bipolar electric fields in the range of 0÷5 kV/mm and in the frequency range of 0.01÷5 Hz using a sinusoidal waveform. Measurements and analysis were performed by means of the Electromechanical Measurement System (STEPHV) and Electromechanical Response Characterization Program (STEP) from TASI Technical software Inc., combining large signal modelling of the mechanical and electrical behavior of ferroelectric materials.

Analysis of large-signal ferroelectric polarization and strain hysteresis loops made it possible to obtain full sets of parameters characterizing the switching processes and ferroelectric hysteresis behavior of the porous and dense piezoceramics and understand the effect of porosity on the polarization-field response of ferroelectric materials. It was shown that the differences in switching behavior of dense and porous piezoceramics are due to the specific features of the domain structure and microstructure of porous piezoceramics. The resulting information provides new insights in the interpretation of the physical properties of porous ferroelectric materials to inform future effort in the design of ferroelectric materials for piezoelectric sensor, actuator, energy harvesting, and ultrasonic transducer applications.

The work was financially supported by the Ministry of Science and Higher Education of the Russian Federation [State assignment in the field of scientific activity, Southern Federal University, 2023, Project No. FENW-2023-0015/(GZ0110/23-08-IF)].

1. J. Schultheiß, J.I. Roscow, J. Koruza, *Phys. Rev. Mater.* **3**, 084408 (2019).
2. A.N. Rybyanets, *IEEE Trans. Ultrason. Ferroelectr. Freq. Control*. **58**, 1492 (2011).

P31

Simulation of resistive switching in nanocrystalline ZnO films for neuromorphic systems of artificial intelligence

I.S. Ugryumov[1], R.V. Tominov[1,2], Z.E. Vakulov[1], V.A. Smirnov[1,2]

[1]*Research Laboratory Neuroelectronics and Memristive Nanomaterials (NEUROMENA Lab), Institute of Nanotechnologies, Electronics and Electronic Equipment Engineering, Southern Federal University, 347922, Taganrog, Russia*
iugryumov@sfedu.ru

[2]*Department of Radioelectronics and Nanoelectronics, Institute of Nanotechnologies, Electronics and Electronic Equipment Engineering, Southern Federal University, Taganrog 347922, Russia*

The development of CMOS technology has led to an era where artificial intelligence and machine learning have become profitable to use, potentially changing the world. There are two classes of neural networks for machine learning: algorithms based on biological mechanisms, which are still in the early stages of research and development, and artificial neural networks (ANNs), which are well understood and already used in all kinds of research and development. With the new GPUs, the ANN has achieved significant success. However, the ANN consumes a lot of energy for both training and logical inference operations when data is moved massively and frequently, which creates significant energy efficiency and performance issues. Neuromorphic computing architecture based on non-volatile memory (NVM) in-memory processing provides a new way to perform ANNs with much higher parallelism and less data transfer than traditional systems. Learning an ANN from an NVM requires many possible read-write operations, reliable memory retention, and the ability to be reversible to the initial state. For offline learning applications, where the entire learning process is performed by the server, the memory requirements are softer, while the accuracy of memory state programming and long-term memory retention are still critical requirements. Among the many NVM options, resistive random-access memory (ReRAM) stands out and becomes a very attractive candidate with its low power consumption, low production cost, high scalability, and good compatibility with CMOS processes. ReRAM is one of the most promising directions for the development of future memory technologies. In recent years, continuous improvements and in-depth research on both materials and electrical switching mechanisms have demonstrated a breakthrough in ReRAM performance. Based on a comparison of different digital memories, ReRAM is the most promising candidate for next-generation memory because of its advantages as both working memory and main memory. Like working memory, ReRAM has very low operating voltages and power, extremely high write/reset speeds, and high reliability. Unlike main memory, ReRAM is non-volatile. Moreover, thanks to its excellent integrated circuit compatibility and scalability, ReRAM has great potential for commercialization and production. However, at present, the fabrication of ReRAM elements requires solving a few problems related to modeling the processes occurring inside the oxide film and studying their influence on the final device resistance. Thus, one of the urgent tasks of modern electronics is to find a convenient model that accurately describes the processes inside the oxide film used in ReRAM memory elements.

A model was developed to solve these problems, which describes the probabilities of generation and recombination of oxygen vacancies under the action of an external electric field in the two-dimensional case. The processes are calculated in the ZnO film volume, with predetermined dimensions along two coordinate axes. For modeling we used the Python programming language with libraries: matplotlib, numpy, math, PIL, io. The simulation process consists of several stages. In the first simulation step, a given number of oxygen vacancies in the oxide film volume is randomly generated. Then the initial temperature distribution, voltage distribution and potential distribution are calculated. Then the generation of oxygen vacancies is simulated by increasing the applied voltage to the oxide film from the initial voltage to the maximum voltage with a given step. After that the voltage applied to the oxide film changes in the opposite direction of the minimum voltage. The results of calculations of temperature distribution, voltage distribution, potential distribution, and oxygen vacancy generation from the numerical data set are converted into a graphical form, as shown in Figure 1a-d.

To investigate the effect of film thickness on the high resistance state/low resistance state (HRS/LRS) ratio, the I-V was simulated (Fig. 1e). The dependence of HRS/LRS ratio on ZnO film thickness is shown in the Figure 1f.

The analysis of the obtained simulation results of the dependence of the HRS/LRS ratio on the film thickness showed that an increase in thickness from 10 to 50 nm leads to an increase in the HRS/LRS from 180 to 1942. The obtained simulation results correlate with the experimental results obtained in [9-11]. The increase in the HRS/LRS ratio can be explained by an increase in the length of the fractured section of the filament with an increase in the ZnO film thickness.

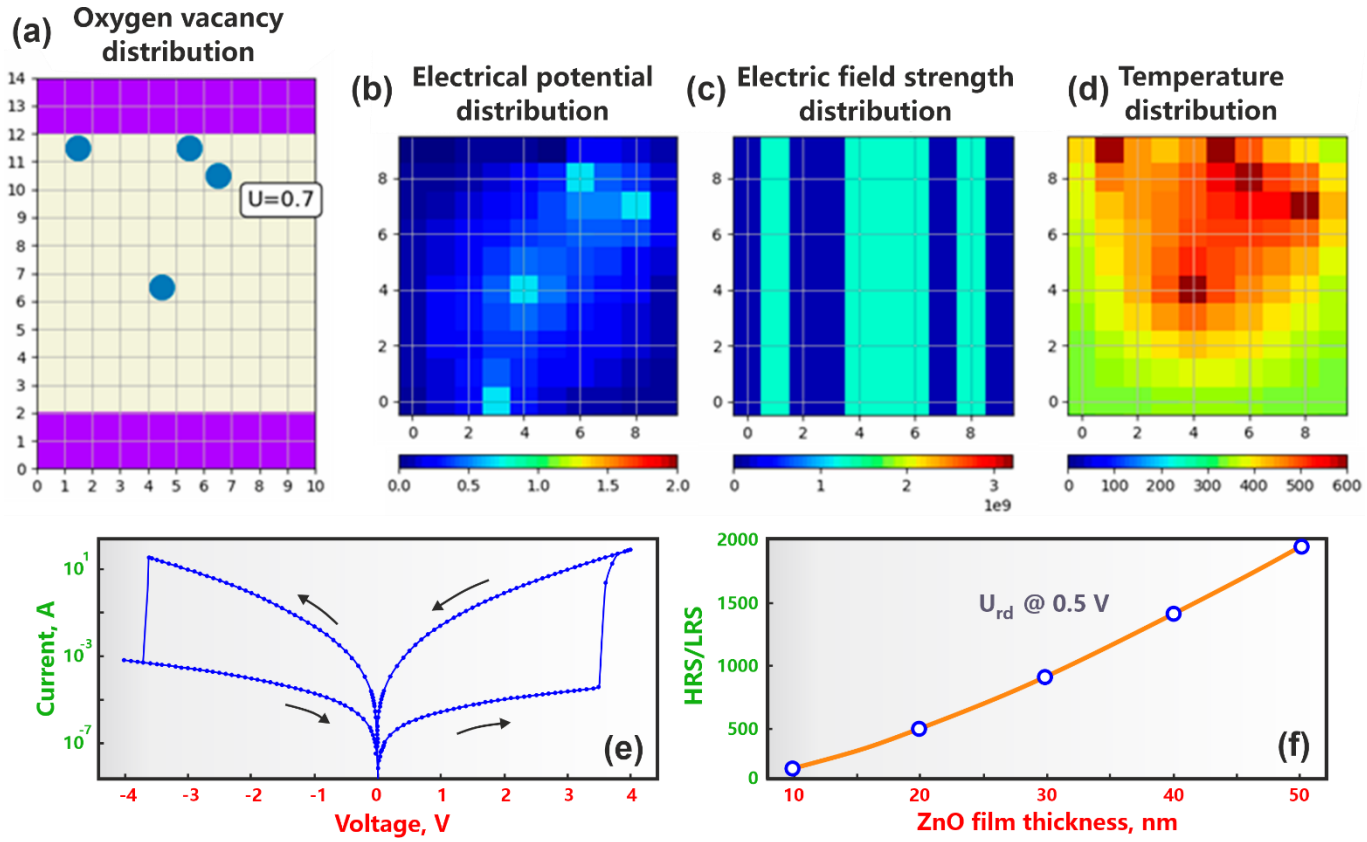

Figure 1. Simulation of the resistive switching in nanocrystalline ZnO films: (a) oxygen vacancy distribution; (b) electric potential distribution; (c) electric field strength distribution; (d) temperature distribution; (e) current-voltage characteristic; (f) HRS/LRS vs. film thickness.

The results obtained can be used in the development of neuromorphic systems based on nanocrystalline ZnO films.

The reported study was funded by the Russian Federation Government (Agreement No. 075-15-2022-1123).

1. D. Ielmini, *Semicond. Sci. Tech.* **31**, 6 (2016).
2. J. Lee, W.D. Lu, *Adv. Mater.* **20**, 1 (2018).
3. F. Pan, S. Gao, C. Chen, C. Song, F. Zeng, *Mater. Sci. Eng.: Rep.* **83**, 1 (2014).
4. Р.В. Томинов, З.Е. Вакулов, В.И. Авилов, и др., *Наноиндустрия* **13**, S5-3 (2020).
5. M. Lee, W. Lee, S. Choi, et al., *Adv. Mater.* **29**, 28 (2017).
6. Р.В. Томинов, З.Е. Вакулов, В.И. Авилов, и др., *Наноиндустрия* **15**, S8-2 (2022).
7. R. Tominov, V. Avilov, Z. Vakulov, et al., *Adv. Electr. Mater.* **8**, 8 (2022).
8. Z. Wang, M. Rao, R. Midya, et al., *Adv. Func. Mater.* **28**, 6 (2018).
9. R.V. Tominov, Z.E. Vakulov, V.I. Avilov, et al., *Nanomaterials* **10**, 5 (2020).
10. R.V. Tominov, Z.E. Vakulov, N.V. Polupanov, et al., *Nanomaterials* **12**, 3 (2022).
11. V.A. Smirnov, R.V. Tominov, V.I. Avilov, et al., *Semiconductors* **53**, 1 (2019).
12. D.B. Strukov, R.S. Williams, *Appl. Phys. A* **94**, 3 (2009).

P32

Fabrication and investigation of a Ti/TiO_x/W memristive crossbar array artificial synapses for promising neuroelectronics elements

L.G. Zhavoronkov, V.I. Avilov, N.V. Polupanov, D.A. Khakhulin, V.A. Smirnov

Southern Federal University, Institute of Nanotechnologies, Electronics and Equipment Engineering, 347922, Taganrog, Russia

zhavoronkov@sfedu.ru

The rapid development of artificial intelligence; big data analytics; systems for collecting, processing, and storing information, creates a need for hardware neural network devices that are characterized by high performance, energy efficiency, as well as reliability and scalability. An analysis of the literature has shown that memristor nanostructures capable of switching between high (HRS) and low (LRS) resistance states at high speed can be used to implement hardware neural networks as artificial synapses and differ from analogues implemented on CMOS circuits with a relatively fast processing, energy efficiency of computing processes, and simplified topology. Memristor nanostructures based on electrochemical titanium oxide have high resistive switching characteristics: a large resistance ratio of the HRS and LRS states, a long state retention time, low switching energy, and multilevel switching in a wide range of resistances [1-5].

Thus, an actual task is to manufacture an artificial synapses crossbar array layout based on the memristor nanostructures and study the regularity of their resistive switching.

The formation of the Ti/TiO_x/W memristor nanostructure was carried out using magnetron sputtering methods; optical lithography; probe nanolithography by local anodic oxidation and ion-stimulated deposition. A thin Ti film was deposited on a Si substrate by magnetron sputtering, then lower contact electrodes were formed by optical lithography, a TiO_x layer was obtained on the lower electrodes using electrochemical oxidation by probe nanolithography, and finally, upper electrodes W were formed by ion-stimulated deposition, as a result, a Ti/TiOx/W memristor crossbar structure was obtained (Fig. 1).

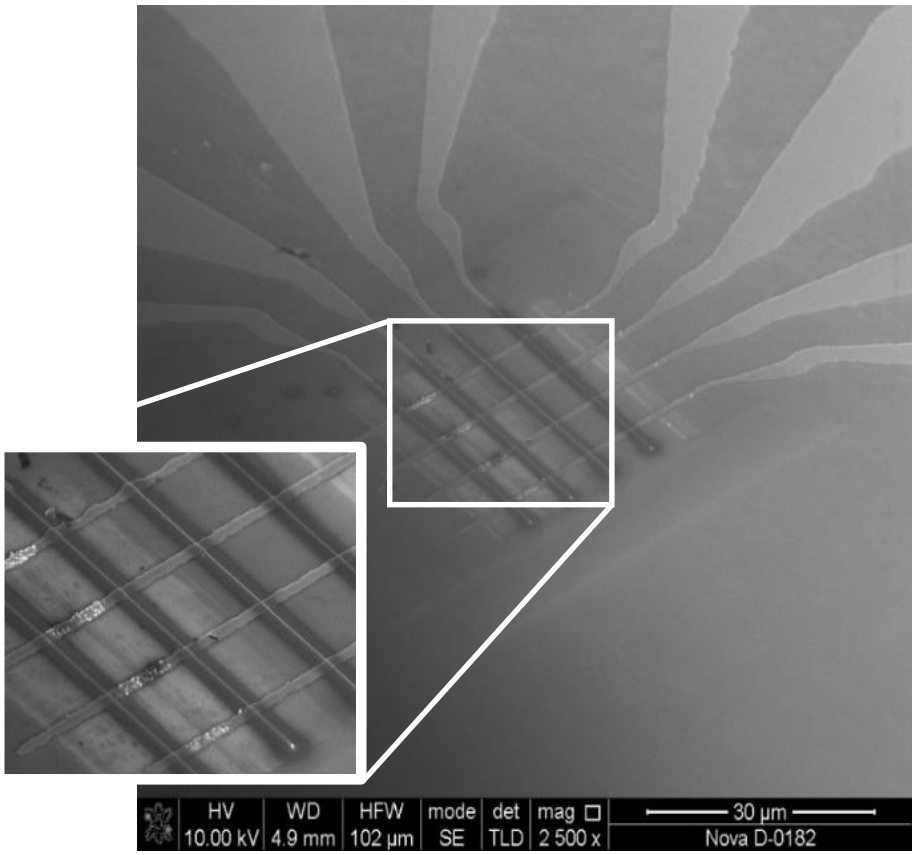

Figure 1. Crossbar array of artificial synapses SEM image.

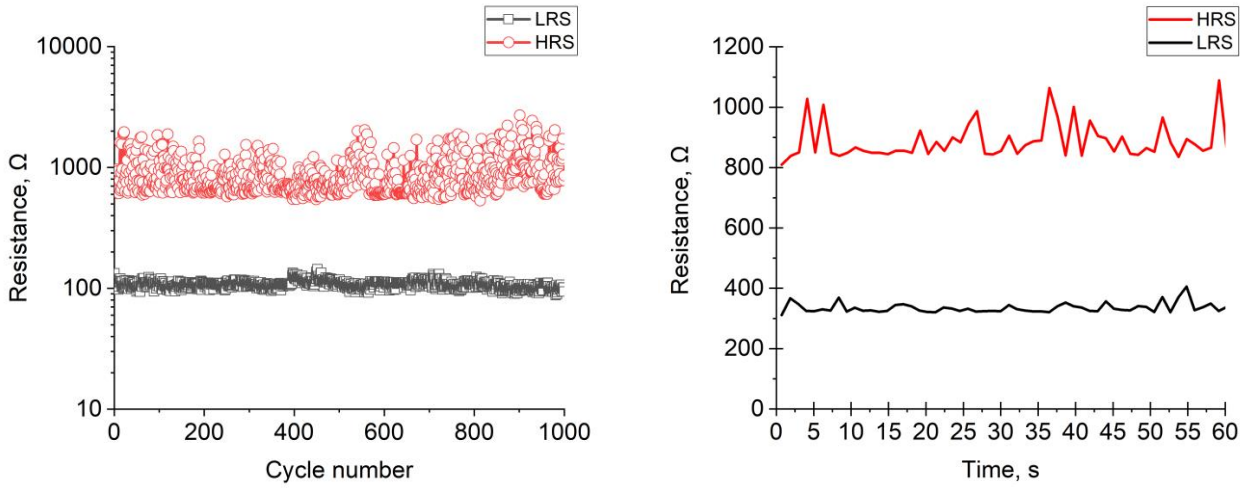

(a) (b)

Figure 2**.** Investigation of the resistive switching regularities of memristor nanostructures: (a) endurance test, (b) retention test.

An endurance and retention study of the Ti/TiO_x/W memristor structure was carried out using an EM-6070A probe station and a Keithley 6517B electrometer. To do this, during the endurance test for 1000 cycles, switching voltage pulses were applied to the LRS state (U_{set}) and to the HRS state (U_{res}) $U_{set/res}$=±0.5V, followed by reading the state at voltage U_{read}= 0.3 V (Fig. 2a).

During the retention test, the switching voltage $U_{set/res}$=±0.4V was initially applied, and then the read voltage pulses U_{read}=0.2V were repeatedly applied for 60 seconds (Fig. 2b).

Data analysis showed that the structure demonstrates resistive switching endurance over 1000 switching cycles, while the average resistance in the LRS state was 100.2 ± 9.1 Ohm, and in the HRS state 890.3 ± 81.7 Ohm, the ratio of the HRS resistance value to LRS is 8.9±1.6. Furthermore, the resistive switching stability test showed the holding of the LRS and HRS states of the structure for 60 seconds, while the average resistance in the LRS state was 335.1 ± 16.5 Ω, and in the HRS state 886.5 ± 60.2 Ω, the relationship between the resistance value of HRS and LRS is 2.7±0.3.

The results obtained can be used in the development of technological processes for the formation of artificial synapses based on titanium oxide memristor nanostructures for the implementation of neuroelectronics and artificial intelligence elements.

The study was supported by a grant from the Russian Science Foundation No. 22-79-10215, https://rscf.ru/project/22-79-10215/, at Southern Federal University.

1. V.I. Avilov, V.A Smirnov, A.A. Fedotov, et al., *IOP Conf. Ser.: Mater. Sci. Eng.* **443**, 012004 (2018).
2. V.I. Avilov, A.S. Kolomiitsev, R.V. Tominov, et al., *J. Phys.: Conf. Ser. Electr. Ed.* **1124**, 022019 (2018).
3. R. Tominov, V. Avilov, Z. Vakulov, et al., *Adv. Electr. Mater.* **8**, 2200215 (2022).
4. V.I. Avilov, R.V. Tominov, L.G. Zhavoronkov, et al., *St. Petersburg Open 2022 Book Abstr.* 426-427 (2022).
5. V.I. Avilov, L.G. Zhavoronkov, V.A. Smirnov, *10th Ann. Int. Conf. PHENMA* 2021-2022 Rostov-on-Don - Taganrog, 51-52 (2022).

P33

Investigation of the kinetics of the domain structure of ferroelectrics during polarization switching in a nonhomogeneous electric field

Yu. Alikin, A. Turygin, V. Shur

School of Natural Sciences and Mathematics, Ural Federal University, 620000, Ekaterinburg, Russia
jury.alikin@at.urfu.ru

Ferroelectrics exhibit spontaneous polarization, the direction of which can be changed by applying an external electric field. In the formation of domain structures, the decisive role is played by the nucleation of domains on the surface and the growth of domains with charged walls in the polar direction. Scanning probe microscopy (SPM) is one of the methods for studying and creating domain structures in ferroelectrics with nanometer spatial resolution. Local switching of polarization on a nonpolar cut using a conducting SPM tip is a unique method for studying the growth of domains with charged walls in the polar direction [1].

Local polarization switching by the SPM tip on a nonpolar Y-cut in MgOCLN led to the formation of isolated wedge-shaped domains. Two modes of switching by rectangular pulses were used: (1) single and (2) multiple with application of series of voltage pulses at one point.

The obtained results were considered in terms of the kinetic approach based on the analogy between the growth of domains and crystals [2]. It was assumed that the growth of the domain during local switching on a nonpolar cut is the result of generation of elementary steps at the domain base and motion of charged head-to-head kinks along the domain wall in the polar direction. The growth of the domain base, which represent a tail-to-tail charged domain wall, is caused by the generation of steps under the action of the polar component of the local field, and the kink motion occurs in the field created by neighboring kinks [1].

The dependences of the tilt of the charged domain walls from the polar direction on the amplitude and pulse number were revealed. It was shown that the domain base width is defined by the spatial distribution of the external electric field [3].

Multiple polarization switching was carried out with 8 min interval between pulses, which made it possible to assume that the depolarization field created by the part of the domain base switched by the previous pulse was completely screened. Only the influence of the residual depolarization field, which appears due to the base increase during the last switching was taken into account. The base growth with the application of each pulse is due to the generation of steps at the base edge. A slight decrease of domain length is caused by backswitching during scanning [3].

There was a study of switching by pair of pulses: first, by a negative pulse and subsequent positive one applied in the point shifted on 10 μm in polar direction, has led to the formation of the single domain localized exactly between the points of voltage application. Static regular domain structures with a period of 0.75 μm and duty cycle of 0.5 were created by local switching by two pulses of different polarity [4].

The results obtained are useful for further development of domain engineering in the crystals of lithium niobate family.

1. M.Y. Gureev, A.K. Tagantsev, N. Setter, *Phys. Rev. B.* **83**, 184104 (2011).

2. A.P. Turygin, Yu.M. Alikin, E.A. Neradovskaia, et al., *Ferroelectrics* **542**, 70 (2019).

3. Yu.M. Alikin, A.P. Turygin, D.O. Alikin, et al., *Ferroelectrics* **574**, 16 (2021).

4. Yu.M. Alikin, A.P. Turygin, D.O. Alikin, et al., *Ferroelectrics* **604**, 25 (2023).

P34

Domain kinetics and periodical poling in single crystals of potassium titanyl-phosphate family for light frequency conversion

M. Chuvakova[1], A. Akhmatkhanov[1], A.A. Esin[1], I.A. Kipenko[1], V. Shur[1], A. Boyko[2,3], D. Kolker[2,3] L. Isaenko[3], S. Zhurkov[3]

[1]*School of Natural Sciences and Mathematics, Ural Federal University, 620000 Ekaterinburg, Russia*
m.a.chuvakova@urfu.ru

[2]*Institute of Laser Physics SB RAS, 630090 Novosibirsk, Russia*

[3]*Novosibirsk State University, 630090 Novosibirsk, Russia*

Single crystals of potassium titanyl-phosphate family with periodical ferroelectric domain structure are one of the promising materials for light frequency conversions [1]. We present the results of measurements of characteristic times and switching fields and *in situ* visualization of domain kinetics in potassium titanyl phosphate Rb:$KTiOPO_4$ (RKTP), potassium titanyl arsenate $KTiOAsO_4$ (KTA) and rubidium titanyl arsenate $RbTiOAsO_4$ (RTA) single crystals.

In situ imaging of domain kinetics in RKTP, KTA and RTA was carried out with the time resolution down to 12.5 μs. The wide range of wall velocities with two orders of magnitude difference was observed for switching in a uniform electric field in RKTP [2]. The kinetic maps allowed analyzing the spatial distribution of wall motion velocities and classifying the walls by velocity. The distinguished slow, fast, and superfast domain walls differed by their orientation. The mobility and the threshold fields for all domain walls were estimated [3]. The revealed increase in the wall velocity with deviation from low-index crystallographic planes for slow and fast walls was considered in terms of determined step generation and anisotropic kink motion.

The domain kinetics and switching fields in RKTP and KTA were compared. The more pronounced input of slow domain walls in KTA results in creation of narrow stripe domains important for periodical poling [4,5]. Spontaneous backswitching was revealed in RTA single crystals. It was shown that the time interval from the end of switching pulse to the start of spontaneous backswitching process ("domain structure stability time") is proportional to the field applied during polarization reversal process.

The periodical domain structure with period of 40 μm was created in 3-mm-thick RKTP single crystals for OPO generation at 2.326 μm using the 1.064 μm pulsed pump with 5.6 ns duration at 20 Hz. The single resonance double-pass optical scheme was used. The threshold power energy 630 μJ and generation efficiency 7% were obtained.

We investigated the characteristics of a PPKTA OPO with a period of 39.2 μm in the low-temperature-grown KTA sample. Under pumping at 1.053 μm, the signal and idler wavelengths were, 1.54 and 3.31 μm, respectively. The parametric generation threshold turned out to be 130 μJ (for a pump intensity of 14.4 MW cm^{-2}), the quantum efficiency was 27%, and the differential efficiency was 12% [6].

The obtained knowledge is important for further development of domain engineering in crystals of KTP family required for creation of high power, reliable, and effective coherent light sources.

The research was made possible by Russian Science Foundation (Grant No. 19-12-00210).

1. V.Ya. Shur, E.V. Pelegova, A.R. Akhmatkhanov, I.S. Baturin, *Ferroelectrics* **496**, 49 (2016).
2. V.Ya. Shur, E.M. Vaskina, E.V. Pelegova, et al., *Appl. Phys. Lett.* **109**, 132901 (2016).
3. V.Ya. Shur, A.A. Esin, M.A. Alam, A.R. Akhmatkhanov, *Appl. Phys. Lett.* **111**, 152907 (2017).
4. A.R. Akhmatkhanov, M.A. Chuvakova, N.A. Dolgushin, et al., *Ferroelectrics* **559**, 1 (2020).
5. A.R. Akhmatkhanov, M.A. Chuvakova, I.A. Kipenko, et al., *Appl. Phys. Lett.* **115**, 212901 (2019).
6. L.I. Isaenko, A.P. Eliseev, D.B. Kolker, et al., *Quantum Electr.* **50**,788 (2020).

P35

Formation of domain structure during focused ion beam irradiation in SBN single crystals

M.D. Kholodenko, E.A. Pashnina, A.R. Akhmatkhanov, M.S. Nebogatikov, V.A. Shikhova, A.S. Slautina, D.S. Chezganov, V. Ya. Shur

School of Natural Sciences and Mathematics, Ural Federal University, 620000, Ekaterinburg, Russia
Maria.Kholodenko@urfu.me

Strontium barium niobate (SBN, $Sr_xBa_{1-x}Nb_2O_6$, x=0.61) single crystals can be used to create electric field-controlled diffraction optical elements [1] and photonic crystals [2]. However, the complicated polydomain structure in as-grown SBN crystals is not desirable for high-performance electro-optic devices. In this work we have studied the features of the domain structure formation induced by ion beam irradiation of the single domain areas of SBN crystals.

The creation of single domain areas was carried out by raster scanning of 460x460 μm^2 region by a focused electron beam with irradiation dose ranging from 100 to 200 μC/cm^2. Local polarization reversal in these areas was realized by focused ion beam irradiation. An artificial dielectric layer (photoresist) was deposited on the irradiated surface, and a solid Cu electrode was deposited on the opposite surface. The obtained domain structure was imaged by second harmonic generation microscopy (SHGM).

Dot irradiation of matrices of 5×5 dots with a period of 10 μm and isolated dots with dose ranging from 10 to 50 pC led to the formation of arrays of round domains (Fig. 1a) and isolated round domains respectively. It was shown that the dose increase leads to increase of the depth of formed domain and a linear increase of its switched area. At the same dose, the isolated domains were 2.7 times smaller than the domains in the matrix. This fact was attributed to the action of electric field of injected charge from neighboring irradiated dots. Isolated domain grow through the sample for doses above 40 pC and domain arrays – for doses above 10 pC.

As a result of irradiation along the lines with dose ranging from 20 to 100 μC/cm, the stripe domains were formed (Fig. 1b). It was shown that the increase of irradiation dose leads to increase of the depth and the width of stripe domains. At the same dose, the stripes in the grating grew 2.5 times deeper than the isolated ones, which is explained by the influence of electric fields from neighboring irradiated regions on the growth of the stripe domain. At doses above 50 μC/cm, the stripe domains in the grating grow through the sample, while isolated stripe domains reach only the middle of the sample. The possibility of creation of domain structure with an arbitrary orientation of the domain walls (sun-like domain shape) was demonstrated (Fig. 1c). The maximum depth of such structures was 370 μm for the irradiation dose 500 μC/cm^2.

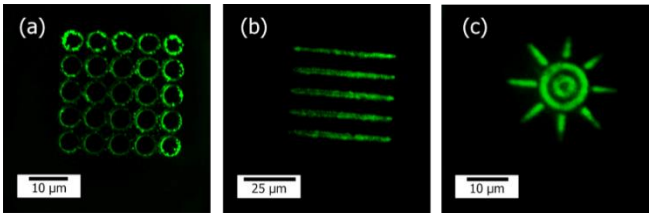

Figure 1. The SHG images of the domains on the surface: (a) matrix of dots; (b) grating of stripes; (c) sun-like domain. The irradiation dose: (a) 40 pC; (b) 100 μC/cm; (c) 250 μC/cm^2.

The obtained results are of considerable interest for the further development of domain engineering methods in SBN crystals.

The equipment of the Ural Center for Shared Use “Modern nanotechnology” Ural Federal University (reg. no. 2968) was used, the work was supported by the Russian Science Foundation (grant 21-72-10160).

1. J. Mávita, L.A. Ríos, C.E. Minor, R.S. Cudney, *Appl. Opt.* **57**, 2208 (2018).

2. J. Li, M. Lu, L. Feng, X. Liu, Y. Chen, *J. Appl. Phys.* **101**, 013516 (2007).

P36

Investigation of the interaction with the domain wall of domains formed by ion beam irradiation in lithium niobate

E.A. Pashnina, A.S. Slautina, A.R. Akhmatkhanov,
M.A. Chuvakova, D.S. Chezganov, V.Ya. Shur

School of Natural Sciences and Mathematics, Ural Federal University, 620000 Ekaterinburg, Russia
elena.pashnina@urfu.ru

Local polarization reversal in ferroelectrics by application of a biased probe of a scanning probe microscope (SPM) or a focused beam of charged particles is a promising method for studying the domain structure, as it allows for the analysis of the domain growth on the submicron scale. The study of the features of the domain interaction is of particular interest. The paper studies the interaction between the domains formed as result of focused ion beam irradiation with the wall of the strip domain.

Local switching was carried out on congruent lithium niobate (CLN) coated with a photoresist layer with a periodically poled domain structure (PPDS) consisting of stripe domains with a width of 9.5 μm. The PPDS was created in two ways: (1) by applying an external field using periodic electrodes (*e-field PPDS*) and (2) by ion beam irradiation (*i-beam PPDS*). To study the effect of screening, the time elapsed from the moment the PPDS was created to the moment of irradiation was about three months for the *e-field PPDS* and three seconds for the *i-beam PPDS*.

Matrix dots irradiation with a period of 4 μm of the samples was carried out. During irradiation near the wall of the stripe domain, two types of changes in the domain structure were revealed (Fig. 1): (1) distortion of the wall shape as a result of domain fusion upon irradiation near the wall, (2) distortion of the wall upon irradiation inside the stripe domain. In the second case the maximum displacement of the wall increases linearly with decreasing distance from the irradiation dot to the wall. In contrast to switching by the SPM probe [1], in the region of irradiation and in the region of distortion of the stripe domain wall, ensembles of nanodomains with a density of about 0.5 μm^{-2} are formed (Fig. 1a). The effect is attributed to spontaneous backswitching under the action of the residual depolarizing field after the relaxation of the charge injected by the ion beam into the photoresist layer. In this case, the presence of the photoresist layer hinders the motion of the domain wall [2]. It is shown that the unscreened depolarization field of the stripe domain of the *i-beam PPDS* structure leads to a decrease in the depth of domains by more than two times. It has been found that domains formed at a distance of less than 2 μm from the wall merge with the stripe domain at a depth of about 10 μm.

The obtained results can be used for the development of domain engineering methods.

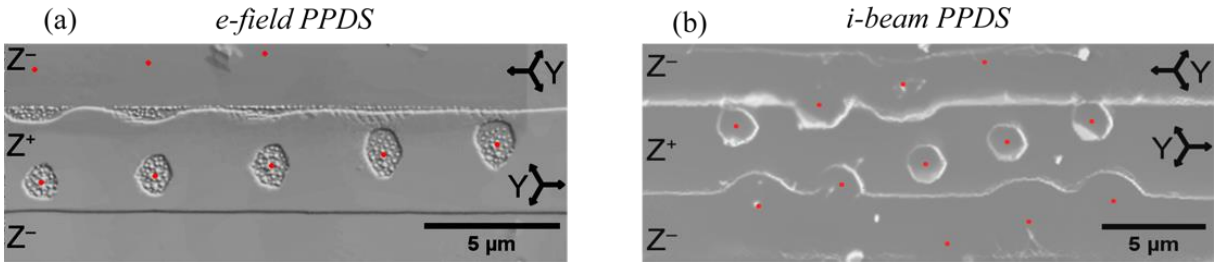

Figure 1. (a) e-field PPDS and (b) i-beam PPDS images of domain structures formed after dot irradiation. The red dots indicate the centers of the positions of the ion beam during irradiation.

The equipment of the Ural Center for Shared Use “Modern nanotechnology” UrFU was used. The research was made possible by Russian Science Foundation (Project № 21-72-10160).

1. A.V. Ievlev, A.N. Morozovska, V.Ya. Shur, et al., *Phys. Rev.* **91**, 214109 (2015).
2. V.Ya. Shur, M.S. Kosobokov, E.A. Mingaliev, et al., *J. Appl. Phys.* **119**, 144101 (2016).

P37

Formation of a regular domain structure and wavelength conversion in lithium niobate modified by the proton exchange

E.D. Savelyev, A.R. Akhmatkhanov, B.N. Slautin, V.Ya. Shur

School of Natural Sciences and Mathematics, Ural Federal University, 620000, Ekaterinburg, Russia
evgeny.savelyev@urfu.ru

One of the most widely used ferroelectric crystals is Lithium Niobate ($LiNbO_3$, CLN) which possesses high values of piezoelectric and non-linear optical coefficients, as well as a high phase-transition temperature which make it possible to create different devices for opto-acoustics, non-linear optics and integrated optics. Optical waveguides in the CLN crystals are created for applications in the telecommunications and integrated optics. One of the most popular methods of creating optical waveguides in CLN is soft proton exchange (SPE) [1]. The creation of periodic domain structures (PDS) in CLN single crystals makes it possible to use the effect of the quasi-phasematching to implement the wavelength conversion with record-high efficiency. Great practical importance is the creation of optical waveguides with a regular domain structure for laser wavelength conversion, which requires investigation of the kinetics of the domain structure in SPE CLN crystals.

In this work, we studied the anomalous growth of stripe domains on the Z- polar surface during polarization switching in SPE CLN single crystals, which was attributed to inefficient screening of the depolarizing field caused by the presence of a dielectric gap. The dependences of the threshold fields of the formation of domains on the Z- polar surface on the duration of the proton exchange process were measured [2]. The observed anomalous decrease of the threshold fields as a result of soft proton exchange was attributed to the formation of an internal bias field caused by the composition gradient in the near-surface layer [2]. It is shown that the magnitude of the composition gradient in the near-surface layer increases with the duration of the proton exchange, which leads to the decrease in the threshold field.

The effect of the formation of quasi-periodic domain structures during the growth of stripe domains from a flat domain wall is revealed. The effect is attributed to the electrostatic interaction of non-through stripe domains. The possibility of creating a stable regular domain structure with a period of 500 nm by polarization switching using the conductive probe of a scanning probe microscope is shown.

Radiation with a wavelength of 374 nm was obtained by generating the second harmonic in a crystal of magnesium-doped lithium niobate with a regular domain structure with a period of 2 μm, created by focused electron beam irradiation [3].

The equipment of the Ural Center for Shared Use “Modern nanotechnology” Ural Federal University (Reg. no. 2968), which is supported by the Ministry of Science and Higher Education RF (Project no. 075-15-2021-677), was used. The research funding from the Ministry of Science and Higher Education of the Russian Federation (Ural Federal University Program of Development within the Priority-2030 Program) is gratefully acknowledged.

1. L. Chanvillard, P. Aschiéri, P. Baldi, et al., *Appl. Phys. Lett.* **76**, 1089 (2000).
2. E. Savelyev, A. Akhmatkhanov, M. Kosobokov, et al., *Crystals* **13**, 72 (2023).
3. E.D. Savelyev, A.R. Akhmatkhanov, D.S. Chezganov, et al., *Ferroelectrics* **576**, 50 (2021).

P38

Study of direct domain growth during local polarization reversal in strontium-barium niobate single crystals

V.A. Shikhova[1], A.S. Slautina[1], A.R. Akhmatkhanov[1], E.A. Pashnina[1], A.P. Turygin[1], M.S. Nebogatikov[1], D.S. Chezganov[1], L.V. Ivleva[2], V.Ya. Shur[1]

[1]*School of Natural Sciences and Mathematics, Ural Federal University, 620000, Ekaterinburg, Russia vera@urfu.ru*
[2]*Prokhorov General Physics Institute, Russian Academy of Sciences, 119991, Moscow, Russia*

Direct growth of the domains formed as a result of local polarization reversal in strontium-barium niobate $Sr_{0.61}Ba_{0.39}Nb_2O_6$ (SBN) single crystals was studied. Local polarization reversal was carried out in two ways: 1) sample irradiation by a focused ion beam; 2) the biased tip of the scanning probe microscope (SPM). The polarization was switched both in the samples with the initial polydomain state representing maze-type nano-domain structure and in the samples with initial single-domain state created by a medium-energy electron beam [1]. The domain structures were imaged on the surface by piezoresponse force microscopy and in the bulk by Cherenkov-type second harmonic generation microscopy (SHGM) [2].

Under dot ion beam irradiation, rounded domains surrounded by a broad domain boundary (BDB) were formed in polydomain samples. The domain size decreased with depth. Thus, the domains had a conical shape, with an average aspect ratio of 11 for the domain and 30 for the BDB. For 2D domain arrays with distance between domains 15 μm the central domain is deeper than that of domains at the edges and isolated domains produced by the same switching pulses. The aspect ratio is 26 for the central domain and 13 for the domains at the edges.

The domains recorded in single-domain samples by ion beam irradiation (Fig. 1) are deeper than in polydomain ones. In the single-domain state the aspect ratio for the central domain is 84; for the domains at the edges 50. In single-domain state the shape of the domain cross section changed from round (on the surface) to close to square (in depth), which corresponds to SBN symmetry – C_{4v}.

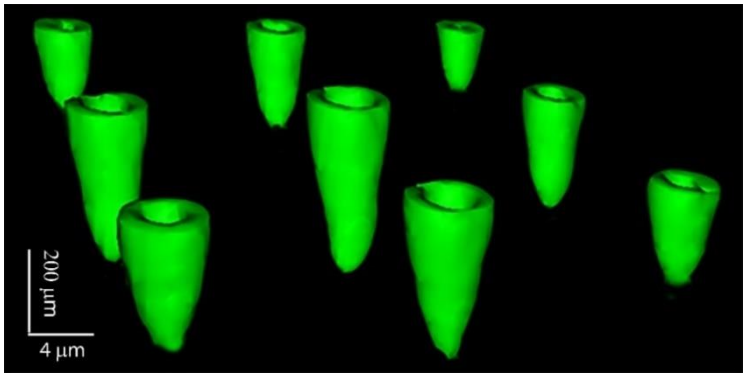

Figure 1. 3D SHGM image of the domains created by ion beam irradiation in single-domain SBN sample. Distance between dots 15 μm. Dose 15 pC.

The isolated domain structures formed by biased SPM tip consisted of conical domains with the aspect ratio equal to 13 in polydomain state and 38 in single-domain state.

The obtained results can be used to create three-dimensional domain structures of arbitrary shape (3D domain engineering) for manufacturing of the non-linear optical devices including controlled diffractive optical elements [3].

The research was made possible by the Russian Foundation for Basic Research (project no. 21-72-10160). The equipment of the Ural Center for Shared Use “Modern nanotechnology” UrFU was used.

1. D.S. Chezganov, V.A. Shikhova, V.V. Fedorovyh, et al., *IEEE Trans. Ultrason. Ferroelectrics Freq. Contr.* **67**, 191 (2020).
2. M. Ayoub, P. Roedig, K. Koynov, et al., *Opt. Express* **21**, 8220 (2013).
3. J. Mávita, L.A. Ríos, C.E. Minor, R.S. Cudney, *Appl. Opt.* **57**, 2208 (2018).

P39

Formation of quasi-regular domain arrays in triglycine sulphate single crystal during scanning by biased SPM tip

A.P. Turygin[1], V.A. Shikhova[1], M.S. Kosobokov[1], A.R. Akhmatkhanov[1], O.N. Sergeeva[2], V.Ya. Shur[1]

[1]*School of Natural Sciences and Mathematics, Ural Federal University, 620000, Ekaterinburg, Russia*
anton.turygin@urfu.ru

[2]*Tver State University, 170000 Tver, Russia*

Triglycine sulfate ($[NH_2CH_2COOH]_3 \cdot H_2SO_4$, TGS) is a well-known uniaxial ferroelectric widely used in infrared receivers and detectors due to its high pyroelectric properties [1]. The spontaneous polarization oriented along the *b* axis arises across a second order phase transition at 49°C. The TGS doping is widely used for tuning its Curie temperature and improvement of pyroelectric properties [2].

We have chosen a deuterated TGS (DTGS) crystal for investigation due to its higher threshold field needed for domain nucleation and growth and a more stable domain structure. The studied DTGS crystals were grown from an aqueous solution. The degree of deuteration was about 80%. The measured phase transition temperature was 59.7°C. For investigation of the domain growth during local switching the single-domain area of 100 × 100 μm^2 was created using scanning by biased SPM tip with a constant voltage of -100 V.

It was demonstrated that the shape of the domains created in single domain area by moving of the biased SPM tip depends on applied voltage and scanning direction (Fig. 1). For scanning along *c* axis the arrays of isolated domains with rounded shape appeared for voltage below 100 V (Fig. 1a). It was shown that the scanning by the biased SPM tip perpendicular to *c* axis led to formation of the quasi-regular array of the isolated dashed domains (Fig. 1b). The average domain period and width increased linearly with voltage.

The obtained results have been attributed to the formation of comb-like domains in the crystal bulk during scanning and their transformation to arrays of isolated domains as a result of partial backswitching [3].

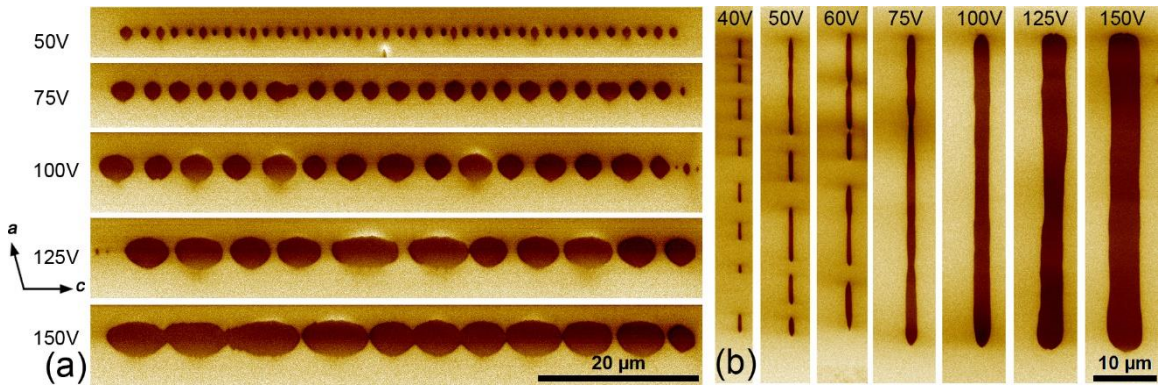

Figure 1. PFM images of domain arrays appeared by scanning with biased tip: (a) along *c* and (b) perpendicular *c* axis. Scanning velocity 1 μm/s.

This research was made possible by the Russian Science Foundation (Project No. 19-12-00210). The equipment of the Ural Center for Shared Use "Modern nanotechnology" Ural Federal University (Reg. No. 2968) was used with the financial support of the Ministry of Science and Higher Education of the Russian Federation (Project No. 075-15-2021-677).

1. A.K. Batra, P. Guggilla, D. Cunningham, et al., *Physica B* **371**, 210 (2006).
2. P. Felix, P. Gamot, P. Lacheau, et al., *Ferroelectrics* **17**, 543 (1977).
3. V.Ya. Shur, M.S. Kosobokov, A.V. Makaev, et al., *Acta Materialia* **219**, 117270 (2021).

P40

Magnetization reversal in thin-film nanostructures under the action of DC current

A.V. Telegin[1], M. Steblii[2], A.V. Ognev[2], A.S. Samardak[2], I.D. Lobov[1], V.D. Bessonov[1]

[1]*M.N. Mikheev Institute of Metal Physics UB of RAS, 620137, Yekaterinburg, Russia*
telegin@imp.uran.ru

[2]*Far Eastern Federal University, Vladivostok, Russia*

Multilayer films with ultra-thin layers of ferromagnetic metals have unique magnetic and transport properties and are promising for the creation, for example, sensor of weak magnetic fields [1]. In metallic nanostructures the spin-orbit interaction is responsible for appearance at the boundary of the heavy non-magnetic metal and the FM layer covering it the interfacial Dzyaloshinskii-Moriya interaction [2]. This antisymmetric exchange interaction can lead to the transformation of the magnetic order and the appearance of nontrivial spin textures, such as skyrmions [3]. In this regard, the question arises of the possibility of controlling the magnetization, for example, with the help of a DC current, as well as the effect of interlayer exchange interaction on the spin torque transfer in nanostructures.

Here we aim to study ferro- and ferrimagnetic thin-film nanostructures synthesized by magnetron sputtering. The magnetic properties are controlled using the vibrating magnetometer and Kerr microscopy. According to the magnetometric data, all the obtained samples have a perpendicular magnetic anisotropy and demonstrate a response to the transmission of a DC current due to a spin-polarized current induced in the structures. It is important, all samples demonstrate a linear dependence of the specific current-induced field. The magnetization reversal of the films occurs at some critical value of the DC current. The processes of magnetization reversal under the action of current were confirmed using Kerr microscopy (Fig. 1). The study of the magnetization of the samples by Kerr microscopy allowed to determine the value of current at which the switching of the magnetization occur. The efficiency of current-induced magnetization reversal achieves about 40% for ferrimagnetic TbCo, which have a bulk nature of the magnetic anisotropy.

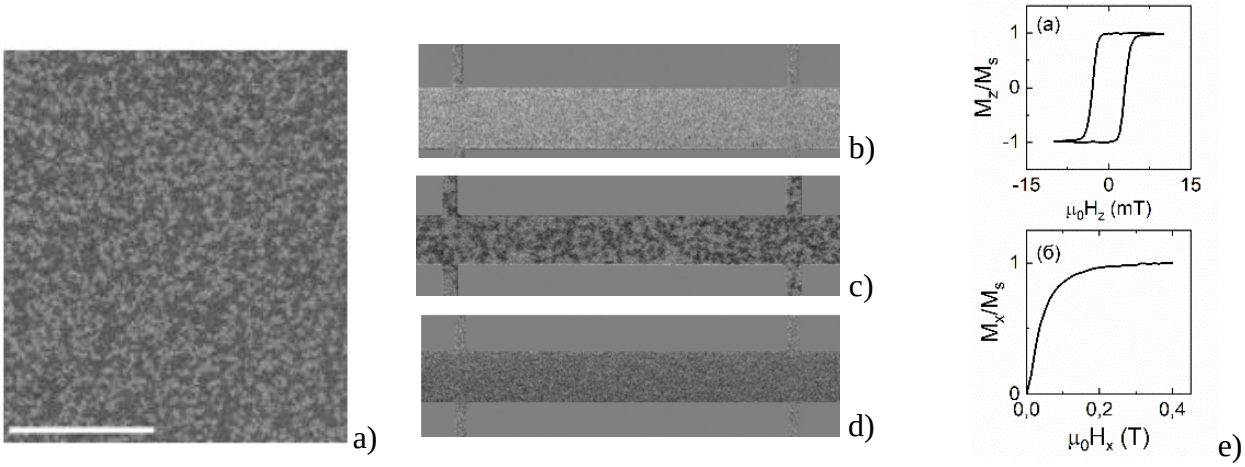

Figure 1. Visualization of magnetization M of the Ru/Co nanostructure: demagnetized film, b) +M magnetized film, c) -M magnetized film, d) DC current is ON, e) hysteresis of M(H) in perpendicular (upper panel) and parallel magnetic field.

Finally, the results of the research of current-induced re-magnetization in the nanostructures can be used for creation and control of various chiral topological textures.

Support of the Russian Science Foundation №21-72-20160 (https://rscf.ru/en/project/21-72-20160) is acknowledged.

1. G.S. Patrin, V.O. Vas'kovskii, *Phys. Met. Metallography* **101**, S63 (2006).

2. J. Park, T. Kim, G.W. Kim, et. al., *Acta Materialia* **241**, 035004 (2022).

3. A. Manchon, A. Belabbes, *Solid State Physics*, Academic Press. **68**, (2017) 89p.

P41

Neutron diffraction studies of system ceramics $(1-x)PbFe_{1/2}Nb_{1/2}O_3$-$xPbFe_{2/3}W_{1/3}O_3$

E.V. Glazunova[1], O.N. Lis[2], L.A. Shilkina[1], I.A. Verbenko[1], L.A. Reznichenko[1]

[1]*Research Institute of Physics, Southern Federal University,344090, Rostov-on-Don, Russia*

kate93g@mail.ru

[2]*Joint Institute for Nuclear Research, Dubna*

Materials that simultaneously combine several types of ordering: ferroelectric (FE), ferro(antiferro-)magnetic (FM, AFM) and ferroelastic are of great interest both in terms of prospects for their application in multifunctional devices for storing and recording information, and from point of view of the study the interaction of electrical and magnetic subsystems and the possibility of discovering new effects. One of the problems of the relationship between FE and magnetic subsystems is their "mutual exclusion" from the point of view of the *B*-cation electron structure. The materials that have in the *B*-position a cation with a partially filled d-sublevel have magnetic properties, while cations with an unfilled d-sublevel cannot be magnetic, but can have FE properties. Result of such a d^n–d^0 separation, the temperatures of the FE and magnetic transitions are far from each other, and the relationship between these subsystems is weak. One of the possible solve to the problem can be the producing of solid solutions with similar temperatures of the FE and magnetic transitions, which manifest themselves in a wide temperature range, in other words, multiferroic-relaxors. Examples of such compounds are solid solutions of the $(1-x)PbFe_{1/2}Nb_{1/2}O_3$-$xPbFe_{2/3}W_{1/3}O_3$ system, in which FE and magnetic properties are manifested in a close temperature range.

Consequently, the purpose of this work is to establish the features of the behavior of the structure and magnetic properties of the solid solutions of the $(1-x)PbFe_{1/2}Nb_{1/2}O_3$-$xPbFe_{2/3}W_{1/3}O_3$ system.

The objects were the solid solutions of the $(1-x)PbFe_{1/2}Nb_{1/2}O_3$-$xPbFe_{2/3}W_{1/3}O_3$ system with x=0.1, 0.6, 1.0. The solid solutions were produced by the two-stage solid-phase synthesis and sintering using conventional ceramic technology: $T_{synth1,2}$ = 800÷900°C; $\tau_{synth1,2}$ = 4÷10 h, $T_{sint.}$ = 870÷1100°C; τ_{sint} = 2 h (depending on composition). Neutron diffraction were carried out on a DN-12 diffractometer of the IBR-2 pulsed high-flux reactor by using a closed cycle helium refrigerator in a wide temperature range of 15÷300 K.

Neutron diffraction spectra of $(1-x)PbFe_{1/2}Nb_{1/2}O_3$-$xPbFe_{2/3}W_{1/3}O_3$ (x=0.1, 0.6, 1.0) compounds obtained in a wide temperature range showed that solid solutions have cubic symmetry *Pm-3m*. The magnetic phase transition found at T_N~ 189 K (x=0.1), in solid solutions with x=0.6 T_N~ 289 K, the AFM transition in $PbFe_{2/3}W_{1/3}O_3$ (x=1.0) occurs at T_N~348 K. In all solid solutions in the temperature range of 15÷300 K, a decrease of the unit cell parameter occurs which is most pronounced at x=0.6. It can be deals with the exclusion of oxygen positions by using crystallographic shear planes that leads to the structure compression.

The magnetic moment increases at rise x, which is consistent with the quantitative content of Fe^{3+} in the study solid solutions. At the temperature ~ 15 K in solid solution with x=0.1 the magnetic moment reaches M=2μ_B, with the increase of x up to 0.6 M=2.6μ_B, and M= 2.9μ_B in $PbFe_{2/3}W_{1/3}O_3$.

The results obtained in this work can be use the development of foundations for magnetoelectric devices.

The study was carried out with the financial support of the Ministry of Science and Higher Education of the Russian Federation (State task in the field of scientific activity in 2023). Project No.FENW-2023-0010/(GZ0110/23-11-IF).

P42

Influence of low-melting additive infiltration on the magnetic hysteresis properties of a nanocrystalline alloy based on the compound $Nd_2Fe_{14}B$

A.A. Golubiatnikova, A.N. Shalaginov, S.V. Andreev, A.S. Volegov

Ural Federal University, Ekaterinburg
a.a.golubiatnikova@urfu.me

Among a variety of magnetic materials, hard magnetic materials are of particular interest. Permanent magnets made of them have found wide application in all fields of science and technology. One of the main materials for the production of permanent magnets is the Nd-Fe-B alloy. The disadvantage of Nd-Fe-B-based magnets is the relatively low Curie temperature of the $Nd_2Fe_{14}B$ phase - 312 ℃, which leads to the impossibility of using them in strong demagnetizing fields at high operating temperatures. When neodymium magnets are heated to 100 ℃, there is almost a twofold decrease in the coercive field compared to that at room temperature.

We investigated a method of increasing the coercivity of a hard magnetic alloy based on the compound $Nd_2Fe_{14}B$ by infiltration of low-melting additives.

Low-melting eutectic additives of the following composition were used: $Nd_{75}Cu_{25}$, $Nd_{75}Co_{25}$, $Nd_{75}(Co_{0,75}Cu_{0,25})_{25}$, $Nd_{75}(Co_{0,5}Cu_{0,5})_{25}$, $Nd_{75}(Co_{0,25}Cu_{0,75})_{25}$. The additives were obtained by melting the pure components in an arc furnace with argon medium. The main hard magnetic material for the experiment was MQP-B brand melt-spun alloy. The powders were mixed in a 20/80 ratio. The prepared mixtures were compressed into parallelepipeds and prepared for annealing in vacuum. The selected annealing temperature range was 550 to 650℃. The annealing time was 1 hour.

Due to the development of additive manufacturing for the production of magnetically hard materials without organic binder by selective laser sintering [1,2], the question of obtaining high coercive field using free powder bulk is of particular interest. Unpressed samples were prepared, the powders were freely poured into the ampoules and annealed at 650℃ for 1 hour. The sample with added $Nd_{75}Cu_{25}$was additionally annealed at 600℃.

The magnetic hysteresis loops of the annealed samples were measured using the PPMS DynaCool.

The obtained values of the coercive field are more than twice as high as the H_c value of pure powder MQP-B (≈9 kOe):

for presses – from 24,4 to 25,6 kOe;

for unpressed – from 22.3 to 25.3 kOe.

The best H_c values are observed at 600 ℃ with the addition of $Nd_{75}Cu_{25}$.

The research was financially supported by Russian Science Foundation (Grant Number 21-72-10104).

1. A.S. Volegov, S.V. Andreev, N.V. Selezneva, et al., *Acta Materialia* **188**, 733 (2020).
2. V.E. Maltseva, S.V. Andreev, D.S. Neznakhin, et al., *Phys. Metals Metallogr.* **123**, 740 (2022).

P43

Simulation and optimization of composite multiferroic with nanostructured magnetic layer

E.V. Kudyukov[1], M.A. Kalinin[1], K.G. Balymov[1], V.O. Vas'kovskiy[1,2]

[1]*Ural Federal University, 620002, Yekaterinburg, Russia*
maks-kalinin-00@inbox.ru

[2]*Institute of Metal Physics, UB RAS, 620137, Yekaterinburg, Russia*

Composite multiferroics is one of the most dynamically growing topics in the scientific community. One of the most promising classes of composite multiferroics are thin-film layered multiferroics. In such materials, ferroelectric and magnetostrictive layers are deposited layer by layer. The large values of the magnetoelectric coupling in such structures are due to the strong mechanical interaction between the layers. Among the promising ferroelectric components for composite multiferroics, one can single out the PVDF polymer, which provides a strong mechanical bond between the layers along with high piezoelectric coefficients in the thin film state [1]. Among the magnetic components, the $Fe_{10}Ni_{90}$ alloy, which has excellent magnetic properties and a significant magnetostriction constant (-20 ppm), is promising. One of the key problems of thin-film multiferroics is the small volume of the magnetostrictive phase, which does not allow the full potential of these systems to be revealed. With an increase in the thickness of the magnetic layer above 150 nm, the appearance of perpendicular magnetic anisotropy is possible, which leads to a sharp deterioration in the soft magnetic properties. The solution to this problem can be the nanostructuring of the magnetostrictive layer by introducing thin nonmagnetic interlayers, which will make it possible to maintain the desired magnetic properties with an overall increase in the volume of the magnetic phase. However, experimental selection of the required configuration is a non-trivial task. It is quite expedient to use modern methods of computer modeling to solve the problem of designing these structures. Thus, the purpose of this work is to build a computer model of a composite multiferroic and further optimize the nanostructuring parameters to achieve the maximum magnetoelectric coefficient.

To build a model of a composite multiferroic, the finite element method implemented on the basis of the COMSOL Multiphysics package was used. Such parameters as the thickness of the PVDF layer, the nanostructuring period of the $Fe_{10}Ni_{90}$ layer, the thickness of the Cu interlayer in the periodic structure, and the thickness of the $Fe_{10}Ni_{90}$ layer were varied.

As a result of this work, the dependences of the magnitude of the magnetoelectric response on the mentioned above optimization parameters were obtained. Based on these dependences, the optimal nanostructuring parameters were chosen. It was also shown that the using of nanostructuring of the $Fe_{10}Ni_{90}$ layer can effectively reduce the damping effect of the glass substrate (Fig. 1).

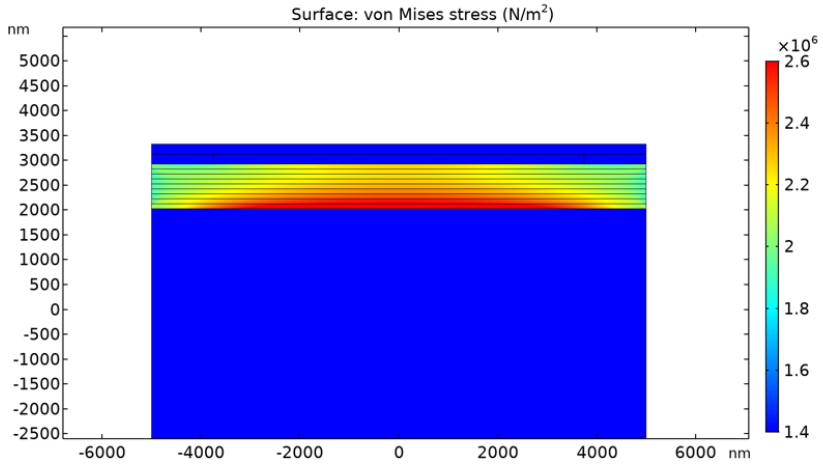

Figure 1. von Mises stress distribution in nanostructured $Fe_{10}Ni_{90}$ layers.

1. E.V. Kudyukov, T.V. Terziyan et al., *Progr. Org. Coatings* **147**, 105857 (2020).

P44

The effect of Ba-doping on the relaxor properties of multiferroic $PbFe_{1/2}Nb_{1/2}O_3$ ceramics

S.I. Kolosov, V.V. Titov, S.I. Raevskaya, S.P. Kubrin, M.A. Evstigneeva, I.N. Zakharchenko, I.P. Raevski

Physics Research Institute and Faculty of Physics, Southern Federal University, Rostov-on-Don, Russia
igorraevsky@gmail.com

Complex perovskite $PbFe_{1/2}Nb_{1/2}O_3$ (PFN) is a multiferroic, i.e., it combines ferroelectric and magnetic properties [1]. Dielectric permittivity ε dependences on temperature for the $Pb_{1-x}Ba_xFe_{1/2}Nb_{1/2}O_3$ solid solution compositions in the $0 \le x \le 0.5$ compositional range were found to change, as x grows, from relatively sharp frequency-independent maxima typical of usual ferroelectrics to the diffused and frequency-dependent maxima typical of relaxors and then to the saturated at low temperatures and frequency-independent ε(T) curves typical of incipient ferroelectrics [2] At the same time Ba-doping leads to the drastic change of magnetic properties of PFN, namely to the drop down of the temperature of the antiferromagnetic phase tramsition (Néel temperature) in the vicinity of the $x \approx 0.15$-0.20 compositional threshold [3].

The scope of the present work is to compare the compositional ranges where the relaxor properties appear with that where the drastic change of magnetic properties of PFN is observed.

To evaluated the degree of the relaxor behavior we used a theoretical framework for $PbB_nNb_mO_3$ relaxors suggested in [4] which takes into account the contributions made by individual NbO_6 octahedra which are believed to be polar units and are said to be «ferroelectrically active». Later it was shown [5] that that the probability, w, of the situation when the Nb ion is surrounded by only the Pb ions for $Pb_{1-x}A_xB_nNb_mO_3$ solid solutions is given by a simple analytical expression $w = (1-x)^{\alpha}$, where $\alpha = 8$. In order to check this model the fall-off in the dielectric permittivity maximum, ε_{max}, with the concentration x for the $Pb_{1-x}Ba_xFe_{1/2}Nb_{1/2}O_3$ solid solution was compared with the computed values of w. In contrast to the model [4], for which $\alpha = 8$ and should not depend on x, the α values estimated from the experimental $\varepsilon_{max}(x)/\varepsilon_{max}(x=0)$ ratio dependence on composition, vary crucially with x at small x values. It seems that this decrease of α with x corresponds to the decrease of the polar volume where the substitutions in the A sites (near the Nb ions) are absent. This implies that the $w = (1-x)^{\alpha}$ dependence is not true at very small x where α exceeds the polar region of the composition with x=0. On the other hand, in the $0.15 < x < 0.4$ compositional range the α values are close to 8 implying that the polar volume reduces to eight unit cells. These data correlate well with the compositional dependence of the activation energy ΔW in the Vogel-Fulcher relation which shows an abrupt increase at $x \approx 0.15$ up to the values typical of the textbook relaxor $PbMg_{1/3}Nb_{2/3}O_3$. Thus the classic relaxor behavior in the $Pb_{1-x}Ba_xFe_{1/2}Nb_{1/2}O_3$ solid solution starts above $x \approx 0.15$, i.e. at the same compositional range where the drastic change of magnetic properties of PFN takes place.

This study was partially supported by the Ministry of Science and Higher Education of the Russian Federation (State assignment in the field of scientific activity, Southern Federal University, 2023, scientific project No. FENW-2023-0015).

1. I.P. Raevski, S.P. Kubrin, S.I. Raevskaya, et al., *IEEE Trans. Ultrason. Ferroelect. Freq. Contr.* **59**, 1872 (2012).
2. I.P. Raevski, V.V. Titov, H. Chen, et al., *J. Mater. Sci.* **54**, 10984 (2019).
3. I.P. Raevski, S.P. Kubrin, S.I. Raevskaya, et al., *Phys. Rev. B* **80**, 024108 (2009).
4. J. Butcher, N.W. Thomas, *J. Phys. Chem. Solids* **52**, 595 (1991).
5. I.P. Raevski, S.A. Prosandeev, *J. Phys.: Cond. Matter* **13**, L299 (2001).

P45

Magnetoelectric properties of skyrmion-like structures

R.F. Mamin, T.S. Shaposhnikova

Zavoisky Physical-Technical Institute, FRC Kazan Scientific Center of RAS, 420029, Kazan, Russia
mamin@kfti.knc.ru

The magnetoelectric effect has long been actively studied. Recently, new materials with interesting characteristics have been obtained for practical application [1, 2]. It is often observed in multiferroics [2], as well as in various inhomogeneous structures consisting of components with different ferroic properties. In this work, within the framework of the phenomenological model, the possibility of the magnetoelectric effect in systems with non-uniform magnetic ordering is considered. The microscopic mechanism of the occurrence of the magnetoelectric effect in such systems is due to the presence of the Dzyaloshinskii-Moriya interaction. The paper considers the occurrence of electric polarization both in small three-dimensional spherical magnetic particles located in a paramagnetic matrix, and in "ordinary" two-dimensional skyrmions. The inhomogeneous distribution of magnetization leads to inhomogeneous electric polarization. As a result, the action of the magnetic field on the magnetic subsystem leads to a change in the inhomogeneous distribution of the electric polarization, and as a result, a magnetoelectric response occurs. The specific form of expressions for the electric polarization and magnetoelectric response is determined by the inhomogeneous distribution of magnetization in the localization regions of such skyrmion-like structures. A non-zero magnetoelectric response to the action of a magnetic field occurs, but it appears only at certain directions of the external magnetic field.

The study was carried out within the framework of the state task of the FRC KazSC RAS.

1. N.A. Spaldin, R. Ramesh, *Nat. Mater*. **18**, 203 (2019).
2. M. Fiebig, T. Lottermoser, D. Meier, M. Trassin, *Nat. Rev. Mater.* **1**, 16046 (2016).

P46

Interplay between structural transformations and diffusion in thin films with antiferromagnetic Ni-Mn

M.E. Moskalev[1], N.A. Kulesh[1], E.A. Kravtsov[2,3], A.N. Gorkovenko[1], V.N. Lepalovskij[1], V.O. Vas'kovskiy[1,2]

[1]*Institute of Natural Sciences and Mathematics, Ural Federal University, 620026, Ekaterinburg, Russia*
mikhail.moskalev@urfu.ru

[2]*Institute of Metal Physics, Ural Branch of the Russian Academy of Sciences, 620066, Ekaterinburg, Russia*

[3]*Institute of Fundamental Education, Ural Federal University, 620062, Ekaterinburg, Russia*

The $L1_0$ θ-NiMn is a potent antiferromagnet with the Néel temperature over 800 ºC, which is capable of providing the exchange bias effect up to temperatures of 350 ºC, making it suitable for industrial applications as a pinning layer in spin valves [1]. However, its implementation into functional spintronics structures may be hindered by diffusion of its components into the adjacent ferromagnetic layer during the annealing, required for the formation of θ-NiMn [2].

In this work we use a combination of X-ray diffractometry in a variety of geometries, such as $\theta/2\theta$, grazing incidence, and X-ray reflectivity, with the total-reflection X-ray fluorescence to assess the diffusion behavior of the constituents in Ni-Mn/$Fe_{20}Ni_{80}$ films. We observe that oversaturating the precursor Ni-Mn layer, although was shown to facilitate the formation of θ-NiMn, leads to excessive diffusion of Mn into the $Fe_{20}Ni_{80}$ layer during the annealing at 300 ºC. We conclude that annealing at lower temperatures does not seem to trigger any noticeable diffusion between the layers. Our results suggest that diffusion of Fe into the Ni-Mn layer, in its turn, might be the reason behind the decomposition of θ-NiMn when reaching 350 ºC, as is indicated by the disappearance of the (111) peak of θ-NiMn in Fig. 1. Our work, thus, may be of both fundamental and applied interest, as it provides additional insight into the mechanisms of diffusion and structural transformations in magnetic thin films, and possible guidelines for industrial implementation of Ni-Mn.

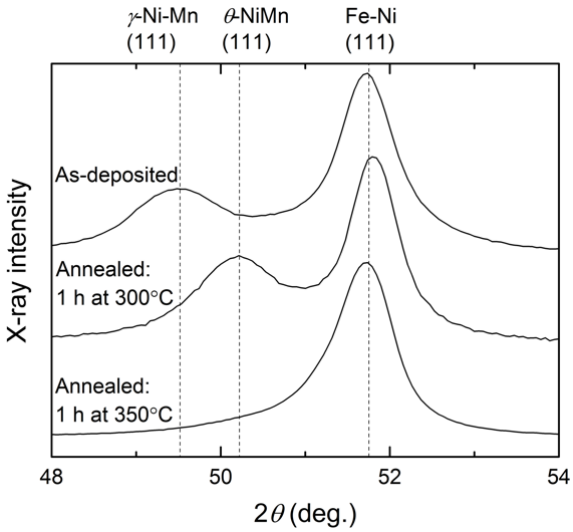

Figure 1. XRD patterns of as-deposited and annealed for 1 h at 300°C and 350°C Ni-Mn (20 nm)/Fe-Ni (40 nm) films.

The research funding from the Ministry of Science and Higher Education of the Russian Federation (Ural Federal University Program of Development within the Priority-2030 Program) is gratefully acknowledged.

1. V.O. Vas'kovskiy, et al., *J. Alloys Compd.* **777**, 264 (2019).
2. V.O. Vas'kovskiy, et al., *Thin Solid Films* **764**, 139616 (2023).

P47

The preparation and study of the multiferroic materials based on $BiFeO_3$-$YMnO_3$ solid solutions

A.V. Nazarenko[1], A.V. Pavlenko[1], E.V. Glazunova[2], A.G. Rudskaya[2], L.A. Shilkina[2], L.A. Reznichenko[2]

[1]*Federal Research Centre, The Southern Scientific Centre of the Russian Academy of Sciences, 344006, Rostov-on-Don, Russia*
avnazarenko1@gmail.com

[2]*Southern Federal University, 344006, Rostov-on-Don, Russia*

An experimental study of multicomponent oxide systems that combine ferroelectric, magnetic, magnetoelectric, and ferroelastic properties is important in studying the possibilities of their further application. Among such oxide systems, materials are singled out in which, under certain conditions, various types of ordering and, as a result, properties simultaneously manifest themselves. Such objects are usually called multiferroics [1]. As a basis for the development of modern multifunctional materials that meet the needs of nano- and microelectronics, heterostructures built using multiferroics with a perovskite-type structure with a common chemical form ABO_3, for instance, bismuth ferrite $BiFeO_3$ (BFO) and yttrium manganese $YMnO_3$ (YMO) [2–10]. There are a number of studies of solid solutions based on the BFO-YMO. However, in most cases, study is limited to low concentrations (up to 20%) of one of the components. This is due to the fact that the phase diagram of these materials has a rather complex composition [11]. At low concentrations, as a rule, the structure of the "parent" is retained, where alloying components are incorporated into the original A- or B-sublattice. In the BFO-xYMO system, compositions with x over 30% have a rather complex structure due to the presence of morphotropic regions of phase coexistence. This attracts much attention from the point of view of studying the mutual influence of multiferroics on each other's properties.

This paper presents the results of studying of the BFO-xYMO system with x = 40, 45, 50%, manufactured in various methods of solid-phase synthesis. In total, six methods were applied, including the use of preliminary mechanical activation of the initial oxides, as well as the reaction from prefabricated components of BFO and YMO. The structure, microstructure and dielectric properties have been studied. It has been shown that, along with perovskite phases, the samples most likely contain a ferrimagnetic composition of the $Y(Fe_{1-y},Mn_y)_2O_5$ type with an orthorhombic structure [12]. For the composition with x = 50%, it was possible to obtain a structure, most likely of the proskite type, with a monoclinic distortion of the unit cell. The study of the dielectric properties of materials showed the presence of anomalies in the temperature-frequency dependences $tg\delta(T,f)$ $\varepsilon'(T,f)$ $\varepsilon''(T,f)$ both in the low-temperature region and at temperatures above room temperature. The results are discussed.

The study is funded by Russian Science Foundation (project No. 22-72-00143, https://rscf.ru/project/22-72-00143/) with the use of equipment of the SSC RAS and SFedU Centers for Collective Use (https://ckp-rf.ru/catalog/ckp/501994/, https://ckp-rf.ru/catalog/ckp/3176/).

1. H. Schmid, *Ferroelectrics* **162**, 317 (1994).
2. P. Royen, K. Swars, *Angewandte Chemie* **69**, 779 (1957).
3. A.I. Zaslavsky, A.G. Tutov, *Doklady AS USSR* **135**, 815 (1960).
4. G.A. Smolenskii, V.A. Bokov, V.A. Isupov et al., *Helvetica Physica Acta* **41**, 1187 (1968).
5. C. Michel, J.-M. Moreau, G.D. Achenbach et al., *Solid State Comm.* **7**, 701 (1969).
6. G. Catalan, J.F. Scott, *Adv. Mater* **21**, 2463 (2009).
7. I. Sosnowska, T.P. Neumaier, E. Steichele, *J. Phys. C: Solid State Phys* **15**, 4835 (1982).
8. D. Sando, A. Bartheemy, M. Bibes, *J. Phys.: Cond. Matter* **26**, 473201 (2014).
9. Z.J. Huang, Y. Cao, Y.Y. Sun et al., *Phys. Rev. B* **56**, 2623 (1997).
10. T. Lonkai, D.G. Tomuta, U. Amann et al., *Phys. Rev. B* **69**, 134108 (2004).
11. A.V. Nazarenko, A.G. Razumnaya, M.F. Kupriyanov et al., *Phys. of the S. St.* **53**, 1599 (2011).
12. A. Muñoz, J.A. Alonso, M.J. Martínez-Lope et al., *Chem. Mater*. **16**, 4087 (2004).

P48

Mössbauer and dielectric studies of perovskite $Bi_{1-x}Nd_xFe_{(1-z)/2}Mn_{(1-z)/2}In_zO_3$ solid solution ceramics fabricated by a high-pressure synthesis

I.P. Raevski[1], S.P. Kubrin[1], A.V. Pushkarev[2], N.M. Olekhnovich[2], Yu.V. Radyush[2], S.I. Raevskaya[1], V.V. Titov[1], M.A. Malitskaya[1], P.A. Shishkina[1], S.I. Kolosov[1],

[1]*Physics Research Institute and Faculty of Physics, Southern Federal University, 344090, Rostov-on-Don, Russia*
igorraevsky@gmail.com

[2]*Scientific-Practical Materials Research Centre of NAS of Belarus, Minsk, Belarus*

Multiferroics - materials that possess two or more order parameters, e.g. ferroelectric and magnetic, attract huge attention due to the possibility of cross-control of their magnetic and electrical properties. The most widely studied perovskite is $BiFeO_3$, in which the temperatures of both ferroelectric and magnetic phase transitions significantly exceed room temperature. One of the main disadvantages of the most widely studied perovskite multiferroic $BiFeO_3$ is that it is an antiferromagnetic. On the basis of first-principal calculations, the possibility of obtaining ferromagnetic properties in $BiFe_{0.5}Cr_{0.5}O_3$ composition was predicted [1]. However, several works failed to find any ferromagnetic or ferrimagnetic properties in $BiFe_{1-x}Cr_xO_3$ ceramics fabricated by a high-pressure synthesis [2,3] (it is the only known method to obtain the perovskite modification of $BiFeO_3$ - based solid solutions compositions with high content of the second component).

$Bi_{1-x}Nd_xFe_{(1-z)/2}Mn_{(1-z)/2}In_zO_3$ (x=0.1, 0.2, 0.4, 0.6) compositions with perovskite structure were fabricated by a high-pressure (T_S=1200-1400 ^oC, P=4–6 GPa) synthesis. X-ray diffraction studies have shown that in such samples the morphotropic region between R3m and Pbam phases lies in the x=0.1÷0.2 compositional range similar to $Bi_{1-x}Nd_xFe_{1-x}Cr_xO_3$.

Thorough studies of Mössbauer spectra measured at 15 K have shown that in $Bi_{1-x}Nd_xFe_{(1-z)/2}Mn_{(1-z)/2}In_zO_3$ compositions a severe clustering of Fe and Cr (Mn) ions takes place. As a result, the volume of the sample is almost completely filled with clusters, either enriched or depleted in Cr (Mn) ions. This clusterisation seems to be the main origin of the absence of ferro-or ferrimagnetic properties in $BiFe_{0.5}Cr_{0.5}O_3$ as well as the similarity of concentration dependences of Neel temperature in solid solutions where Fe ions are replaced by paramagnetic ones [4, 5]

The temperature dependences of tgδ and both the real ε' and imaginary ε" parts of the complex permittivity ε* of $Bi_{1-x}Nd_xFe_{0.5}Cr_{0.5}O_3$ compositions were studied in a wide range of temperatures (15÷450 K) and frequencies (100Hz÷1MHz) using an E7-20 impedance meter. Measurements at higher temperatures were not carried out because of the fast increase of conductivity and thedanger of transformation of the metastable perovskite phase obtained by synthesis under high pressure into other phases stable at atmospheric pressure. While the tgδ(T) and ε"(T) curves show several maxima the temperature of which increase with the measuring frequency, the anomalies at the ε'(T) curves have the step-like form and the low-frequency values of ε' are very large. Such behavior is typical , e.g. for materials with the relaxation of the Maxwell-Wagner type. Conductivity activation energy (0.44 eV) corresponding to grain boundaries is substantially larger than activation energies of tgδ and ε" (0.13 eV) which confirms the supposition of the relaxation of the Maxwell-Wagner type.

This study was partially supported by RNF (project 23-42-10024) and by the Belarussian Republican Foundation for Fundamental Researches (project T23RNF-169).

1. P. Baettig, N.A. Spaldin, *Appl. Phys. Lett*. **86**, 012505 (2005).
2. F. Chang, N. Zhang, F. Yang, et al., *J. Phys. D: Appl. Phys*. **40**, 7799 (2007).
3. I.P. Raevski, S.P. Kubrin, A.V. Pushkarev, et al., *Ferroelectrics* **525**, 1 (2018).

P49

Magnetic Properties of Sintered and Rapidly Quenched $Sm_{10,5}Fe_{89,5-x}V_x$ Alloys (x = 10,0; 15,4) with $ThMn_{12}$ Type Structure

A.N. Shalaginov, A.A. Golubiatnikova, S.V. Andreev, A.S. Volegov

Ural Federal University, 620014, Ekaterinburg, Russia

Arkady.Shalaginov@urfu.ru

Every year the world is under increasing pressure to reduce its carbon footprint in the atmosphere through the reduction of fossil fuel use. Alternative ways of obtaining energy from renewable sources are used: wind, solar, and tidal energy, to this end. Carbon emissions from land transport are decreasing due to the partial replacement of petrol and diesel vehicles by electric or hybrid vehicles. This trend is leading to an increase in the use of high-efficiency permanent magnets, which are produced using rare-earth metals (REM). Due to the high cost of REM, it is economically advantageous to produce such permanent magnets in which their content would be minimized. One such compound is $Sm(Fe,T)_{12}$ (T = Ti, V, Co, etc.) with a $ThMn_{12}$ crystal structure. This compound contains 7,7 at. % REE, compared to 11,8 at. % in the compound $Nd_2Fe_{14}B$. Along with this, Sm is much cheaper than Nd.

The present work is devoted to establishing the effect of the fabrication method on the hysteresis magnetic properties of $Sm_{10,5}Fe_{89,5-x}V_x$ alloys (x = 10,0; 15,4). Two methods of obtaining the magnetically hard material based on the $Sm_{10,5}Fe_{74,1}V_{15,4}$ alloy were used: rapid quenching and sintering technology. Amorphous ribbons of homogenized $Sm_{10,5}Fe_{74,1}V_{15,4}$ alloy were obtained at a quenching surface speed of 30 m/s. The rapidly quenched alloys (RQA) were heat-treated at different temperatures in a vacuum as well as in an argon environment for 30 minutes. This allowed us to determine the annealing temperature at which the optimal microstructure is formed to obtain the maximum possible coercive field of the obtained RQA. The highest H_c value obtained was 7,8 kOe and $(B{\cdot}H)_{max}$ = 4,9 MGOe.

An attempt was made to sinter pressed particles of $Sm_{10,5}Fe_{74,1}V_{15,4}$ powder of the size of the order of 1 micron. Preparation for sintering was carried out in two different ways. The sintering was carried out at temperatures of 850 °C and 1140 °C for 1 – 4 hours.

The report will present the major demagnetization curves of RQA $Sm_{10,5}Fe_{89,5-x}V_x$ (x =10,0; 15,4) heat-treated at different conditions and their analysis. The results of measurements of the initial magnetic susceptibility of the alloys and the magnetic hysteresis loop for sintered alloys $Sm_{10,5}Fe_{74,1}V_{15,4}$ will also be given.

The research was financially supported by Russian Science Foundation (Grant Number 21-72-10104).

P50

The magnetic properties of toroidal samples produced by selective laser melting from iron powder

K.A. Stepanova, V.E. Maltseva, S.V. Andreev, A.S. Volegov, E.A. Stepanova, V.A. Kataev

Ural Federal University, 620026, Ekaterinburg, Russia
ksenia.stepanova@urfu.ru

Soft magnetic materials are used as electromagnetic cores. Their design is laminated thin sheets of steel. For nowadays it is not possible to produce cores with lower losses, due to limits of minimum sheet thickness and maximum silicon content [1]. Moreover, making complex shape cores is also not possible because of high brittleness such sheets. Additive manufacturing can help to overcome these limitations.

Additive manufacturing of soft magnetic materials allows to realize promising designs due to the flexibility of the production process. Currently study [2] offers various designs of cores that cannot be implemented by classical production methods. The development of additive manufacturing researches makes possible to create energy efficient soft magnetic components with all the advantages of additive technologies.

In works [2,3] strong influence of processing parameters, powder structure and annealing on the structure and properties of printed samples was shown. In [2] was found that high values of laser power lead to slow cooling of the section. Therefore, larger grains are observed, but residual stresses increase. Also, in [3] was shown that annealing can decrease residual stresses and the percentage of internal defects, as well as support domain growth and domain walls motion.

In this work the effect of processing and heat treatment parameters on the magnetic properties of torus-shaped samples obtained from carbonyl iron powder on an additive selective laser melting system Coherent Creator RA was studied. The static magnetic properties were measured with an MMKS-0.5 (NII STT, Smolensk). Relative measurement error of magnetic flux density and magnetic field strength ± 3% and ± 2%, respectively. The samples were annealed at 650 °C for 2 hours under vacuum.

Figure 1 shows a comparison of the magnetization curves and the values of the maximum magnetic permeability in the initial and annealed states. Based on the obtained results it was possible to observe only small changes in the magnetic properties due to changes in the processing parameters: laser power, scanning pattern. A significant difference was observed (Fig. 1) in samples fabricated with a power laser 200 W and a scanning rate 2000 mm/s (instead of 1000 mm/s). The reason is samples ‘structure that differs from other ones. The density of these samples is 5.1 g/m^3, while the density of other samples is ~6.1 g/m^3.

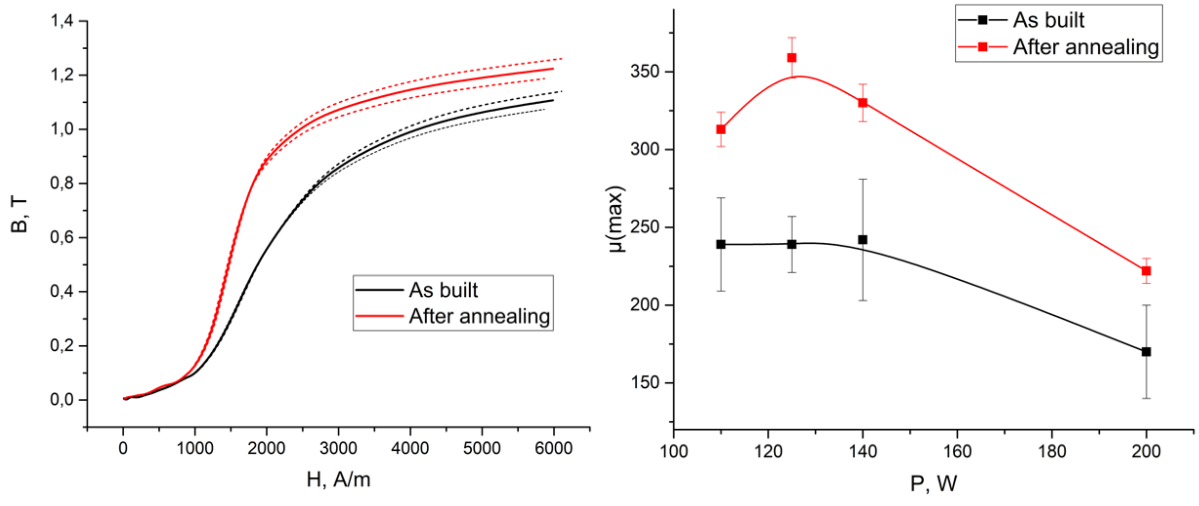

a) b)

Figure 1. Comparison of the magnetic properties of samples in the initial and annealed states: (a) magnetization curves, (b) dependence of the maximum magnetic permeability on the laser power.

Moreover, a significant improvement of the magnetic properties after annealing was found. The magnetization curve of the annealed sample (Fig. 1a, red line) indicates an easier process of magnetization in comparison with the initial state. The reason could be increasing grains size as a result of heat treatment. Besides, the maximum magnetic permeability of the sample fabricated with a laser power 125 W is 239, and after annealing it increases to 359. However, the hysteresis loss power of the annealed samples increased relative to the initial state.

In this work, a technique for producing soft magnetic samples by selective laser melting was tested. The key points of the technology for manufacturing magnetic circuits were identified. Although the magnetic properties are not yet suitable for practical use, however, ways to improve the properties, density, and to texture optimal grains size were determined.

As the result of this work, it can be concluded that the selection of the optimal processing and annealing parameters is necessary to control the structure of samples (such as porosity, grains size, fractures) and to improve their magnetic properties, probably due to an increase grains size and a decrease in residual stresses. Considering the current results will make possible to realize the advantages of the method: the creation of magnetic circuits of complex shape with acceptable properties for certain applications.

1. A.J. Moses, *Scripta Materialia* **67**, 560 (2012).

2. D. Goll et. al., *Additive Manufacturing* **27**, 428 (2019).

3. H. Shokrollahi, K. Janghorban, *J. Magn. Magn. Mater.* **317**, 61 (2007).

P51

Origin of dielectric dispersion in multiferroelectric $LuFeO_3$ doped by Sc

A.P. Turygin[1], D.O. Alikin[1], A.D. Ushakov[1], A.S. Abramov[1], V.I. Pryakhina[1], E.D. Greshnyakov[1], A. Zhaludkevic[2], D. Karpinskiy[2], V.Ya. Shur[1]

[1]*School of Natural Sciences and Mathematics, Ural Federal University, 620000, Ekaterinburg, Russia*
[2]*Scientific-Practical Materials Research Centre of NAS of Belarus, 220072, Minsk, Belarus*
anton.turygin@urfu.ru

Interest in multiferroics in the last decade has experienced significant growth of researchers in the field of new functional materials. The recently discovered multiferroics of the $REFeO_3$ series (RE = Lu, Yb) possesses ferroelectric and magnetic properties at room temperature [1, 2]. These compositions belong to multiferroics of the second type, where ferroelectric properties are caused by the magnetic ordering [3]. The interaction between magnetic and ferroelectric subsystems in this type of the materials is of considerable interest for the fabrication of the magnetic sensors, memory devices, and capacitors for the energy storage [4]. However, polar hexagonal phase of $REFeO_3$ possess multiferroic properties, which is not energetically favorable and thereby should be somehow stabilized, for example in thin film, by the stress from the substrates. In the case of the bulk ceramics, stabilization of the hexagonal phase is much more difficult task, and advanced chemical substitution schemes should be implemented instead.

In the present work, $LuFeO_3$-based solid solutions with Sc substitution were fabricated using the solid-phase synthesis method, and the dielectric properties of these compositions were studied and interpreted. The measured dielectric characteristics in $Lu_{1-x}Sc_xFeO_3$ showed a diffuse peak in the temperature range from 200 to 240°C, which had been interpreted previously as a relaxor phase transition or the ordering of charged defects, leading to conductivity increase.

Our high-resolution measurements using piezoresponse force microscopy allows to reveal that $Lu_{1-x}Sc_xFeO_3$ possessed the properties of a relaxor ferroelectric. The coexistence of nanoscale polar and non-polar phases could be discriminated in certain ceramic grains. Another subset of grains showed absence of piezoelectric response but displayed relatively high electrical conductivity, which increased significantly with temperature. Despite the minor deviation of the chemical composition in ceramics from the data obtained from energy-dispersive spectroscopy, confocal Raman microscopy revealed significant changes in the spectra across the grains. These changes could be attributed to local variations in symmetry, indicating the coexistence of hexagonal (ferroelectric) and orthorhombic (non-ferroelectric) phases. The dielectric maximum could be attributed to a rapid increase in electronic conductivity within the orthorhombic phase measured by conductive AFM caused by activation of oxygen vacancies at elevated temperatures. The PFM measurements allows to confirm existence of the diffuse phase transition within this temperature range.

This research was made possible by the RFBR (project # 20-52-04011) and BRFFR (project # T21RM-040). The equipment of the Ural Center for Shared Use “Modern nanotechnology” Ural Federal University (Reg. No. 2968) was used with the financial support of the Ministry of Science and Higher Education of the Russian Federation (Project No. 075-15-2021-677).

1. S. Dong, J.-M. Liu, S.-W. Cheong, et al., *Adv. Phys.* **64**, 519 (2015).
2. Y.K. Jeong, J.-H. Lee, S.-J. Ahn, H.M. Jang, *Chem. Mater.* **24**, 2426 (2012).
3. U. Chowdhury, S. Goswami, D. Bhattacharya *et al.*, *Appl. Phys. Lett.* **105**, 052911 (2014).
4. N.A. Spaldin, R. Ramesh, *Nat. Mater.* **18**, 203 (2019).

P52

Simple spin-reorientation model in rare-earth orthoferrites and orthochromites

E.V. Vasinovich, A.S. Moskvin

Ural Federal University, 620100, Ekaterinburg, Russia
e.vasinovich@gmail.com

Rare-earth orthorhombic perovskites, orthoferrites RFeO$_3$ and orthochromites RCrO$_3$ (where R is a rare-earth ion and yttrium), exhibit many important features, such as weak ferro- and antiferromagnetism, which are an overt and hidden canting of magnetic sublattices, magnetization reversal, anomalous circular magnetooptic, etc. Spin reorientation (SR) is one of their unique properties that attracted a lot of attention back in the 1970s [1].

The revival of interest in the mechanism of the spontaneous spin reorientation and magnetic compensation in rare-earth perovskites in recent years is related to the discovery of the magnetoelectric and exchange bias effects, which can have a direct application in magnetoelectronics.

In this work, we consider a simple microscopic theory of the SR transition in a certain plane of the rare-earth orthoferrite induced by the *4f–3d* interaction, more specifically, the interaction of the well-isolated ground-state Kramers doublet or non-Kramers quasidoublet of the *4f* ion with an effective magnetic field induced by *3d* sublattice. For instance, a thermodynamic potential of the model for the SR transition $G_x - G_z$ in the *ac* plane ($\boldsymbol{G}$ is the antiferromagnetic vector of the *3d* sublattice) can be written as

$$\Phi(\theta) = K_1 \cos 2\theta + K_2 \cos 4\theta - kT \ln 2 \cosh \frac{\Delta(\theta)}{2kT}, \qquad (1)$$

where K_1 and K_2 are the first and second anisotropy constants of the *3d* sublattice [2], θ is the orientation angle, $\Delta(\theta)$ is the lower doublet (quasi-doublet) splitting of the 4f ion. Minimizing $\Phi(\theta)$ leads to two equations:

$$\sin 2\theta = 0 \text{ (phases } G_x \text{ and } G_z\text{)},$$
$$\alpha\mu + \beta\mu^3 = \tanh\frac{\mu}{\tau} \text{ (angular phase } G_{xz}\text{)}, \qquad (2)$$

where $\tau = T/T_{sr}$, $T_{sr} = \left[\Delta^2(0) - \Delta^2\left(\frac{\pi}{2}\right)\right]/16kK_1$, $\mu = \Delta(\theta)/2kT_{sr}$, and α, β are the parameters, which depend on the K_1, K_2, $\Delta(0)$, and $\Delta\left(\frac{\pi}{2}\right)$.

Figure 1 shows typical solutions for the master equation (2). This model can describe a variety of the SR scenarios including rather typical smooth SR via one or two second-order phase transitions (see SO region in Fig. 1), sharp first-order phase transition (see FO region), and unconventional "mixed" SR via combination of the second and first-order phase transitions (see MO$_{1,2}$ regions).

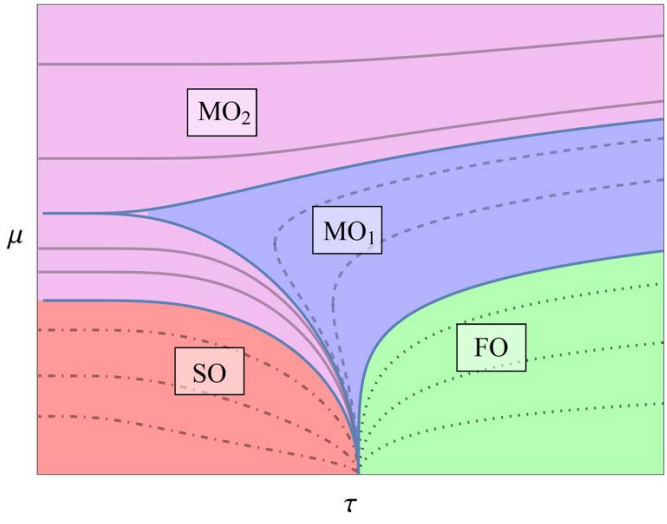

Figure 1. $\mu - \tau$ phase diagram of the model.

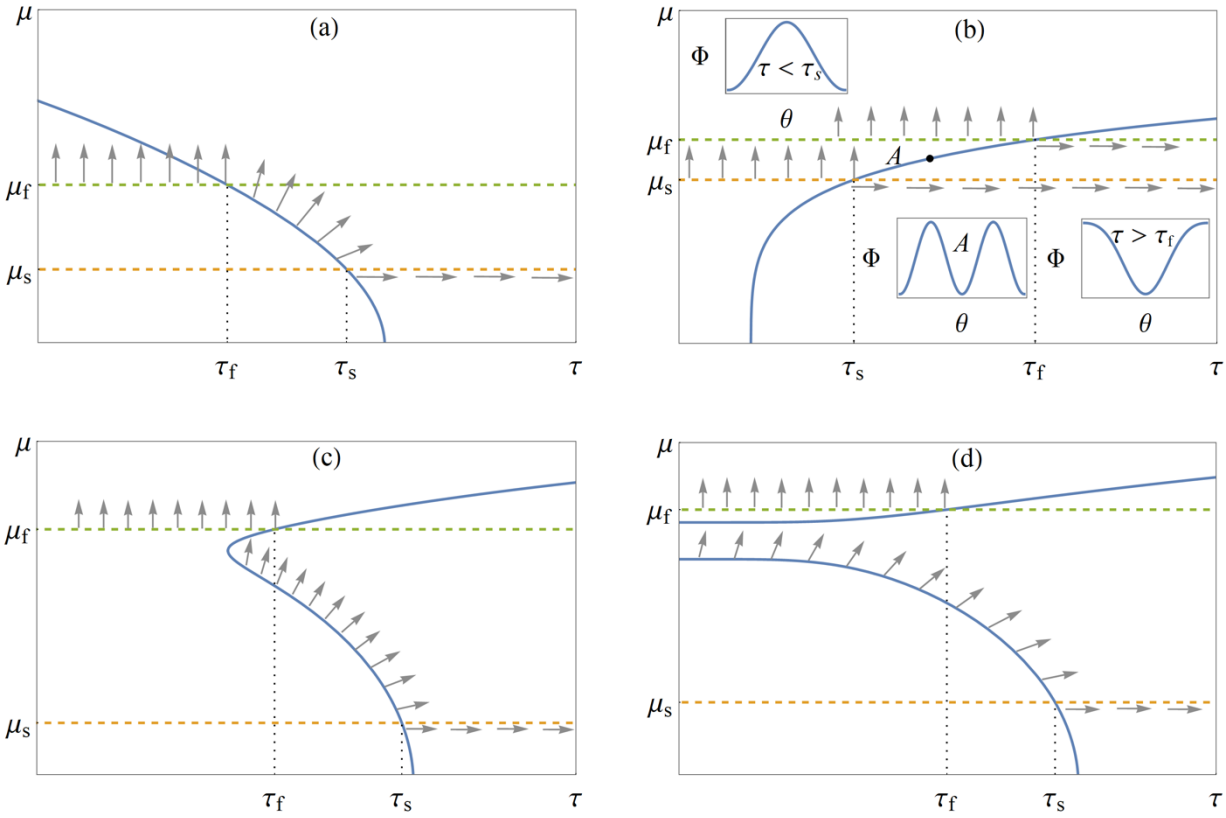

Figure 2. Illustrations of (a,b) typical and (c,d) unconventional SR transitions predicted by the model. The arrows indicate the direction of the antiferromagnetic vector $\boldsymbol{G}$ in the *ac* plane.

Figure 2 shows detailed examples of the phase diagram. Figure 2a describes a typical smooth SR transition with two second-order phase transitions $G_x - G_{xz}$ at the beginning (τ_s) and $G_{xz} - G_z$ at the end (τ_f) of the spin reorientation. Figure 2b describes an abrupt first-order SR transition: for $\tau > \tau_f$ there is the G_x-phase, which can remain stable up to τ_s when cooled; for $\tau < \tau_s$ there is the G_z-phase, which can remain stable up to τ_f when heated.

Figures 2c and 2d describe the more interesting cases when the model predicts the existence of mixed-type SR transitions. At τ_s, there is the smooth second-order phase transition $G_x - G_{xz}$. At $\tau \leq \tau_f$, we have two stable phases, G_z and G_{xz}: at those temperatures the sharp first-order phase transition $G_x - G_{xz}$ can happen, or the system could stay in the angular G_{xz}-phase.

The main results have been published in [3].

The work was supported by RSF project № 22-22-00682.

1. K.P. Belov, A.K. Zvezdin, A.M. Kadomtseva, R.Z. Levitin, *Orientation Phase Transitions in Rare Earth Magnetic Materials* (Nauka, Moscow), 317 (1979).
2. A. Moskvin, *Magnetochemistry* **7**, 111 (2021).
3. A. Moskvin, E. Vasinovich, A. Shadrin, *Magnetochemistry* **8**, 45 (2022).

P53

Piezoceramic lithium metaniobate: possibilities for improving mechanical properties

S.I. Dudkina, K.P. Andryushin, L.A. Shilkina, I.N. Andryushina, I.A. Verbenko, L.A. Reznichenko

Research Institute of Physics, Southern Federal University, 344090, Rostov-on-Don, Russia
s.i.dudkina@yandex.ru

Despite the unique characteristics of lithium metaniobate (MNL) - uniaxiality and one of the highest among ferroelectrics (FE) Curie temperature (T_c ~ 1200 °C) - it has not found wide practical application in the form of the ceramics, which is largely due of its by the low mechanical strength and a tendency to self-destruct. Attempts to improve the mechanical properties of MNL by the modification, the designing binary systems, using various methods and technological procedures for the obtaining did not lead to significant results. Meanwhile, the creation of such high-temperature piezoactive ceramics is of undoubted interest not only in applied terms, but also in scientific terms due to the possibility of comparing the properties of single- and polycrystals of a representative of a small class of uniaxial FEs belonging to the least studied (than, for example, perovskites) to structural type of the pseudoilmenites.

The paper presents the results of a comprehensive study of the crystal structure, microstructure, electrical and mechanical properties of the solid solutions (SS) of binary systems of the form $(1\text{-}x)LiNbO_3 - xA^{2+}TiO_3$, where is A^{2+} – Cu, Ni, Co, x = 0.005 - 0.030. SS have been prepared by using conventional ceramic technology.

The solubility boundaries of the components, the symmetry and parameters of the unit cells of the formed SS were determined by X-ray diffraction. Two groups of systems have been distinguished: with the formation of continuous series of TS in the studied concentration ranges and with limited solubility of the components.

The table shows the main electrical and mechanical characteristics of the best of the developed materials in comparison with pure MNL.

Table. Characteristics of the developed material and pure MNL.

Material	Maximum operating temperature, K	Electrophysical parameters*)					
		σ, MPa	$\varepsilon_{33}^T/\varepsilon_0$	d_{33}, pC/N	V_R, km/s	K_t	K_t/K_p
Designed (with $0.005CoTiO_3$)	1300	300	54	11.9	5.4	0.30	25
MNL	1200	150	45	9.8	4.6	0.20	15

*) σ is the mechanical strength, $\varepsilon_{33}^T/\varepsilon_0$ is the relative permittivity of polarized samples, d_{33} is the piezoelectric modulus, V_R is the speed of sound, K_t, K_p are the electromechanical coupling coefficients of the thicknessed and radial vibration modes of the samples, respectively, K_t/K_p is the anisotropy of the piezoelectric properties.

High mechanical strength and sufficiently high piezoparameters and sound speed make it possible to use the developed compositions for creating piezoelectric elements for devices of high-frequency measuring equipment designed to control objects that experience extreme external influences (temperature, pressure, shock, vibrations).

The study was carried out with the financial support of the Ministry of Science and Higher Education of the Russian Federation (State task in the field of scientific activity in 2023). Project No. FENW-2023-0010/(GZ0110/23-11-IF) "Multicomponent intelligent structures: phase transition crossing effects and strategies for accelerated design of eco-systems for technologies for digital design of devices for controlling the parameters of physical media." The equipment of the Center for Collective Use of the Scientific Research Institute of Physics of the Southern Federal University "Electromagnetic, electromechanical and thermal properties of solids" was used.

P54

Features of obtaining lead-free ferro-piezoceramics based on sodium niobate

S.I. Dudkina, K.P. Andryushin, I.N. Andryushina, M.O. Moysa,
I.A. Verbenko, L.A. Reznichenko

Research Institute of Physics, Southern Federal University, 344090, Rostov-on-Don, Russia
s.i.dudkina@yandex.ru

The group of lead-free ferro-piezoceramic materials (FPCM) based on sodium niobate (NN) has a number of physical properties that are not realized in well-known industrially produced compositions based on PZT ($Pb(Ti,Zr)O_3$) compositions. The advantages of such FPCMs are the high speed of sound, which determines the high-frequency (HF) range of operation of the converter, as well as the ability to obtain a given frequency on less thin plates, which simplifies the technology for manufacturing HF devices due to the possibility of increasing their resonant dimensions; low experimental density, leading, on the one hand, to a significant reduction in the weight of products, and, on the other hand, to a decrease in acoustic impedance; very low dielectric constant, which is important for electrical matching with the generator and the load; increased electromechanical coupling coefficient of the oscillation mode by the thickness; sufficient anisotropy of the piezoproperties, which improves the signal-to-noise ratio and simplifies the production technology, eliminating the operation of cutting the material; low dielectric and moderate mechanical losses, which is important for obtaining short pulses and uniform amplitude-frequency characteristics.

One of the limitations that prevent their mass production is the long firing during the sintering process due to high temperatures and also low mechanical strength, which provokes self-destruction of products. One of the ways to accelerate the production of FPCM, including those based on sodium niobate, is the hot pressing (HP) method, the essence of which is the simultaneous application of high temperatures and pressures to the workpiece from the press powder. In addition to the high performance, the advantages of the HP are its versatility; the possibility of manufacturing practically non-porous ceramics with a density close to theoretical and with a controlled microstructure; preservation of the stoichiometry of the composition; increasing the efficiency of FPCM compared to that when using conventional ceramic technology. At HP the transfer of the pressure to the workpiece , as a rule, is carried out with the help of various media, most often loose bodies - fillings. The use of the filling during FPCM sintering by the HP method is dictated, first of all, by the need to exclude direct contact of the sample with the material of the matrix and punches, as well as normal pressure transfer to it, uniform supply and removal of heat from the fired products.

To eliminate the above negative effects, we have developed a filling composition that makes it possible to reduce the sintering temperature (T_{sint}) of lead-free FPCMs and significantly improve their mechanical strength. At the same time, the composition of the filling for sintering FPCM based on sodium niobate, including Al_2O_3 and an additive, differs in that it contains powdered manganese oxide MnO and manganese carbonate $MnCO_3$ as an additive. The introduction of MnO and $MnCO_3$ into the filling composition leads to the depletion of the atmosphere surrounding the sample in the working volume with oxygen due to its binding during the oxidation of MnO and displacement by carbon dioxide during the decomposition of $MnCO_3$, that is, the formation of a reducing atmosphere in the matrix. Sintering under these conditions promotes the formation of oxygen vacancies. Participating in mass transfer processes, these vacancies facilitate diffusion processes, accelerate them, and lead to a decrease in T_{sint}. Conservation of a given stoichiometry at such low firing temperatures improves the properties of sintered niobate materials. The use of this filling makes it possible to use the investigated media to create high-performance materials with a wide spectrum of action with desired properties.

The study was carried out with the financial support of the Ministry of Science and Higher Education of the Russian Federation (State task in the field of scientific activity in 2023). Project No. FENW-2023-0010/(GZ0110/23-11-IF) "Multicomponent intelligent structures: phase transition crossing effects and strategies for accelerated design of eco-systems for technologies for digital design of devices for controlling the parameters of physical media." The equipment of the Center for Collective Use of the Scientific Research Institute of Physics of the Southern Federal University "Electromagnetic, electromechanical and thermal properties of solids" was used.

P55

Resonance response of antiferroelectrics with a low content of ferroelectric components in the microwave range

P.A. Astafev[1], K.P. Andryushin[1], A.A. Pavelko[1], A.R. Borzykh[2], I.A. Ivanov[2]

[1]*Research Institute of Physics, Southern Federal University, Rostov-on-Don, 344090, Russia*
l.6.e.9.w.4.a.9.p@yandex.ru

[2]*Department of Physics, Southern Federal University, Rostov-on-Don, 344006, Russia*

Two-component and multicomponent ferroelectric solid solutions can be used in various electronic components [1]. However, at present, not much attention is paid to the electrodynamic properties of these materials in the areas of concentration and temperature phase transitions. Our previous experience in measuring ferroelectric, antiferroelectric materials, as well as ferroelectric relaxors, showed the presence of resonant behavior of samples of various shapes and sizes in electromagnetic fields of the microwave range of various configurations [2, 3]. Both two-component and multicomponent solid solutions based on $(x\text{-}1)PbZrO_3\text{-}xPbTiO_3$ were considered in the range of concentration and temperature phase transitions, while high-Q resonances were found only in the antiferroelectric phase. From the point of view of environmental friendliness, a more interesting ferroelectric-antiferroelectric system is $(x\text{-}1)NaNbO_3\text{-}xKNbO_3$, in which we also found, presumably, resonance behavior in compositions with a low content of $KNbO_3$.

Thus, the purpose of this work was to determine the nature of the absorption maxima of potassium sodium niobate samples in the microwave range.

The objects of this study were samples of solid solutions of the two-component system $(x\text{-}1)NaNbO_3\text{-}xKNbO_3$. The materials were obtained by double solid-phase synthesis followed by sintering (temperatures varied in the range (1200÷1370) ºC) using conventional ceramic technology. The samples are made in the form of cylinders with a diameter of 12 mm and a height of 1.2 mm. Machining of surfaces was carried out with a diamond tool according to the 6th accuracy class. The error of the diameters and thicknesses of the samples is no more than 4% for the thickness and no more than 1% for the diameter. The compositions with $KNbO_3$ concentration in the range $0 < x < 0.04$ were chosen for measurements.

The measurements were carried out using a P9375A "Keysight" vector network analyzer and two measuring cells, which are straight segments of microstrip lines (MPL) on substrates of various materials. To achieve the best agreement with the measuring setup and the lowest level of losses, the MSLs had different widths, which depended on the permittivities of the substrates. During the measurements, the samples were located in the center of the cell, on the MSL surface, and also on the substrate, next to the MSL, while the dependences of the real parts of the scattering matrix coefficients on frequency were recorded. Measurements on the MSL surface were performed to assess the level of microwave absorption in the material [4], and next to the MSL, to check for the presence of electromagnetic wave resonances in material samples.

The experiment showed that in the case of the location of the samples on the surface of the MSL (Fig. 1a,b), the intensity of the absorption maxima at a frequency of 5.5 GHz increases as the molar fraction of $KNbO_3$ increases from 0 to 1%, and then sharply increases to 50% and in does not change on average up to 4% $KNbO_3$. The maximum at a frequency of 7 GHz is weakly distinguishable or indistinguishable at all. When the samples are located next to the MSL on the substrate (Fig. 1c,d), there is no absorption maximum at a frequency of 5.5 GHz, while a maximum at a frequency of 7 GHz becomes visible, the intensity of which decreases with increasing $KNbO_3$ concentration.

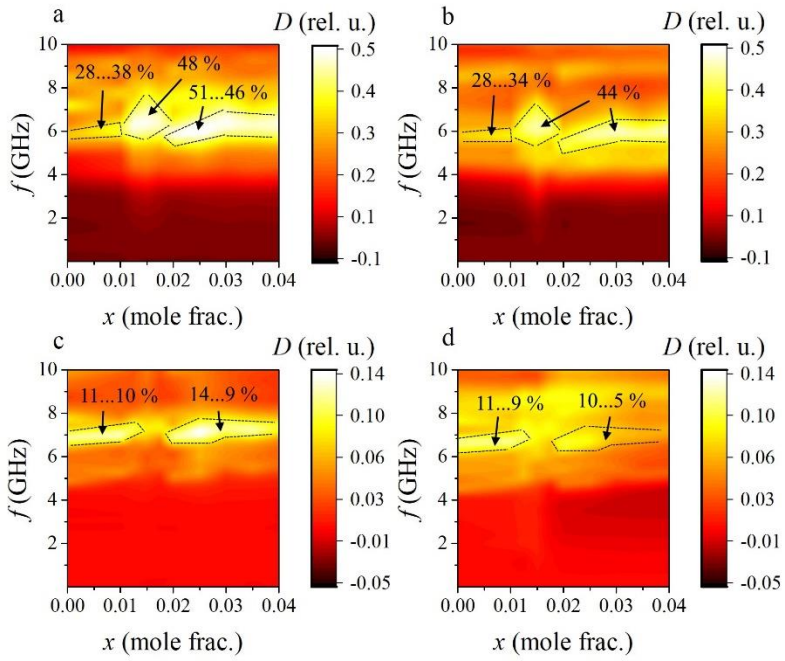

Figure 1. Dependences of the absorption coefficient of samples (1-x)$NaNbO_3$-(x)$KNbO_3$ on the frequency and concentration of KNbO3 under different experimental conditions: (a) sample on MSL, measuring cell 1; (b) sample on MSL, measuring cell 2; (c) sample next to the MSL on the substrate, measuring cell 1; (d) the sample next to the MSL on the substrate, measuring cell 2. The dotted line marks the areas with the maximum absorption level.

These observations, as well as the fact of the existence of an electromagnetic energy absorption maximum when the sample is in a region with a weak electric field density, indicate the different nature of the occurrence of the described maxima, in particular, confirms the resonant nature of the maximum at a frequency of 7 GHz. All detected features are associated exclusively with material samples, which is confirmed by measurements using a different measuring cell.

The study was carried out with the financial support of the Ministry of Science and Higher Education of the Russian Federation (State task in the field of scientific activity in 2023). Project No. FENW-2023-0010/(GZ0110/23-11-IF).

1. A.K. Tagantsev, V.O. Sherman, K.F. Astafiev, et al., *J. Electroceramics* **11**, 1 (2003).
2. P. Astafev, A. Pavelko, A. Lerer, et al., *Crystals* **12**, 4 (2022).
3. P. Astafev, A. Pavelko, K. Andryushin, et al., *Materials* **15**, 24 (2022).
4. Ya.A. Reizenkind, A.B. Kleshchenkov, A.M. Lerer, Yu.M. Noikin, *Proc. Int. Symp. "Physics of Lead-Free Piezoactive and Related Materials. Modeling of eco-systems (Analysis of Current State and Prospects of Development)"* **2**, (2021).

P56

Effect of light on the resistance of the $LaMnO_3/Bi_4Ti_3O_{12}/Ba_{0,4}Sr_{0,6}TiO_3/MgO$ and $Ba_{0.8}Sr_{0.2}TiO_3/LaMnO_3/Ba_{0.8}Sr_{0.2}TiO_3/MgO$ heterostructures

A.O. Chibirev, A.V. Leontiev, N.N. Garig'yanov, M.I. Bannikov, R.F. Mamin

Zavoisky Physical-Technical Institute, FRC Kazan Scientific Center of RAS, 420029, Kazan, Russia
chibirev12@mail.ru

The creation of quasi-two-dimensional metallic states at the interface and the control such states by light is impossible without the use of new design interfaces. A high-mobility electron gas has been discovered at the interface between two oxide insulators $LaAlO_3$ (LAO) and $SrTiO_3$ (STO) [1]. The effect of infrared, green, and ultraviolet laser radiation on the electrical resistance of the heterostructure $Ba_{0.8}Sr_{0.2}TiO_3/LaMnO_3$ was investigated here. In this work, we investigated the effect of infrared, green, and ultraviolet laser radiation on the electrical resistance of the heterostructure $BaTiO_3/LaMnO_3$ on $LaMnO_3$ single crystal and in heterostructures $LaMnO_3/Bi_4Ti_3O_{12}/Ba_{0,4}Sr_{0,6}TiO_3$ and $Ba_{0.8}Sr_{0.2}TiO_3/LaMnO_3/Ba_{0.8}Sr_{0.2}TiO_3$ on MgO substrate.

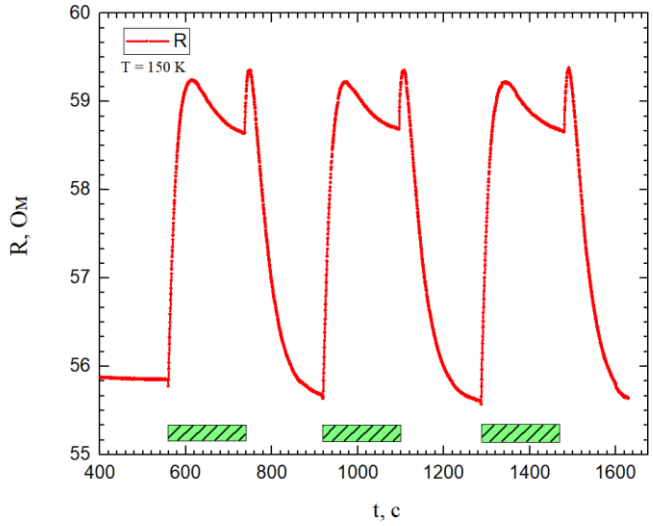

Figure 1. Multiple on-off switching of electrical resistance of the $LaMnO_3/Bi_4Ti_3O_{12}/Ba_{0,4}Sr_{0,6}TiO_3/MgO$ heterostructure at 150 K by green illumination.

Dependencies of the electrical resistance on temperature light exposure were studied for $Ba_{0.8}Sr_{0.2}TiO_3/LaMnO_3$ heterosctructure, as well as for $LaMnO_3/Bi_4Ti_3O_{12}/Ba_{0,4}Sr_{0,6}TiO_3/MgO$ and $Ba_{0.8}Sr_{0.2}TiO_3/LaMnO_3/Ba_{0.8}Sr_{0.2}TiO_3/MgO$ heterosctructures. An unfocused laser beam with a diameter of 4 mm, with a Gaussian shape, irradiated the space between the contact pads through the optical window of the cryostat. We observed at both $LaMnO_3/Bi_4Ti_3O_{12}/Ba_{0,4}Sr_{0,6}TiO_3/MgO$ and $Ba_{0.8}Sr_{0.2}TiO_3/LaMnO_3/Ba_{0.8}Sr_{0.2}TiO_3/MgO$ heterosctructures an increase in resistance when exposed to light at all wavelengths used and a recovery of resistance in the dark state. These changes of resistance are positive and up to 8-10% of the steady-state resistance, the time constant associated with the transient component is ~ 4-50 s. The response to green light exposure was the most prominent. It was found that when illuminated with light of different wavelengths, there was a cumulative effect, a change in resistance over several on/off cycles green and infrared light. The observed effect cannot be explained by direct heating of the sample by laser pulses, because the laser pulse repetition rate is low and, therefore, the cumulative thermal effects should be negligible. Measurements in the Kelvin mode of atomic force microscopy showed that illumination has a similar effect on the surface charge concentration, which confirms our hypothesis that the effect is associated with partial screening of the ferroelectric polarization by photogenerated charge carriers. This example shows that quasi-two-dimensional high conductance at ferroelectric/dielectric interfaces can be controlled by light.

The reported study was funded by Russian Scientific Foundation, research project No. 21-12-00179.

1. A. Ohtomo, H. Ywang, *Nature* **427**, 6973 (2004).

P57

The influence of doping by tin (II) cations on antimony sulphoiodide longitudinal piezo module values

D.V. Chirkova[1], I.V. Lisnevskaya[2]

[1]*Federal Research Centre, The Southern Scientific Centre of the Russian Academy of Sciences, 344006, Rostov-on-Don, Russia*

sdanamail@list.ru

[2]*Southern Federal University, Chemistry department, 344015, Rostov-on-Don, Russia*

Antimony sulphoiodide (SbSI) is one of the important ferroelectric materials of A(V)B(VI)C(VII) group. It exhibits one of the biggest among known materials bulk piezomodulus (d_v= 800÷900 pC/N) and some other high electrophysical characteristics [1]. These properties make it promising for electromechanical transducers, sensors and detectors. The main limitation of SbSI wide practical application is its low (22ºC) temperature of phase transition into paraelectric phase (Tc). One of the possible ways to overcome this challenge is modifying of material properties by doping [2]. However, there are few published results on the electrophysical properties of doped materials.

On the basis of synthesis method described in [2] the samples of doped materials SbSI:xSn were obtained. The synthesized powders were dark red in color and had a needle-like structure characteristic for SbSI. The amount of dopant *x* was varied in the range from 1 to 10 mol.%. Using Brigman-Stokbarger technique the polycrystalline textures of doped materials were grown. The textures were diced on the samples of 0.4 cm thick. The samples obtained were covered with electrodes. The determined values of piezomodulus d_{33} for samples under study are presented in Figure 1. The highest value is registered for material with *x*=5 mol%.

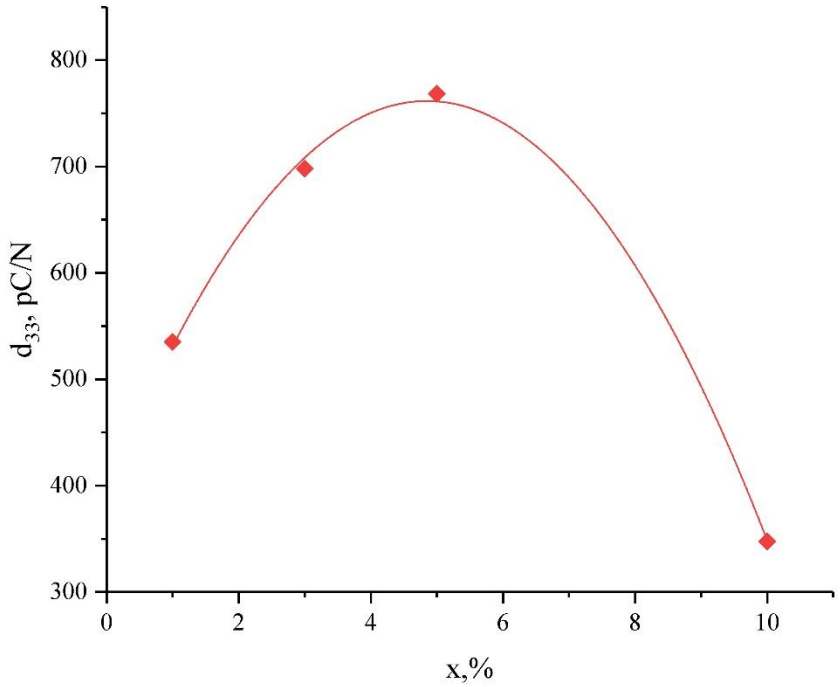

Figure 1. Dependence of the longitudinal piezo module of SbSI:xSn samples on the amount of the dopant introduced.

The work was carried out within the framework of the SSC RAS state task (project number 122020100294-9)

1. E.I. Gerzanich, V.M. Fridkin, *Segnetoelectrics of A(V)B(VI)C(VII) type* (Nauka), 220 (1982).
2. T.G. Lupeiko, D.V. Chirkova, I.V. Lisnevskaya, *Ferroelectrics* **493**, 183 (2016).

P58

Composite effect of conductivity in systems $MeWO_4$-Al_2O_3 (Me – Ca, Sr)

V.A. Gardt, A.F. Guseva, N.N. Pestereva, D.K. Kuznetsov

Ural Federal University, 620002, Yekaterinburg, Russia
Vitiagt@mail.ru

Composites (1-*x*)$MeWO_4$–*x*Al_2O_3 (Me – Ca, Sr) obtained by the solid-phase method. The phase composition of the composites and their thermodynamic stability were confirmed by XRD and TG-DSC. The SEM-EDA method was used to study the morphology of the composites.

The conductivity of composites was studied by the method of electrochemical impedance as a function of temperature, oxygen pressure in the gas phase, and the content of the dispersed additive Al_2O_3.

Figure 1 shows the dependences of the electrical conductivity of (1-*x*)$CaWO_4$–*x*Al_2O_3 and (1-*x*)$SrWO_4$–*x*Al_2O_3 composites on the mole fraction of aluminum oxide. The concentration dependence of the (1-*x*)$CaWO_4$–*x*Al_2O_3 and (1-*x*)$SrWO_4$–*x*Al_2O_3 composites conductivity has the form of a curve with a gentle maximum. The dome-shaped nature of the concentration dependence of the conductivity of the studied composites is explained in terms of the percolation model [1, 2]. The dependence obtained is satisfactorily described by the mixing equation [2].

The addition of a low-conductivity Al_2O_3 nanopowder to a low-conductivity alkaline earth metal tungstate causes an increase in conductivity in the $CaWO_4$–Al_2O_3 system by a maximum of 12 times, and in the $SrWO_4$–Al_2O_3 system by a maximum of 4 times. The increase in electrical conductivity is related to the high ionic conductivity of the $MeWO_4$|Al_2O_3 interphase boundary, which is formed at the site of contact between the matrix and the disperse additive. The segregation of small grains of Al_2O_3 in the near-surface region of large grains of the alkaline earth metal tungstate matrix, detected in this work by the SEM-EDA method, contributes to the formation of a connected system of conducting interfaces $CaWO_4$|Al_2O_3 ($SrWO_4$|Al_2O_3).

Reaching the maximum value, the electrical conductivity begins to decrease due to the discontinuity of the interphase boundary by dielectric particles Al_2O_3. The maximum conductivity is observed at a content of ~50 mol. % Al_2O_3 in the $CaWO_4$–Al_2O_3 system and ~30 mol. % Al_2O_3 in the $SrWO_4$–Al_2O_3 system.

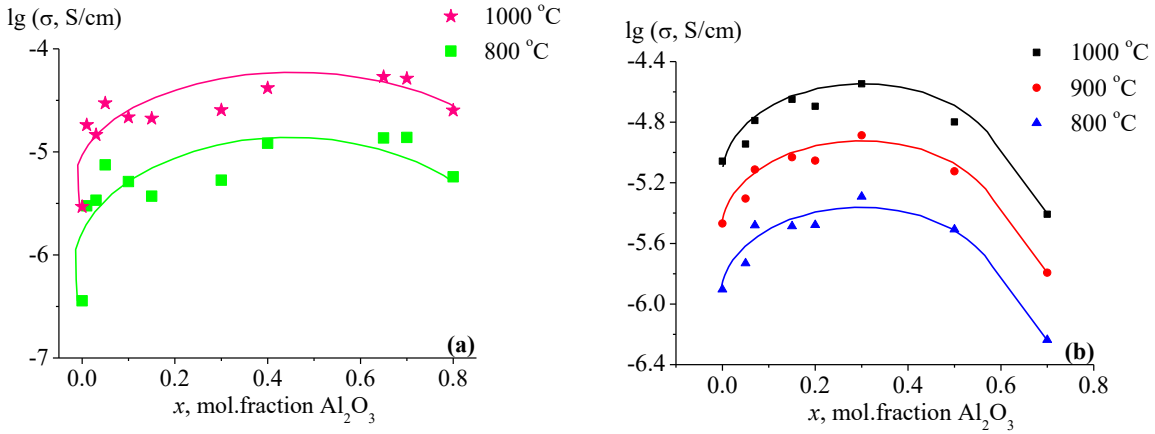

Figure 1. Electrical conductivity as a function of the mole fraction of Al_2O_3 at different temperatures: a) (1-*x*)$CaWO_4$–*x*Al_2O_3, b) (1-*x*)$SrWO_4$–*x*Al_2O_3

The research results were obtained within the framework of the state task of the Ministry of Science and Higher Education of the Russian Federation (project number 123031300049-8) using the equipment of the UCKP "Modern Nanotechnologies" UrFU (reg. No. 2968), supported by the Ministry of Science and Higher Education of the Russian Federation (project No. 075-15-2021-677).

1. N.F. Uvarov, *Solid State Ionics* ***136-137***, 1273 (2000).
2. N.F. Uvarov, *Composite solid electrolytes*, Novosibirsk: ISSC SB RAS Publ., 259, (2008).

P59

Oxygen-ion composites MWO_4-SiO_2 (M – Sr, Ba)

V.A. Gardt, N.N. Pestereva, A.F. Guseva, D.V. Korona

Ural Federal University, 620002, Yekaterinburg, Russia
Vitiagt@mail.ru

Composites (1-*f*)$SrWO_4$-*f*SiO_2 and (1-*f*)$BaWO_4$-*f*SiO_2, where f is the volume fraction of dispersed SiO_2 additive, were prepared by solid-phase method. The obtained composites were investigated by XRD, TG-DSC, SEM-EDA methods.

The electrical conductivity of the composites was measured by the electrochemical impedance method as a function of temperature, partial pressure of oxygen in the gas phase and composition. To assess the contribution of ionic conductivity, the sum of ionic transfer numbers was measured by the EMF method.

In the systems under study the addition of low-conducting SiO_2 nanopowder to low-conducting tungstate causes the increase of conductivity in the $CaWO_4$-SiO_2 and $BaWO_4$-SiO_2 systems by a maximum of 12 times, and in the $SrWO_4$-SiO_2 system by approximately 2 orders of magnitude. The growth of conductivity is related to the high ionic conductivity of the $MeWO_4|SiO_2$ interface, formed at the contact of the matrix and disperse additive. The segregation of small grains of SiO_2 in the near-surface area of large grains of tungstate matrix detected in this work by SEM-EDA contributes to the formation of a coherent system of conductive $MeWO_4|SiO_2$ interphase boundaries.

Passing through the maximum, the conductivity begins to decrease due to the discontinuity of the interfacial boundary by SiO_2 dielectric particles.

To calculate the conductivity of (1-*f*)$SrWO_4$-*f*SiO_2 and (1-*f*)$BaWO_4$-*f*SiO_2 composites as a function of SiO_2 content, the mixing equation [1] was used. The calculated concentration dependences of conductivity obtained are in satisfactory agreement with the experimental results (Fig. 1).

The discrepancy between the calculated and experimental conductivity curves is due to the fact that the real composite differs from the model system. In the model, average grain sizes are taken for calculation, but the powders of the components are not monodisperse. Nevertheless, the calculated dependence correctly reflects the general tendency of conductivity change with increasing concentration of disperse additive.

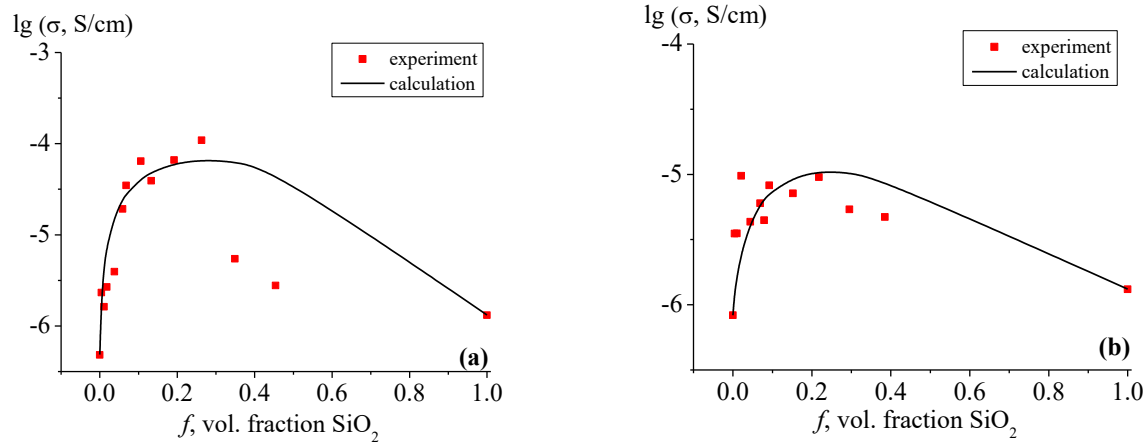

Figure 1. Experimental and calculated electrical conductivity of composites at 900 °C: a) (1–*f*)$SrWO_4$–*f*SiO_2; b) (1–*f*)$BaWO_4$–*f*SiO_2.

The research results were obtained within the framework of the state task of the Ministry of Science and Higher Education of the Russian Federation (project number 123031300049-8) using the equipment of the UCKP “Modern Nanotechnologies” UrFU (reg. No. 2968), supported by the Ministry of Science and Higher Education of the Russian Federation (project No. 075-15-2021-677).

1. N.F. Uvarov, *Composite solid electrolytes*, Novosibirsk: ISSC SB RAS Publ., 259, (2008).

P60

Evolution of the domain structure during polarization reversal and phase transitions in $BaTiO_3$ ferroelectric ceramics

L.V. Gimadeeva, A.D. Ushakov, A.A. Nikulin, D.O. Alikin, V.Ya. Shur

Ural Federal University, 620000, Ekaterinburg, Russia
lv.gimadeeva@urfu.ru

Ferroelectric $BaTiO_3$ (BTO) ceramics is classical ceramics with well-known crystal structure and macroscopic properties and widely used for capacitors, resistors with positive temperature coefficient, ultrasonic transducers, and piezoelectric devices. Piezoelectric performance of polycrystalline materials predominantly depends on by extrinsic mechanisms with dominating contributions of reversible and irreversible domain wall motion [1-3], which postulates importance of the domain structure analysis using the methods of the high resolution. Here, we study domain structure evolution after polarization reversal in external electric field and ferroelectric phase transition in bulk BTO ceramics using piezoresponse force microscopy.

The domain structure obtained after thermal depolarization was shown to represent a large domain band («superdomains») filled with twins of various orientations and 180-degree domain walls crossing the boundaries of twins in the individual ceramic grains. The domain structure and average value of the piezoelectric response depends significantly on the cooling rate during the ferroelectric phase transition. Low cooling rates provides better compensation for mechanical stresses and the depolarizing field, which stimulates a decrease of the domains size and leads to the formation of nanodomain structure with 180-degree domain walls. At high cooling rate, domain sizes are larger, and average piezoelectric response is higher due to a better alignment of the polarization. The formation of the domain structure under the colling from paraelectric state is supposed to be influenced by the mechanical stresses, which is limited at high cooling rates as result of the limited rate of twinning in the ceramic and unavoidable temperature gradient in the “out of plane” direction.

The application of a uniform electric field leads to a significant change in the twin domain structure inside the superdomains, while position and orientation of superdomains boundaries often conserved. Three main stages of the domain structure evolution were revealed: (1) reorientation of twin systems under the action of mechanical stresses caused by the converse piezoelectric effect; (2) the main stage of polarization reversal representing 180-degree domain walls movement, following by non-180-degree walls rearrangement as result of mechanical stress compensation. The complete rearrangement of the domain structure was observed in some grains of ceramics; (3) final stage of polarization reversal with non-180-degree domain wall motion and an increase of the density of twins. The observed evolution of the domain structure in the electric field is in line with the structural change revealed by in situ X-ray diffraction performed earlier for ferroelectric ceramics [4].

The equipment of the Ural Center for Shared Use “Modern nanotechnology” of Ural Federal University (reg. no. 2968), which is supported by the Ministry of Science and Higher Education RF (project no. 075-15-2021-677), was used. The reported study was funded by the Ministry of Science and Higher Education of the Russian Federation (project FEUZ-2023-0017).

1. D. Damjanovic, M. Demartin, *J. Phys.: Cond. Matter* **9**, 4943 (1997).
2. G. Arlt, *Ferroelectrics* **76**, 451 (1987).
3. S. Wada et al., *J. Appl. Phys.* **98**, 014109 (2005).
4. J. Schultheiß et al., *Acta Mater.* **157**, 355 (2018).
5. L.V. Gimadeeva et al., *Ferroelectrics* **605**, 36 (2023).
6. L.V. Gimadeeva et al., *Ferroelectrics* **559**, 83 (2020).

P61

Record value of the operating temperature zone of a superconducting spin-valve with two ferromagnetic Heusler alloy layers

A.A. Kamashev[1], N.N. Garif'yanov[1], A.A. Validov[1], V. Kataev[2], Ya.V. Fominov[3,4], I.A. Garifullin[1]

[1]*Zavoisky Physical-Technical Institute, FRC Kazan Scientific Center of RAS, 420029, Kazan, Russia*
kamandi@mail.ru

[2]*Leibniz Institute for Solid State and Materials Research IFW Dresden, D-01069, Dresden, Germany*
[3]*D. Landau Institute for Theoretical Physics RAS, 142432, Chernogolovka, Russia*
[4]*Laboratory for Condensed Matter Physics, HSE University, 101000, Moscow, Russia*

To increase the efficiency of the superconducting spin valve (SSV), special attention should be paid to the choice of ferromagnetic materials for the F1/F2/S SSV multilayer. Here, we report the preparation and the superconducting properties of the SSV heterostructures where Pb is used as the superconducting S layer. In the magnetic part of the structure, we use the same starting material, the Heusler alloy $Co_2Cr_{1-x}Fe_xAl_y$, for both F1 and F2 layers. We utilize the tunabilty of the magnetic properties of this alloy, which depending on the deposition conditions forms either an almost fully spin-polarized half-metallic F1 layer or a weakly ferromagnetic F2 layer. We demonstrate that the combination of the distinct properties of these two layers boosts the generation of the long-range triplet component of the superconducting condensate in the fabricated SSV structures and yields superior values of the triplet spin-valve effect of more than 1K and of the operational temperature window of the SSV up to 0.6 K (Fig. 1).

The achieved values of ΔT_c^{trip} and ΔT_c^{full} set new benchmarks for the design of the superconducting spin valves as the prototype elements for applications in superconducting spintronics. They demonstrate the by far not yet exhausted potential for the optimization of ferromagnetic materials in an F1/F2/S SSV structure together with the simultaneous simplification of its fabrication. The observed boosting of the SSV effect by increasing the strength of the rotating external magnetic field on the background of the overall suppression of T_c calls for further experimental and theoretical studies for a better understanding of the underlying physics of this phenomenon.

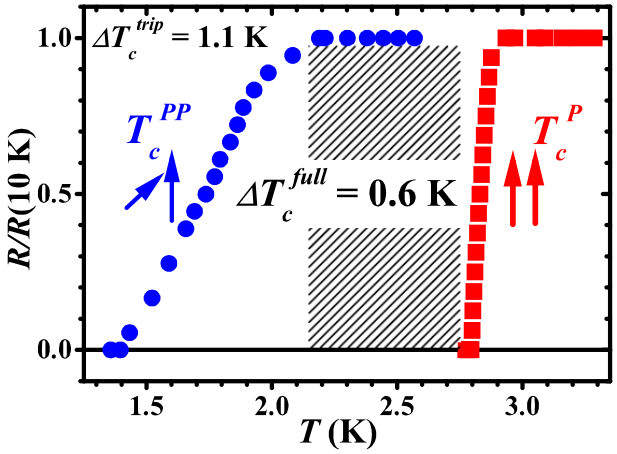

Figure 1. Superconducting transition curves for the P ($\alpha = 0°$) and PP ($\alpha = 90°$) configuration of the cooling field used to fix the direction of the magnetization of the HA^{RT} layer and the applied magnetic field H_0 = 4 kOe that rotates the magnetization of the HA^{hot} layer for the sample HA^{hot}(20nm)/Al(4nm)/HA^{RT}(5nm)/Al(1.2nm)/Pb(60nm). The shaded area marks the operational temperature window of the SSV.

P62

Structural modelling of non-stoichiometric $Pb(Mg_{1-y}Nb_y)O_{3-z}$ solid solutions

A.R. Lebedinskaya[1], A.G. Rudskaya[2]

[1]*Academy of Architecture and Arts, Southern Federal University, 344090, Rostov-on-Don, Russia*
lebed1989@rambler.ru

[2]*The Department of Physics, Southern Federal University, 344090, Rostov-on-Don, Russia*

Today, compositionally and structurally disordered materials are being actively studied, which are considered promising for a wide range of practical applications due to the unique combinations of ferroelectric, ferroelastic, ferroelectric, magnetic, semiconductor and superconducting properties, which are very important in the development of functional materials for new generation of microelectronic materials in the development of materials for new generation of applications. Particular attention among them is attracted by complex perovskite-like piezo and ferro-materials of oxygen octahedral type with a perovskite structure $(A'_p A''_{p-1})(B'_y B''_{y-1})O_3$ [1-3].

In this work a method for calculating the structural parameters for solid solutions $AB_{1-y}B'_yO_{3-z}$ with a perovskite structure was considered. A formula has been obtained for determining the nonstoichiometric coefficients y and z on the basis of taking into account the emerging "deformation" of the unstressed anion-cationic bonds A-O, B-O, B'-O in the compound under consideration due to the existing non-stoichiometry of the composition. The questions of the change in the structural parameters of the compounds under consideration due to the arising oxygen vacancies and the possible violation of this requirement of electroneutrality are discussed.

Samples of stoichiometric and non-stoichiometric PMN obtained by solid-phase synthesis from a mixture of PbO, MgO, and Nb_2O_5 oxides selected in the appropriate proportions, corresponding to the investigated compositions. The following cases of non-stoichiometry were considered:

1. $y = z = 0$ – stoichiometry for all cations and anions;

2. $0 \leq y \leq 0.5$; $z = 0$ - stoichiometry for Pb cations and anions and non-stoichiometry for type B (Mg/Nb) cations;

3. $0 \leq y \leq 0.5$; $z = 0{,}25$ - stoichiometry only for Pb cations and non-stoichiometry for type B (Mg/Nb) cations and anions. The method for estimating the values of the nonstoichiometric coefficients z and y from the average parameter of the reduced perovskite cell, the lengths of interatomic bonds, and the stiffness coefficients of the bonds is given in [ ]

The X-ray diffraction patterns of the initial precursors obtained by the solid state methods for each composition of $Pb(Mg_{1-y}Nb_y)O_{3-z}$ with y = 0.25; 0.50; 0.75 and z= 0; 0.25 taken at room temperature, are the typical X-ray diffraction profiles for the X-ray ceramic samples ($Pb(Mg_{1/4}Nb_{3/4})O_3$, $Pb(Mg_{½}Nb_{½})O_{2,75}$ and $Pb(Mg_{3/4}Nb_{1/4})O_3$.

Satisfactory agreement was obtained between the calculated and experimentally obtained structural data for all solid solution compositions.

The deviation from stoichiometry in solid solutions based on lead magnoniobate may result in a change in the distribution of internal electric fields due to violation of the electroneutrality of the compositions.

At present, there are a sufficient number of works that make it possible to reveal the features of the oxygen sublattice in perovskite-like compounds. However, they consider the situation of structures containing disordered oxygen vacancies. Revealing their localization while maintaining a predominantly statistical position is a separate task.

1. S. Pandya, J. Wilbur, J. Kim, et al., *Nature Mater.* **17**, 432 (2018).
2. T. Kolodiazhnyi, J. Padchasri, R. Yimnirun, *J. Eur. Cer. Soc.* **38**,1517 (2018).
3. G.A. Smolensky, V.A. Bokov, V.A. Isupov, et al., *Ferroelectrics and Antiferroelectrics* (L: Nauka), 476 p (1971).
4. D.I. Rudsky, A.R. Lebedinskaya, I.A. Verbenko, et al., *Ferroelectrics* **590**, 167 (2022).

P63

Leakage currents in monocrystalline SBN60 thin films at T = 303...453 K

N.V. Makinyan[1,2], A.V. Pavlenko[1,2]

[1]*Federal Research Center, The Southern Scientific Centre of the Russian Academy of Sciences, 344006, Rostov-on-Don, Russia*
norair.makinyan@yandex.ru

[2]*Research Institute of Physics, Southern Federal University, 344090, Rostov-on-Don, Russia*

In the case of ferroelectric thin films, leakage currents are important for their application, for example, in integrated circuits (ICs). In the practical application of films, as well as in their experimental studies in large electric fields, their value should be less than a certain threshold. For this reason, the study of the mechanisms of electrical conductivity of promising thin-film materials, which include strontium-barium niobates, is important both from a practical and fundamental point of view [1]. It is known that several basic types of conductivity are realized in dielectrics, related both to the near-electrode region and to the volume of the dielectric layer. The first include Schottky emission, and the second include such mechanisms as Pool–Frenkel emission (PF) and space-charge-limited conduction (SCLC).

In this work, we measured leakage currents in a thin film $Sr_{0,6}Ba_{0,4}Nb_2O_6$ (SBN60) at different temperatures using a measuring complex based on TF Analyzer 2000 E and Linkam THMS600 stage (Fig. 1).

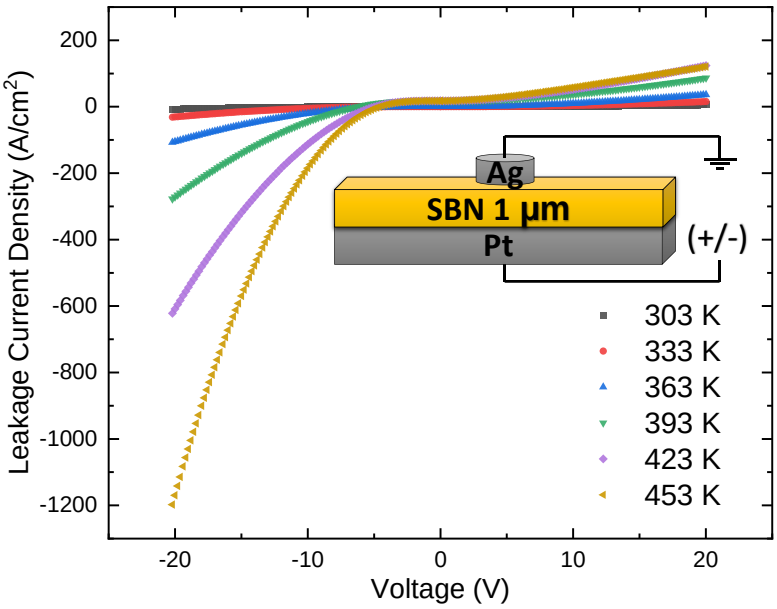

Figure 1. Leakage currents in SBN60 thin film at different temperatures.

After analyzing the forward and reverse bias at room temperature, it was found that in SBN60 at a field strength of E = 4.5 – 9.5 MV/m, the predominant conduction mechanism is the emission of PF, and starting from E = 10 MV/m, the conductivity is caused by the limitation of the spatial charge. It is established that starting from T = 393 K, Schottky emission already makes the main contribution to the SBN60 leakage currents when a positive voltage is applied to the bottom electrode. The reasons for the revealed patterns are discussed.

The study was carried out with the financial support of the Ministry of Science and Higher Education of the Russian Federation (State task in the field of scientific activity in 2023). Project No. FENW-2023-0010/(GZ0110/23-11-IF).

1. F.-C. Chiu, *Adv. Mater. Sci. Eng.* **2014**, 1 (2014).

P64

Leakage currents in $Ba_2NdFeNb_4O_{15}$ thin films at room temperature

N.V. Makinyan[1,2], A.V. Pavlenko[1,2]

[1]*Federal Research Center, The Southern Scientific Centre of the Russian Academy of Sciences, 344006, Rostov-on-Don, Russia*
norair.makinyan@yandex.ru

[2]*Research Institute of Physics, Southern Federal University, 344090, Rostov-on-Don, Russia*

For the application of thin dielectric films, an important characteristic is the leakage current, which can be due to both the chemical composition and structure of the material and its defect. Depending on external influences, both the mechanism and the magnitude of the conduction current can change, which can directly affect the correct operation of the corresponding devices. In the case of more complex electronic devices with more functionality, for example, based on multiferroics, which include $Ba_2NdFeNb_4O_{15}$ (BNFNO), leakage currents can cause great damage to the device. It is known that in the region of large electric fields there are several basic types of conductivity associated with both the near-electrode region and the volume of the dielectric layer. The first include Schottky emission, and the second include such mechanisms as Pool–Frenkel emission (PF) and space-charge-limited conduction (SCLC) [1]. In this work, we investigated leakage currents in BNFNO thin film at room temperature using the TF Analyzer 2000 E measuring system (Fig. 1).

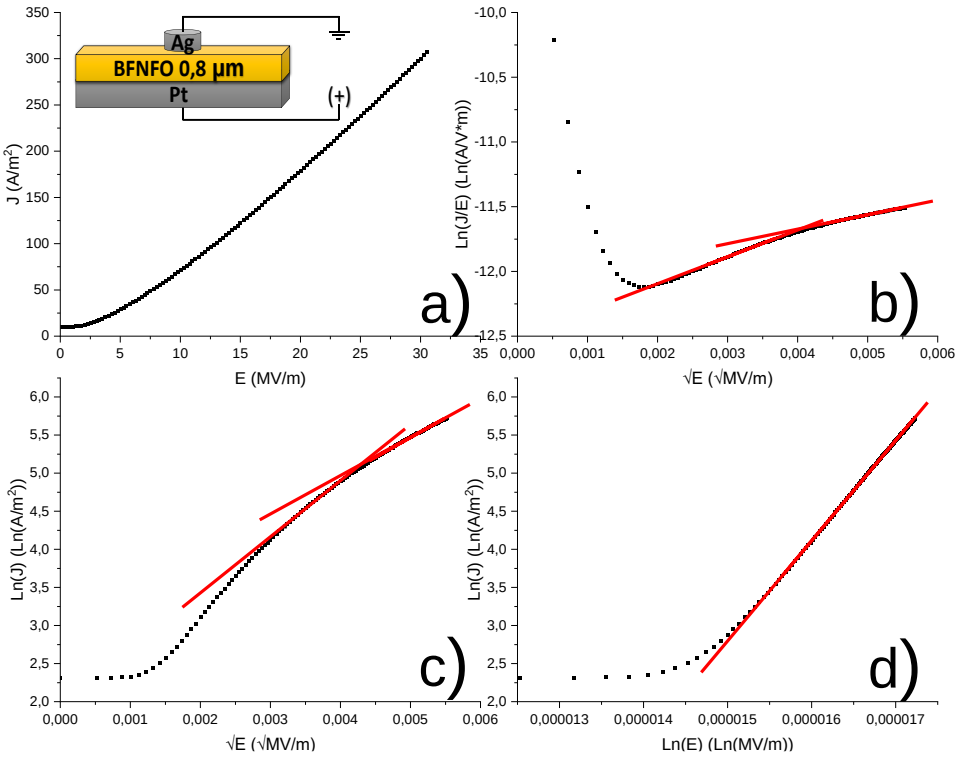

Figure 1. Dependence of the leakage current density on the field strength in BNFNO thin film in coordinates J–E (a), Poole – Frenkel (b), Schottky (c), SCLC (d)

After calculations and analysis of the obtained dependencies, taking into account [1], it was found that at E = 0...13 MV/m, it is not possible to identify the mechanism unambiguously, i.e there is most likely the coexistence of several conduction mechanisms, and at E = 14...30 MV/m, the main mechanism that makes the greatest contribution to the electrical conductivity in BNFNO thin film is Schottky emission associated with the injection of electrons in the near-electrode region.

The work was financially supported by the Russian Science Foundation, grant No.21-72-10180 with the use of equipment of the Centers for Collective Use No.501994.

1. F.-C. Chiu, *Adv. Mater. Sci. Eng.* **2014**, 1 (2014).

P65

Structure and ferroelectric properties of 0.91NNO-0.09SZO thin film grown on $SrTiO_3$:Nb substrate

Ya.Yu. Matyash[1], D.V. Stryukov[1], A.V. Pavlenko[1,2], N.V. Ter-Oganesyan[2]

[1]*Federal Research Centre the Southern Scientific Centre of the Russian Academy of Sciences, 344006, Rostov-on-Don, Russia*
matyash.ya.yu@gmail.com

[2]*Research Institute of Physics of Southern Federal University, 344090, Rostov-on-Don, Russia*

Antiferroelectric (AFE) materials, especially in the thin films form, have a great potential for application in microelectronics [1]. The most studied AFE are solid solutions (SS) based on zirconate $PbZrO_3$ [2]. However, the need to create and use environmentally friendly materials has led to the research of lead-free AFE, among which the most promising are SS based on sodium niobate $NaNbO_3$ (NNO). At room temperature, NNO can exist in two phases: AFE P-phase (Pbma) or ferroelectric (FE) Q-phase (P21ma) [3]. The Q phase in sodium niobate can be obtained, for example, by applying an electric field or doping [4], but after the field action, the reverse transition to the AFE P phase does not occur. A stable AFE phase is obtained in SS $(1-x)NaNbO_3$-$xSrZrO_3$ [5] and $(1-x)NaNbO_3$-$xCaZrO_3$ [6] at $0<x<0.10$. This work is devoted to studying a thin (~30 nm thick) $0.91NaNbO_3$–$0.09SrZrO_3$ (NNSZO) film grown by RF cathode sputtering on STO(001) substrates.

The structure and nanostructure, as well as ferroelectric and dielectric properties, were studied by X-ray diffraction, scanning probe microscopy (SPM), and dielectric spectroscopy.

According to the X-ray diffraction study, no crystalline impurities were found in the film, which correlates with the data of atomic force microscopy (AFM). The crystallographic axes [001] of the film and substrate are co - directional. The film lattice parameter in the direction normal to the substrate surface was c = 4.11 Å. A comparison of the film lattice parameters with the unit cell parameters of a bulk ceramic sample (c_{bulk} = 3.921 Å) showed that the unit cell in the film is strongly stretched. The film unit cell deformation relative to the ceramic cell was 4.8%. An analysis of the AFM scans showed that the surface of the NNSZO film is characterized by a smooth relief and a low RMS roughness (~0.3 nm). The results obtained point to a layered growth mechanism. Using SPM methods, stable regions of different orientations (toward and away from the substrate) were formed on the surface of the NNSZO film, which is a manifestation of the FE phase. This fact is also indicated by the results of the dielectric hysteresis loops measurements, from which it can be seen that the P(U) dependence of the FE type is characteristic of the film. The reason for the stabilization of the FE phase in the 30-nm-thick NNO-SZO film on the STO(001) substrate is supposedly due to the detected significant deformation of the unit cell.

The work was carried out within the framework of the state task of the SSC RAS under project No. 122020100294-9.

1. Z. Liu, T. Lu, J. Ye, et al., *Adv. Mater. Technol.* **3**, 1800111 (2018).
2. N. Izyumskaya, Y.-I. Alivov, S.-J. Cho, et al., *Crit. Rev. Solid State Mater. Sci.* **32**, 111 (2007).
3. A.M. Glazer, H.D. Megaw, *Acta Cryst.* **A29**, 489 (1973).
4. E.A. Wood, R.C. Miller, J.I. Remeika, *Acta Cryst.* **15**,1273 (1962).
5. H. Guo, H. Shimizu, Y. Mizuno, C.A. Randall, *J. Appl. Phys.* **117**, 214103 (2015).
6. H. Shimizu, H. Guo, S.E. Reyes-Lillo, et al., *Dalton Trans.* **44**, 10763 (2015).

P66

Structure, ferroelectric and dielectric properties of a two-layer BNFNO/SBN60 film grown on a SRO/MgO(001) substrate

Ya.Yu. Matyash[1], D.V. Stryukov[1], A.V. Pavlenko[1,2]

[1]*Federal Research Centre the Southern Scientific Centre of the Russian Academy of Sciences, 344006, Rostov-on-Don, Russia*
matyash.ya.yu@gmail.com

[2]*Research Institute of Physics of Southern Federal University, 344090, Rostov-on-Don, Russia*

Currently, materials based on ferroelectrics (FE) and multiferroics (MF) in the form of nanoscale films are being actively studied. Such structures not only have great potential for applications in microelectronics, but are also of fundamental interest to scientific teams. Solid solutions thin films based on FE and MF have a number of properties such as high dielectric permittivity, piezo- and pyroactivity, dielectric nonlinearity, and electro-optical effect [1]. A completely new properties set can be realized in multilayers based on such films due to mechanical stresses depending on the growth mechanism [2], the preparation method, and size effects. In this paper, we study the structure and ferroelectric properties of a two-layer BNFNO/SBN60/SRO/MgO(001) film grown by RF sputtering in an oxygen atmosphere.

The two-layer heterostructure was studied by X-ray diffraction and atomic force microscopy in the Kelvin mode.

X-ray diffraction analysis showed that all layers of the heterostructure were grown epitaxially, and the films and substrate axes were in complete parallel orientation. No traces of impurity phases were detected. To illustrate the ferroelectric (Fig. 1) properties on the SBN60/BNFNO/SRO/MgO heterostructure surface in the lithography mode, the regions corresponding to the inscription were polarized. The applied voltage during polarization was +10V. After that, the surface potential of the heterostructure was measured in the KM mode using the two-pass technique. As a result, stable, polarized regions were formed, which we could not achieve in similar regimes on single-layer samples of SBN60/SRO/MgO and BNFNO/SRO/MgO.

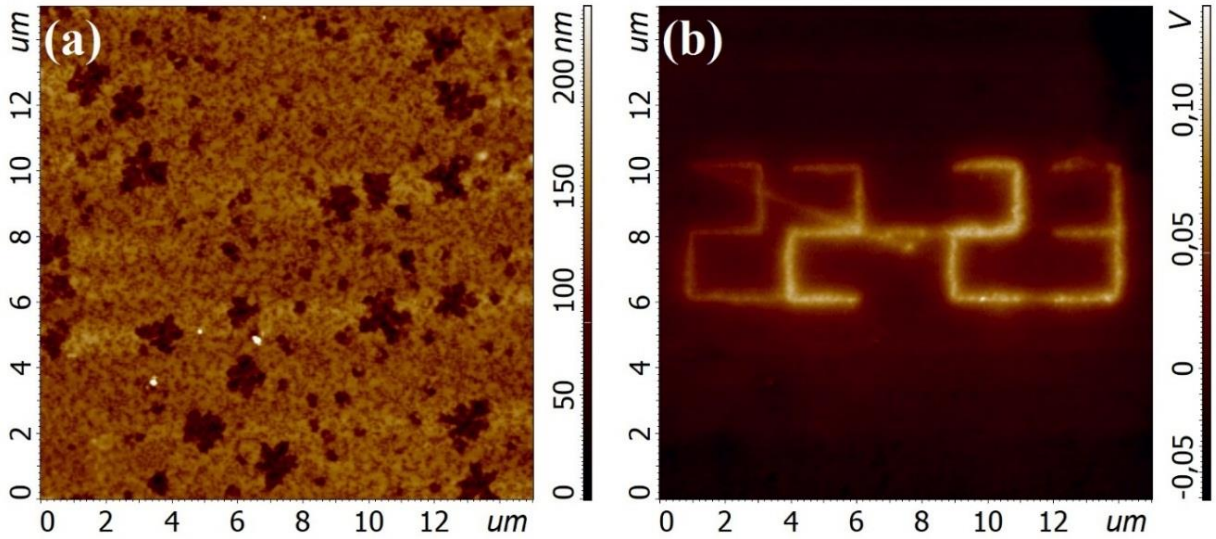

Figure 1. Surface topography (a) and surface potential signal of the BNFNO/SBN60/SRO/MgO heterostructure after polarization (b).

This work was financially supported by the Russian Science Foundation [grant No. 21-72-10180].

1. K.M. Rabe, C.G. Ana, J.M. Triscon, *Physics of ferroelectrics: a modern view* (M.: BINOM. Lab. Knowledge), 440 (2011).
2. A.R. Shugurov, A.V. Panin, *Tech. Phys.* **65**, 1881 (2020).

P67

Magnetodielectric effect in solid solutions of the system based on bismuth ferrite and sodium-potassium niobates

M.O. Moysa[1], A.S. Pavlenko[1]

[1]*Research Institute of Physics, Southern Federal University, 344090 Rostov-on-Don, Russia*
moysa@sfedu.ru

Multiferroid media attract the attention of researchers due to the coexistence of magnetic, ferroelectric and ferroelastic properties. This fact allows them to be used in microelectronics, digital memory, touch sensors and spintronics [1, 2]. The legislative Directives of the European Parliament adopted in recent decades with strict requirements for the environmental safety of industrial production [3,4] have made it necessary to search for non-toxic bases for these materials. In this regard, we have designed a triple system based on ferroelectric (FE) ((Na0.5K0.5)NbO3) and magnetic (BiFeO3) components. In this paper, we investigated the magnetoelectric effect (ME) in the SS of the (1-x)(Na0.5K0.5)NbO3-xBiFeO3 system.

The objects of the study were the SS systems (1-x)(Na0.5K0.5)No3-x BiFeO3 x=0.60-0.80. The samples were obtained by solid-phase synthesis in two stages and sintered using conventional ceramic technology (Tsint.1= 1123K, τ=4 hours, Tsint.2= 1123K, τ=4 hours; T= (1303-1323) K, τ =2 hours).The study of the behavior of C(f) and the frequency range of the electric field f = (25÷10^6) Hz at a constant magnetic field of 0.85 Tl was carried out on unpolarized samples using a measuring stand based on the Agilent 4980A LCR meter.

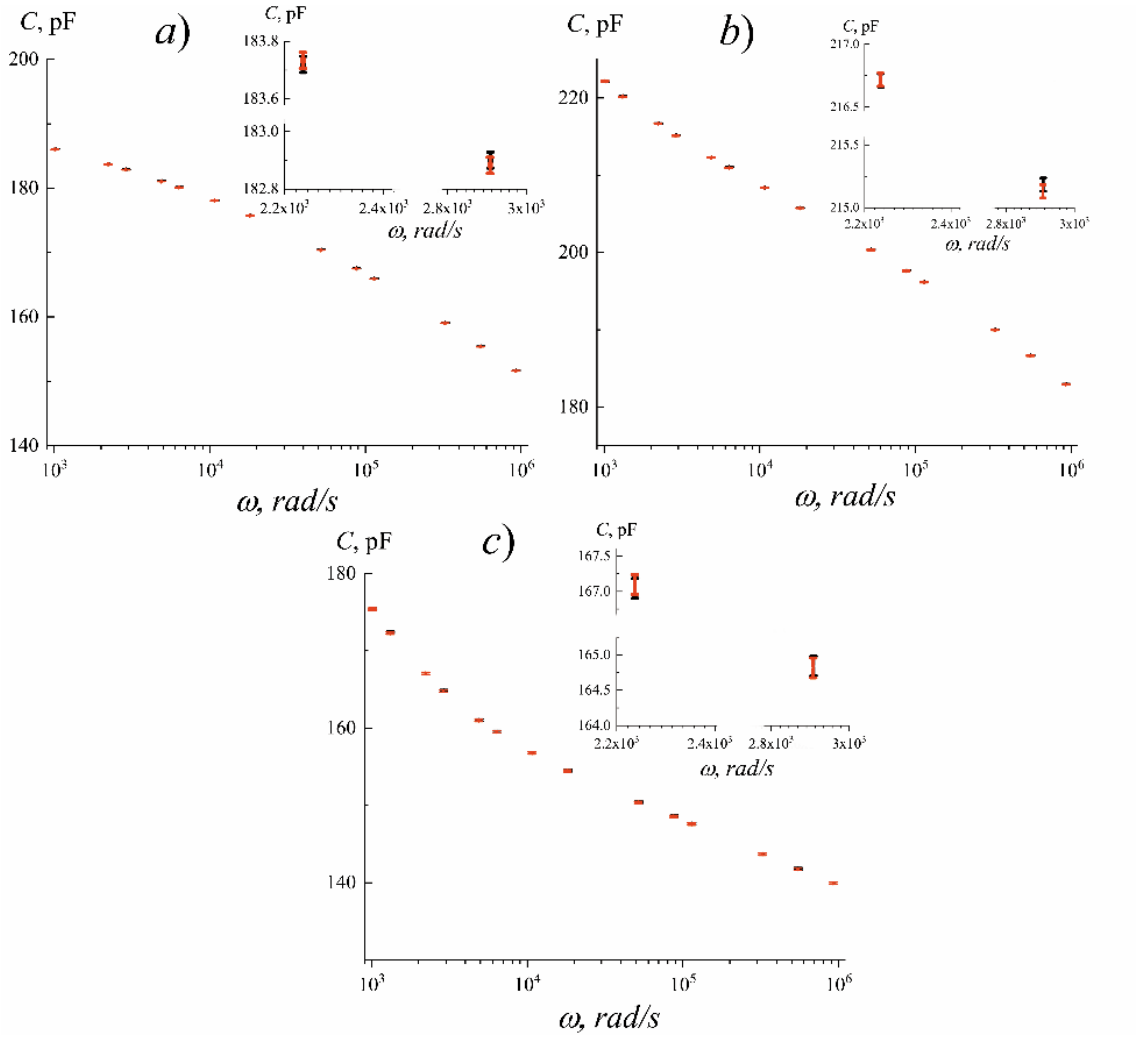

Figure 1. Dispersion of the SS capacity of the system (1-*x*)($Na_{0.5}K_{0.5}$)NbO_3-*x*$BiFeO_3$ *x*=0.60-0.80 in the frequency range (1-1000) kHz in a magnetic field of 0.85 Tl (red icons) and without it (black icons) at a temperature of 300 K.

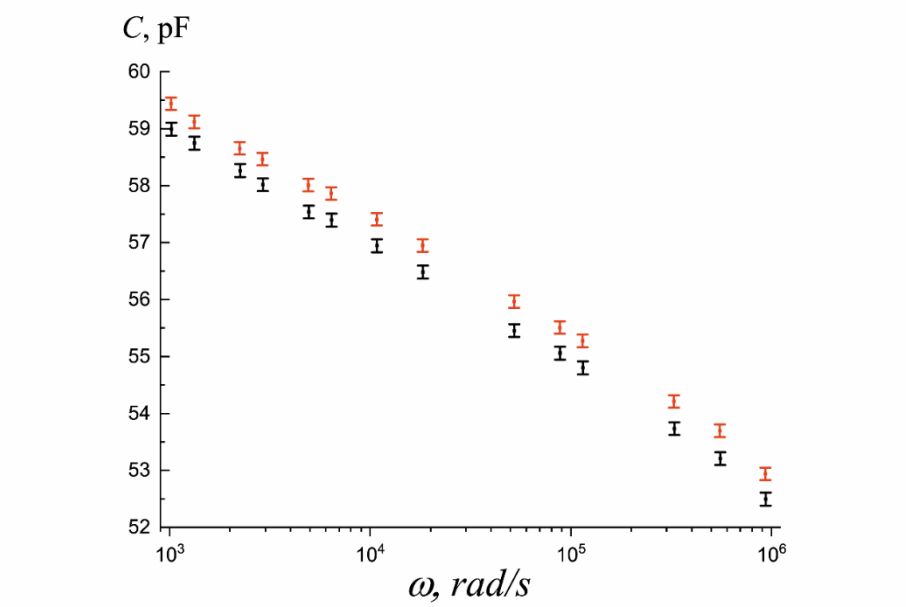

Figure 2. Dispersion of the SS capacity of the system (1-*x*)($Na_{0.5}K_{0.5}$)NbO_3-*x*$BiFeO_3$ *x*=0.80 in the frequency range (1-1000) kHz in a magnetic field of 0.85 Tl (red icons) and without it (black icons) at a temperature of 77 K.

Figure 1 illustrates the behavior of the capacitance of the TP system (1-*x*)($Na_{0.5}K_{0.5}$)NbO_3-*x*$BiFeO_3$ *x*=0.60-0.80 in the frequency range (1-1000) kHz and a magnetic field of 0.85 Tl (and without it) at a temperature of 300 K. It is established that in these SS, the change in capacitance under the influence of the magnetic field of the previously specified value in the entire research frequency range is manifested within the error. This fact indicates the absence of a connection between the magnetic and dielectric subsystems in the studied SS under the established conditions.

Figure 2 shows the behavior of the capacitance of the SS system (1-*x*)($Na_{0.5}K_{0.5}$)NbO_3-*x*$BiFeO_3$ *x*=0.80 in the frequency range (1-1000) kHz and a magnetic field of 0.85 Tl (and without it) at a temperature of 77 K. In the studied SS, a change in capacitance under the influence of a magnetic field was detected.

The study of DC resistance at a constant magnetic field of 0.85 ttl was carried out on unpolarized samples using a measuring stand based on high resistance meter Agilent 4339B. The magnitude of magnetoresistivity was determined by the ratio:

$$MR = \frac{\rho(H) - \rho(0)}{\rho(0)} * 100\%$$

The resistance of an object in a magnetic field and without it at a constant current at a given temperature was also measured. It was revealed that the magnetoresistivity of the studied SS is 55%, which can contribute to the value of the SS capacity.

The study was carried out with the financial support of the Ministry of Science and Higher Education of the Russian Federation (State task in the field of scientific activity in 2023). Project No. FENW-2023-0010/(GZ0110/23-11-IF).

1. R. Jasrotia, R. Khargotra, A. Verma, et al., *Applications of multiferroics, in: ferrites and multiferroics*, Springer, 215 (2021).
2. C. W. Nan, M.I. Bichurin, et al. *Appl. Phys.* **103**, 031101 (2008).
3. Directive 2002/95/EU of the European Parliament and of the Council of 27 January 2003 on the restriction of the use of certain hazardous substances in electronic equipment, in Official Journal of the European Union. L. 37. (2003) V. 46. 19-23.
4. Directive 2011/65/EU of the European Parliament and of the Council of 8 June 2011 on the restriction of the use of certain hazardous substances in electrical and electronic equipment, , in Official Journal of the European Union. L. 174. (2011) V.54. 88.

P68

Microstructural studies of $0.91NaNbO_3$-$0.09SrZrO_3$ films obtained by RF-cathode sputtering

A.V. Nazarenko[1], A.V. Pavlenko[1]

[1]*Federal Research Centre, The Southern Scientific Centre of the Russian Academy of Sciences, 344006, Rostov-on-Don, Russia*
avnazarenko1@gmail.com

At present, in micro- and nanoelectronics, there is a need to use ferroelectric (FE) and antiferroelectric (AFE) materials made in the form of thin films. In particular, since the beginning of the 21st century, research has been actively conducted on the use of lead-free materials as active elements. The most promising object in this area is sodium niobate $NaNbO_3$ (NNO) fabricated in various solid states. This material has a perovskite type structure with a large number of different phase transitions [1-2]. At room temperature, NNO can be both in the FE and in the AFE phase. However, the last one often is not stable in pure NNO [3]. Therefore, the solid solutions are made on the basis of NNO, for example, $(1-x)NaNbO_3$-$xSrZrO_3$ [4]. The films obtained on their basis have good perspectives for application in the form of capacitor structures in modern devices. In particular, films based on $0.91NaNbO_3$–$0.09SrZrO_3$ (NNO–9SZO) are of great interest. These films were first obtained in 2022 on a single-crystal magnesium oxide MgO(001) substrate by RF cathode sputtering method with a $SrRuO_3$ (SRO) sublayer [5].

This work presents the results of their microstructural study. An analysis of morphology of the chipped NNO-9SZO films edge showed that the films are homogeneous, the texture is practically absent. The thickness of the studied film is ~1.6 μm, which corresponded to a growth rate of ~6-7 nm/min. A layer of the lower SRO electrode is observed between the substrate and the film, which is confirmed by energy dispersive analysis (fig. 1). The surface of the film is covered with "hubbles" of irregular shape, the size of which is in the range of 0.5-0.75 μm. It is possible that this "hubbles" are the nucleuses of the growth of subsequent layers. Between the "hubbles" the film surface is homogeneous (smooth, without any inclusions of impurity phases, cavities, pores and other defects).

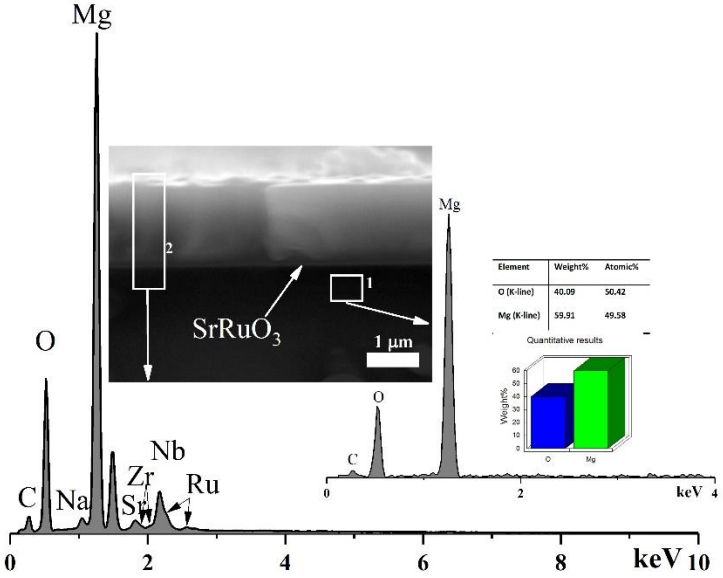

Figure 1. General results of microstructural studies of the edge of chipped NNO-9SZO films.

This work was financially supported by the Ministry of Education and Science of the Russian Federation SSC RAS (project No. 122020100294-9)

1. H.D. Megaw, *Ferroelectrics* **7**, 87 (1974).
2. A.M. Glazer, H.D. Megaw, *Acta Cryst.* **A29**, 489 (1973).
3. E.A. Wood, R.C. Miller, J.I. Remeika, *Acta cryst.* **15**, 1273 (1962).
4. H. Guo, H. Shimizu, Y. Mizuno, C.A. Randall, *J. Appl. Phys.* **117**, 214103 (2015).
5. A.V. Pavlenko, D.V. Stryukov, V.G. Smotrakov, et al., *Ferroelectrics* **590**, 227 (2022).

P69

Conservation of the polar state above Curie temperature in $BaTiO_3$ ceramics and single crystals

D.O. Alikin[1], A. A. Nikulin[1], L.V. Gimadeeva[1], A.D. Ushakov[1], Q. Hu[2], H. Yan[3], L. Jin[2], V.Ya. Shur[1]

[1]*School of Natural Sciences and Mathematics, Ural Federal University, 620000, Ekaterinburg, Russia*

[2]*Xi'an Jiaotong University, 710049, Xi'an, China*

[3]*Queen Mary University of London, London, United Kingdom*
denis.alikin@urfu.ru

The conservation of polar phase residual regions in ferroelectric materials with higher Curie (Tc) temperatures has been a topic of interest since its prediction in the mid-20th century [1]. Subsequent experimental evidence supporting this prediction was established through second harmonic generation spectroscopy in barium titanate ceramics, revealing the existence of a second harmonic signal up to 10°C higher than the typical T_c for BTO ceramics [2]. Recently, significant strides in high-resolution scanning transmission electron microscopy have enabled the visualization of polar nano-regions above Tc at the atomic scale in barium titanate ceramics, covering nearly the entire visualized surface area [3].

Despite considerable progress in understanding above-Curie ferroelectricity, its origin remains a subject of discussion, with some attributing it to local strains leading to the relaxor properties of barium titanate. In this contribution, we present compelling evidence for the first time, demonstrating the conservation of macroscopic domains more than 20°C above T_c and their stability even after local polarization reversal. Our investigations were conducted on barium titanate ceramics and single crystals undergoing the ferroelectric phase transition, utilizing piezoelectric response force microscopy (PFM) with precise surface temperature control achieved through an on-the-surface resistive thermometer with an accuracy of below 0.1°C. Complementing the acquired data were macroscopic measurements of dielectric permittivity, polarization loops, and piezoelectric coefficients, obtained through optical interferometry.

Remarkably, we observed partial retention of the polar state above the phase transition temperature, which we attribute to the segregation of charged defects and their consequent screening effect. Additionally, our findings indicate that macroscopic defects, such as dislocations and grain boundaries, act as regions of non-uniformity influencing the above-Curie ferroelectricity. The insights gained from this research contribute to a deeper understanding of the fundamental mechanisms governing ferroelectric behavior, opening new possibilities for tailoring the properties of these materials for various technological applications.

The equipment of the Ural Center for Shared Use "Modern nanotechnology" of Ural Federal University (reg. no. 2968), which is supported by the Ministry of Science and Higher Education RF (project no. 075-15-2021-677), was used. The reported study was funded by the Ministry of Science and Higher Education of the Russian Federation (project FEUZ-2023-0017).

1. W. Känzig, *Art. Helv. Phys. Acta.* **24**, 343 (1951).
2. A.M. Pugachev, et al., *Phys. Rev. Lett.* **108**, 247601 (2012).
3. A. Bencan, et al., *Nat. Commun.* **12**, 3509 (2022).

P70

Features of ferroelectric properties in metal-ferroelectric-semiconductor structures based on nanosized films with the TTB structure

A.V. Pavlenko[1], T.S. Ilyina[1,2], D.A. Kiselev[2], D.V. Stryukov[1], Ya.Yu. Matyash[1]

[1]*Federal Research Centre the Southern Scientific Centre of the Russian Academy of Sciences, 344006, Rostov-on-Don, Russia*

tolik_260686@mail.ru

[2]*The National University of Science and Technology MISIS, 119049 Moscow, Russia*

In solid state physics, nanosized thin films of active dielectric materials having the structure of tetragonal tungsten bronze (TTB) with the general chemical formula $(A1)_2(A2)_4(C)_4(B1)_2(B2)_8O_{30}$ [1] receive much attention. This is due both to the prospects for their application in nanoelectronics and MEMS, and to the fundamental interest associated with the establishment of regularities in the size effects manifestation in this type of functional structures. In this work, we studied the ferroelectric properties of barium strontium niobates (SBN60) and barium neodymium ferroniobate (BNFNO) thin films, as well as two-layer structures based on them, grown on a Si(001) substrate by RF cathode sputtering in an oxygen atmosphere.

According to X-ray diffraction analysis, it was found that heterostructures with different alternation of Si(001)/BNFNO/SBN, Si(001)/SBN/BNFNO, Si(001)/BNFNO, and Si(001)/SBN layers, in which the thicknesses of each of the layers varied from 40 to 500 nm were obtained without the formation of impurity phases. When analyzing the objects surface using piezoelectric force microscopy, the domain structure traces were recorded (in Fig. 1), however, it was not possible to distinguish a specific type and shape of domains, since the regions had different shapes and were oriented differently, which is mainly observed in a number of relaxor ferroelectrics.

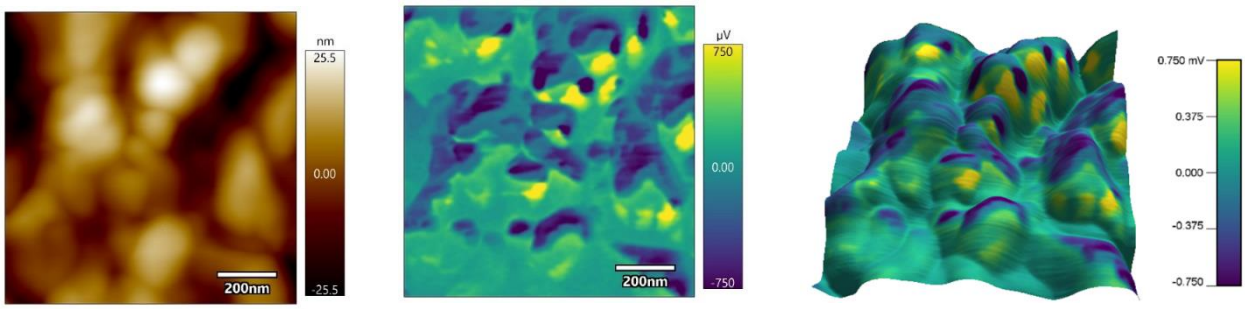

(a) (b) (c)

Figure 1. Topography (a), piezoresponse signal (b) and 3D image of the signal topography + SBN60/BNFNO/Si film piezoresponse (c)

When analyzing the capacitance-voltage characteristics of the synthesized materials, it was found that in all cases, at a measuring field frequency of 10^4 Hz, high-frequency C(U) dependences were recorded. While in all single-layer samples, due to the natural unipolarity of the films domain structure, the field effect was clearly manifested (the substrate surface was in depleted/inverted state). An analysis of polarization switching processes and the corresponding memory effects showed that the most promising properties are manifested in heterostructures of the SBN60/BNFNO/Si(001) type. The reasons for the revealed regularities are discussed.

1. Yu.S. Kuzminov, *Ferroelectric crystals for controlling laser radiation*, Science, M. (1982). 400 p.

P71

Dielectric characteristics and energy efficiency of the BNFNO(420 nm)/SBN60(420 nm)/SRO/MgO(001) heterostructure

A.V. Pavlenko

Federal Research Centre the Southern Scientific Centre of the Russian Academy of Sciences, 344006, Rostov-on-Don, Russia
tolik_260686@mail.ru

Currently, ferroelectric and multiferroic functional materials in the form of nanoscale films grown on dielectric and semiconductor substrates are being intensively studied. This is connected both with the prospects for their application in modern technology and with the interest in studying new effects arising in two-layer structures. This paper presents the study results of the dielectric and ferroelectric characteristics of the BNFNO(420 nm)/SBN60(420 nm)/SRO/MgO(001) multilayer heterostructure. Nanosized BNFNO, SBN60, and SRO films were synthesized by RF cathode sputtering in an oxygen atmosphere (intermittent sputtering technology was used). During sputtering, we used ceramic targets of stoichiometric compositions of BNFNO, SBN60 and SRO, respectively, with a diameter of 50 mm and a thickness of 3 mm.

When measuring the dielectric characteristics, the applied electrical voltages to the multilayer heterostructure were 2 times higher than those applied to the corresponding single-layer heterostructures. This is due to the interaction between the layers. To study the ferroelectric characteristics and energy efficiency parameters of the heterostructure, the dependences P(U) were measured using the TFAnalyzer2000 analyzer. The calculated energy efficiency parameters are shown in Figure 1.

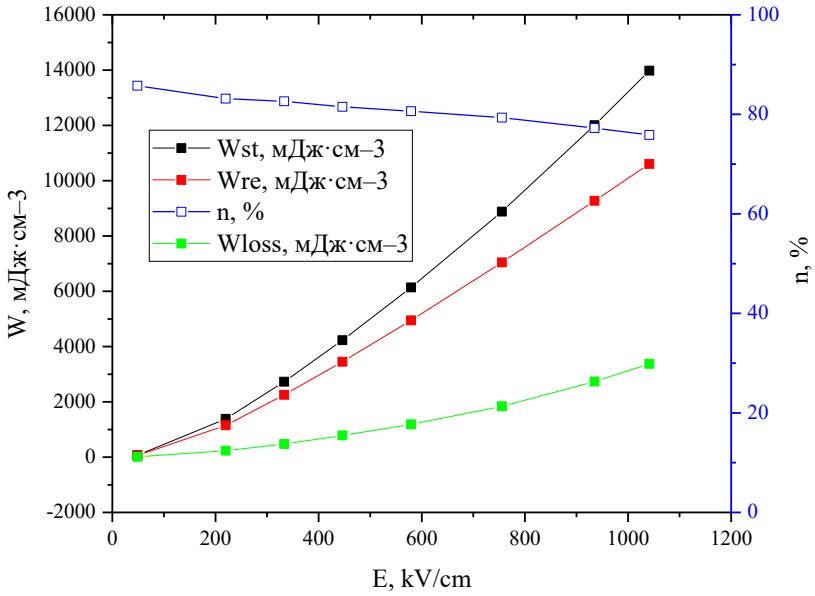

Figure 1. Dependence of *n*, W_{loss}, W_{st} and W_{re} on the electric field magnitude for the Au/BNFNO(420 nm)/SBN60(420 nm)/SRO/MgO(001) heterostructure at room temperature.

It can be seen that at room temperature at E=0...1050 kV/cm for the object under study, the value of W_{st} reaches ~ 14000 mJ cm^{-3}, and n is at least 78%. When analyzing the samples ferroelectric fatigue, it was found that the degradation of their ferroelectric parameters is practically not fixed up to 10^{10} switching cycles at an electric field frequency of 10^7 Hz. The reasons for the revealed regularities are discussed.

The work was financially supported by the Russian Science Foundation grant No. 21-72-10180.

P72

Critical character of field dependence of giant values of inverse piezoelectric moduli in polycrystalline ferroelectric relaxors

I.P. Raevski[1], J. Zeng[2], K. Zhao[2], W. Ruan[2], X. Ruan[2], L. Zheng[2], Shi Xue[2],G. Li[2], S.I. Raevskaya[1], V.V. Titov[1], M.A. Malitskaya[1], P.A. Shishkina[1], S.I. Kolosov[1]

[1]*Physics Research Institute and Faculty of Physics, Southern Federal University, 344090, Rostov-on-Don, Russia*
igorraevsky@gmail.com

[2]*Key Laboratory of Inorganic Functional Ceramics and Devices, Shanghai Institute of Ceramics, Chinese Academy of Sciences, 200050, Shanghai, China*

Single crystals of solid solutions based on relaxor ferroelectrics, characterized by giant values of piezoelectric, dielectric, electrostrictive, pyroelectric, and other responses in a wide temperature range are of great interest for applications. The huge values of different responses in relaxors are due to the presence of polar nanoregions in them, which are very sensitive even to a small external effect. It was previously established that in single crystals of solid solutions of the classical relaxor $Pb(Mg_{1/3}Nb_{2/3})O_3$ (PMN) with the ferroelectric $PbTiO_3$ (PT), the giant piezoelectric response (corresponding to the direct piezoelectric effect) has a critical nature [1,2]. There is a line of critical points in the x, E, T-phase diagram of the PMN-PT system and the compositions from the morphotropic region (MO) approach this line [1]. Later the possibility of a significant increase of piezoelectric moduli for the direct piezoelectric effect (hereinafter, for brevity, direct piezoelectric moduli) of PMN-PT single crystals, the composition of which is far from MO, by applying the electric field was established [2]. Such effect "shifts" these compositions towards the critical point and the field dependences of the maximum values of the piezoelectric moduli are critical.

In contrast to crystals, in PMN-PT ceramics, it has not yet been possible to achieve giant values of piezoelectric moduli for the direct piezoelectric effect, even in highly textured samples. At the same time, the values of the piezoelectric modulus in the case of the converse piezoelectric effect (hereinafter for brevity -the converse piezoelectric modulus) in PMN-PT ceramic samples and soft ferroelectric multicomponent piezoelectric ceramics in a certain field range are comparable to those for the single crystals [3]. This is due to the fact that, unlike conventional ferroelectrics, for ferroelectrics with a diffuse phase transition (DPT) and relaxors, the contribution of small domains and polar nanoregions, as well as electrostriction, to the total value of the piezoelectric modulus d_{ij} is large, therefore, the d(E) dependence is nonlinear and the converse piezoelectric modulus is usually much larger than the direct one, which is promising for practical use.

Revealing the nature of the field dependence of the inverse piezoelectric moduli near the critical point on the E,T phase diagram, will make it possible to determine ways to increase dramatically the piezoresponse of PMN-PT ceramics. This, in turn, will significantly reduce the size of many piezoelectronic devices and expand the scope and scale of their application.

This study was partially supported by RNF (project 23-42-10024).

1. Z. Kutnjak, J. Petzelt, R. Blinc, *Nature* **441**, 956 (2006).
2. S.I. Raevskaya, A.S. Emelyanov, F.I. Savenko, et al., *Phys. Rev. B* **76**, 11580R (2007).
3. A.V. Turik, A.A. Yesis, L.A. Reznitchenko, *J. Phys.: Condens. Matter*. **18**, 4839 (2006).

P73

Size effect of the piezoelectric properties in thin films of $BiFeO_3$

V.A. Safina[1], B.N. Slautin[1], A.S. Abramov[1], M.S. Kosobokov[1], V.Ya. Shur[1], A.V. Pavlenko[2], D.O. Alikin[1]

[1]*School of Natural Sciences and Mathematics, Ural Federal University, 620002, Ekaterinburg, Russia*
v.a.safina@urfu.ru

[2]*Research Institute of Physics SFU, 344090, Rostov-on-Don, Russia*

$BiFeO_3$ (BFO) is a unique multiferroic material that combines a high value of spontaneous polarization with anti-ferromagnetic behavior at room temperature [1,2]. Due to such combination of properties, BFO is an excellent candidate for various applications including ferroelectric memory and mem-computing devices, where electric-magnetic writing/reading access is required. However, producing thin epitaxial BFO films that conserve ferroelectric properties remains a challenging task, as the native phase instability and large leakage current pose significant obstacles. Here we introduced new method for quantitative evaluation of the piezoelectric properties using advanced piezoresponse force microscopy, which excludes parasitic electromechanical phenomena such as charge injection and electrical current. The effective piezoelectric coefficient of hetero-epitaxial BFO films was analysed as a function of the thickness and parameters of the hysteresis loop measurements (Fig. 1). The recalculated coercive and bias fields were found to be almost constant except of the film with a minimal thickness – 9 nm. In 9 nm-thick film, the coercive filed increases, while residual response decreases, which can be explained by the compressive stress caused by the clamping of the material to the substrate.

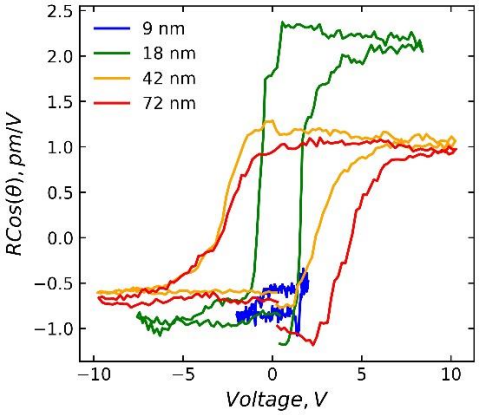

Figure 1. Piezoelectric hysteresis loop in the BFO films with different thicknesses after PUND correction.

The research funding from the Ministry of Science and Higher Education of the Russian Federation (Ural Federal University Program of Development within the Priority-2030 Program) is gratefully acknowledged. The equipment of the Ural Center for Shared Use “Modern nanotechnology” UrFU was used.

1. G. Catalan, J.F. Scott, *Adv. Mat.* **21**, 2463 (2009).
2. S. Fujino et al., *APL* **92**, 202904 (2008).

P74

PFM study of spherulite perovskite islands in PZT thin films

S.V. Senkevich[1,2], I.P. Pronin[1], D.A. Kiselev[3], V.P. Pronin[2], I.I. Khinich[2]

[1]*Ioffe Institute, 194021, St. Petersburg, Russia*
SenkevichSV@mail.ioffe.ru

[2]*Herzen State Pedagogical University of Russia, 191186, St. Petersburg, Russia*

[3]*National University of Science and Technology «MISiS», 119049, Moscow, Russia*

The structural, ferroelectric, and piezoelectric properties of thin $Pb(Zr,Ti)O_3$ (PZT) spherulite films formed by RF magnetron sputtering have been studied. The films were fabricated in two stages on a $Pt/TiO_2/SiO_2/Si$ substrate. At the first stage, the films were deposited at a substrate temperature of 150°C, and at the second stage, for the crystallization of the perovskite phase, they were annealed at 530–570°C. The film thickness was 500 nm. Both single-phase perovskite films and those consisting of separate spherulitic islands located in a low-temperature pyrochlore matrix were studied

The films were studied using an EVO-40 (Zeiss) scanning electron microscope and MFP-3D SA (Asylum Research) and Ntegra Prima (NT-MDT) atomic force microscopes. The composition of the films corresponded to the morphotropic phase boundary with the elemental ratio Zr/Ti=54/46.

The microstructure, growth orientation, phase state, and composition of the formed films were studied by electron microscopy. Surface morphology, normal and lateral piezoelectric responses, as well as surface potential of individual perovskite spherulitic islands were studied by atomic force microscopy.

Figure 1 shows the lateral response of an individual perovskite island (Fig. 1a) and its surface potential (Fig. 1c), as well as the profiles of these signals (Fig. 1b and d, respectively). The effect of a nonuniform distribution of the piezoelectric response and surface potential over the surface of a perovskite island is found, from the maximum response near its boundary to the minimum one in the center of the island. It is assumed that the observed effect is due to the peculiarities of the formation of radiant spherulites. The paper discusses possible physical mechanisms leading to such inhomogeneities.

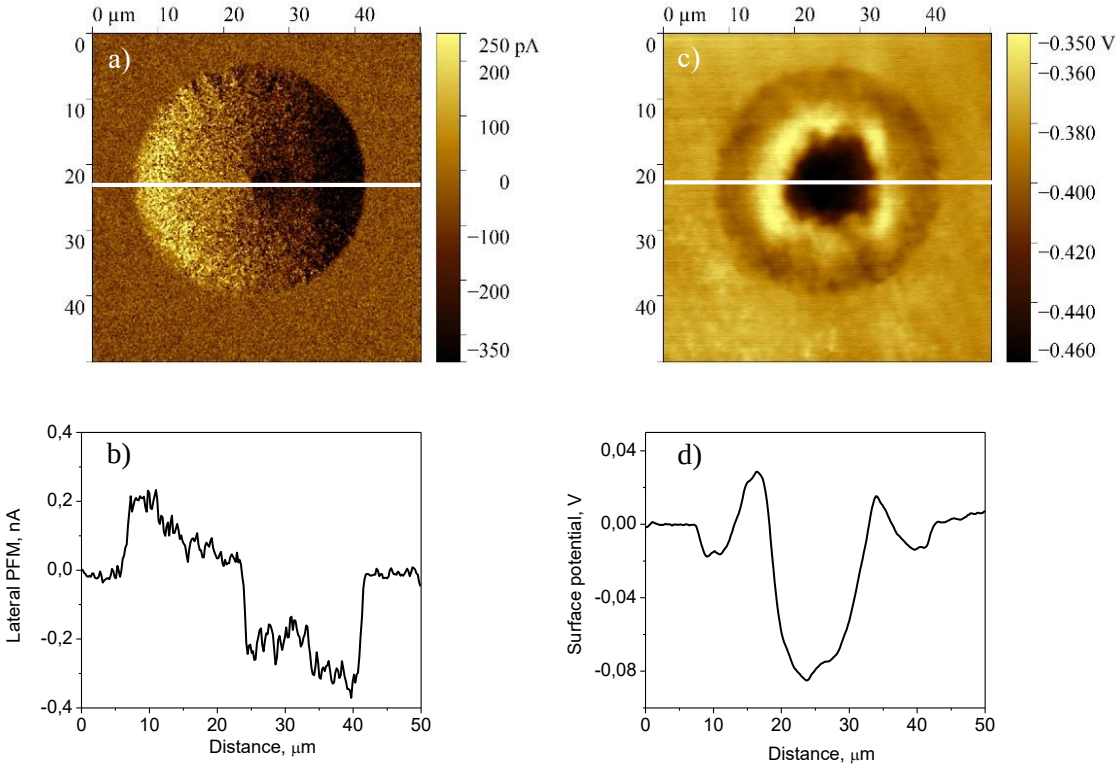

Figure 1. Image and profiles of the lateral piezoelectric response (a, b) and surface potential (c, d) of a perovskite island.

The work was supported by an internal grant from the Herzen State Pedagogical University of Russia.

P75

Effect of thermal treatment in an indium atmosphere on the magnetic properties of soft magnetic materials

L.G. Shaimardanova, E.A. Stepanova, A. A. Fedeschenko, D.S. Neznakhin

[1]*Ural Federal University named after the first President of Russia B.N. Yeltsin, 620002, Yekaterinburg, Russia*
Lilia.Shaymardanova17@gmail.com

This work is devoted to the study of heat treatments in the presence of indium vapor on the magnetic properties of samples of soft magnetic alloys in the form of thin films. It was found that indium vapor atmosphere during heat treatment affects the magnetic properties of soft magnetic materials.

Amorphous soft magnetic films are of great interest, both scientifically and in application, among the soft magnetic materials, because they have unique physical properties and can be used without pretreatments and insulating coatings. But to change the properties, including magnetic properties, various heat treatments (HT) are carried out.

A number of studies have found that placing materials in a chemically active environment and subsequent heat treatment have an effect on their properties. Usually various mixtures of inert gases, hydrogen or water vapor are used [1-3]. However, of great scientific interest is the change in the properties of films after heat treatment in an atmosphere of metal vapors that do not react chemically with the components of the alloy composition. For example, in the presence of indium, since its vapor can be obtained at relatively low temperatures (less than the crystallization temperature).

The effect of heat treatment in indium atmosphere was studied on films of Finemet composition: $Fe_{73,5}Nb_3Cu_1Si_{13,5}B_9$, 70 nm thick, and $Fe_{72,5}Nb_{1,5}Mo_2Cu_{1,1}Si_{14,2}B_{8,7}$, 1000 nm thick. The dimensions of the samples were 4x6 mm^2. The films are produced by high-frequency ion-plasma deposition at the ATC ORION 8 UHV. All samples were placed in individual heat-resistant perolitic glass tubes and sealed with or without a piece of indium.

HT took place in a muffle furnace MIMP-3UE. The heating rate was 10 C/min. To analyze the chemical composition of the surface of the samples used X-ray fluorescent spectrometer on the full reflection «NANOHUNTER». The surface magnetic properties were studied using a Kerr effect magneto-optical microscope. The atomic force microscope «BRUKER MULTIMODE 8» was used to study the surface structure.

Studies have shown that the change in the magnetic properties of the samples is also largely influenced by the mechanism of the HT itself. Therefore, the most effective one was determined experimentally: temperature 300°C, isothermal exposure time 240 minutes.

The surface of the films was studied by atomic force microscopy. The results for samples of 1000 nm thickness after HT are shown in Figure 1. It is clear from Figure 1б that indium does not cover the whole surface of the sample but is distributed chaotically in the form of droplets on it. The same results were obtained for 70 nm thick films.

Studies of the films surface showed that their roughness practically did not change after HT.

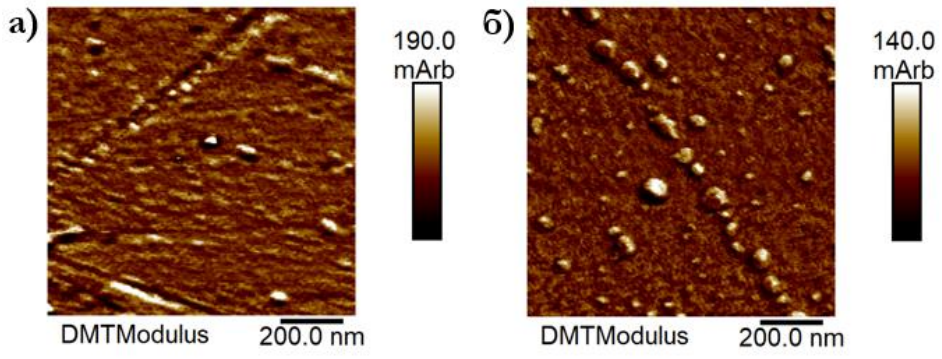

Figure 1. Image of films with a thickness of 1000 nm: а – sample after HT, б – sample that underwent HT in an indium atmosphere.

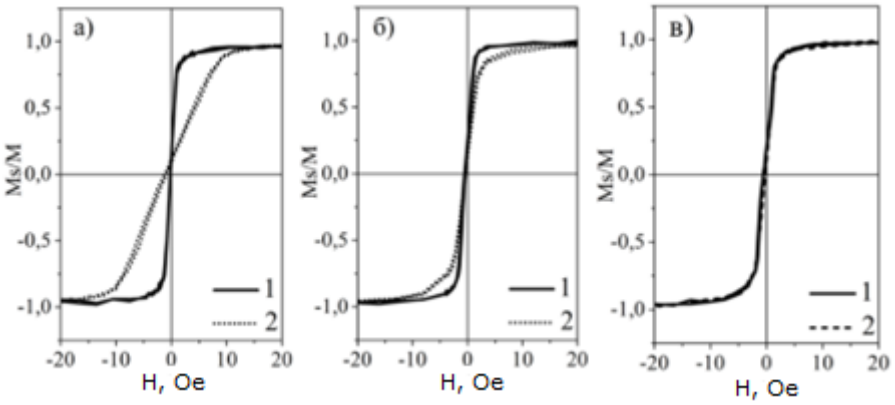

Figure 2. Magneto-optical hysteresis loops of 1000 nm thick films: (a) immune state; (b) after HT; (c) after HT in the indium atmosphere. 1 – measured when a magnetic field is applied along the easy direction (ED), 2 – measured when a magnetic field is applied and perpendicular to the ED.

Magneto-optical hysteresis loops were also investigated. A magnetic field was applied along and perpendicular to the light magnetization axis. The trend of changes in the magnetic properties of the films of different thicknesses after HT was similar. As can be seen from Figure 2, HT of the samples led to a decrease in the induced magnetic anisotropy of the films. However, in the sample after HT in an indium atmosphere the magnetic anisotropy disappeared completely.

Thus, the presence of indium during heat treatment leads to a change in the surface magnetic properties of the film samples. This can be explained by the fact that stress relaxation occurs during heat treatment and indium possibly introduces additional stresses.

E. A. Bolyachkina for her help in examining samples on the magneto-optical Kerr microscope and atomic force microscope.

This work was carried out with the financial support of the Ministry of Science and Higher Education FEUZ 2023 0020.

1. A. Nourmohammadi, H.M. Fesharaki, *Jap. J. Appl. Phys.* **12**, 123002 (2018)
2. N. A. Skulkina, *Physics of metals and materials science* **12**, 1242 (2015)
3. N. A. Skulkina, *Physics of metals and materials science* **10**, 1015 (2016)

P76

Complex electromechanical parameters and microstructure peculiarities of PZT-type porous piezoceramics

N.A. Shvetsova, I.A. Shvetsov, E.I. Petrova, D.I. Makarev, A.N. Rybyanets

Southern Federal University, 344090, Rostov-on-Don, Russia
nashvecova@sfedu.ru

Porous piezoceramics based on different piezoceramic compositions are widely used now in ultrasonic transducers and sensors for various technical applications such as medical ultrasonic devices, nondestructive testing, underwater acoustics, and others [1]. However, despite numerous studies and long observation regarding pore effects on material properties, many aspects of the relationship between the microstructure peculiarities and electromechanical parameters of porous piezoceramics are still unclear. Besides, the reasons for the frequency dependences of the complex parameters, as well the microstructural and physical mechanisms of elastic losses and dispersion in porous piezoceramics seems not yet clear.

In this work, we studied the microstructure peculiarities and complex electromechanical parameters of porous piezoelectric ceramics based on the PZT system. Piezoelectric ceramics of the composition $Pb_{0.95}Sr_{0.05}Ti_{0.47}Zr_{0.53}O_3$ + 1% Nb_2O_5 with different relative porosity in the range of 0÷50% and average pore size of 10÷30 μm were chosen as the object of the study. Experimental samples of porous piezoceramics were obtained using a modified method of pore formers burning-out. Microstructural studies were performed on polished and chipped surfaces of porous piezoceramics samples using the scanning electron microscopes (JEOL JSM-6390LA and TM-100, Hitachi). The complex elastic, dielectric, and piezoelectric parameters of the piezoceramics elements were measured on standard samples using Agilent 4294A impedance analyzer and the piezoelectric resonance analysis (PRAP) software. The frequency dependences of the complex parameters of the experimental samples in the frequency range up to 20 MHz were studied by analyzing the impedance spectra for the fundamental and higher-order resonances of thickness vibrational mode.

As the result of SEM microstructure analysis, it was found that at any connectivity type (3-0, 3-3) and porosity up to 50% the real structures of the studied porous were close to the matrix medium structure with continuous coral-like piezoceramic skeleton. It was revealed that the following microstructural features define the dielectric, piezoelectric and electromechanical properties of the studied porous piezoelectric ceramics - the branched flexible three-dimensional piezoceramics skeleton and the quasi-rod piezoceramics structure in the direction of residual polarization of porous piezoceramics. The study of the frequency dependences of the complex elastic moduli C_{33}^{E} and C_{33}^{D} in the frequency range up to 20 MHz using the PRAP method allowed us to identify areas of normal and anomalous elastic dispersion in porous ferroelectric ceramics. It was shown that the cause of the normal elastic dispersion in a porous piezoceramics is the rapid grows in the attenuation of ultrasonic waves with a frequency caused by Rayleigh scattering of elastic waves in pores. In its turn, the anomalous dispersion of the elastic properties of the studied porous piezoceramics is due to its microstructural features, namely, the presence of a rigid three-dimensional piezoceramic frame and a quasi-rod structure.

The study was financially supported by the Russian Science Foundation grant No. 22-11-00302, https://rscf.ru/project/22-11-00302/ at the Southern Federal University.

1. A.N. Rybyanets, D.I. Makarev, N.A. Shvetsova, *Ferroelectrics* **539**, 101 (2019).

P77

Influence of component dispersion on electrical properties of $CaWO_4$-Al_2O_3 composites

A.A. Tushkova, A.G. Baranova, A.F. Guseva, N.N. Pestereva

Ural Federal University, 620002, Yekaterinburg, Russia
Anastasiatu14@gmail.com

It was found earlier that the addition of Al_2O_3 nanopowder to $CaWO_4$ leads to an increase in ionic conductivity by approximately one order of magnitude. Since the high composite conductivity is due to the processes occurring at the interfacial boundaries [1], in this work an attempt was made to study the effect of the dispersion of the components on the electrical conductivity of the composites. For this purpose, aluminum oxide nanopowder obtained by electroexplosion with different specific surface area 20, 40, 60; 69, 77 m^2/g and calcium tungstate obtained by solid-phase synthesis with an average grain size 12 μm, as well as calcium tungstate ground in a ball mill, were used to prepare composites. The phase composition of the composites and their thermodynamic stability were confirmed by XRD and TG-DSC.

The conductivity of composites was studied by the method of electrochemical impedance as a function of temperature, the content of the dispersed additive Al_2O_3, $CaWO_4$ and Al_2O_3 dispersion.

Figure 1 shows the $(1-x)CaWO_4–xAl_2O_3$ electrical conductivity versus the mole fraction of Al_2O_3 at different dispersity of aluminum oxide (a) and calcium tungstate (b).

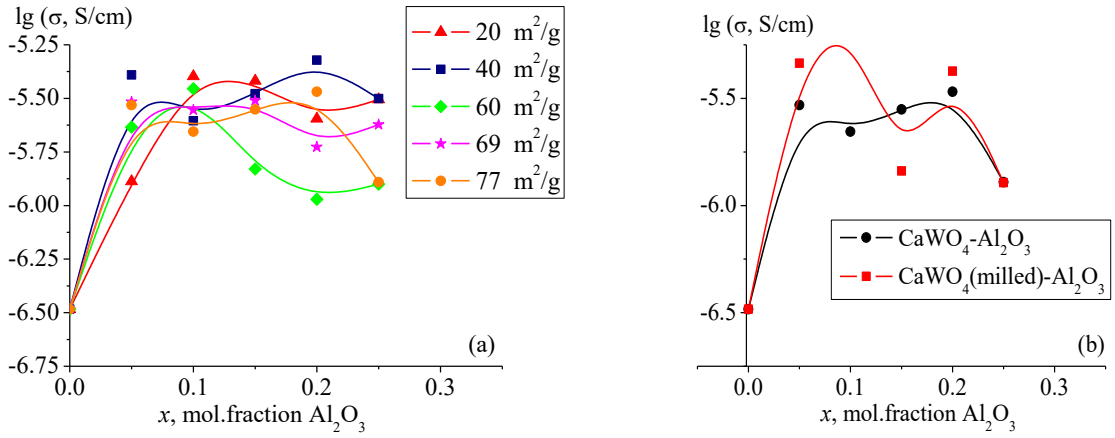

Figure 1. Electrical conductivity as a function of the mole fraction of Al_2O_3 at different dispersity of aluminum oxide (a) and calcium tungstate (b).

The addition of 5 mol% Al_2O_3 to calcium tungstate leads to an increase in ionic conductivity by more than an order of magnitude. The introduction of a larger amount of alumina into the composite leads to stabilization and a subsequent decrease in conductivity. The high composite conductivity is related to the high ionic conductivity of the $CaWO_4|Al_2O_3$ interphase boundary, which is formed at the site of contact between the matrix and the disperse additive. Therefore, the dispersion of the composite components should lead to an increase in the composite conductivity. Indeed, the grinding of calcium tungstate leads to an increase in the conductivity of the composites (Fig. 1b). However, the use of aluminum oxide with different specific surface area 20 - 77 m^2/g did not lead to significant changes in the conductivity of the composite (Fig. 1a). This is probably due to the polydispersity of Al_2O_3 nanopowders used for the preparation of composites.

Reaching the maximum value, the electrical conductivity of $(1-x)CaWO_4–xAl_2O_3$ composites decreases due to the discontinuity of the interphase boundary by dielectric particles Al_2O_3.

The research results were obtained within the framework of the state task of the Ministry of Science and Higher Education of the Russian Federation (project number 123031300049-8) using the equipment of the UCKP “Modern Nanotechnologies” UrFU (reg. No. 2968), supported by the Ministry of Science and Higher Education of the Russian Federation (project No. 075-15-2021-677).

1. N.F. Uvarov, *Composite solid electrolytes*, Novosibirsk: ISSC SB RAS Publ., 259, (2008).

P78

The spherulite microstructure study of lead zirconate titanate thin films obtained by RF magnetron sputtering

A.R. Valeeva[1], I.P. Pronin[1], E.Yu. Kaptelov[1], S.V. Senkevich[1], M.V. Staritsyn[2], V.P. Pronin[3]
[1]*Ioffe Institute, 194021, St. Petersburg, Russia*
ValeevaAR@mail.ioffe.ru
[2]*NRC "Kurchatov Institute", CRISM "Prometey", 191015, St. Petersburg, Russia*
[3]*Herzen State Pedagogical University of Russia, 191186, St. Petersburg, Russia*

Interest in studying the nature of the spherulitic crystal structures formation has noticeably grown. It is well known that these structures are formed under certain conditions in most known materials (regardless of their composition) [1,2]. A lot of attention to spherulites is mainly connected with the miniaturization of piezoelectric quartz generators and, as a result, the use of thin-film technologies [2,3]. One of the most spreading forms of spherulites are radiant spherulites, in which rotation of the growth axis is observed in the process of radial growth. This leads to structural disturbances and apparently has a negative effect on the oscillatory properties of the grown quartz films.

Recent studies show spherulitic structures are typical for thin ferroelectric films, and in particular lead zirconate titanate (PZT) which are the main materials for creating various microelectromechanical devices [4,5]. However, the features of the spherulitic microstructure crystallization in thin PZT films have not been practically studied up to now, just as the relationship between the microstructure and their physical properties has not been studied. The purpose of this work is to study the microstructure of thin PZT films, the composition of which corresponds to the region of the morphotropic phase boundary, with varying the sizes of spherulitic blocks and changing their dielectric properties.

Thin-film PZT structures were fabricated by a two-stage method of RF magnetron sputtering. Films were deposited on platinized silicon substrates (Pt/TiO2/SiO2/Si). The sputtered ceramic target composition corresponded to the elemental ratio of zirconium and titanium atoms Zr/Ti = 54/46 and corresponded to the region of the morphotropic phase boundary. Two types of films were prepared, differing in: a) 100% crystallization of the perovskite phase, consisting of spherulite blocks and b) spherulite islands of the perovskite phase in a pyrochlore matrix. To vary the size of the spherulites, the target-substrate distance was changed in the range from 30 to 70 mm. To study the dielectric characteristics an array of platinum contact pads was fabricated on the surface of the prepared films.

The crystal structure and phase state of the films were controlled by X-ray diffraction analysis (θ-2θ), Rigaku Ultima IV. Microimages of perovskite films were studied using a Tescan Lyra 3 scanning electron microscope equipped with a detector for recording electron backscattering diffraction patterns. The dielectric properties were studied using an E7-20 immitance meter and a modified Sawyer-Tower circuit.

In this work, the change in the crystal structure, the nature of the microstructure and the dielectric properties of the samples depending on the linear size of the spherulites was studied. It was found that the formation of a spherulitic structure is realized through an intermediate perovskite phase, which is characterized by a lower density. The structural and dielectric parameters of the formed films reached at certain sizes of spherulites anomalously high values. The paper discusses the causes and mechanisms responsible for the behavior of the observed changes.

1. A.G. Shtukenberg, Yu.O. Punin, E. Gunn, B. Kahr, *Chemical Review* **112**, 1805 (2012).
2. N.R. Lutjes, S. Zhou, J. Antoja-Lleonart, B. Noheda, V. Ocelík, *Sci. Rep.* **11**, 14888 (2021).
3. E.J. Musterman, V. Dierolf, H. Jain, *Int. J. Appl. Glass Sci.* **13**, 402 (2022).
4. L. Song, S. Glinsek, E. Defay, *Appl. Phys. Rev* **8**, 041315 (2021)
5. A.A. Bukharaev, A.K. Zvezdin, A.P. Pyatakov, Yu.K. Fetisov, *Successes of physical sciences* **188**, 1288 (2018).

P79

Superconducting spin-valve structure Co1/Pb/Co2 with insulator layers in F/S interfaces

A.A. Validov, M.I. Nasyrova, R.R. Khabibullin, I.A. Garifulin

[1] *Zavoisky Physical-Technical Institute, FRC Kazan Scientific Center of RAS, 420029 Kazan, Russia*
validov@kfti.knc.ru

Now the classical SSV structures have been studied in sufficient detail and well. Latest results show (see, e.g., [1, 2]), the limiting values of the SSV effect have already been practically achieved using various alloys and elemental materials in F1/F2/S structures. In this regard, it is necessary to study non-standard unusual SSV models. One of such possible variants of models can be SSV structures with insulator layers. The possibility of observing a significant SSV effect $\Delta T_c \sim 0.3$ K in SSV structures with insulator layers was demonstrated by Deutscher and Meunier in 1969 [3].

In present work are given our first experimental investigation of the superconducting properties of Co1/Pb/Co2 SSV structure with insulator layers. We created thin oxide layers into Co1/Pb and Pb/Co2 interfaces similarly in Ref.[3]. Electrical resistivity measurements were carried out by standard DC four-point method. An external magnetic field was always applied in-plane of the sample in all measurements. The superconducting critical temperature T_c was defined as the midpoint of the transition curve.

Fig. 1 depicts superconducting transition curves at P ($H_0 = +1$ kOe) and AP ($H_0 = -1$ kOe) orientations of the Co1 and Co2 layers's magnetization, respectively. The value of SSV effect $\Delta T_c = 0.2$ K. The figure shows that the $\Delta T_c > \delta T_c$. Thus, the full SSV effect was observed.

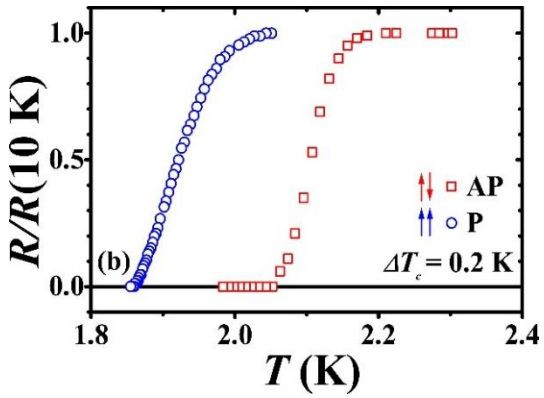

Figure 1. Superconducting transition curves at P ($H_0 = +1$ kOe) (○) and AP ($H_0 = -1$ kOe) (□) orientations of the Co1 and Co2 layers' magnetizations, respectively.

Our results demonstrate the possibility of observing the SSV effects in SSV structures with insulator layers. It seems that the observation of SSV effects in such structures is not obvious, since S/F interface is bad. But from our experimental results and the results in Ref.[3] quite large SSV effects are observed.

We investigated superconducting properties of Co1/Pb/Co2 heterostructures with insulator layers. In these heterostructures were formed thin oxide layers (insulator layers) into Co1/Pb and Pb/Co2 interfaces. We have observed full superconducting spin valve effect with value of ΔT_c reached 0.2 K. It can be assumed that investigation of SSV structure with insulator layers is a promising area of research. We have also studied superconducting properties of Co1/Pb/Co2 structures with similar parameters, but without insulator layers. T_c for these samples was not registered until 1.4 K. This is due to the free penetration of Cooper pairs from the S-layer into the F-layers.

The research was supported by the Russian Science Foundation grant No. 22-22-00916.

1. Y. Gu, G. B. Hal´asz, J. W. A. Robinson, M. G. Blamire, *Phys. Rev. Lett.* **115**, 067201 (2015).
2. A. Singh, S. Voltan, K. Lahabi, and J. Aarts, *Phys. Rev. X* **5**, 021019 (2015).
3. G. Deutscher and F. Meunier, *Phys. Rev. Lett.* **22**, 395 (1969).

P80

Temperature dependences study of the SBN61 films transmission spectra

K.M. Zhidel[1], A.V. Pavlenko[1,2]

[1]*Research Institute of Physics, Southern Federal University, 344090, Rostov-on-Don, Russia*
karinagidele@gmail.com

[2]*Federal Research Centre, The Southern Scientific Centre of the Russian Academy of Sciences, 344006, Rostov-on-Don, Russia*

Strontium-barium niobate solid solutions ($Sr_xBa_{1-x}Nb_2O_6$, SBN) [1] attract much attention of researchers due to their electro-optical [2], pyroelectric [3], and piezoelectric [4] properties, which open up great prospects for their use in microelectronic devices. SBN crystals are attractive materials for new optoelectronic devices. Of particular interest is the high photorefractive sensitivity and large electro-optical coefficient r_{33} [5], which makes it possible to use it for modern devices for optical data processing [6], optical storage devices [7], and optical conjugation [8].

SBN thin films are a promising material for application. The most interesting are heteroepitaxial films, which are obtained by methods and high-frequency sputtering [9, 10] of targets.

Despite the obvious practical possibilities of SBN, there are very few publications in the literature devoted to studying the dependence of the optical properties of these crystals on temperature.

In this work, we study the optical properties of SBN61 thin films synthesized by high-frequency RF sputtering in an oxygen atmosphere on single-crystal MgO(001) substrates. When controlling the optical characteristics of layers of various materials, the method of spectrophotometry is widely used.

The spectral coefficients of directional transmission of SBN61 thin films were measured using an SF-56 UVI spectrophotometer. The following parameters were set as measurement parameters: "Scanning" mode, spectral range 190–1100 nm, sampling step 1 nm, measurement time 0.2 s, slit width: 6.0 nm. The sample was placed in an LN-121-SPECTR nitrogen filled optical cryostat in vacuum. The temperature range was changed from +20°C to +180°C.

The transmission spectra show a pronounced sequence of interference maxima and minima, as well as a shift of peaks and absorption edge regions during temperature measurements. A detailed analysis of the optical spectra will make it possible to reveal the nature of the features of this material, make significant progress in the study of optical properties, and make it possible to develop recommendations for the use of these materials in the development of new devices.

The work was performed with the use of equipment of the Center for Collective Use «Integrated Centre of scientific-technological equipment SSC RAS (research, development, approval)», the Southern Scientific Centre of the Russian Academy of Sciences (No. 501994).

The study was carried out with the financial support of the Ministry of Science and Higher Education of the Russian Federation (State task in the field of scientific activity in 2023). Project No. FENW-2023-0010/(GZ0110/23-11-IF).

1. Yu.S. Kuzminov, *Ferroelectric crystals for controlling laser radiation*. Nauka, Moscow (1982), 400 p.
2. P.V. Lenzo, E.G. Spencer, A.A. Ballman, *Appl. Phys. Lett.* **11**, 23 (1967).
3. A.M. Glass, *J. Appl. Phys*. **40**, 4699 (1969).
4. R.R. Neurgaonkar, W.K. Cory, J.R. Oliver, *Ferroelectrics* **51**, 3 (1983).
5. R.R. Neurgaonkar, W.K. Cory, J.R. Oliver, et al., *Opt. Eng.* **26**, 392 (1987).
6. P. Yeh, A.E.T. Chiou, *Opt. Lett*. **12**, 138 (1987).
7. J.E. Ford, Y. Fainman, *J. Opt. Soc. Am. A* **9**, 1183 (1992).
8. G.L. Wood, W.W. Clark, M.J. Miller, et al., *IEEE J. Quantum Electron* **23**, 2126 (1987).
9. M.K. Ryu, S.H. Lee, H.J. Joo, et al., *Ferroelectrics* **260**, 99 (2001).
10. M. Cuniot-Ponsard, J.M. Desvignes, B. Ea-Kim, E. Leroy, *J. Appl. Phys*. **93**, 1718 (2003).

P81

Optical properties of the BNFNO films depending on temperature

K.M. Zhidel[1], A.V. Pavlenko[1,2]

[1]*Research Institute of Physics, Southern Federal University, 344090, Rostov-on-Don, Russia*
karinagidele@gmail.com

[2]*Federal Research Centre The Southern Scientific Centre of the Russian Academy of Sciences, 344006, Rostov-on-Don, Russia*

At present, nonlinear dielectrics with the structure of tetragonal tungsten bronze (TTB) with the general chemical formula $(A1)_2(A2)_4(C)_4(B1)_2(B2)_8O_{30}$ [1], which include multiferroics $Ba_2LnFeNb_4O_{15}$ (Ln is a rare earth element), are intensively studied [2–4]. Since 2009, studies of $Ba_2LnFeNb_4O_{15}$ ceramics have shown that they can be used to create new multiferroic structures that combine ferroelectric and magnetic properties at room temperature [2]. In subsequent years, these structures were obtained in a nanoscale form, which made it possible to consider their application in functional electronics and sensor technology [5]. Unlike barium–strontium niobates, the most well-known materials with the TTB structure [1], the crystal structure of $Ba_2LnFeNb_4O_{15}$ is filled [6, 7], however, during the synthesis of ceramics and single crystals, vacancies arise in the Ln positions, which strongly affects the dielectric properties and phase composition materials [6].

An analysis of publications in scientific journals has shown that there is no information about the optical characteristics of the material of this composition. When controlling the optical characteristics of layers of various materials, the method of spectrophotometry is widely used.

This work consisted in studying the dependence of the optical properties on high temperatures in films of neodymium barium ferroniobate ($Ba_2NdFeNb_4O_{15}$, BNFNO) grown on a MgO(001) substrate.

The spectral coefficients of directional transmission of neodymium barium ferroniobate thin films on a single-crystal MgO substrate were measured using an SF-56 UVI spectrophotometer. The following parameters were set as measurement parameters: "Scanning" mode, spectral range 190–1100 nm, sampling step 1 nm, measurement time 0.2 s, slit width: 6.0 nm. The sample was placed in an LN-121-SPECTR nitrogen filled optical cryostat in vacuum. The temperature range was changed from +20°C to +180°C.

The transmission spectra show a pronounced sequence of interference maxima and minima, as well as a shift of peaks and absorption edge regions during temperature measurements. A detailed analysis of the optical spectra will make it possible to reveal the nature of the features of this material, make significant progress in the study of optical properties, and make it possible to develop recommendations for the use of these materials in the development of new devices.

The work was performed with the use of equipment of the Center for Collective Use «Integrated Centre of scientific-technological equipment SSC RAS (research, development, approval)», the Southern Scientific Centre of the Russian Academy of Sciences (No. 501994).

The research was funded by the Russian Science Foundation (project No. 21-72-10180).

1. Yu.S. Kuzminov, *Ferroelectric crystals for controlling laser radiation*. Nauka, Moscow (1982), 400 p.
2. T. Hajlaoui, C. Harnagea, A. Pignolet, *Mater. Lett.* **198**, 136 (2017).
3. A R. Bodeux, D. Michau, M. Josse, M. Maglione, *Solid State Sci*. **38**, 112 (2014).
4. M. Josse, O. Bidault, F. Roulland, et al., *Solid State Sci*. **11**, 1118 (2009).
5. H. Wu, A. Tatarenko, M.I. Bichurin, Y. Wang, *Nano Energy* **83**, 105777 (2021).
6. M. Albino, P. Veber, S. Pechev, et al., *Cryst. Growth Des*. **14**, 500 (2014).
7. E. Castel, P. Veber, M. Albino, et al., *J. Cryst. Growth* **340**, 156 (2012).

P82

Research on the $KV_3O_8 \cdot 0.75H_2O$ -Methyl cellulose flexible nanocomposite films and electrochromic property

Q.Y. Zhu [1], K. S. Sun[1], S. C. Cui [1,2], J. X. Dong[1], Y. Q. Zhang[1], J. Y. Zhang[1,2]

[1]*School of Materials Science and Engineering, Wuhan University of Technology, 430070, Wuhan, People's Republic of China*

cglamri@whut.edu.cn

[2]*State Key Laboratory of Advanced Technology for Materials Synthesis and Processing, Wuhan University of Technology, 430070, Wuhan, People's Republic of China*

KV_3O_8-0.75H_2O nanowires were fabricated by sol-gel method. The KV_3O_8-0.75H_2O-carboxymethyl cellulose nanowires with combined by centrifuge cleaning and ultrasonic dispersion assisted. The flexible nanocomposite films were obtained from the rotational coating. Figure 1 shows characterization and electrochemical properties of the flexible nanocomposite films. The potassium was present in the interlayer structure through ions and expanding the channel space for the transport of Li^+ in the composite nanocomposite film (Fig. 1a). Simultaneously, the methylcellulose provided the sites for the growth of the films [1], showing a nanowire-like one-dimensional morphology (1D) with a film layer spacing of 0.81 nm (Fig. 1b). The combined support of K^+ and 1D shape is the main reason for the significant improvement in the electrochemical stability of the films. Nanostructures provide faster ion transport rates and a significant active reaction surface area that can effectively facilitate electrochromic reactions [2,3]. The electrochemical testing in a lithium perchlorate electrolyte. The results are shown in Figure 1c, films were driven at ±1 V and remained in good working order after 2000 cycles. The films had exhibited a range of yellow, green and orange colour modulations when stimulated, as shown in Figure 1d. The flexible nanocomposite film therefore not only enhances the electrochemical properties of vanadium oxides, but also broadens the choice of materials for flexible electrochromic functional devices.

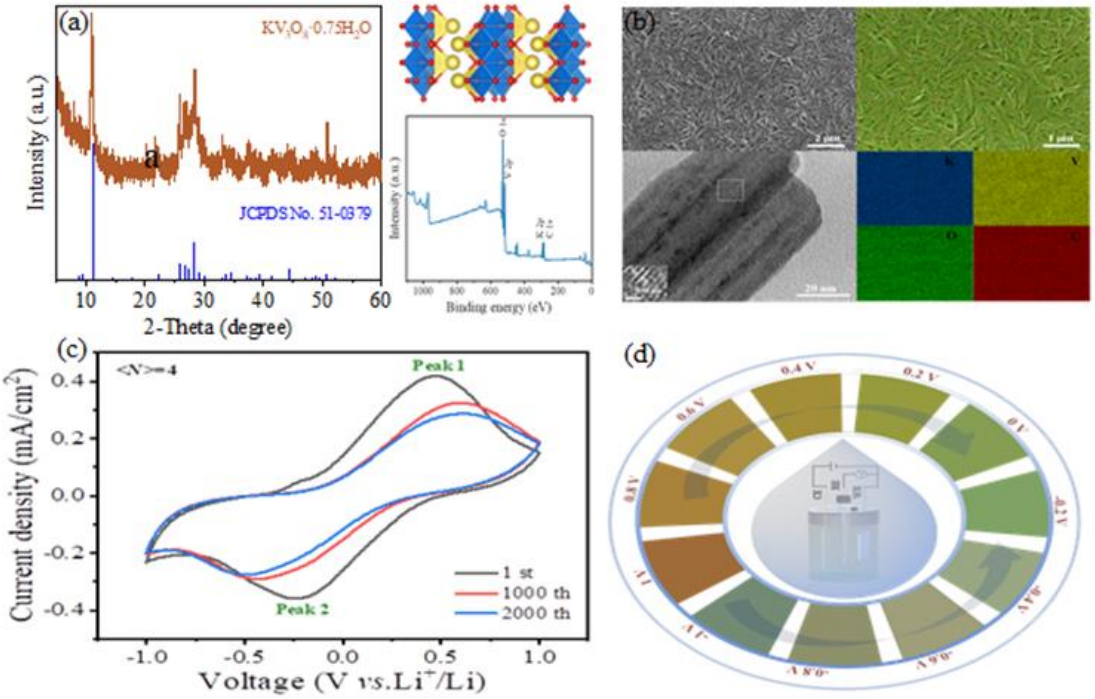

Figure 1. KV_3O_8-0.75H_2O-carboxymethyl cellulose flexible nanocomposite films characterization and electrochemical properties.

1. S.K. Sun, S.C. Cui, Q.Y. Zhu, J.Y. Zhang, *ACS Appl. Electr. Mater.* **4**, 4724 (2022).
2. G.J. Yang, Y.M. Zhang, Y.R. Cai, et al., *Chem. Soc. Rev.* **49**, 8687 (2020).
3. G.F. Cai, A.L-S. Eh, L. Ji, and P.S. Lee, *Adv. Sustainable Syst* **12**, 1700074 (2017).

P83

Ferroelectric and photoelectronic properties of peptide nanotubes and nanostructures based on various amino acids

V.S. Bystrov[1], E.V. Paramonova[1], O.R. Ledeneva[2], E.V. Belova[2], P.S. Zelenovskiy[3,4], V.M. Fridkin[5]

[1]*Institute of Mathematical Problems of Biology, Keldysh Institute of Applied Mathematics, RAS, 142290 Pushchino, Russia*

vsbys@mail.ru

[2]*Physics Faculty, Lomonosov Moscow State, 119991 Moscow, Russia*

[3]*School of Natural Sciences and Mathematics, Ural Federal University, 620000 Ekaterinburg, Russia*

[4]*Department of Chemistry and CICECO−Aveiro Institute of Materials, University of Aveiro, 3810-193 Aveiro, Portugal*

[5]*Shubnikov Institute of Crystallography, Federal Scientific Research Center "Crystallography and Photonics" of Russian Academy of Sciences, 119333 Moscow, Russia*

Peptide nanotubes based on diphenylalanine (FF PNT) possessing ferroelectric and piezoelectric properties are an example of well-studied nanostructures widely used in various fields [1–6]. However, recently, it was found that they also exhibit pronounced photoelectronic properties [6,7], which differ for dipeptides of various chirality L-FF/D-FF dipeptides [1, 3]. In this work, we used quantum chemical calculations to analyze photoelectronic properties of PNTs based on other dipeptides: dileucine (Leu-Leu/LL) and diisoleucine (Ile-Ile/II) of L and D chiralities. The calculations were performed in HyperChem package using semi-empirical quantum-chemical PM3 method in the restricted Hartree-Fock approximation.

The models of FF PNT representing stacks of parallel rings (ring structures) of 6 L-FF or D-FF molecules each were taken from the experimental X-ray data [1-4]. Both models demonstrated high spontaneous polarization directed along the nanotube axis, and high values of coercive electric fields and piezoelectric coefficients. Their characteristic energy levels E_LUMO, E_HOMO, and the band gap E_g = E_LUMO - E_HOMO were found to be noticeably different for L and D molecules [8].

The computer model of L-LL PNTs based on experimental data [5, 6] also predicts a significant polarization directed along the nanotube axis, and high values of piezoelectric coefficients and E_g. However, currently, there is no experimental crystallographic data for D-LL. The synthesis and characterization of D-LL are ongoing now, and new results are expected soon. Likewise, there is no experimental data for D-II PNTs. Therefore, artificial helical models of FF, LL, and II of both types of chirality were constructed. These models would predict the expected characteristics of the structures for future experiments.

The calculations performed on artificial and experimental helical models showed the band gap Eg values are noticeably higher than that for the experimental models (Table 1). Similarly, artificial helical models demonstrated higher values of Eg than those of experimental. These results indicate a higher level of optimization typical for natural crystal structures.

Regarding the discrepancy between experimental and artificial models, a similar trend for Eg values is observed for the models of different chiralities. For L-II and L-FF PNTs, the band gap is typically smaller than for D-II and D-FF (Table 1). Therefore, this difference cannot be attributed to a computational error.

Table 1. Band gap Eg values (in eV) calculated for PNTs based on various dipeptides.

№	PNT type	Artificial 2-rings model	Experimental helical 2-coils model	Artificial helical 2-coils-model
1	L-FF	8.5865	3.4410	
2	D-FF	8.7027	3.5750	
3	L-LL	8.3411	3.2296	
4	D-LL	9.0976		6.5440
5	L-II	8.7533		5.3967
6	D-II	9.5261		6.2945

Thus, it can be concluded that helical structures based on dipeptides of various amino acids possess smaller Eg values than their ring counterparts. This effect may be of great evolutionary importance for biomolecular structures, since most of them include helical amino acid/dipeptide sequences. During their self-assembly, it would be energetically more preferable to switch from ring structures to helical ones. Such switching can be considered as a kind of topological phase transition to a more stable organization of biomacromolecules [9].

It is also important to note that Eg values fall in the range of spectral characteristics close to the solar-blind ultraviolet region associated with the absorption of sunlight by the ozone layers of the atmosphere. From a practical point of view, the absence of such absorption, in the case of "ozone holes", the radiation passes through the atmosphere and can be detected using photodetectors based on such PNTs [7, 8]. It is important that the Eg depends on the applied electric field, which makes it possible to adjust the recorded range [7–10]. Polymeric ferroelectrics and layers of graphene/dichalcogenodes are well suited for this purpose [8, 10-12]. Such works are now actively developed in the world.

1. V. Bystrov, J. Coutinho, P. Zelenovskiy, et al., *Nanomaterials* **10**, 1999 (2020).
2. P.S. Zelenovskiy, A.S. Nuraeva, S. Kopyl, et al., *Crystal Growth & Design* **19**, 6414 (2019).
3. V.S. Bystrov, J. Coutinho, O.A. Zhulyabina, et al., *Ferroelectrics* **574**, 78 (2021).
4. V. Bystrov, *Computer Simulation Nanostructures: Bioferroelectric Amino Acids. Bioferroelectricity: Peptide nanotubes and thymine nucleobase* (LAP LAMBERT Academic Publishing), 137 (2020).
5. C.H. Gorbitz, *Chem. Eur. J.* **7**, 5153 (2001).
6. C.H. Gorbitz, *Acta Cryst. B* **74**, 311 (2018).
7. V.S. Bystrov, *Comput. Cond. Matter.* **14**, 94 (2018).
8. V. Bystrov, E. Paramonova, P. Zelenovskii, et al., *Symmetry* **15**, 504 (2023).
9. V.S. Bystrov, P.S. Zelenovskiy, et al., *Math. Biol. & Bioinf.* **14**, 94 (2019).
10. V.S. Bystrov, E.V. Paramonova, P.S. Zelenovsky, et al., *Proc. Int. Conf. "Math. Biol. & Bioinf."*. Ed. V.D. Lakhno. Pushchino: IMPB RAS. **9**, e18 (2022).
11. X. Wang, et al., *Adv. Mater.* **27**, 6575 (2015).
12. V.S. Bystrov, E.V. Paramonova, X. Meng, et al., *Abstr. book: 15th Int. Conf. Adv. Comp. Eng. Exp.* (ACEX2022, Florence, Italy), 49 (2022).

P85

Formation of $BaTiO_3$ thin films for energy-efficient memristive applications

D.A. Dzyuba[1,2], Z.E. Vakulov[1], R.V. Tominov[1,2], V.A. Smirnov[1,2]

[1]*Research Laboratory "Neuroelectronics and Memristive Nanomaterials" (NEUROMENA Lab), Institute of Nanotechnologies, Electronics and Electronic Equipment Engineering, Southern Federal University, 347922, Taganrog, Russia*
dmdzyuba@sfedu.ru

[2]*Department of Radioelectronics and Nanoelectronics, Institute of Nanotechnologies, Electronics and Electronic Equipment Engineering, Southern Federal University, 347922, Taganrog, Russia*

Due to the wide range of possible applications, oxide materials and ferroelectrics have attracted the attention of the scientific community [1]: non-volatile memory devices [2-5], converters and MEMS [6], and energy harvesting devices [7]. Barium titanate ($BaTiO_3$) can be used in many applications due to its ferroelectric properties, high dielectric permittivity and large electro-optical coefficients. RF sputtering, molecular beam epitaxy, sol-gel method, and pulsed laser deposition (PLD) [8, 9] can be used to fabricate $BaTiO_3$ thin films. The oxygen pressure value under PLD is one of the key parameters affecting the growth mechanism, crystal orientation, degree of defectiveness and microstructure of $BaTiO_3$ film. Thus, the purpose of this work is to study the processes of $BaTiO_3$ films production by pulsed laser deposition, considering the synthesis conditions for energy-efficient memristor devices.

$BaTiO_3$ nanocrystalline films were formed by PLD method using the Pioneer 180 module (Neocera, USA). For controlled and reproducible ablation of rotating $BaTiO_3$ target (Kurt J. Lesker, 99.9% purity), a COMPex Pro 102 F excimer KrF laser (Coherent Inc., Germany) with a laser wavelength of 248 nm was used. The target was in a vacuum chamber evacuated to 1×10^{-6} Torr. Films were formed on silicon substrates in oxygen medium in a wide pressure range (from 1×10^{-5} Torr to 1×10^{-2} Torr). The distance from the target to the substrate was 100 mm, and the laser radiation power density and laser pulse repetition rate were 1.5 J/cm^2 and 10 Hz, respectively.

It was found that with increasing oxygen pressure from 1×10^{-5} Torr to 1×10^{-2} Torr, the concentration of charge carriers increases from $(4.8\pm0.4)\times10^{13}$ cm^{-3} to $(2.3\pm0.2)\times10^{14}$ cm^{-3} with the mobility of charge carriers in the films decreasing from (8.0 ± 0.6) cm^2/(V·s) to (2.6 ± 0.2) cm^2/(V·s). The resistivity of the obtained films increases 4 times from $(2.0\pm0.2)\times10^4$ Ω·cm to $(8.8\pm0.8)\times10^4$ Ω·cm. The change in the electrophysical parameters can be related to the influence of the oxygen pressure value on the phase composition of $BaTiO_3$ films [10], and the charge carriers in $BaTiO_3$ films can be generated by oxygen vacancies [11]. An increase in oxygen pressure leads to an increase in the number of vacancies, which leads to an increase in the concentration of charge carriers. The dependence of the mobility of charge carriers on the pressure has the opposite character. The growth of specific resistance can be associated with a decrease in the mobility of charge carriers, as well as the intensification of oxidation processes of the material condensed on the surface of the substrate and in the transition space at increasing oxygen pressure. The chemical composition of $BaTiO_3$ films was investigated by XPS technique on a K-Alpha Thermo Scientific spectrometer with an Al Kα monochromatic ray source (energy 1486.6 eV). High-resolution spectra were recorded in constant energy CAE transmission mode with an energy value of 20 eV, resolution was 0.1 eV, and statistical accumulation was n=10. In order to minimize the impact of non etch regions during ion profiling on the probe, the scanning beam diameter was 0.1 mm and the ion etching region was 1 mm. The etching depth was ~10 nm per cycle. Quantification was performed using modified Schofield library sensitivity factors.

Figure 1 (a) shows survey spectra of $BaTiO_3$ thin films formed on silicon substrates at oxygen pressures of 1×10^{-5} Torr and 1×10^{-2} Torr. Survey spectra shows that the surface composition before the ion etching is represented by the O, C, Ba elements. The concentration of titanium on the surface of the samples before etching is too low- and high-resolution spectra were recorded for quantitative calculation. The low intensity of the spectral lines of titanium can be related to the defectiveness of the perovskite film and surface contamination by atmospheric carbon. Atmospheric carbon can adsorb on perovskite film defects and interact with barium to form carbonates, as evidenced by the shape and position of Ba 3d photoelectron lines.

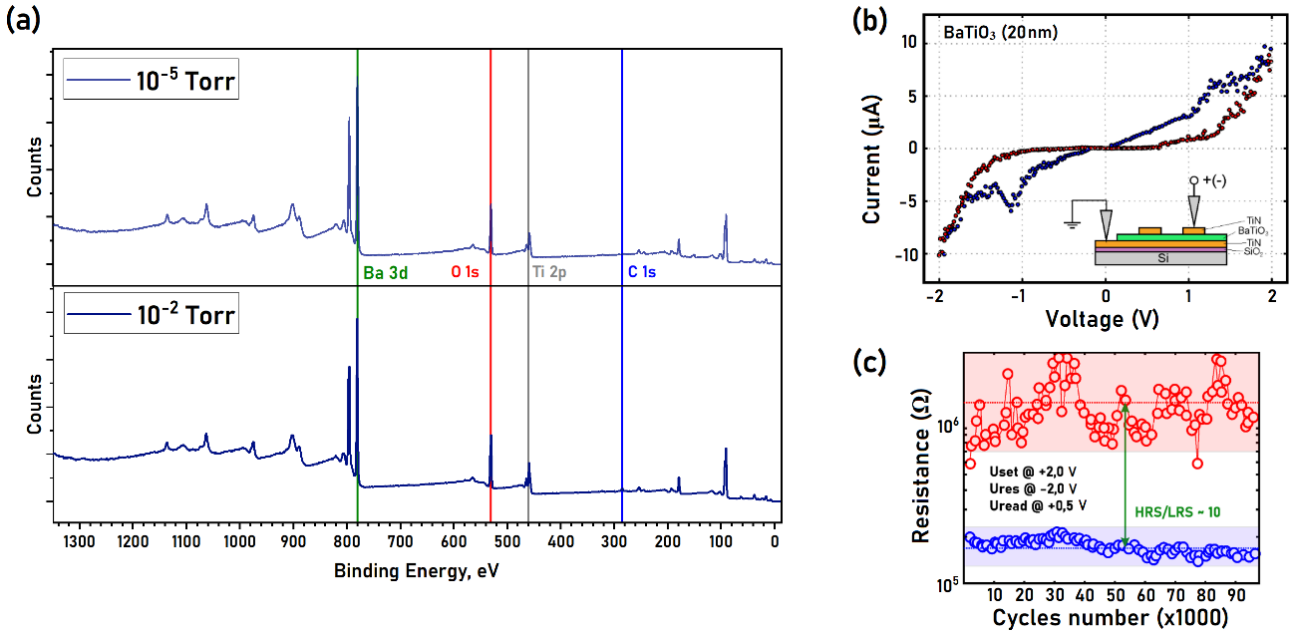

Figure 1. (a) Survey XPS spectra; (b) CVC and (c) endurance test of fabricated $BaTiO_3$ thin films.

It was found that after two etching cycles, at a depth of ~ 40 nm, the composition of the samples approaches the characteristics of perovskite and correlates as 1 Ba/1 Ti/ 3 O. For the sample obtained at oxygen pressure of 1×10^{-2} Torr a slight deviation in Ba/Ti ratio is observed. Comparing the intensities of photoelectron lines of Ti 2p and Ba 3d samples in the dynamics it can be assumed that this effect is due to the different thickness of the films obtained at different pressures. Figure 1 (b, c) shows the results of memristor properties study. It was found that the 20 nm thick $BaTiO_3$ film (10^{-2} Torr) maintained stable HRS and LRS states for 100k cycles with an HRS/LRS ratio of ~10 with U_{set} = +2 V, U_{res} = -2 V, and U_{read} = +0.5 V. The obtained results were used in the fabrication of energy-efficient memristor structures based on $BaTiO_3$ films.

The study was carried out with the financial support of the Russian Federation Government (Agreement No. 075-15-2022-1123).

1. Z.E. Vakulov, D.A. Khakhulin, E.G. Zamburg, et al., *Materials* **14**, 17 (2021).
2. P.M. Razi, R.B. Gangineni, *Thin Solid Films* **685**, 59 (2019).
3. R. Tominov, V. Avilov, Z. Vakulov, et al., *Adv. Electr. Mater.* **8**, 8 (2022).
4. Р.В. Томинов, З.Е. Вакулов, В.И. Авилов и др., *Наноиндустрия*, **15**, S8-2 (2022).
5. R.V. Tominov, Z.E. Vakulov, N.V. Polupanov, et al., *Nanomaterials* **12**, 3 (2022).
6. D. Kim, M.D. Rossell, M. Campanini, et al., *Appl. Phys. Lett.* **119**, 1 (2021).
7. H. Su, X. Wang, C. Li, Z. Wang, et al., *Nano Energy* **83**, (2021).
8. R.V. Tominov, Z.E. Vakulov, V.I. Avilov, et al., *Nanomater.* **10**, 5 (2020).
9. V.A. Smirnov, R.V. Tominov, V.I. Avilov, et al., *Semicond.* **53**, 1 (2019).
10. V.B. Shirokov, Y.I. Yuzyuk, B. Dkhil, V.V. Lemanov, *Phys. Rev.B* **75**, 22 (2007).
11. S.R. Gilbert, L.A. Wills, B.W. Wessels, et al., *J. Appl. Phys.* **80**, 2 (1996).

P86

Technological optimization of the BZN-based ceramics preparation

M.A. Marakhovskiy, M.V. Talanov

Southern Federal University, 344090, Rostov-on-Don, Russia
marmisha@mail.ru

Technological operations of sintering ceramic layers and burning conductive electrodes are carried out synchronously during the manufacture of thermostable ceramic capacitors with internal Ag–Pd electrodes, as well as microwave filters. In addition, the temperatures of these processes must be coordinated. The dielectric materials with pyrochlore structure of the Bi_2O_3-ZnO-Nb_2O_5 (BZN) system used in this case are characterized by sintering temperatures of 1000÷1100°C, which requires the use of of Ag – Pd pastes with a Pd content of up to 30% in the internal electrodes of the ceramic elements. Reducing sintering temperatures to values below 1000° C will allow the use of Ag-Pd pastes with a Pd content < 30%., which will significantly reduce the cost of such converters [1-3]. One of the widely used methods for reducing the sintering temperature, which is used in the production of ceramic elements, is spark plasma sintering. But, until this date, it was not known about the results of using spark plasma sintering in the manufacture of the BZN-based dielectric ceramics. Thus, the aim of the work was to establish optimal manufacturing regimes for the dielectric ceramic material of the BZN system without losing its properties due to the use of spark plasma sintering technology.

The BZN ceramics are characterized by high values of the relative dielectric permittivity ($\varepsilon/\varepsilon_0$ ~ 140÷160), low dielectric losses (tg δ < 1%) and has high temperature stability. Ceramic elements of the specified composition were obtained by solid-phase synthesis and sintered using traditional ceramic technology (chamber furnace with atmospheric pressure), as well as by spark plasma sintering with DC pulses. The sintering quality of the ceramic elements was assessed by microstructure images obtained with a scanning electron microscope (JEOL JSM-6390LA) and by density values measured by hydrostatic weighing.

The analysis of the obtained results showed the relevance of using the spark plasma sintering method to increase the values of the relative dielectric permittivity by 20-25% (up to the values of $\varepsilon/\varepsilon_0$ = 170÷180), while maintaining low values of the tangent of the dielectric loss angle (tg δ < 1%), the temperature coefficient (TCE = -180 − -416 10^{-6} $grad^{-1}$) and with a decrease in the sintering temperature (to T_{sint} = 930÷950 ° C), as well as with a reduction in the duration of the sintering process (to t = 30 – 60 sec.). The established modes of spark plasma sintering of ceramic material based on the BZN system can be used in the industrial manufacture of capacitor elements with increased functional characteristics.

The research was carried out at the expense of the grant of the Russian Science Foundation No. 22-72-10022, https://rscf.ru/project/22-72-10022/.

1. J.C. Nino, M.T. Lanagan, C.A. Randall, *J. Appl. Phys.* **89**, 4512 (2001).
2. Q. Wang, H. Wang, X. Yao, *J. Appl. Phys.* **101**, 104 (2007).
3. R.A.M. Osman, N. Maso, A.R. West, *J. Am. Ceram. Soc.* **95**, 296 (2012).